Pulsed Electromagnetic Field Exposure:

A Novel Microwave Technique in

Potential Breast Cancer Treatment

Zhe Zhao

Centre for High Frequency Engineering, School of Engineering, Cardiff University

Cardiff China Medical Research Collaborative, School of Medicine, Cardiff University

A thesis submitted to Cardiff University for the degree of Doctor of Philosophy

April 2020

DECLARATION

This work has not previously been accepted in substance for any degree and is not concurrently submitted in candidature for any degree.

Signed…… (candidate) Date……..

Statement 1

This thesis is being submitted in partial fulfilment of the requirements for the degree of PhD.

Signed…… (candidate) Date……..

Statement 2

This thesis is the result of my own independent work/investigation, except where otherwise stated. Other sources are acknowledged by explicit references.

Signed…… (candidate) Date……..

Statement 3

I hereby give consent for my thesis, if accepted, to be available for photocopying and for inter-library loan, and for the title and summary to be made available to outside organisations.

Signed…… (candidate) Date……..

Statement 4

I hereby give consent for my thesis, if accepted, to be available for photocopying and for inter-library loans after expiry of a bar on access previously approved by the Graduate Development Committee.

Signed…… (candidate) Date……..

Abstract

The main objectives of this study are to uncover the potential mechanism of pulsed electromagnetic field exposure (PEFE) at the microwave range in inducing cell death in breast cancer cell lines *in vitro* and to confirm its clinical significance using a nude mouse model xenografted with human breast cancer cells. This novel technique can potentially contribute to the clinical treatment of breast cancer.

A dedicated microwave system was constituted and calibrated for precise PEFE generation and delivery. PEFE induced cell death included necrosis and apoptosis. Necrosis was discovered to be mainly due to the breakdown of membrane structure and cellular organelles, whilst apoptosis was triggered by disruption of tight junctions. The disrupted tight junction of the human breast cancer cells caused an under expression of ZO-1, a key component of the tight junction and HSP90, a heat shock protein involved in cell death. The decreased level of HSP90 activated caspase-dependent apoptotic signalling pathways with the subsequent overexpression of Caspase3/9 inhibiting glycolysis in metabolic signalling pathways, which was confirmed by a series of metabolic assays.

Furthermore, a neural regulator, namely Kidins220, was discovered to be a biomarker for PEFE treatments. Increased efficacy of the PEFE treatment was demonstrated in breast cancer cell lines with Kidins220 knockdown.

In conclusion, PEFE can exert its efficacy of cell-killing in breast cancer cells, reflecting its potential application in clinical breast cancer treatments. Independent of the thermal effect of microwaves, this minimally invasive technique can be cost-effective with less pain and side effects.

Acknowledgements

I would like to express my most sincere thanks to my supervisors, Professor Johannes Benedikt, Professor Wenguo Jiang, and Dr. Tracey Martin for their consistent help and scrupulous guidance throughout my PhD study. With their encouragement and expertise, we overcome many difficulties in my study and eventually achieve this great research. Furthermore, I also appreciate all of the advice, explanations, and improvements from them during the writing of this thesis.

I acknowledge the assistance from Professor Chang Gong from Sun Yat-sen University Zhongshan School of Medicine. With her expertise and support, we achieved the *in vivo* experiments successfully.

I would like to offer my thanks to Dr. Lin Ye, for his assistance in the establishment of Kidins220 Scramble and knockdown in breast cancer cell lines, Miss Fiona Ruge for assistance in histological and immununohislogical assays and Dr Christopher von Ruhland of Central Biological Service at Cardiff University for his help in the electron microscopy studies.

I also would like to offer my thanks to Miss Fiona Ruge, Dr. Jane Lane and Dr. Gregory M. Harrison for their help with the proof reading of my thesis.

I am very grateful to my wife, Dr. Shuo Cai for her accompanying and consistent support in experimental techniques throughout my PhD study. We have had a really fantastic time in Cardiff studying and living together. Her valuable encouragement is another motivation for me to finish my PhD study.

I also would like to give my deepest thanks to the family of my wife's and mine, for the unfaltering support and encouragement.

Publications

Zhao, Z., Martin, T.A., Benedikt, J., Cai, S., Ye, L., Davies, E., Mansel, R.E. and Jiang, W.G., 2020.: Kinase D interacting substrate 220 (Kidins220) and disease progression of breast cancer, the role of heat shock protein90 (HSP90). ***Cancer Research***, 80 (4), P3-01-18-P3, DOI: 10.1158/1538-7445.SABCS19-P3-01-1

Zhao, Z., Martin, T.A., Benedikt, J., Cai, S., Ye, L., Mokbel, K., Davies, E., Mansel, R.E. and Jiang, W.G., 2020. Kidins220 (kinase D interacting substrate 220) has a connection with neutrotrophic related factors, BDNF and NGF, in human breast cancer. ***Cancer Research***, 80 (4), P2-07-01, DOI: 10.1158/1538-7445.SABCS19-P2-07-01

Content

List of Figures

Chapter 1

Chapter 2

Chapter 3

Chapter 4

Chapter 5

Chapter 6

Chapter 7

List of Tables

Chapter 1

Chapter 2

Chapter 3

Chapter 4

Chapter 5

Abbreviations

ACC: acetyl-CoA carboxylases

ACL: ATP citrate lyase

ATCC: American Type Culture Collection

APS: Ammonium persulphate

ATP: adenosine triphosphate

BBB: blood-brain barrier

BSA: Bovine serum albumin

BSS: Balanced salt solution

cDNA: complementary DNA

CMI: confocal microwave imaging

CRUK: Cancer Research UK

CT: computed tomography

DC: direct current

DEPC: Diethylpyrocarbonate

dH2O: distilled water

DMEM: Dulbecco's Modified Eagles' Medium

DMSO: Dimethylsulphoxide

DNA: Deoxyribonucleic acid

ECIS: Electric Cell-Substrate Impedance Sensing

EDTA: Ethylenediaminetetraacetic acid

EEG: electroencephalogram

EMF: electromagnetic field

ERK: Mitogen-activated protein kinase

FAK: focal adhesion kinase

FAS: fatty acid synthase

FBS: foetal bovine serum

FCS: Foetal calf serum

FMT: focused microwave thermotherapy

GFP: green fluorescent protein

GLS: glutaminase

GSH: glutathione

GSM: Global System for Mobile Communications

GSSG: Oxidized glutathione

HCC: hepatocellular carcinoma

HMI: holographic microwave imaging

HSP: heat shock protein

IFC: Immunofluorescence

JAKs: Janus kinase

JAMA: Junctional adhesion molecule A

Kidins220: Kinase D-interacting substrate of 220kDa

LDH/LDHA: lactate dehydrogenase

LED: light-emitting diode

MEK: Dual specificity mitogen-activated protein kinase

MI: microwave imaging

MIST: microwave imaging via space time

MRI: Magnetic resonance imaging

MSA: multi-static adaptive

MW: microwave

MWA: microwave ablation

NAD: nicotinamide adenine dinucleotide

NADH: nicotinamide adenine dinucleotide

NADPH: nicotinamide adenine dinucleotide phosphate

OXPHOS: oxidative phosphorylation

PAK: Serine/threonine-protein kinase

PBS: Phosphate-buffered saline

PCR: Polymerase chain reaction

PDEs: partial differential equations

PET/CT: Positron emission tomography

PN: partial nephrectomy

PTFE: Polytetrafluoroethylene

qPCR: quantitative real-time polymerase chain reaction

RCC: Renal cell carcinoma

RF: radio frequency

RN: radical nephrectomy

RNA: Ribonucleic acid

RNAi: RNA interference

ROS: reactive oxygen species

SAR: specific absorption rate

SDS: Sodium dodecyl sulphate

SDS-PAGE: Sodium Dodecyl Sulphate Polyacrylamide Gel Electrophoresis

STATs: Signal transducer and activator of transcription

TAMP: tight junction associated transmembrane protein

TBE: Tris-Boric-Acid

TBS: Tris Buffered Saline

TBST: Tris Buffered Saline with 0.2% Tween 20

TEM: Transmission electron microscopy

TEMED: Tetramethyl ethylenediamine

TSAR: tissue sensing adaptive radar

VAV1: Proto-oncogene vav

Vis: Virtual Instruments

VSWR: voltage standing wave ratio

WHO: World Health Organization

ZO: Zonula Occluden

Chapter 1 Introduction

1.1 Microwave energy

Microwaves are ultra-high frequency signals with frequency ranging from 300MHz to 300GHz. Microwaves are a crucial energy carrier since they consist of electric and magnetic fields which are perpendicular to each other. As shown in Figure 1.1, this frequency range can be divided into varied bands. The band designation in the microwave range is listed in Table 1.1. Microwaves can be generated by dedicated devices, including semi-conductor devices and electric vacuum devices. In recent decades, microwaves have been evolved into various powerful devices in a number of important fields, including (but not limited to) communication, military, measurement, detection, heating, and synthesis. Due to certain particular characteristics, microwave applications have also been attempted in the area of medicine and medical technologies, such as disease detection, imaging and treatments.

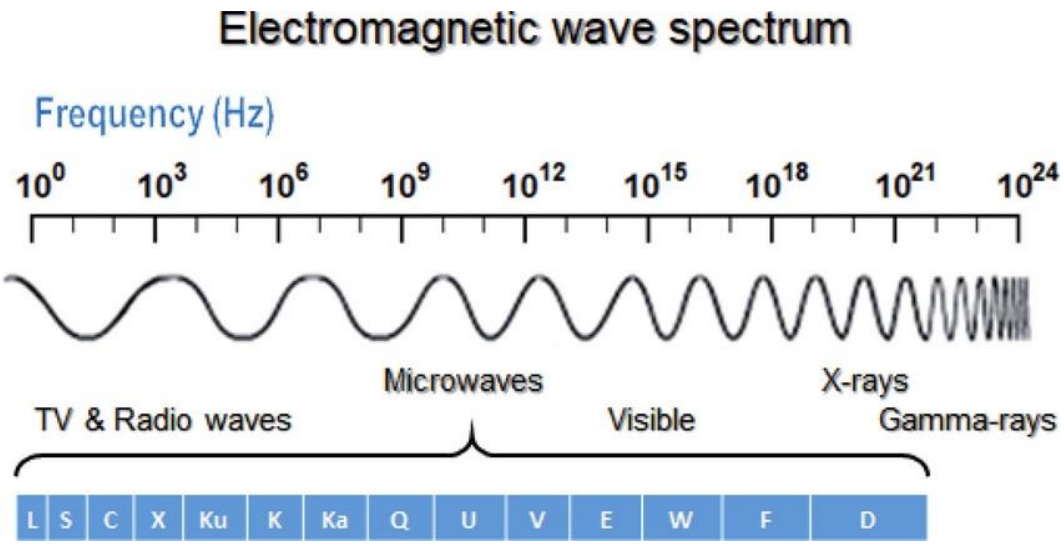

Figure 1.1 Microwave in electromagnetic wave spectrum(Ari Adi et al., 2019)

Table 1.1 Band designation in microwave range

Band Designation	Nominal Frequency Range
UHF	300 MHz—1000 MHz
L	1000 MHz—2000 MHz
S	2000 MHz—4000 MHz
C	4000 MHz—8000 MHz
X	8000 MHz—12000 MHz
Ku	12 GHz—18 GHz
K	18 GHz—27 GHz
Ka	27 GHz—40 GHz
V	40 GHz—75 GHz
W	75 GHz—110 GHz
mm	110 GHz—300 GHz

1.2 Microwave application in medical fields

Microwave applications in medical fields can be broadly categorised into that in diagnosis and in treatment (Rosen et al., 2002). For the past few decades, research on interactions between biological materials and electromagnetic fields has become well established (Gabriel et al., 1996). Investigations targeting physical characteristics of biological tissues at microwave range, such as dielectric properties and electromagnetic emission, have contributed to different techniques in diagnosis and treatment (Edrich, 1979).

Diagnostic applications employing microwave technologies are largely composed of two distinct stages, passive diagnosis and active diagnosis (Töpfer and Oberhammer, 2017). Microwave techniques have been successively applied in breast imaging and brain imaging with regard to diagnosis. Other potential applications in clinical diagnosis includes accumulated fluid monitoring in the torso (Ahdi Rezaeieh et al., 2017), bone imaging (Chandra et al., 2015) and non-invasive thermometry (Grodzinsky and Sund Levander, 2020).

As for treatment, many techniques have been developed based on the theory that polar molecules in biological tissue would respond to electromagnetic fields in microwave range. The realignment of polar molecules under oscillating microwave will rapidly increase the local tissue temperature through friction, contributing to thermal therapy such as microwave ablation (MWA) (Knavel and Brace, 2013), and some adjuvant treatments utilising hyperthermia (Riggs et al., 2020). MWA is mainly applied in cancer treatments in liver cancer, and to some limited degree to lung, breast, and kidneys. Other clinical applications include undesired tissue ablation in thyroid (Teng et al., 2019) and bones (Rinzler et al., 2019). As an adjuvant treatment, hyperthermia delivered by microwave can assist some well-established therapies such as chemotherapy and radiotherapy to enhance their efficacy (Hassan, 2010).

1.3 Microwave application in cancer diagnosis

Cancer is a global challenge in health. It is now the biggest killer in developed countries, overtaking heart diseases. According to the World Health Organisation (WHO), one in every six deaths in the world is the result of cancer, amounting to 9.6 million deaths globally in 2018. Of all the cancer types, lung cancer, breast cancer, colorectal cancer, prostate cancer and skin cancers are the top five in terms of incidence. When considering mortality, lung cancer, colorectal cancer, gastric cancer, liver cancer and breast cancer are the top five leading causes of death.

Early diagnosis of cancer is extremely important since it can reduce mortality in cancer patients. As an imaging technique, microwave has been applied in breast cancer detection. Compared to traditional imaging techniques in breast cancer, microwave imaging (MI) has some advantage in terms of accuracy, specificity and low cost. Additionally, MI is non-ionic irradiation, thus it is harmless to biological tissues (Cheng and Fu, 2018).

1.3.1 Theory of microwave diagnosis

As demonstrated in section 1.2, microwave imaging (MI) has two approaches, namely through passive and active methods. Passive diagnosis is from detection of electromagnetic emission from biological tissues. A calibrated radiometry is

employed to receive the radiation and the results can be reflected by temperature distribution of the target area. If morbidity is exists and is detected, changes should be observed locally in the measured temperature distribution compared to normal tissues or organs (Töpfer and Oberhammer, 2017).

Active diagnosis in cancer relies on modelling of dielectric properties of biological tissues and organs, including permittivity and conductivity (Töpfer and Oberhammer, 2017). It has been well documented that when normal cells become cancerous, the cellular water content increases dramatically due to the increased hydration and morphological alterations (Ross and Gordon, 1982). For example, liver cancer cells have 5% more water in their cytoplasm than normal liver cells (Ross and Gordon 1982). In mammary tissues, as another example, breast cancer tissues have significantly higher proportion of free water than normal tissues (Chung et al., 2008). Furthermore, plasma which is mainly water based (92%) accounts for 60% of the blood. Once the tumour is formed, the water content in tumour microenvironments is significantly elevated, resulting from the increased blood capillaries. Taken together, the increased water content in cancer cells and tissues contributes to significant changes in dielectric properties compared to normal tissues or organs. Active diagnosis utilises an external microwave source to deliver microwaves to target areas in a test organ or tissue, and the transmitted and reflected signals are then measured. Compared with normal tissues or organs, the altered dielectric properties lead to changes in the transmitted and reflected signals, which would then allow interrogation of the information for a diagnostic purpose, in this case for the possible presence of cancer.

1.3.2 Microwave cancer diagnosis techniques

Microwave thermography is a typical passive diagnosis technique, which has been applied in breast cancer detection. Active diagnosis can be subgrouped into microwave tomographic imaging and radar-based microwave imaging. Microwave tomographic imaging can be operated either in single frequency or with multi-frequencies in order to achieve better diagnosis. Radar-based microwave imaging can be further classified into five techniques based on the algorithms applied to the technologies. They include confocal microwave imaging (CMI), tissue sensing

adaptive radar (TSAR), microwave imaging via space time (MIST), multi-static adaptive (MSA) microwave imaging and holographic microwave imaging (HMI) (Bolomey and Jofre, 2010).

1.4 Microwave application in cancer treatments

The concept and investigation of microwave application in medical treatments can be traced back as early as the 1960s (Rojavin and Ziskin, 1998). This has led to the development of mature microwave technology used in cancer therapies for decades (Midorikawa et al., 2000, Lu et al., 2001, Izumi et al., 2001, Dong et al., 1998). These technologies work alone or combined with other therapies (Riggs et al., 2020). However, the mechanism of microwave treatments underlying these early developments are rather complicated and has limited the scope of application, arguing for more research into both the mechanisms and areas of applications (Chu and Dupuy, 2014). One key challenge here is that the existing evidence from both scientific research and clinical trials indicates that so far, the microwave based medical treatments are based on their thermal effect.

1.4.1 Microwave ablation (MWA)

As a typical application of thermal effect, microwave ablation has been widely used in liver, lung breast and renal cancer treatments, mostly guided by imaging tools. In those applications, microwave is delivered into lesions through varied types of applicators manufactured using microwave antennas, then local high temperature is produced as a result of dielectric heating. In order to produce local high temperature effectively, continuous microwave signals are applied. For instantaneous cell death, the required local temperature is usually in the excess of 60°C (Reimann et al., 2018, Schena et al., 2017, Tal and Leviatan, 2017, Bertram et al., 2006), whereas, prolonged treatments are required if the produced temperature is between 42°C and 60°C (Knavel and Brace, 2013). Traditional MWA is conducted at 915 MHz or 2.45 GHz (Martin et al., 2010, Lubner et al., 2010) while more precise ablation requires much higher frequency such as 5.8GHz – 10GHz due to the limited shallow energy penetration (Surducan et al., 2010). Additionally, the size of the ablation zones is also affected by the varied types of applicators (Cazzato et al., 2020).

1.4.2 Theory of microwave ablation

In microwave ablation, microwave is delivered to lesions through varied modalities, interacting with polar molecules, such as water, which eventually leads to rapid temperature increase. The produced local high temperature elicits tissue necrosis. The water content in biological tissues can be characterised by its complex relative permittivity and conductivity(Kishk, 2011). The complex relative permittivity ($\varepsilon^* = \varepsilon' - j\,\varepsilon''$) is frequency and temperature dependent, shown in Figure 1.2. The real part of ε^* represents the ability to be polarized by the external electric field, whistle the imaginary part is the dielectric loss, and quantifies the efficiency with which electromagnetic energy is converted to heat.

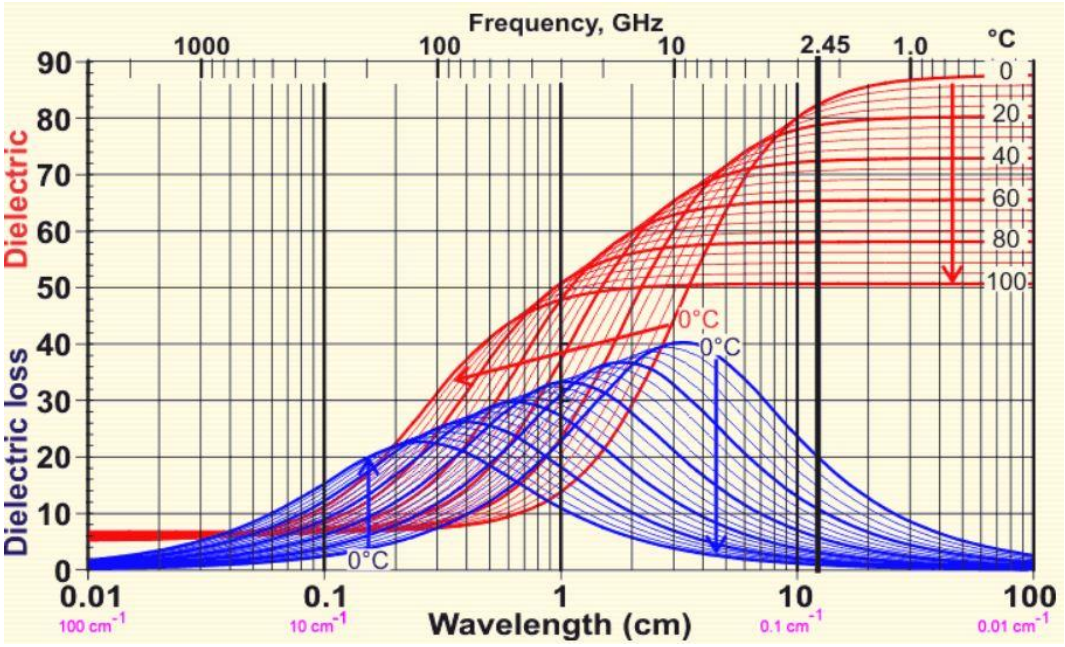

Figure 1.2 Dielectric permittivity and dielectric loss of water between 0°C and 100°C, the arrows showing the effect of increasing temperature or increasing water activity(Hasted, 1972, Buchner et al., 1999). It can be seen that both frequency and temperature can induce alteration in dielectric loss.

In some clinical trials, microwave ablation was performed *ex vivo*. The biological tissues were maintained in aqueous electrolyte which is water based and contains

ions. The dissolved ions can affect the relative permittivity. An example demonstrating the relative permittivity of saline is illustrated in Figure 1.3.

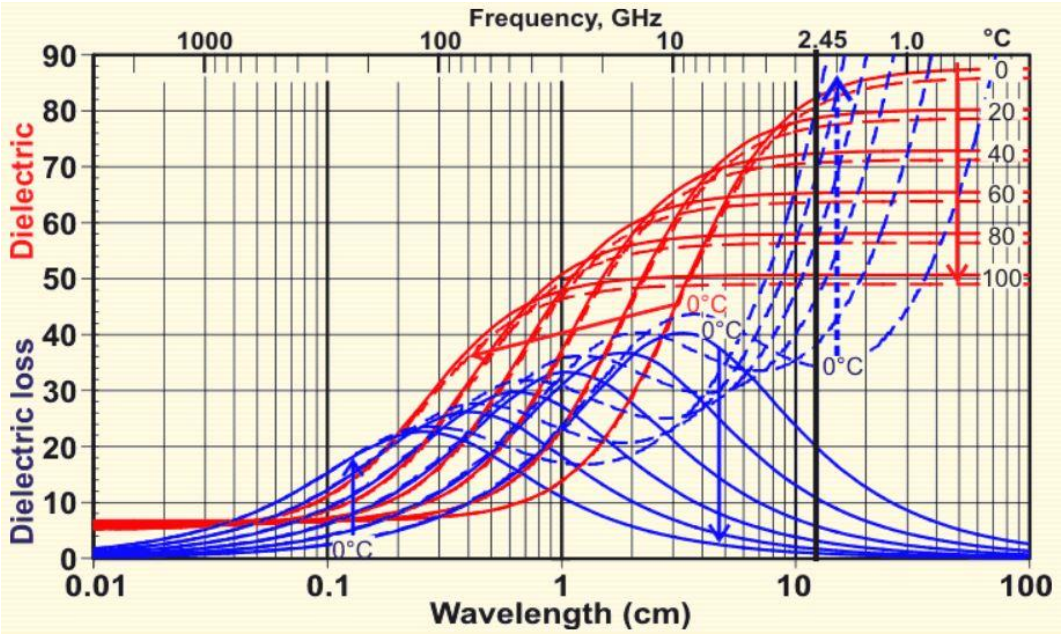

Figure 1.3 Dielectric permittivity and dielectric loss of a salt solution between 0°C and 100°C, the arrows showing the effect of increasing temperature(Meissner and Wentz, 2004, Risman and Wäppling-Raaholt, 2007). The solid lines represent the pure water as shown in Figure 1.2. The dashed lines represent the salt solution. In addition to frequency and temperature, the dissolved ions can also induce alterations in dielectric loss.

Furthermore, another component contributing to heat is conductivity. It has been studied that the electromagnetic energy deposition in biological tissue can be described in the following equations(Metaxas and Meredith, 1988, Chiang et al., 2013):

$$SAR = \frac{\sigma_{eff}}{2\rho}|E|^2$$

$$\sigma_{eff} = \sigma + 2 \times \pi \times f \times \varepsilon_0 \varepsilon''$$

where σ is the conductivity of the tissue (S/m), σ_{eff} represents the effective dielectric conductivity, $|E|$ is the electric field amplitude (V/m), ρ is tissue mass density (kg/m^3), $\varepsilon_0 = 8.854 \times 10^{-12}$ F/m, ε'' is the imaginary part of complex permittivity of

the tissue, and *SAR* is the specific absorption rate (*W/kg*). *SAR* is effectively a measurement of the rate of energy deposition in the tissue and will determine the power transferred to the tissue, consequently governing the damage inflicted to the tissue.

1.4.3 Microwave delivery techniques in microwave ablation

Microwaves can be irradiated from antennae, from which they penetrate inside the surrounding medium. The modalities of delivering a microwave to lesions have contributed to two major therapies in medicine, namely focused microwave thermotherapy (FMT) and percutaneous microwave ablation.

FMT is a minimally invasive treatment that is mainly used in breast cancer treatments (Dooley et al., 2010). When performing FMT, two compression plates made of microwave waveguide applicators are used to deliver the focused microwave fields to breast tumours transcutaneously, as depicted in Figure 1.4. A rectangular aperture with well-designed geometry locates in each compression plate, allowing a cooling system to be applied to alleviate the burn on the skin surface. Typically, the desired elevation of local temperature of the tumour in FMT ranges from 43℃ to 52℃. A sensor catheter, integrated within the microwave focusing probe and a temperature sensor, is inserted in the tumour site, monitoring the microwave field amplitude and temperature, respectively. This sensor catheter is placed under the guidance of ultrasound transducers which are placed in the rectangular aperture on each compression plate. The measured data can be fedback to adjust the input microwave power to achieve the required temperature in the tumour region.

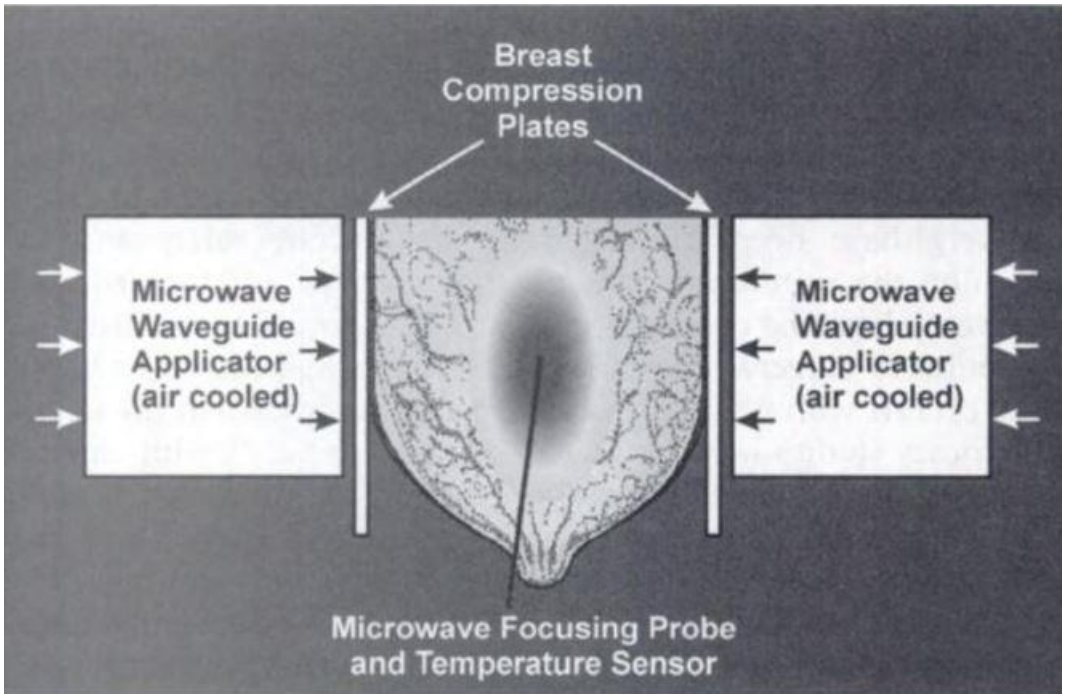

Figure 1.4 Externally applied focused microwave phased array thermotherapy treatment of cancer in the intact breast (Fenn, 2007).

Percutaneous microwave ablation has been widely used in cancer treatments for lung (Aufranc et al., 2019), liver (Yu et al., 2017), breast (Zhou et al., 2012) and kidney (De Cobelli et al., 2020). This technique requires a dedicated microwave applicator inserted through tissues, precisely reaching the tumour region guided by imaging tools, such as ultrasound and computed tomography (CT) (Deshazer et al., 2016), as shown in Figure 1.5. The key feature for the technology is generating thermally induced damage to cells and tissues. During the ablation, local high temperature is produced to achieve rapid tissue necrosis, thus a cooling system is integrated in the microwave applicator to avoid damage to surrounding normal tissues. Different kinds of microwave applicators have been designed and manufactured to increase local temperature effectively and achieve a larger ablation zone (Ahmed et al., 2011).

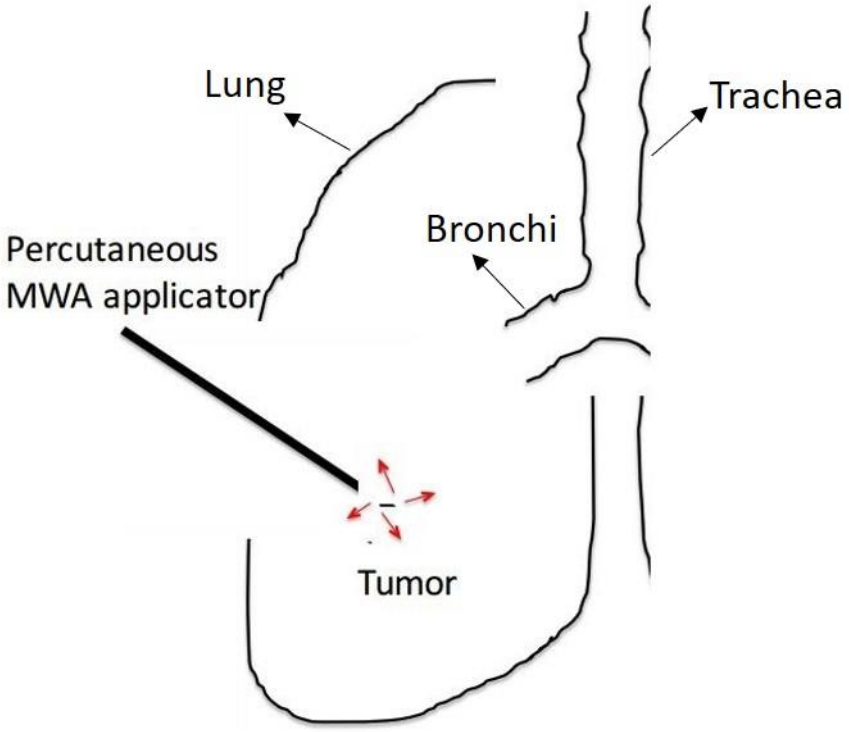

Figure 1.5 An example illustrating how percutaneous MWA was performed in pulmonary tumours (Pfannenstiel et al., 2017).

1.4.4 Previous investigation of microwave ablation

Although MWA has been widely applied in clinical treatments, some significant drawbacks which limit its further and wider application cannot be ignored. Typically, MWA is performed at low frequencies (915MHz or 2.45GHz) and delivers several tens of watts of power. Such high-power levels require equipment of larger size and produces excessive levels of heat that leads to collateral damage to the surrounding normal tissues and nearby organs. Thus, a cooling system is required to minimise the collateral damage, nevertheless increasing the cost of the entire system accordingly. In addition, a large proportion of the delivered energy returns to the microwave circuit due to the mismatched impedance between tumour tissue and microwave applicator during MWA. This unexpected mismatched impedance leads to unpredictable ablation zones, making it challenging to achieve complete ablation of tumour lesions (Jones et al., 2012). In recent years, a few studies have been considering how to improve and advance the technology by

targeting at different frequency and power levels. Yoon *et al*, conducted a comparative study performing MWA at higher frequencies (up to 30GHz) and lower power levels (1-3 watts), using a nude mouse model. Their results revealed that 18GHz had the highest ablation efficiency and this consideration was supported by the *in vivo* study. The *in vivo* study exhibited complete cessation in tumour growth without any recurrence elevated at day 100 (Yoon et al., 2011). This interesting observation does indeed point to a promising indication that MWA operating at higher frequency and low power level may suppress the growth of breast tumours, whilst minimising collateral damage. Similarly, Jones, *et al*, also conducted MWA at high frequency (14.5GHz) to investigate ablation efficiency (Jones et al., 2012). According to their results, higher power levels were able to generate significantly larger ablation zones through automatic impedance matching adjustment. Taken together, frequency and power level can be targeted to elevate the ablation efficiency of MWA.

Regarding the potential mechanism of MWA induced cell death, many studies have been conducted to confirm that the elicited cell death results from the affected tumour microenvironment and damages occurred in membrane and subcellular levels (Nikfarjam et al., 2005). The lesions undergoing MWA exhibit three zones (Ahmed et al., 2011): (1) central zone, which is immediately next to the microwave applicator; (2) transitional zone, beyond the central zone, exhibiting cell apoptosis or reverse injury; (3) normal tissues, which surround the transitional zone and are unaffected by MWA (Chu and Dupuy, 2014), as shown in Figure 1.6.

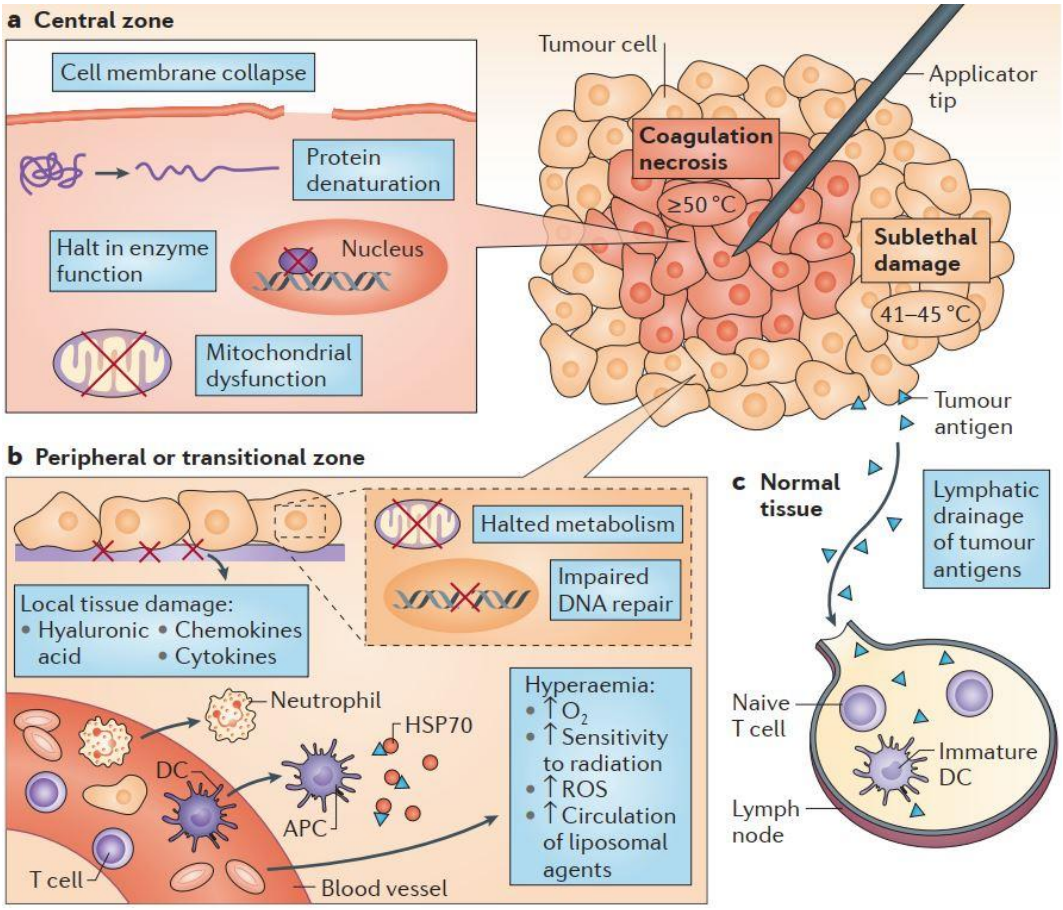

Figure 1.6 The zones of lesions undergoing MWA. The applicator tip is surrounded by three zones. (a) The central zone undergoes coagulative necrosis at temperatures ≥ 50°C. Cell membrane collapse, protein denaturation, a halt in enzyme activity and DNA polymerase function, and mitochondrial dysfunction all occur (b) The peripheral or transitional zone has a steep negative temperature-gradient. At temperatures between 41 °C and 45 °C there is still heat-induced injury, but it is sublethal and reversible. (c) The normal surrounding tissues (Nikfarjam et al., 2005).

During MWA, direct cellular damage is triggered and the main cause for induced cell death is thought to be alterations in membrane integrity which eventually leads to cytolysis (Nikfarjam et al., 2005, Fajardo et al., 1980). Another cause of cell death is considered to be mitochondrial dysfunction response to heat-induced injury (Wheatley et al., 1989, Willis et al., 2000). The denaturation of some crucial enzymes and proteins related to DNA replication can also contribute to cell death (Warters and Joseph, 1982). Furthermore, some other potential factors assist cell death under MWA and compromise disrupted synthesis of RNA, release lysosomal

enzymes and impair Golgi apparatus (Fajardo et al., 1980, Nikfarjam et al., 2005). In addition to direct cellular damage, MWA would also initiate indirect damage. For example, it has been shown that apoptosis, ischaemia due to impaired vascular function and accordingly reperfusion induced damage, and release of lysosomal contents as well as a change in cytokine expression (Fajardo et al., 1980, Nikfarjam et al., 2005). As a result, the mechanism of MWA induced cell death remains complicated and further investigations are required to completely uncover this novel technique.

1.4.5 Microwave ablation in clinical trials

As a well-established ablation technique, microwave ablation has been studied in clinical trials as a minimally invasive therapy for certain types of solid cancers for several decades.

Given the treatment choices for patients with cancer, the anatomical location of the tumours, stage and patient's conditions, microwave ablation as an alternative treatment has only been used as an alternative to certain tumour types, mostly in liver, lung, breast and renal cancers.

Lung cancer

Globally, lung cancer is the leading cancer type both in incidence and in mortality. In 2014, almost 1.6 million people died from lung cancer worldwide (Stewart and Wild, 2014). This trend increases over time, for example almost 1.8 million people died of lung cancer in the world in 2018 (WHO). In the UK, lung cancer survival over 1, 5, and 10 years are respectively 32.1%, 9.5% and 4.9% for men and women combined (Cancer Research UK data, www.cancerresearchuk.org, 2010-2011 results).

Although surgical resection has been a standard treatment for patients diagnosed with early stage lung cancer, unfortunately only around 30% of those with early stage lung cancer are eligible for surgical procedure, due to factors beyond the cancer itself. These factors can be multiple including medical comorbidities, poor cardiopulmonary function and older age (greater than 75 years of age). Patients who cannot receive surgical lobectomy are traditionally offered chemotherapy and/or

radiation therapy as alternatives, although other treatments including targeted therapies and cell based and immune therapies are now available. However, without cytoreduction (removing tumours), these treatments did not show a significant increase in reducing patients' mortality (Sidoff and Dupuy, 2017). Microwave ablation has been reported to be a safe, cost-effective, minimally invasive treatment for patients who do not qualify for surgery. There have been a number of clinical trials conducted using microwave ablation for these patients. The number of trials tend to be small, as are the number of patients in each study. Table 1.2. lists some of the trials.

Table 1.2 Clinical outcomes of microwave ablation in lung cancer treatments

NO	Patients	Lesions	Outcome (YS[1], Local recurrence)	Date
1	80	130	1-YS: 91.3% 2-YS: 75%	2002(Feng et al., 2002)
2	50	82	1-YS: 65% 2-YS: 55% 3-YS: 45%	2008(Wolf et al., 2008)
3	80	130	1-YS: 91.3% 2-YS: 75%	2011(Vogl et al., 2011)
4	56	69	1-YS: 69% 2-YS: 54% 3-YS: 49%	2012(Belfiore et al., 2013)
5	47	47	1-YS: 89% 2-YS: 63% 3-YS: 43%	2014(Yang et al., 2014)
6	47	103	1-YS: 82.7% 2-YS: 67.5% 4-YS: 16.6%	2016 (Vogl et al., 2016)
7	61	79	Local recurrence:3.7%	2019(Aufranc et al., 2019)

1 YS: year survival

Liver cancer

The sixth most common cancer all over the world (Globocan, 2012) in terms of incidence is liver cancer. Liver cancer has multiple histological types, including hepatocellular carcinoma (HCC), intrahepatic cholangiocarcinoma and sarcomas. HCC is the most common type of all the liver cancers diagnosed (Omata et al., 2017) and is the third most lethal type of cancer (Lau and Lai, 2009, Ferlay et al., 2010). In 2018, liver cancer resulted in 782 thousand deaths throughout the world

according to the World Health Organisation (WHO). Liver cancer also commands a poor clinical outcome. In the UK, the 5-year survival for patients with liver cancer is 23% (15-39 years old) and 6% (80-99 years old) for men, 30% and 2% for the women of the same age groups (Cancer Research UK, 2009-2011).

As with many other solid tumours, the first-choice treatments for HCC are restricted to hepatectomy and liver transplantation for those suitable for the procedure. This treatment option provides best clinical outcomes for patients. Unfortunately, only approximately 10%-20% of the patients with HCC are suitable for surgical resections (Lai and Lau, 2005, Lau, 2008). The majority are poor candidates due to various factors related to the cancer and within the patients, including patients with multiple tumours in both left and right liver lobes, excessive tumour size with poor liver reserve, and unfavourable tumour location (namely too close to vital structures for safe surgical procedures) (Qian et al., 2012). Given the particular features of the liver, namely the size of the organ (the largest solid organ in the body), giving reasonable ease of access to the tumour, microwave ablation has been more widely used for unresectable and recurrent HCC patients, than any other cancer types. The ablation also results in a high percentage of complete tumour necrosis and better year survival rate. Clinical outcomes in recent years after microwave ablation in HCC are listed in Table 1.3.

Table 1.3 Clinical outcome of microwave ablation in HCC

NO	Patients	Lesions	CA[1]	local Recurrence or tumour progression (LTP) complications	Date
1	234	339	92.8%	Local recurrence:30.77%	2002(Dong et al., 2003)
2	36	46	89%	--	2002(Shibata et al., 2002)
3	8	11	90.9%	--	2005(Abe et al., 2005)
4	49	98	94.9%	Local recurrence:11.8%	2005(Lu et al., 2005)
5	87	224	--	Local recurrence:2.7% Regional recurrence:43%	2007(Iannitti et al., 2007)
6	90	133	93.2%	LTP:5%	2007(Kuang et al., 2007)
7	50	--	86%	--	2009(Yin et al., 2009)
8	1136	1928	--	Major complications:2.6%	2009(Liang et al., 2009)

9	100	270	98%	Local recurrence:2%	2009(Martin et al., 2010)
10	39	125	100%	Local recurrence:9.6%	2011(Lorentzen et al., 2011)
11	22	22	95.5%	LTP:18.2%	2012(Qian et al., 2012)
12	736	1037	--	Major complications:2.9%	2012(Livraghi et al., 2011)
13	144	194	94.3%	Local progression:5.1%	2013(Poggi et al., 2013)
14	77	105	86.7%	LTP:10.5%	2013(Zhang et al., 2013)
15	113	131	98.5%	Local recurrence:10.9% Major complications:2.7%	2013(Ding et al., 2013a)
16	75	107	--	Overall survival rate (14 month):76.0%	2014(Ziemlewicz et al., 2015)
17	129	173	--	Major complication:2.2%	2016(Thamtorawat et al., 2016)
18	99	136	--	LTP:8.8%	2016(Potretzke et al., 2016)
19	203	265	--	1-year, 3-year and 5-year LTP:1.1%, 4.3%, 11.4%	2017(Yu et al., 2017)
20	70	70	--	--	2019(Tinguely et al., 2019)
21	59	66	96.6%	Primary recurrence:5%	2019(Darweesh and Gad, 2019)
22	28	34	100%	Major complication:7.2% Local recurrence:9.1%	2019(Kamal et al., 2019)
23	44	52	92.3%	Complication rates:13.6% Local recurrence (1 year):6.91%	2020(Suwa et al., 2020)
24	66	--	95.0 ± 11.2%	--	2020(An et al., 2020)
25	64	--	85.7 ± 9.4%	--	2020(An et al., 2020)

1 CA: Complete ablation.

Breast cancer

Breast cancer is the most common female malignant disease worldwide with increasing incidence especially in developing countries (Jemal et al., 2009). In the UK, breast cancer constituted 15% of all the 54,500 new cases of cancer in 2016 (Cancer Research UK (CRUK)). It is noteworthy that almost a quarter (24%) of the breast cancers are seen in women over 75 years of age (CRUK). Women at advanced age with breast cancer present a significant challenge as patients and to the healthcare sector due to the general wellbeing and health conditions of the patients which often makes this group of patients not eligible for aggressive therapies including surgery and chemotherapy.

Due to the development of screening techniques, patients with breast carcinomas can be diagnosed at an early stage (tumour diameter $\leqslant$ 3cm) (Ahmed et al., 2015, Elmore et al., 2005). Currently, microwave ablation is promising in small breast carcinomas and many studies have reported satisfying clinical outcomes, listed in Table 1.4.

Table 1.4 Clinical outcomes of microwave ablation in breast cancer treatments

NO	Sample (N)	Size	CA[1]	Complications	Date
1	10	1 to 8 cm	--	flap necrosis, blister	2002(Gardner et al., 2002)
2	25	0.7–2.8 cm	68%	Short-lived erythema, pain, Burn, oedema	2004(Vargas et al., 2004)
3	41	0.7–2.73 cm	85.3%	Skin burn, nipple retraction, seroma, abscess	2010(Dooley et al., 2010)
4	15	2.0–7.8 cm	--	Skin burn	2010(Dooley et al., 2010)
5	41	1.0–3.0 cm	90%	skin injury, pectoralis muscle injuries	2012(Zhou et al., 2012)

1 CA: complete ablation.

Renal cell carcinoma (RCC)

Renal cell carcinoma (RCC) is one of the most frequently diagnosed cancers worldwide with 403,262 incidences and 175,098 mortalities in 2018 (Capitanio et al., 2019). In the UK, it is seventh highest incidence of cancer, with 13,100 new cases reported (CRUK 2015-2017). When age is considered, members of the population aged between 85-89 have the highest incidence, again presenting a significant challenge for treatment options as the patients tend to have underlying medical conditions excluding them from receiving aggressive treatment procedures. The overall survival rate for patients with kidney cancers are good, 72%, 56% and 50% surviving after 1, 5 and 10 years, respectively (CRUK, 2010-2011).

Although surgery is the gold standard for RCC, percutaneous ablation techniques are an alternative for patients who are poor candidates for surgery, owing to at least the size of the organ (namely kidneys being one of the largest solid organs in the body) and the lack of vital body structures in and around the kidney (Motzer et al., 2017, Ljungberg et al., 2019). A few clinical trials have been conducted to evaluate MWA in RCC treatments. Shapiro *et al.*, compared MWA with traditional surgeries such as partial nephrectomy (PN) and radical nephrectomy (RN) in a clinical cohort of 325 patients who had stage T1b RCC. Local recurrence-free, metastasis-free, cancer-specific and overall survival were estimated in the study and the results revealed that MWA could be a feasible alternative to surgery (Shapiro et al., 2020). De Cobelli *et al.*, compared MWA with other ablation techniques using separate patient cohorts. The results failed to exhibit any significant differences except for shortened treatment time in MWA, indicating that MWA has equivalent safety and efficacy compared to cryoablation (De Cobelli et al., 2020). To investigate the efficacy of MWA in T1a and T1b renal cell carcinomas, Aarts *et al*, reported clinical trials of 100 patients who underwent MW treatment (108 RCC tumours included 85 T1a and 23 T1b) relating the treatment to local tumour recurrence (LTR), morbidity and mortality. The outcomes exhibited equivalent safety of MWA in both T1a RCC and T1b RCC, and significantly higher efficacy in T1a nodules (Aarts et al., 2020). As for treatments of T1c RCC, Zhou and Arellano *et al.*, reported safe outcomes in 44 patients who underwent CT-guided MWA. Furthermore, the results

also revealed that MWA had the advantage of shorter treatment time and less sedation compared to other ablative techniques (Zhou and Arellano, 2018).

Other cancer types

MWA has also been attempted in the treatment of pancreatic cancer and thyroid microcarcinomas. In pancreatic cancer, a clinical trial of 10 patients with locally advanced, surgically nonresectable, nonmetastatic pancreatic head cancer underwent MWA and the results were encouraging (Carrafiello et al., 2013). These findings indicated that MWA can be a feasible approach in the palliative treatment of pancreatic cancer. In a study of thyroid microcarcinoma, a large cohort of 185 patients underwent MWA (Teng et al., 2019). The results revealed that MWA is safe and efficient to be a potential therapy in primary papillary thyroid microcarcinoma treatments.

Microwave ablation in other medical conditions

In addition to cancer treatments, MWA has also been applied in osteoid osteoma treatments (Rinzler et al., 2019, Prud'homme et al., 2017, Kostrzewa et al., 2014, Basile et al., 2014). These studies have reported impressive success rates (>90%), and a low rate of minor complications and side effects.

1.4.6 Advantages of microwave ablation

Compared to other ablation techniques, the advantages of MWA are described below:

Active heating. Microwave ablation produces local high temperature by oscillations of polar molecules when interacting with electric fields (Andreano and Brace, 2013). The heat thus generated is most likely substantially produced from friction. As a result, microwave ablation can effectively avoid charring and nerve damage compared to radiofrequency ablation (Jones et al., 2012).

Effective heating. Microwave ablation triggers local high temperatures more effectively (Dong et al., 2019), especially when the ablation zone is near the blood vessels (Simon et al., 2005). The blood vessels can act as a heat sink, which dissipates the high temperature energy produced by microwaves through blood

circulation. Microwave ablation is not affected by this heat sink phenomenon, thus achieves more consistent tumour destruction. Furthermore, microwave ablation can achieve larger ablation zones under the same conditions compared to other ablation techniques (Andreano and Brace, 2013).

Selectivity. Microwave power produces local heat in the tumour without damaging the surrounding healthy tissue due to the difference in electric properties between healthy and tumour breast tissues (Sha et al., 2002, Vargas et al., 2004).

Low local recurrence rate. A review of the efficacy of microwave ablation has been carried out by Martin *et al*, in which 100 patients underwent ablations for hepatic malignancies (Martin et al., 2010). The significant finding was that local recurrence of the tumour at the ablated site occurred in only 2% of patients. This would have been further strengthened with studies of larger cohorts.

1.4.7 Disadvantages of microwave ablation

Costs. Microwave ablation is usually performed with a continuous wave at high power levels. The microwave devices involved in ablation systems need to produce high power and generate high temperatures. These devices are much more expensive than those that operate at low power levels, leading to relatively high cost (Jones et al., 2012).

Complexity due to cooling. When performing microwave ablation, the generated local high temperature can cause pain to patients and collateral damage to neighbouring tissues and organs. As a result, cooling devices have been considered and produced in order to relieve the side effects produced by heat including pain. This will also increase the cost of microwave ablation and increase the complexity of the entire microwave ablation system due to the integrated cooling system (Jones et al., 2012).

Side effects. Ablation may generate undesired tissue damage and will induce side effects, including periprocedural pain, fever, and slight pleural effusion. These side effects commonly exist in thermal ablations (Lahat et al., 2014). In addition to side effects, microwave ablation still can cause complications to patients depending on the ablation location (Ding et al., 2013b).

1.4.8 Microwave hyperthermia as an adjunct to enhance other therapies

In addition to thermal ablation, microwaves may have a role to play in assisting other types of cancer treatments, by enhancing their efficacy (Hassan, 2010). These complementary effects have been reported with established radiotherapy and chemotherapy. It has been shown in clinical trials that the cell killing effect of radiotherapy and chemotherapy can be further enhanced by hyperthermia in which tumours were placed at temperature ranging between 40℃ to 43℃ (Riggs et al., 2020, Issels, 2008). For this purpose, many microwave adapters or systems have been manufactured to deliver the desired hyperthermia for cancer treatments (Wust et al., 2002).

1.5 Biological effects of microwaves on biological samples

Due to the rapid development of communication systems, especially mobile phones and other wireless technologies, the human environment has been more involved with electromagnetic exposure at microwave frequencies (Bhangari et al., 2019). Extensive research interests have been directed to investigate these, for example, whether this exposure to electromagnetic signals can have an adverse and/or significant effect on biological samples, on the human brain, and even on human bodies (Parmar et al., 2019a). When biological samples are exposed to an electromagnetic field (EMF) at a microwave frequency, either the electric field or the magnetic field will interact with the sample, and the nature and degree of interaction will depend on the frequency. In the extreme low frequency range, the magnetic field is the likely dominant form to interact with biological samples. Conversely, the electric field mainly impacts on biological samples in the microwave frequency range (Kim et al., 2019). A number of studies have reported alterations in biological tissues exposed to high frequency electromagnetic fields under different conditions, while some other studies have reported no influence on biological tissues. In addition, only a few studies have reported how microwaves interact with cancer cells without hyperthermia (Kim et al., 2019).

1.5.1 Previous study on normal biological samples

Since the effects of microwave interaction with biological samples remain controversial, only those findings showing an influence on biological tissues were investigated in this research. Previous experiments have been conducted on different models *in vitro* and *in vivo*, exhibiting alterations mainly in brain and nerve activities, males and females reproductive systems, hormone levels, genotoxicity, gene and protein expression, and oxidative stress (Kim et al., 2019).

1.5.1.1 Non-thermal exposure on brain and nerve activities

A good number of studies have demonstrated changes in the electrical activity of the brain using electroencephalogram (EEG) recordings when exposed to microwaves. These changes occurred in event-related potentials (Vecchio et al., 2012a), alpha-wave power of the electroencephalogram (Vecchio et al., 2012b, Vecchio et al., 2010), slow-wave activity in human subjects (Lustenberger et al., 2013), spread of neural synchronization (Vecchio et al., 2007), and human cortical neural efficiency (Vecchio et al., 2012a). Furthermore, it has also been reported that EMF exposure can induce changes in electroencephalogram during sleep (Loughran et al., 2012). These acute changes in EEG in response to microwaves do not show pathological changes leading to diseases or necessarily adverse health effects but do illustrate that there are likely changes relating to the functioning of brain.

High frequency EMF exposure has also been shown to induce varied electrophysiological changes in the brain, leading to a series of altered behavioural effects. The conclusions were made from human studies or *in vivo* experiments. The induced behavioural alterations in human studies comprise reduction in behavioural arousal (de Tommaso et al., 2009), and affect sleep latency (Hung et al., 2007), cognitive functions (Vecchio et al., 2012b), spatial memory (Luria et al., 2009), well-being (Redmayne et al., 2013), thermal pain threshold (Vecsei et al., 2013), and motor activity (Lustenberger et al., 2013). Similarly, behavioural alterations in animal studies include memory (spatial and non-spatial) functions (Razavinasab et al., 2016), learning functions (Qin et al., 2014), cognitive functions (Deshmukh et al., 2013b), emotional behaviour (Bouji et al., 2012), motor functions

(Odacı et al., 2013), stress behaviour (Junior et al., 2014), hypoactivity (Kumar et al., 2009), analgesic effect (Mathur, 2008), passive avoidance deficit (Narayanan et al., 2010), and anxiety-related behaviour (Sokolovic et al., 2012).

Some other studies have investigated the effect of microwaves on the permeability of the blood-brain barrier (BBB). Research group (Eberhardt et al., 2008) found that pulse-modulated exposure at 915MHz in rats without any hyperthermia for 2 hours (0.2mW/Kg-0.2W/Kg, whole body SARs) resulted in increased albumin entering the brain, indicating that non-thermal pulsed microwave exposure could have a damaging effect via the BBB. Similar results were also observed by Nittby *et al*, (Nittby et al., 2009) and Sirav *et al*, (Sirav and Seyhan, 2011), under different exposure conditions.

Furthermore, electromagnetic field (EMF) exposure was demonstrated to impact brain metabolism, evaluated by enzyme levels (Ammari et al., 2008) and glucose consumption (Kwon et al., 2011). Aboul Ezz *et al.*, (2013) also reported that EMF affected levels of neurotransmitters in different parts of the brain in rats, in *in vivo* models (Aboul Ezz et al., 2013).

1.5.1.2 Non-thermal exposure on reproduction

1.5.1.2.1 Male fertility

Microwave exposure from mobile phones has been said to be able to significantly decrease spermatozoa quality by decreasing the motility, normal morphology, sperm count, and viability. Erogul *et al*, reported that 5-minute-exposure from mobile phone (900MHz GSM, average power density 0.2W/m) induced decreased motility in human spermatozoa *in vitro* (Erogul et al., 2006). Similarly, Agarwal *et al* also found that exposure to a mobile phone (1 hour, 850MHz GSM, 1 – 40μW/cm, 0.01 – 0.4W/m) would decrease the motility and viability, *in vitro*, of human spermatozoa, while it would increase oxidative stress of spermatozoa (Agarwal et al., 2009). *In vivo* experiments, to expose rabbits to low power microwave from a mobile phone (0.9GHz GSM, 8h/day, 09.00-17.00, for 12 weeks, at an average 2.92V/m highest exposure, 0.487V/m lowest exposure) showed a significantly decreased sperm motility as well as semen fructose

concentrations after 10 weeks (Salama et al., 2009). At the cell morphology level, there have been reports showing that microwave exposure from mobile phones induced morphological abnormality in spermatozoa (Otitoloju et al., 2010, Kesari and Behari, 2010). Furthermore, cohort studies on human volunteers have revealed that prolonged exposure to microwaves results in decreased quality of spermatozoa (Wdowiak et al., 2007, Fejes et al., 2005, Agarwal et al., 2008).

Microwave exposure can also exert influence on the levels of harmful reactive oxygen species (ROS) in spermatozoa by inducing an increase. *In vivo* experiments with rabbits have shown that low microwave exposures (SAR at 8 X 10^{-4} W/kg) at 50GHz for 2 hours a day for 45 days significantly altered antioxidant enzyme activity in spermatozoa samples. Meanwhile, increased apoptosis and decreased histone kinase activity were also observed under the experimental setting. The cell death and kinases changed were argued to be induced by ROS overproduction (Kesari and Behari, 2010). Similar results were observed by Kesari and Behari when exposing small animals, rats, to 0.9GHz radiation.

There is ample evidence showing that microwave exposure from mobile phones was able to cause DNA damage to spermatozoa *in vitro* and *in vivo*. Aitken *et al* subjected mice to intermittent mobile phone radiation at 900MHz (0.09W/Kg, 12h/day) and observed DNA damages in sperm after one week of treatments (Aitken et al., 2005). De Iuliis *et al* applied mobile phone exposure (1.8GHz, SAR of 0.4 – 27.5 W/Kg) to human sperm *in vitro* for 16 hours and found a significant increase in DNA oxidative damage and DNA strand breaks/DNA fragmentation when specific absorption rates were at 2.8W/Kg and above (p<0.001) (De Iuliis et al., 2009).

1.5.1.2.2 Pregnancy and female fertility

Chronic microwave exposure during pregnancy can decrease the female fertility, verified by alterations in offspring. In a study involving pregnant women (18-33 years of age, n=90) and full term new infants (n=30), Rezk *et al* found that exposing both future mothers and the infants to a mobile phone (10 minutes, dialling mode) would significantly increase the heart rate of both foetal and neonatal progeny and significantly decrease the stroke volume and cardiac output of their hearts (Rezk et

al., 2008). Odaci *et al* reported that, using a rat model, consistent exposure at the prenatal stage to an electromagnetic field (0.9GHz, 1mW/cm or 10W/m) had an impact on the formation and differentiation of neural stem cells during embryonic development (Odaci et al., 2008). The results also exhibited a significant reduction in the number of neurones compared to a control group in their offspring, when measured in 4 weeks old models. Gul *et al* reported a possible toxic effect induced by microwave exposure on rat ovaries. In this study, pregnant rats were exposed to a mobile phone in standby mode for 11 hours and 45 minutes, and in speech mode for 15 minutes, at a frequency of every 12h during the pregnancy (Gul et al., 2009). The follicles in the offspring were calculated at 21 days after birth and a significant reduction of follicles (average of 30% fewer) in their ovaries was observed compared to the control group.

1.5.1.3 The hormone melatonin

Melatonin is a hormone in the body that regulates sleep and sleeping patterns. A substantial effort has been made to understand if microwaves may influence sleeping by affecting the levels of melatonin in the body. Interestingly, most of these studies were carried out on human subjects. Exposure to mobile phones (>25 minutes/day, mean average 34 minutes/day, for 13 days) has been associated with significantly decreased nocturnal concentrations of the hormone melatonin in adults as seen by a 34% decrease in the metabolites of melatonin in urine (Burch et al., 2002)). Jarupat *et al* also found significantly decreased melatonin (36% decrease, measured by melatonin in the saliva, 02.00h). The test conditions exposed the volunteers to 30 minutes continuous use of a mobile phone every hour from 17.00-01.00h (1.96GHz, 2.5mW/cm) (Jarupat et al., 2003). Wood *et al* found significantly reduced melatonin concentrations immediately following 30 minutes of digital mobile phone exposure in the evening (27% decrease, 0.895GHz-GSM, 0.25W average power, measured by metabolite in the urine) (Wood et al., 2006).

1.5.1.4 Genotoxicity

There has been mounting evidence to show that microwave exposure under different conditions can elicit genotoxicity in certain circumstances, such as DNA damage, changes in chromosomal conformation and the formation of micronuclei.

This genotoxicity was observed in human fibroblasts (Schwarz et al., 2008), human lymphocytes and human leukocytes (Zhang et al., 2002), human lens epithelial cells (Yao et al., 2008), human Molt-4 leukaemia cells (Philips et al 1998), primary cultured neurons (Xu et al., 2010), human hair root cells (Cam and Seyhan, 2012), rat granulosa cells (Diem et al., 2005), human sperm (Avendano et al., 2012), human SH-SY5Y neuroblastoma cells (Luukkonen et al., 2009), rat and mouse brain cells (Deshmukh et al., 2013a), Chinese hamster cells (Zhang et al., 2006), rat renal and liver cells (Trosic et al., 2011), mouse embryonic stem cells (Ferreira et al., 2006), mouse sperm (Liu et al., 2013b), rat and cow erythrocytes (Ferreira et al., 2006), rat bone marrow cells (Atli Sekeroglu et al., 2013), rat hepatocytes (Furtado-Filho et al., 2014), rat lymphocytes (Gajski and Garaj-Vrhovac, 2009), blood cells and serum of rats (Kumar et al., 2010), calf thymus DNA (Hekmat et al., 2013), earthworms *Eisenia fetida* (Tkalec et al., 2013), and embryos of quails (Burlaka et al., 2013). Although the observations appear to be consistent, these studies were nonetheless conducted on cells *in vitro*, using conditions not commonly seen in the range of normal mobile phone microwave energy.

1.5.1.5 Gene and protein expression

Electromagnetic exposure at microwave frequencies on gene expression was initially examined by cDNA microarray (Harvey and French, 1999). Subsequently, various methods were applied in the follow up investigations, including gene expression (SAGE) method, gene expression microarray, GeneChip and Gene Array. In this section, previous studies which have been confirmed using multi-methods are investigated.

Some studies revealed altered expression of genes regulating cell apoptosis when exposing cells to chronic microwave irradiation. In primary cultures of neurons and astrocytes, pro-apoptosis molecules such as caspase-2, caspase-6, Asc, and Bax exhibited up-regulation (Zhao et al., 2007b), after exposure to GSM at 1900MHz for 2 hours. Using cultured acute T-lymphoblastic leukaemia cells (CCRF-CEM), certain apoptotic genes and activated cell cycle arrest genes were similarly found to overexpress after continuous microwave exposure at 900 MHz for 2 hours and 48 hours (Trivino Pardo et al., 2012). Buttiglione *et al* demonstrated that exposing

human neuroblastoma cells to a 900 MHz-modulated RF radiation would result in both Egr-1 gene expression and cell regulatory functions that involved apoptosis inhibitors like Bcl-2 and survivin (Buttiglione et al., 2007). Furthermore, reduction in the expression of the STAT3 gene after exposure to applied microwave (10.715 GHz, SAR of 0.725 W/kg, 6 h in 3 days at 25°C) was reported in cultured mouse brain cells (Karaca et al., 2012). Conversely, apoptosis inhibitor genes, including HSP70, were also affected by chronic microwave exposure (Lixia et al., 2006) (Trivino Pardo et al., 2012).

In addition to apoptosis, some other genes which play a role in cell morphology, the cytoskeleton, signal transduction pathway, metabolism (Zhao et al., 2007a) and structural maintenance (Chen et al., 2012) were also reported to be affected by microwave exposure under different conditions.

At the protein level, chronic microwave exposure has induced an altered expression of a few proteins. These alterations have been evaluated and verified using different techniques as stated in the following: Nylund and Leszczynski *et al* investigated the effects of GSM 900 MHz RF EMF exposure for 1 hour on EA.hy 926 cells (SAR of 2.0 W/kg) (Nylund and Leszczynski, 2004). Under these conditions, the cells exhibited an overexpression of a 27 kD heat shock protein (HSP27), together with an increase in its hyper-phosphorylation status.

In the subsequent experiments, the authors confirmed that a similar exposure (35 GHz continuous microwave exposure for 46 mins, power density at 75mW/cm^2) was able to elicit alterations in expression of 11 other proteins regulating cytoplasmic structures in rat cells (Sypniewska et al., 2010). These altered proteins were associated with inflammation, oxidative stress, and energy metabolism. Fragopoulou *et al* applied long-term whole-body irradiation to Balb/c mice under different conditions. Under this experimental setting, a few proteins related to neural function and brain metabolism exhibited altered expression (Fragopoulou et al., 2012).

1.5.1.6 Oxidative stress

The biological consequences of oxidative stress induced by microwave exposure have been well studied for decades. Using an *in vitro* approach, an increase in reactive oxygen species (ROS) level was seen in human semen (Agarwal et al., 2009, De Iuliis et al., 2009), human lens epithelial cells (Yao et al., 2008), embryos of Japanese quails (Burlaka et al., 2013), and in different cell types from rats (Campisi et al., 2010, Gajski and Garaj-Vrhovac, 2009, Kumar et al., 2010, Liu et al., 2013a). Furthermore, *in vivo* experiments also showed overproduction of ROS induced by different microwave irradiation (Guler et al., 2010, Guler et al., 2012, Kesari and Behari, 2009). Interestingly, Atasoy *et al* reported a decreased level of catalase and glutathione peroxidase activity ($p<0.05$) (Atasoy et al., 2013) in Wistar albino male rats after exposure to indoor Wi-Fi Internet access devices (2.437 GHz, 24h/day for 20 weeks). Collectively, it can be concluded that the chronic exposure to microwaves could result in changes in reactive oxygen species (ROS) *in vitro* and *in vivo.* However, the nature and magnitude of changes differ according to experimental conditions and cell types.

1.5.2 Biological effects on cancer cells

In radiofrequency research, a recent development in cancer therapy termed 'oncothermia' (Andocs et al., 2009, Szasz, 2013) was introduced, implying that this method can achieve cancer cell death under normothermic radiofrequency irradiation. By conducting the same experiments with conventional heating methods such as a water bath, the efficacy of cell-killing cannot be achieved, which implies the possible existence of 'nonthermal effects' of microwave on the death of cancer cells. Based on these reports, one would argue that the microwaves itself, rather than the heat it has generated, can be attributed to causing the death of cancer cells. If cancer cells can be killed by microwave irradiation without hyperthermia, this might be applied as a new cancer therapy in the future.

This idea received support from a recent successful study by Asano *et al* (Asano et al., 2017a). The authors exposed different cultured cancer cell lines to continuous microwave irradiation for 1 hour, using a dedicated microwave irradiation system. During exposure, the temperature of the cultured cells was maintained precisely at

37℃. To investigate whether the induced cell death was cell type or cell line specific, multiple cell lines from different cancer types were used including MCF-7 (breast cancer), T98G (glioblastoma), KATOIII (gastric cancer), HGC-27 (gastric cancer), HL-60 (leukaemia), MDA-MB-231 (breast cancer), Panc-2 (pancreatic cancer) and MCF-12A (immortalised normal mammary epithelial cells) cells. After microwave irradiation, a significantly decreased viability was observed in each cell line excluding MCF-12A, a very interesting observation that in addition to induction of cell death of cancer cells, the irradiation technologies might have a differential action on cancer cells and normal cells.

Subsequent experiments were also conducted in order to investigate the mechanism of normothermic microwave irradiation induced cancer cell death at molecular levels (Asano et al., 2017b). Three main kinds of cell death were examined sequentially, including apoptosis, necrosis and autophagy. The results revealed that cancer cells irradiated by normothermic microwaves underwent apoptosis that was independent of caspase activity. Furthermore, normothermic conditions were also confirmed by evaluating levels of the 70 kD heat shock protein (HSP70) which did not exhibit any increase in expression, indicating no heat response was induced.

1.6 A focus on breast cancer

1.6.1 Incidence of breast cancer

Breast cancer is one of the most frequent malignancies and accounts for almost 15% of all different cancer cases in the UK in females (Figure1.7) (Akram et al., 2017). The incidence of breast cancer was rose from 641,000 cases in 1980 to more than 1.6 million in 2010 worldwide, and 2.1 million women were estimated to have breast cancer in 2018. The cause of breast cancer is multifactorial with contributing factors including genetic, environmental, hormonal, dietary, and age. The highest incidence rate was found in older people, and a quarter (25%) of new breast cancer cases in the UK were over 75 years old in the UK (Cancer Research UK) (Figure 1.8).

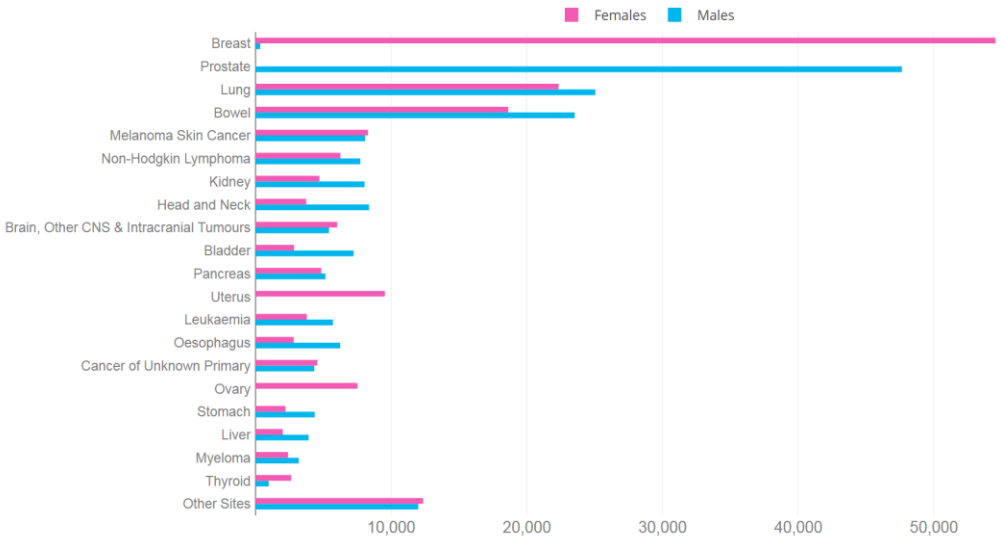

Figure 1.7 The incidence of breast cancer in the UK. Source: Cancer Research UK.

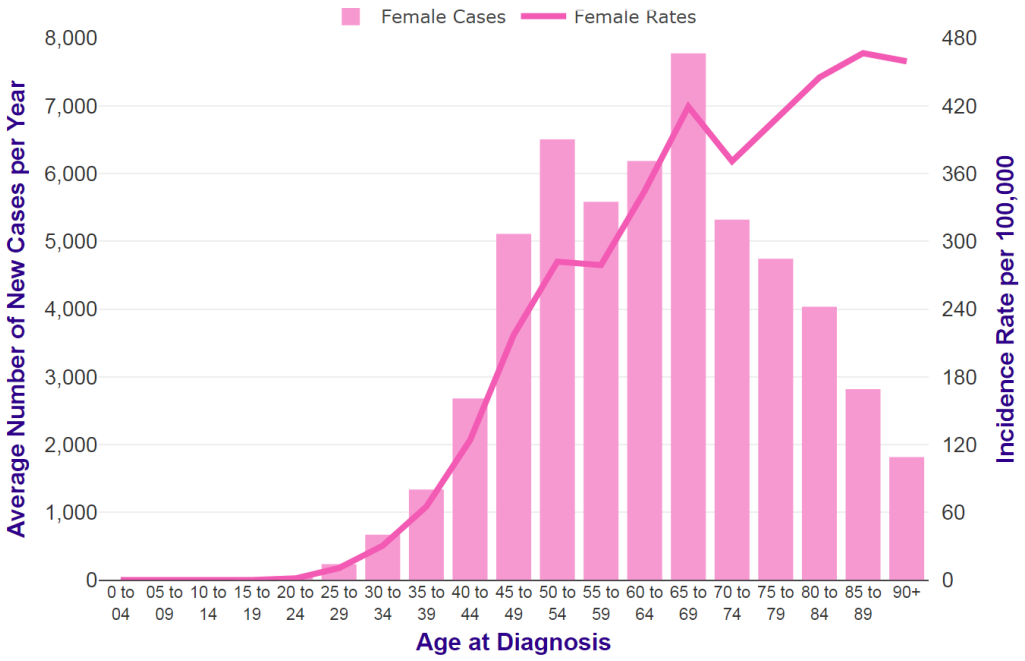

Figure 1.8 Average number of new breast cancer diagnosis at different age in the UK, incidence rates per 100,000 Population, 2014-2016 (Cancer Research UK).

1.6.2 Mortality of breast cancer

The five-year survival of breast cancer is quite different in different countries. It is 80% in developed countries and falls to 40% in developing countries (Coleman et al., 2008). Breast cancer is the 4th most common cause of cancer death in the UK, with around 11,400 breast cancer deaths every year in 2015-2017 (Figure 1.9) (Cancer Research UK). Due to the early detection and effective treatment, the mortality of breast cancer in North America and the European Union has decreased in recent years, and the mortality of breast cancer in the European Union was expected to drop by 8% since 2011(Malvezzi et al., 2016, Harbeck and Gnant, 2017).

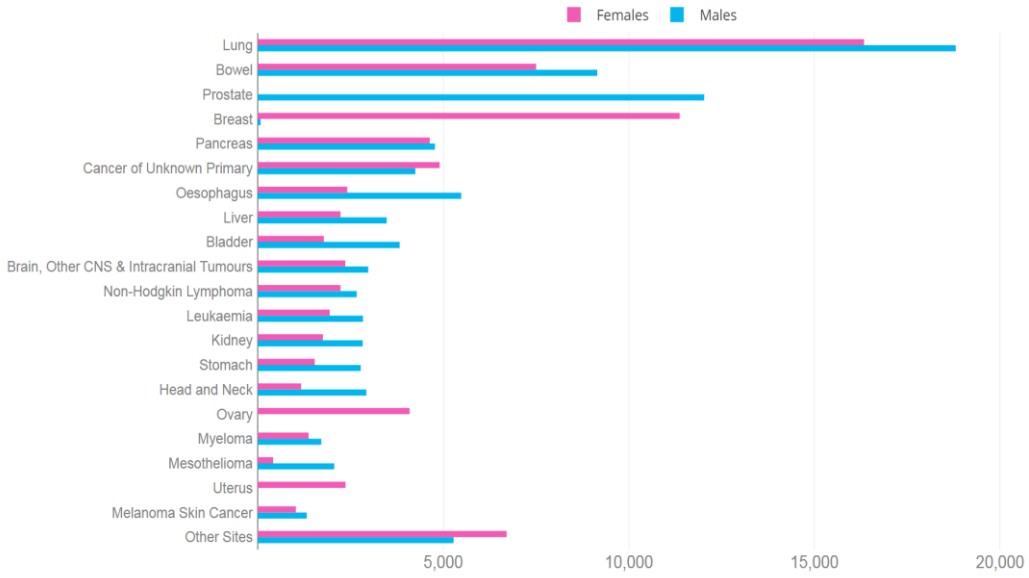

Figure 1.9 The mortality of breast cancer in the UK, 2017 (Cancer Research UK).

1.6.3 Staging of breast cancer

Staging of cancers is important in assessing the outcome of the patients and therapeutic decision making. The most accepted method of tumour staging is the TNM classification of breast cancer, by considering the size of the tumour (T), lymph node status (N) and if distant metastasis exists (M). Table 1.5. is a summary of the current staging system in breast cancer.

Table 1.5 Staging and TNM classification of breast cancer (Cancer Research UK)

Stage-I	**Tumour less than 2 cm and no spread to lymph nodes.**
Stage-IIA	Tumour less than 2cm and spread to 1-3 lymph nodes in armpit; or tumour 2-5cm and no spread to lymph nodes.
Stage-IIB	Tumour2-5 cm and spread to 1-3 lymph nodes in armpit; or tumour more than 5cm and no spread to lymph nodes.
Stage-IIIA	Tumour less than 5cm but spread to 4-9 lymph nodes in armpit or any lymph nodes under breastbone; or tumour more than 5cm and spread to 1-9 lymph nodes.
Stage-IIIB	Tumour any size but spread to nearby muscle and skin
Stage-IIIC	Tumour any size but spread to at least 10 lymph nodes in armpit; or to at least 1 node under breastbone and at least 1 in armpit; or to at least 1 node near collarbone.
Stage- IV	Breast cancer has spread to other parts of the body (metastasis)

1.6.4 Diagnosis of breast cancer

1.6.4.1 Symptoms and screening

Early diagnosis of breast cancer generally relies on awareness of symptoms and screening. Women with breast cancer may have symptoms including pain, a palpable mass and abnormalities in size and shape of the breast (McDonald et al., 2016). Mammography is the only screening method used to prevent and reduce mortality of breast cancer, as recommended by the American Cancer Society for women from the age of 45 (Pace and Keating, 2014, McDonald et al., 2016). In UK, all women at the age of 50 to 71 are invited to have breast cancer screening using mammography every 3 years (https://www.nhs.uk/conditions/breast-cancer-screening/). Over the years, mammography screening had led to an overall 19% reduction in the mortality of women with breast cancer. One of the limitations of this screening is false-positive findings. The false-positivity in mammography screening produces a 61% chance of misdiagnosis for women between the age of 40 and 50 years old (Pace and Keating, 2014). An example of a patient of 53 years old who received mammography screening and was diagnosed with breast cancer is shown in Figure 1.10.

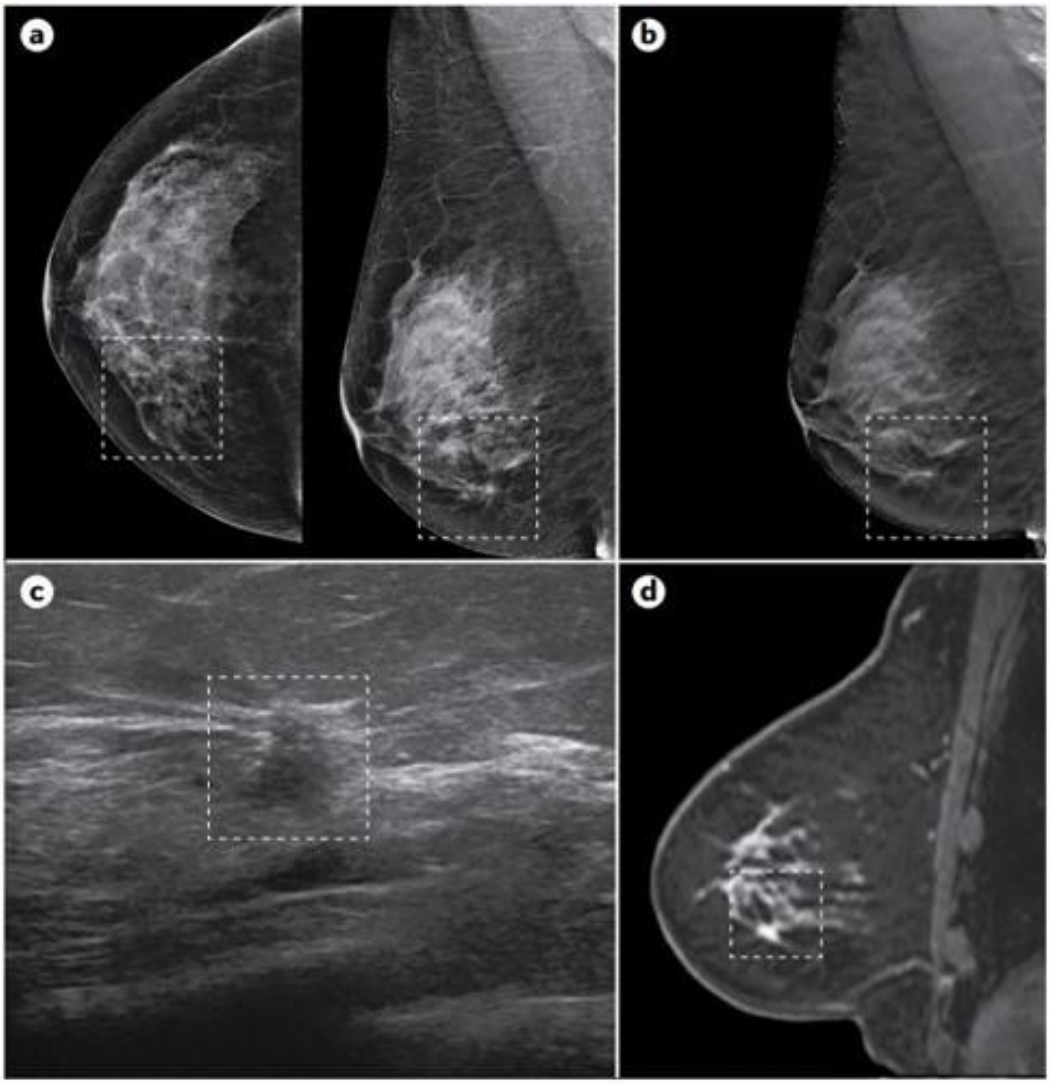

Figure 1.10 A 53-year-old woman in postmenopausal condition who did not have family history of breast cancer. She had no clinical findings before conducting the routine mammography screening. One lesion was found in the right breast. The tumour was squared in dashed line in each image (Harbeck et al., 2019).

1.6.4.2 Ultrasonography

Ultrasonography is a highly versatile tool to estimate the size and locate the position of breast tumours and is used for imaging-guided percutaneous biopsy (Loh and Chew, 2011).

1.6.4.3 Magnetic resonance imaging (MRI)

MRI has been used to evaluate breast cancer with clear clinical indications. It provides accurate and clear imaging compared with conventional imaging methods. MRI is suggested for assessment of diagnosed invasive lobular cancers and is a benefit to women with genetic mutations of BRCA1 and BRCA2 genes (Richardson et al., 2007).

1.6.4.4 Positron emission tomography (PET/CT)

PET/CT is an extremely precise tool for identifying lymph nodal and distant metastasis in comparison with regular imaging, as well as assessing primary tumours. PET/CT is also used in evaluating the treatment efficiency and the management of breast cancer recurrence (Antoch et al., 2004, Akram et al., 2017).

1.6.4.5 Breast biopsy

A breast biopsy is the most simple and effective technique for the diagnosis of breast cancer (Diego et al., 2016). In order to enhance the precision and avoid false negative results, the triple combination of breast examination, imaging and biopsy of breast tissue are routinely performed for the diagnosis of breast cancer (Akram et al., 2017).

1.6.4.6 Oestrogen (ER) and progesterone (PR) receptors

Breast cancer is hormone related and can be subgrouped based on hormone receptor status, including oestrogen and progesterone receptor expression. Additionally, other receptors can also be assessed, such as the human epidermal growth factor receptor (HER) family, which has four members, EGFR (Her1), Her2, Her3 and Her4. Of the four members, Her2 is routinely assessed in today's practice. These tests give some essential information regarding the aggressiveness of the cancer and allows for decision making when deciding the prospective response of the patients to certain drugs (Akram et al., 2017).

1.6.5 Traditional breast cancer therapy

The main objective for treating breast cancer patients is to prolong life whilst preserving the quality of life. Different types of standard treatment can currently be

chosen from for breast cancer patients, depending on their diagnosis. Moreover, some breast cancer patients are involved in clinical trials, which help to improve current treatments or obtain further information on using more effective therapies.

1.6.5.1 Surgery

Surgery is often the option for those individuals whose breast cancer has not metastasized to other areas of the body and surgical removal of the tumour is a common treatment for breast cancer (Houssami et al., 2017). Breast-conserving surgery, also known as lumpectomy, aims to preserve the breast itself by only removing breast tumours and surrounding tissues within a safe margin. During this procedure, small parts of tissues from the chest wall might be removed if the cancer is adjacent to it (Fisher et al., 1995, Akram et al., 2017). In a mastectomy, the breast is completely removed. This usually happens when the tumour is too large (more than 5cm) for a lumpectomy. In the process of simple mastectomy, only breast tissue and the muscles underneath the mammary gland are removed, and some of the lymph nodes under the arm may be sent for pathological evaluation (Czajka and Pfeifer, 2020). Modified radical mastectomy is the most common type of mastectomy. In this procedure, the underlying tissue muscle beneath the breast and all visible lymph nodes in axilla are removed. The breast tissue is then separated from the muscle underneath and sent for pathological examination. To avoid unnecessary dissection of the axilla, a sentinel node biopsy technique was introduced in the 1990s. The procedure involved identifying and dissecting the sentinel lymph node, the first lymph node draining the lymphatics from the region where the breast tumour is located. This highly skilled procedure has been introduced as an essential procedure for breast surgery (Mansel et al., 2006, Schmauss et al., 2015). It has spared a large number of patients from unnecessary radical mastectomy and axillary clearance. After surgery, some patients may be given chemotherapy, radiation therapy, targeted therapy, or hormone therapy to kill any remaining cancer cells and to reduce the possibility of cancer relapse. Some patients may also choose to have breast reconstruction after a mastectomy by using the patient's own non-breast tissue or implants filled with saline or silicone gel (Ahmed et al., 2005).

1.6.5.2 Chemotherapy

Chemotherapy is used for cancer patients to kill cancer cells or to stop cells from dividing. It is mainly used for breast cancer patients at stage 2 to stage 4 and is particularly beneficial for patients with oestrogen receptor-negative (ER-) disease. Depending on the diagnosis/prognosis of the patients, chemotherapy can be either used before and/or after surgery (Akram et al., 2017). "AC" (Adriamycin and Cyclophosphamide) is one of the most common used combination. It combines cyclophosphamide with doxorubicin hydrochloride (Adriamycin), and sometimes a taxeme drug, such as docetaxel (Cleator et al., 2006) . Although chemotherapy has some severe side effects, it can help to control disease progression for several years for those patients with cancer metastasis (Muller et al., 2001).

1.6.5.3 Radiation therapy

Radiation therapy kills cancer cells or can keep them from growing by using high-energy X-rays or other types of radiation (Chang-Qing et al., 2020). Radiation therapy includes external and internal radiation therapy. External radiation therapy is used to treat breast cancer and works by using the instrument to send radiation from outside of the body towards the cancer. Internal radiation therapy works by placing needles, wires, or catheters with radioactive substances directly into or near the cancer. Internal radiation therapy is able to relieve the pain caused by bone metastasis by using strontium-89 (Sadeghi et al., 2010).

1.6.5.4 Hormone therapy

Hormones are released by endocrine glands and circulated in the bloodstream. By acting on their specific receptors, hormones participate in a wide range of functions of the target cells and organs. They are also contributing factors in the development of cancers. The female hormone oestrogen, made mainly by the ovaries and acting on the oestrogen receptors (ER), can promote the growth and spread of breast cancer cells. Hormone therapies can stop cancer cells from growing by preventing hormone secretion or by blocking their function. Treatment by preventing the ovaries from making oestrogen is called ovarian ablation. Hormone therapy by targeting the oestrogen receptor (ER) with Tamoxifen is often given to patients with

early localized ER positive breast cancer who have the chance to have surgery. It is also suitable for those patients with metastatic breast cancer. Hormone therapy does have side effects, for example, treatment with tamoxifen or oestrogens can act on cells all over the body and may increase the chance of developing endometrial cancer (Gompel and Santen, 2012). However, compared with more aggressive chemotherapy, hormone therapy is considered to have very few side effects.

1.6.5.5 Targeted therapy

Targeted therapy is a type of treatment that uses drugs or other substances to target a specific molecule (marker) on cancer cells which in turn leads to an attack on cancer cells without harming normal cells. Monoclonal antibodies, tyrosine kinase inhibitors, cyclin-dependent kinase inhibitors, mammalian target of rapamycin (mTOR) inhibitors, and PARP inhibitors are types of targeted therapies used in the treatment of breast cancer (Masoud and Pages, 2017, Wilkes, 2018).

1.6.5.6 Immunotherapy

Immunotherapy, also called biotherapy or biological therapy, relies on the patient's immune system to fight against cancer (Hadden, 1999). It works by using cells from the human body or partially made in the laboratory to boost the defence of the body against cancer. Immunotherapy, in many different forms, plays a significant role in the management of breast cancer, an example of which is the development and use of vaccines. Parts of cancer cells can also be used for the production of vaccines and then facilitate the human immune system in fighting the cancer (Akram et al., 2017).

1.7 Kidins220

As discussed in earlier sections, microwave energy has been shown to influence nerve and brain cells, seemingly more prominently than other cell types. A number of neurotrophic factors, which primarily act on neuronal cells, are also known to have a direct influence on non-neuronal related cells. One such factor is Kindins220, which has been shown to have intimate links with neuronal and non-neural cancers but with strong neurological and endocrine links(Cai et al., 2017).

1.8 Metabolism and abnormal metabolics of cancer cells

Metabolism is a series of chemical reactions in organisms that sustain growth, reproduction, and response to environment. These reactions can be categorized as catabolism and anabolism. Catabolism is the procedure that breaks down compounds, such as nutrition to generate energy. Conversely, anabolism is the procedure that synthesizes necessary compounds with substrates and energy consumption (Vander Heiden et al., 2009).

Most mammalian cells rely on glucose for energy and nutrition. Glucose is metabolised by way of glycolysis, which is a multi-step procedure, eventually converting glucose to pyruvate. In normal cells, most of the pyruvate enters the mitochondria and undergoes oxidative phosphorylation through the Krebs Cycle under normal oxygen levels (Figure 1.11). Subsequently, adenosine triphosphate (ATP) is produced and used for life-sustaining processes (Cairns et al., 2011, Ryan et al., 2019).

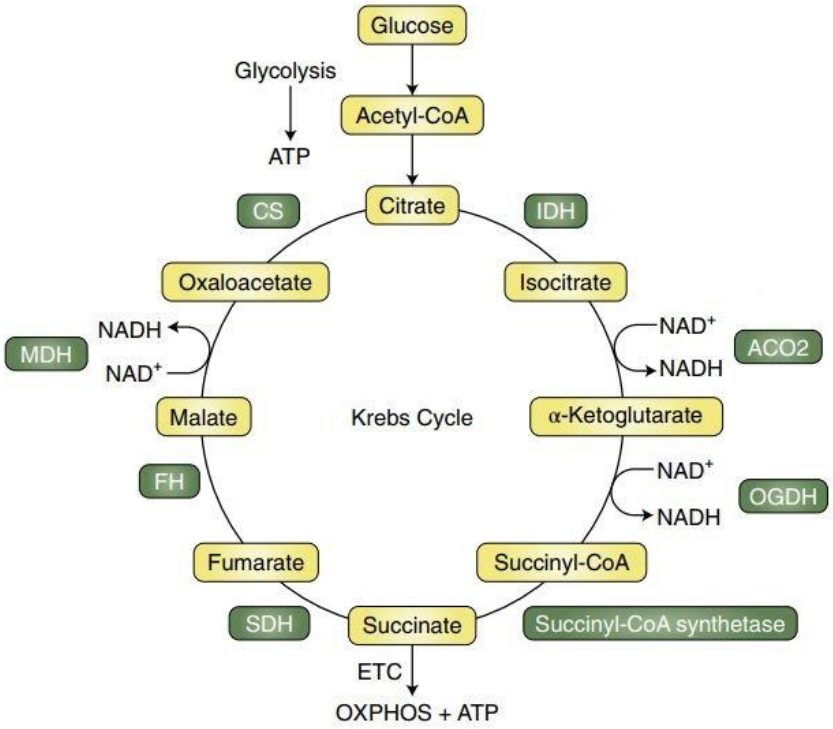

Figure 1.11 Krebs Cycle. Pyruvate enters mitochondria and undergoes oxidative phosphorylation through the Krebs Cycle, under normal oxygen levels (Ryan et al., 2019).

However, cancer cells have an altered cell cycle when compared with normal cells. Cancer cells are known to sustain uncontrolled proliferation and replicative immortality (Hanahan and Weinberg, 2011); thus, vast amounts of energy and biosynthetic substrates are required for the rapid growth and rapid division. To meet this demand, cancer cells shift the main mechanism of ATP generation from oxidative phosphorylation to aerobic glycolysis in the presence of oxygen. In aerobic glycolysis, most of the pyruvate produced from glycolysis, is transferred away from the mitochondria to interact with lactate dehydrogenase (LDH/LDHA) instead, resulting in ATP and lactate production (Figure 1.12). Interestingly, it has been shown that aerobic glycolysis is less efficient than oxidative phosphorylation in ATP generation. Since a great amount of energy is required for cancer cells, the question is why do cancer cells rely on a less efficient pathway?

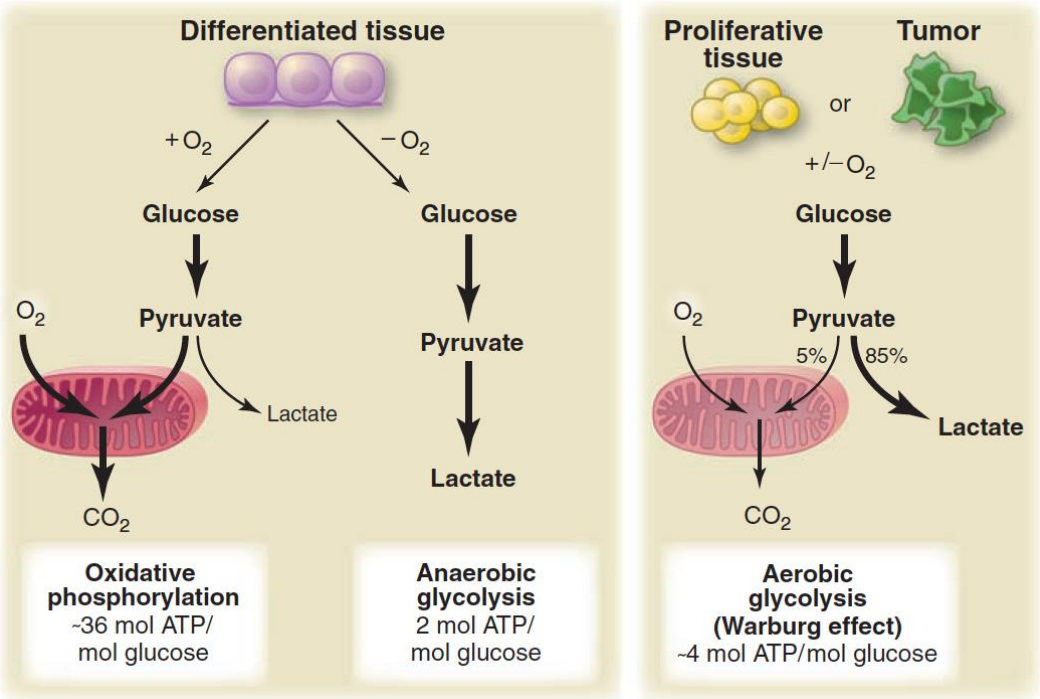

Figure 1.12 Oxidative phosphorylation (left) and aerobic glycolysis (right) (Vander Heiden et al., 2009)

In addition to increased division rates, cancer cells are also able to avoid apoptosis and are thus able to sustain consistent and uncontrolled growth. Cancer cells maintain a steady state of reactive oxygen species (ROS) at a much higher level

than that in normal cells. This elevated level of ROS helps cancer cells evade growth suppressors and resist cell death. Based on the increased ROS level, oxidative phosphorylation will further elevate its level through many oxidative reactions, which can effectively cause oxidative stress and eventually induce cell necrosis or apoptosis dependent on dose. As a result, cancer cells must manage this elevated ROS level, minimize the oxidative phosphorylation and turn to aerobic glycolysis (Panieri and Santoro, 2016).

In addition to energy, varied biosynthetic precursors are also essential for highly proliferative cancer cells to synthesize excess lipid, nucleotide, and amino acids. As another important fuel source, glutamine contributes to this biosynthesis (Hsu and Sabatini, 2008). Glutamine is converted to glutamate through a deamination reaction catalysed by glutaminase (GLS) inside mitochondria. Glutamate is subsequently converted to an intermediate in the TCA cycle, which assists with the ATP and amino acid production (Hensley et al., 2013). One of the converted intermediates in the TCA cycle, termed citrate, exits the mitochondria and becomes a critical component of amino acid and fatty acids. Fatty acids are essential for new membrane production (Fenton et al., 2000). More importantly, glutamine also plays a role in redox homeostasis. The glutamine in the cytosol, is involved in the synthesis of nucleotides and hexosamines by donating amide nitrogen (Hensley et al., 2013). After losing amide nitrogen, glutamine is converted to glutamate. Cytosolic glutamate is critical for maintaining redox homeostasis and protecting cells against oxidative stress through the production of glutathione (GSH) (Hensley et al., 2013), as shown in Figure 1.13.

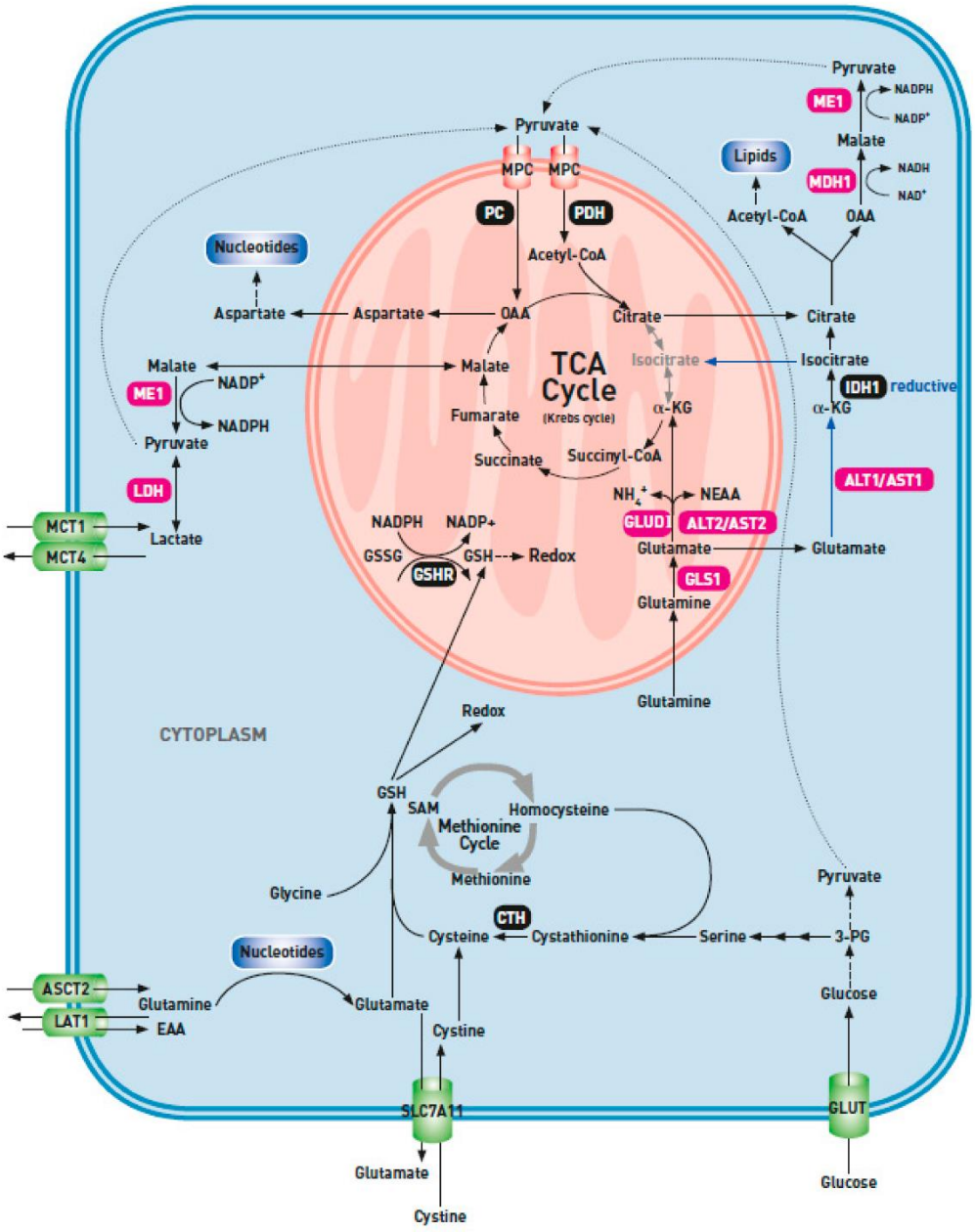

Figure 1.13 Glutamine metabolism in cancer cells. Glutamine is converted to glutamate inside mitochondria. Glutamate is subsequently converted to an intermediate form in the TCA cycle, which assists with ATP and amino acid production(Vanhove et al., 2019).

Compared with normal cells, metabolic signalling pathways in cancer have been reprogrammed to adapt to the microenvironment of the tumour and meet the requirements of fuel and biomass. This altered metabolism is a hallmark of cancer cells (Hanahan and Weinberg, 2011).

Based on the altered signalling pathway and steady state of homeostasis, many techniques have been proposed to target metabolism as a new venture for cancer treatments. These techniques can be catalogued into two aspects, including enzyme inhibition in metabolic signalling pathways and elevated ROS levels (Rodríguez-Enríquez et al., 2009, Mates and Sanchez-Jimenez, 2000). As demonstrated in section 1.4 and 1.5, microwave exposure can induce alteration in expression of proteins and cellular ROS level. This aspect has formed part of the present study, a worthy approach in order to evaluate if new microwave technologies induced cancer cell death may be via changes in metabolism. This can assist the exploration on how microwaves exert their cell-killing effects in cancer treatments.

1.9 Objectives, hypothesis and aims of this study

The overarching objective of this study was to develop, test and understand a new technology and its potential to treat human breast cancer. The technology, pulsed electromagnetic field exposure (PEFE), will be further refined for use and investigated as to its mode of action. This is a distinct area of unmet clinical need in patients with breast cancer who cannot receive current therapies.

The hypothesis is as follows: pulsed electromagnetic field exposure (PEFE) is able to induce apoptosis in cancer cells via a hitherto unknown mechanism and that this technology could be used as a clinical tool when treating breast cancer.

The aims of this study were as follows:

1. To develop a new technique namely pulsed electromagnetic field exposure (PEFE) attempting to kill breast cancer cells *in vitro* and *in vivo* and evaluate its potential significance in clinical application.

2. To explore the underlying mechanism involved as to how pulsed electromagnetic field exposure (PEFE) interacts with cancer cells at molecular level.

3. After the identification of proteins involved in apoptosis, Kidins220, a regulator in neuronal activities involved in cell apoptosis, was investigated to determine its ability to regulate the efficacy of PEFE treatments in breast cancer.

4. In addition to potential mechanism at molecular level, it was also determined whether PEFE treatments could induce cancer cell death through altered metabolism.

1.10 Thesis outline

This study is a combination of microwave engineering and breast cancer research. The main contribution of each chapter is summarized as follow:

Chapter1: Investigations on microwave applications in medical field, especially in cancer treatments. The biological effect of microwave was studied, which is potentially able to impact biological samples. In the area of cancer research, breast cancer was studied including incidence, mortality, staging, modalities of diagnostic techniques and therapies. As a regulator of neural activities, the role of Kidins220 in breast cancer and how it could potentially affect PEFE treatments was also investigated. Furthermore, the characteristics of metabolism in cancer cells was studied. This chapter demonstrated the background and significance of the thesis.

Chapter2: This chapter illustrated the materials used in this research, preparation of experimental reagents, and the techniques used in biological experiments.

Chapter3: The PEFE system was constructed and calibrated at desired frequency and power levels. The irradiation pattern was simulated using COMSOL Multiphysics to show the high level of electric field on the cell surface during the treatments. Moreover, some initial experiments were conducted to handle the probe appropriately, better understand the temperature profile, and assess the cell viability more precisely.

Chapter4: Intensive PEFE treatments were conducted *in vitro* and *in vivo*. A series of direct heating experiments without microwave were conducted to confirm the PEFE induced temperature increase did not impact cell viability. Many factors which could potentially impact the *in vitro* treatments were investigated. The results revealed that frequency, energy, and cell types do not impact treatments. Higher electric filed was required for better efficacy and the treatments are waveform specific. According to the analysis of the number of dead cells over time, rapid cell necrosis and prolonged cell death were found to be elicited by intensive PEFE. The

necrosis resulted from membrane structure and intracellular organelles breakdown, whistle the prolonged cell death was potentially triggered by the disruption of intercellular junctions, confirmed by transmission electron microscopy. *In vivo* study was conducted with in the collaboration with Sun Yet-Sen university. Significant tumour reduction was observed in mice underwent PEFE compare to control group, indicating the potentially clinical significance in the future breast cancer treatments. Furthermore, Kidins220 was investigated to impact cellular migration in breast cancer cells and enhance the efficacy of PEFE treatments, indicating Kidins220 can be examined as a potential biomarker if PEFE is applied in clinical breast cancer treatments.

Chapter5: Chronic PEFE was conducted *in vitro* to investigate PEFE induced prolonged cell death. Direct heating was also conducted to confirm the induced temperature increase did not impact cell viability over time or trigger any heat shock stress during the treatments. The prolonged cell death was studied to be cell apoptosis, confirmed by morphology alterations, DAPI staining and overexpression of Caspase3/9. Kinexus protein array revealed strong links between cell motility and apoptosis after PEFE treatments. Thus, the important component of tight junction-ZO-1 was first investigated using Western Blot and IFC staining. The disrupted tight junction eventually led to cell apoptosis.

Chapter6: A series of metabolic assays were conducted to investigate how PEFE impacted metabolic signalling pathways in cancer cells. The results revealed that PEFE induced cell apoptosis was not through metabolic signalling pathways.

Chapter7: In this chapter, we summarised the mechanism on how intensive PEFE and chronic PEFE induced cancer cell death. Furthermore, we introduced future work on PEFE system improvement and supplementary experiments for better verification of our results.

Chapter 2 Methodology

2.1 Materials

2.1.1 Cell lines

2.1.1.1 Cancer cell lines

The cell lines involved in this research were established human breast cancer cells, including MDA-MB-231, MCF-7, BT549, and T47D. They were all purchased from sLGC Standard (Teddington, Middlesex, England) who supply cell lines in the UK for the American Type Culture Collection (ATCC, Rockville, MD, USA). All cell lines were verified at source for their identity and were low passage on acquisition. Full details of these cell lines are listed in Table 2.1. Dulbecco's Modified Eagles' Medium (DMEM) supplemented with 10% foetal bovine serum (FBS) and antibiotics were used for cell culture.

Table 2.1 Details of breast cancer cells used in this research

	MDA-MB-231	MCF-7	BT549	T47D
Species	Human	Human	Human	Human
Tissue	Mammary gland/breast	Mammary gland, breast	Mammary gland, breast	Mammary gland
Gender	Female	Female	Female	Female
Age	51	69	72	54
Morphology	Epithelial	Epithelial	Epithelial	Epithelial
Culture Properties	Adherent	Adherent	Adherent	Adherent
Disease	Adenocarcinoma	Adenocarcinoma	Ductal carcinoma	Ductal carcinoma

2.1.1.2 Normal breast cells

Primary cultured normal mammary epithelial cell stocks were purchased from Lonza (Basel, Switzerland). The normal epithelial cells, with limited ability to multiply, were maintained in a specific medium supplied by Lonza and used within early passages.

2.1.2 General compounds

The chemicals and reagents used in this research are listed in Table 2.2.

Table 2.2 Chemicals and reagents

Material/Reagent	Supplier
10% Foetal calf serum (FCS)	PAA Laboratories, Coelbe, Germany
A/G protein agarose beads	Insight Biotechnology, UK
Acetic acid	Fisher Scientific, Leicestershire, UK
Acrylamide mix (30%)	Sigma-Aldrich, Poole, Dorset, UK
Agarose	Melford Laboratories Ltd, Suffolk, UK
Ammonium persulphate (APS)	Sigma-Aldrich, Poole, Dorset, UK
Amphotericin B	Sigma-Aldrich, Poole, Dorset, UK
Ampicillin	Sigma-Aldrich, Poole, Dorset, UK
Bio-Rad DC™ Protein Assay	Bio-Rad Laboratories, Hercules, CA, USA
Boric acid	Duchefa Biochemie, Haarlem, Netherlands
Bovine serum albumin (BSA)	Sigma-Aldrich, Poole, Dorset, UK
Bromophenol Blue	Sigma-Aldrich, Poole, Dorset, UK
Calcium chloride ($CaCl_2$)	Sigma-Aldrich, Poole, Dorset, UK
CellTiter-Glo® 2.0 Assay	Promega, UK
Chloroform	Sigma-Aldrich, Poole, Dorset, UK
Coomassie Blue	Sigma-Aldrich, Poole, Dorset, UK
Crystal violet	Sigma-Aldrich, Poole, Dorset, UK
Diethylpyrocarbonate (DEPC)	Sigma-Aldrich, Poole, Dorset, UK
Dimethylsulphoxide (DMSO)	Fisons Scientific Equipment, Loughborough, UK
Disodium phosphate ($NaHPO_4$)	BDH Chemicals Ltd, Poole, Dorset, UK
Dithiothreitol	Sigma-Aldrich Ltd, Dorset, UK
Dulbecco's Modified Eagles' Medium/Nutrient mixture F12	Sigma-Aldrich, Poole, Dorset, UK
Ethylenediaminetetraacetic acid (EDTA)	Duchefa Biochemie, Haarlem, Netherlands
Ethanol	Fisher Scientific, Leicestershire, UK
Formalin	Sigma-Aldrich Ltd, Dorset, UK
GoTaq® Green Master Mix	Promega, UK
G418	Sigma-Aldrich, Poole, Dorset, UK
Glucose-GloTM Assay	Promega, UK
Glutamine/Glutamate-Glo™ Assay	Promega, UK
Griess Reagent System	Promega, UK
GSH/GSSG-Glo™ Assay	Promega, UK
Hydrochloric acid (HCl)	Sigma-Aldrich, Poole, Dorset, UK
Isopropanol	Sigma-Aldrich, Poole, Dorset, UK
Lactate-Glo™ Assay	Promega, UK
Matrigel®	BD Biosciences, Oxford, UK
Methanol	Fisher Scientific, Leicestershire, UK
Mitochondrial ToxGlo™ Assay	Promega, UK
NAD(P)H-Glo™ Detection System	Promega, UK
Disodium phosphate (Na_2HPO_4)	BDH Chemicals Ltd., Poole, Dorset, UK

Sodium azide (NaN_3)	Sigma-Aldrich, Poole, Dorset, UK
Nitrocellulose membrane	Amersham, Cardiff, UK
Penicillin	Sigma-Aldrich, Poole, Dorset, UK
Ponceau S Stain	Sigma-Aldrich, Poole, Dorset, UK
Precision qScript™ RT PCR kit	Primerdesign Ltd, Southampton, UK
Potassium chloride (KCl)	Fisons Scientific Equipment, Loughborough, UK
REDTaq® ReadyMix™ PCR Reaction Mix	Sigma-Aldrich, Poole, Dorset, UK
ROS-Glo™ H_2O_2 Assay	Promega, UK
RPMI	Sigma-Aldrich, Poole, Dorset, UK
Bovine serum albumin (BSA)	Sigma-Aldrich, Poole, Dorset, UK
Sodium dodecyl sulphate (SDS)	Melford Laboratories Ltd, Suffolk, UK
Sodium chloride (NaCl)	Sigma-Aldrich, Poole, Dorset, UK
Sodium fluoride (NaF)	Sigma-Aldrich, Poole, Dorset, UK
Sodium hydroxide (NaOH)	Sigma-Aldrich, Poole, Dorset, UK
Sodium orthovanadate (Na_2VO_4)	Sigma-Aldrich, Poole, Dorset, UK
Sodium pyrophosphate ($Na_4P_2O_7$)	Sigma-Aldrich, Poole, Dorset, UK
Streptomycin	Sigma-Aldrich, Poole, Dorset, UK
Sucrose	Fisons Scientific Equipment, Loughborough, UK
SYBR®Safe DNA gel stain	Life Technologies Ltd, Paisley, UK
TBS Automation Wash Buffer	
Tetramethylethylenediamine (TEMED)	Sigma-Aldrich, Poole, Dorset, UK
TRI Reagent	Sigma-Aldrich, Poole, Dorset, UK
Tris-Cl	Melford Laboratories Ltd, Suffolk, UK
Triton X-100	Sigma-Aldrich, Poole, Dorset, UK
Trypsin	Sigma-Aldrich, Poole, Dorset, UK
Tween 20	Melford Laboratories Ltd, Suffolk, UK
Vectastain Universal ABC kit	Vector Laboratories Inc, Peterborough, UK
Zinc chloride (ZnCl)	Sigma-Aldrich, Poole, Dorset, UK

2.1.3 Instruments, software and other general plastic consumables

The instruments, software and general plastic consumables are listed in Table 2.3.

Table 2.3 Instruments, culture vessels and software

Microwave Instruments	
Hardware	**Manufacturer**
N5181B MXG X-Series RF Analog Signal Generator, 9kHz-6GHz	Keysight Technologies UK Limited
MILMEGA AS1860-50 Broadband Power Amplifier	MILMEGA Limited UK
Altan TecRF AS7122 Circulator	Atlantic Microwave Ltd
Directional Coupler 1.5-9.0GHz	Cardiff University
U2021XA 50MHz-18GHz USB Peak and Average Power Sensor X 2	Keysight Technologies UK Limited
Times Microwave Unterminated to Unterminated RG 405 Coaxial Cable	RS Components Ltd. Corby, Northants, UK
LUXTRON Fibre Optic Temperature Sensors	LumaSense Technologies Inc. Littlehampton, UK
Biological Instruments	
0.4 μm filtration unit	Sigma-Aldrich Co, Poole, Dorset, UK
25 cm^2 and 75cm^2 culture flasks	Cell Star, Germany
Lecia DM IRB microscopy	Lecia GmbH, Bristol, UK
Countess™ II Automated Cell Counter	Fisher Scientific UK Ltd
Invitrogen™ Countess™ Cell Counting Chamber Slides	Fisher Scientific UK Ltd
Neubauer haemocytometer counting chamber	Reichert, Austria
Protein spectrophotometer	BIO-TEK, Wolf Laboratories, York, UK
RNA spectrophotometer	BIO-TEK, Wolf Laboratories, York, UK
UV light chamber	Germix
Software	
LabView2017	National Instruments Corporation Austin, TX, USA
Image J	Public Domain
Prism8	GraphPad Software, San Diego, USA
Microsoft Excel	Microsoft In., Redmond, WA, USA
ECIS	Applied BioPhysics, Inc. New Jersey, USA

2.1.4 Primers for polymerase chain reaction (PCR)

Primers used in this research were designed using Beacon Design Programme (Biosoft International, Palo Alto, California, USA) and synthesised by Sigma Genesis (Poole, Dorset, UK). They were stored at -20℃ and were defrosted at room temperature when needed. Primer sequences used for quantitative real-time polymerase chain reaction (qPCR) are shown in Table 2.4.

2.1.5 Antibodies

Antibodies used in this research and their source are listed in Table 2.5. Primary antibodies were supplied by Insight Biotechnology (Insight Biotechnology, UK) and Abcam (Cambridge, England, UK), secondary antibodies were from Sigma-Aldrich (Poole, Dorset, UK).

Table 2.4 Primers for qPCR

Primer name	Primer sequence (5'-3')	Product size (bp)
GAPDHF1	AAGGTCATCCATGACAACTT	1070
GAPDHZR1	ACTGAACCTGACCGTACAGCC ATCCACAGTCTCTG	
Kidins220F2	AGACGTTCCATGCTCAGA	136
Kidins220ZR2	ACTGAACCTGACCGTACATGC CTTCTTCGGTAAGTG	

Table 2.5 Antibodies used in this research

Antibodies	Molecular weight (kDs)	Supplier	Product code
Rabbit anti-Kidins220	220	Insight Biotechnology/Santa Cruz	sc48738
Mouse anti- β-actin	42	Insight Biotechnology/Santa Cruz	sc47778
HSP90	90	Insight Biotechnology/Santa Cruz	Sc69703
ZO-1	220	Invitrogen	61-7300
Caspase3	32	Insight Biotechnology/Santa Cruz	Sc56053
Caspase9	47	Insight Biotechnology/Santa Cruz	Sc17784
Rabbit anti-mouse (whole molecule) IgG peroxidise conjugate	Dependent on primary	Sigma-Aldrich	A5278
Goat anti-rabbit (whole molecule) IgG peroxidise conjugate	Dependent on primary	Sigma-Aldrich	A0545
Rabbit anti-goat (whole molecule) IgG peroxidise conjugate	Dependent on primary	Sigma-Aldrich	A5420

2.2 Reagents, buffers and standard solutions used in this research

2.2.1 Solutions used in cell culture

2.2.1.1 Complete cell culture medium

Complete cell culture medium consisted of 500ml Dulbecco's Modified Eagle's Medium (DMEM), 50ml heat inactivated foetal calf serum (FCS) (Sigma-Aldrich Company, LTD Irvine, Ayrshire, UK) and 5ml of an antibiotic cocktail (Sigma-Aldrich Co, Poole, Dorset, UK) comprising penicillin, streptomycin and amphotericin B (Sigma-Aldrich Company, LTD Irvine, Ayrshire, UK). This medium was stored in a freezer at 4°C.

2.2.1.2 Balanced salt solution (BSS)

The ingredients of BSS were 79.5g NaCl, 2.2g KCl, 1.1g Na_2HPO_4, 2.1g KH_2PO_4 and 10 litres of distilled water (dH_2O). When mixing, the pH was maintained at 7.2 by adding 1M NaOH (Sigma-Aldrich, Inc., Poole, Dorset, England, UK). The BSS buffer was then autoclaved and stored at room temperature.

2.2.1.3 0.05M EDTA

As a stock solution, 0.05M EDTA was made containing 40g NaCl, 1g KCl (Fisons Scientific Equipment, Loughborough, UK), 5.72g Na_2HPO_4 (BDH Chemical Ltd., Poole, England, UK), 1g KH_2PO_4 (BDH Chemical Ltd., Poole, England, UK) and 1.4g EDTA (DuchefaBiochemie, Haarlem, The Netherlands) in 5 litres of dH_2O. NaOH was used to adjust the pH value of the solution to 7.4, and the solution was autoclaved before use.

2.2.1.4 Trypsin (25mg/ml)

This solution was prepared by dissolving 500mg trypsin in 20ml 0.05M EDTA. After filtering with a 0.2µm mini-star filter (Sartorious, Epsom, UK), it was stored in a -20°C freezer. When detaching cells, 250µl of trypsin/EDTA solution was dissolved in 10ml of BSS buffer to form a working solution. Any unused working solution was stored in a 4°C freezer.

2.2.1.5 Phosphate-buffered saline (PBS)

One litre of 1× PBS was prepared with 8g NaCl, 0.2g KCl, 1.44g Na_2HPO_4 and 0.24g KH_2PO_4 added to 800ml dH_2O. Additional HCl was used to lower the pH value to 7.4 and augment the total solution volume to 1 litre. After autoclaving, this solution was stored at room temperature.

2.2.1.6 Antibiotics stock solution

This material was prepared by dissolving 5g streptomycin, 3.3g penicillin, and 12.5mg amphotericin B in DMSO into 0.5 litre BSS. Filtered through a 0.2µm mini-star filter in advance, 5ml of the solution was added 500ml DMEM for use.

2.2.2 Solutions used in molecular biology

2.2.2.1 Tris-Boric-Acid (TBE) electrophoresis buffer

The 5 × TBE solution contained 540g Tris-HCl (Melford Laboratories Ltd, Suffolk, UK), 275g Boric acid (Melford Laboratories Ltd, Suffolk, UK), 46.5g EDTA and 10L dH_2O. The pH value was increased to 8.3 by the addition of NaOH. This solution was stored at room temperature. To constitute agarose gel and DNA electrophoreses, 200ml of this solution was diluted with dH_2O at 1:4 ratio, before autoclaving.

2.2.2.2 Diethylpyrocarbonate (DEPC) water

DEPC water was prepared by diluting 500µl of DEPC stock solution (Sigma-Aldrich, Inc., Poole, Dorset, England, UK) with distilled water at 1:19 ratio.

2.2.2.3 DNA electrophoresis loading buffer

This loading buffer was constituted by mixing 10ml H_2O with 25mg bromophenol blue (Sigma-Aldrich, Inc., Poole, Dorset, England, UK) and 4g sucrose (Fisons Scientific Equipment, Loughborough, UK) dissolved in. The prepared buffer was stored at 4°C freezer.

2.2.3 Solutions for Western blot

2.2.3.1 Lysis Buffer

This solution contained 8.76g NaCl, 6.05g Tris, 200mg of 0.02% sodium azide, 5g of 0.5% sodium deoxycholate, 15ml of 1.5% Triton × 100, 1mg Aprotinin (1µg/ml), 1mg Leupeptin (1µg/ml) and l litre dH_2O, and was stored in 4°C freezer.

2.2.3.2 Tris Buffered Saline (TBS)

This TBS solution contained 1 litre H_2O with 0.5M Tris and 1.38M NaCl dissolved in. HCl was used to lower the pH value to 7.4. The prepared TBS was stored at room temperature.

2.2.3.3 10% ammonium persulphate (APS)

This solution was constituted by dissolving 1g APS (Sigma-Aldrich) in 10ml dH_2O, then stored in a 4°C freezer.

2.2.3.4 10 × Running buffer

The ingredients of this solution included 303g Tris, 100g SDS (Melford Laboratories Ltd., Suffolk, UK), 1.44kg Glycine (Melford Laboratories Ltd., Suffolk, UK) and 10 litres of dH_2O. After dissolving all of the solid materials in dH_2O, the pH value was adjusted to 8.4 by adding NaOH. This running buffer was stored at room temperature and diluted with dH_2O at 1:9 ratio before use.

2.2.3.5 Transfer buffer

This buffer was prepared by dissolving 15.15g Tris and 72g glycine in 1 litre of methanol (Fisher Scientific, Leicestershire, UK), then diluted with 4 litres of dH_2O.

2.2.4 MTT solution used in MTT assays

Five milligrams of MTT (methylthiazolyldiphenyl-tetrazolium bromide, Sigma-Aldrich) was dissolved into 1ml of PBS followed by vortexing until completely dissolved. The solution was then filtered using a 0.2μM filtration disc. Once prepared, the MTT solution was stored at 4℃ protected from light.

2.2.5 Solutions used in metabolic assays

2.2.5.1 Glucose Detection Reagent used in Glucose-Glo™ Assay

The product components of Glucose Detection Reagent used in this assay were purchased from Promega and are listed in Table 2.6. The ingredients were Luciferin Detection Solution, Reductase, Reductase Substrate, Glucose Dehydrogenase and NAD. The 10mM Glucose was used for generating positive control.

The preparation of the detection kit was as instructed by the manufacturer. Briefly, all the components, stored in a -80℃ freezer, were thawed to room temperature to form homogeneous solutions. Once thawed, the Luciferin Detection Solution was equilibrated at room temperature, and the other components were added into the Luciferin Detection Solution at the ratio of 1:100, followed by gently inverting 5

times, to constitute Glucose Detection Reagent. The unused components were returned to the -80℃ freezer for storage.

Table 2.6 Glucose Detection Reagent components

Glucose-Glo™ Assay	Size
Luciferin Detection Solution	5ml
Reductase	55µl
Reductase Substrate	55µl
Glucose Dehydrogenase	200µl
NAD	30µl
Glucose (10mM)	50µl

2.2.5.2 Lactate Detection Reagent used in Lactate-Glo™ Assay

The product components of Lactate Detection Reagent (Promega) used in this assay are listed in Table 2.7. The ingredients were Luciferin Detection Solution, Reductase, Reductase Substrate, Lactate Dehydrogenase and NAD (nicotinamide adenine dinucleotide). A solution of 10mM Lactate was used for generating positive control.

When preparing this reagent, all the components were taken out of the -80℃ freezer and thawed at room temperature to form homogeneous solutions. Once thawed, the Luciferin Detection Solution was equilibrated at room temperature and the Lactate Dehydrogenase was dissolved into 275µl of water followed by gently mixing, to form reconstituted Lactate Dehydrogenase. Other components, together with Reconstitute Lactate Dehydrogenase were mixed with Luciferin Detection Solution at the ratio of 1:100, by gently inverting 5 times, to constitute Lactate Detection Reagent. The unused components were returned to the -80℃ freezer for storage.

Table 2.7 Lactate Detection Reagent components

Lactate-Glo™ Assay	Size
Luciferin Detection Solution	5ml
Reductase	55µl
Reductase Substrate	55µl
Lactate Dehydrogenase	1 vial
NAD	30µl
Lactate (10mM)	50µl

2.2.5.3 Glutamate Detection Reagent used in Glutamine/Glutamate-Glo™ Assay

The components of this reagent were supplied by Promega, UK, and included Luciferin Detection Solution, Reductase, Reductase Substrate, Glutamate Dehydrogenase, NAD, Glutaminase, Glutaminase Buffer and Glutamate. Further details are listed in Table 2.8.

When preparing this reagent, the Luciferin Detection Solution was thawed, then equilibrated at room temperature while other components were placed on ice prior to use. Reductase, Reductase Substrate, Glutamate Dehydrogenase, and NAD were added to the Luciferin Detection Solution sequentially at the ratio of 200:200:50:50:1. A homogeneous solution was formed by gently inverting five times, prior to use.

Table 2.8 Glutamate Detection Reagent components

Glutamine/Glutamate-Glo™ Assay	Size
Luciferin Detection Solution	50ml
Reductase	275µl
Reductase Substrate	275µl
Glutamate Dehydrogenase	1ml
NAD	1ml
Glutaminase	125µl
Glutaminase Buffer	25ml
Glutamate (10mM)	50µl

2.2.5.4 NAD(P)H-Glo™ Detection Reagents used in NAD(P)H-Glo™ Detection System

The components of this reagent were purchased from Promega UK, including Reductase, Reductase Substrate, Luciferin Detection Reagent (lyophilized), Reconstitution Buffer. Further details are listed in Table 2.9.

Prior to NAD(P)H-Glo™ Detection Reagent preparation, the Luciferin Detection Reagent was reconstituted by transferring the entire contents of the Reconstitution Buffer to the amber bottle containing lyophilized Luciferin Detection Reagent, after both materials were thawed and equilibrated at room temperature.

When preparing the NAD(P)H-Glo™ Detection Reagent, the thawed Reductase and Reductase Substrate were immediately added into Luciferin Detection Reagent, at the ratio of 200:200:1. After gently inverting five times, a homogeneous solution of this reagent was formed.

Table 2.9 NAD(P)H-Glo™ Detection Reagent components

NAD(P)H-Glo™ Detection System	Size
Reductase	55µl
Reductase Substrate	55µl
Luciferin Detection Reagent (lyophilized)	1 vial
Reconstitution Buffer	10ml

2.2.5.5 CellTiter-Glo® 2.0 Reagent used in CellTiter-Glo® 2.0 Assay

When preparing this ready-to-use reagent, CellTiter-Glo® 2.0 Reagent, supplied by Promega. UK was taken from the -80℃ freezer, then kept at 4℃ overnight. The use of a 22℃-water bath was then required to equilibrate this reagent at room temperature. A homogeneous solution of this reagent was formed by gentle mixing.

2.2.5.6 Reagents used in GSH/GSSG-Glo™ Assay

The reagents used for the GSH/GSSG-Glo™ Assay were Total Glutathione Lysis Reagent, Oxidized Glutathione Lysis Reagent, Luciferin Generation Reagent and Luciferin Detection Reagent. The entire components of this assay are listed in Table 2.10, and the materials for Total Glutathione Lysis Reagent, Oxidized Glutathione Lysis Reagent, and Luciferin Generation Reagent are listed in Table 2.11 to 2.13, respectively. When preparing these three reagents, the necessary components for each reagent, were gently mixed to form homogeneous solutions. As regards the Luciferin Detection Reagent, the entire Reconstitution Buffer with Esterase was transferred to the amber bottle containing lyophilized Luciferin Detection Reagent. Then, the mixture was inverted until the substrate was thoroughly dissolved.

Table 2.10 Entire components of GSH/GSSG-Glo™ Assay

GSH/GSSG-Glo™ Assay	Size
NEM, 25mM	250µl
Passive Lysis Buffer, 5×	5ml
DTT, 100mM	1.25ml
Luciferin Detection Reagent (lyophilized)	1 vial
Reconstitution Buffer with Esterase	50ml
Glutathione Reaction Buffer	50ml
Luciferin-NT	500µl
Glutathione, 5mM	2 X 100µl
Glutathione S-Transferase	3 X 500µl

Table 2.11 Total Glutathione Lysis Reagent components

Components	Volume per Reaction
Luciferin-NT	1.0µl
Passive Lysis Buffer, 5×	10.0µl
Water	39.0µl
Final volume per reaction	50.0µl

Table 2.12 Oxidized Glutathione Lysis Reagent components

Component	Volume per Reaction
Luciferin-NT	1.0µl
NEM, 25mM	0.5µl
Passive Lysis Buffer, 5×	10.0µl
Water	38.5µl
Final volume per reaction	50.0µl

Table 2.13 Luciferin Generation Reagent components

Component	Volume per Reaction
100mM DTT	1.25µl
Glutathione-S-Transferase	3.0µl
Glutathione Reaction Buffer	45.75µl
Final volume per reaction	50.0µl

2.2.5.7 ROS-Glo™ Detection Solution used in ROS-Glo™ H_2O_2 Assay

The components of this reagent were from Promega (UK) and are listed in Table 2.14. When preparing this reagent, reconstituted Luciferin Detection Reagent was produced by transferring the entire contents of thawed Reconstitution Buffer to the amber bottle containing lyophilized Luciferin Detection Reagent. Immediately

before use, 10µl each of d-Cysteine and Signal Enhancer Solution was added to per 1ml of Luciferin, producing the ROS-Glo™ Detection Solution.

Table 2.14 ROS-Glo™ Detection Solution components

ROS-Glo™ H_2O_2 Assay	Size
H_2O_2 Substrate, 10mM	40µl
Signal Enhancer Solution	100µl
d-Cysteine, 100×	100µl
H_2O_2 Substrate Dilution Buffer	2ml
Luciferin Detection Reagent	1 vial
Reconstitution Buffer	10ml

2.3 Cell culture, maintenance and storage

2.3.1 Cell culture

All of the wild type cell lines involved in this research were cultured in complete cell culture medium as illustrated in section 2.2.1.1. The lentivirus-transfected cell lines (MDA -MB-231 and MCF-7) were initially cultured in DMEM with 500µg/ml G418 (Geneticin) for selection, then cultured in DMEM with 100µg/ml G418 for maintenance.

All cell lines were initially cultured in 25cm^2 flasks (Greiner Bio-One Ltd, Gloucestershire, UK), then subcultured to 75cm^2 flasks (Greiner Bio-One Ltd, Gloucestershire, UK) when confluency reached 80%. These flasks were kept in a dedicated incubator (Sanyo, UK) at 37°C, 95% humidification and 5% CO_2 supply.

2.3.2 Cell maintenance

Cell culture medium was changed every 2-3 days. Viability and confluency were checked visually by an inverted phase contrast microscope (Lecia GmbH, Bristol, UK). Confluency was approximately calculated by assessing the area of the flask surface covered by cultured cells. Cell handling was performed inside a Class II laminar flow cabinet (SafeF ST Classic, FASTER) to avoid contamination.

2.3.3 Cell detachment

Cell culture medium was aspirated using a dedicated and sterile glass pipette. The cells were washed by prepared PBS solution to remove the remaining cell culture medium containing serum, which could inactivate the trypsin performance.

One millilitre trypsin solution was applied to cells, then aspirated using a glass pipette after the cell surface was fully covered by the solution. The remaining trypsin was enough to detach the cells so that cell membranes would not be damaged. Further incubation for 5-10 minutes and inspection under a microscope were necessary to ensure complete cell detachment.

Once detached, 5ml complete cell culture medium was applied to neutralise the trypsin and form a cell suspension. This cell suspension was transferred to a 30ml universal (Greiner Bio-One Ltd, Gloucestershire, UK), followed by centrifugation at 1700rpm for 5 minutes.

After centrifugation, the supernatant was aspirated, and the cell pellet was resuspended with fresh complete cell culture medium. This cell suspension was then used immediately for re-culturing or in experimental work.

2.3.4 Cell counting

A Neubauer haemocytometer counting chamber (Mod-Fuchs Rosenthal, Hawksley, UK) was used to perform cell counting. This chamber constituted of 9 squares at 1mm × 1mm × 0.1mm and estimated the number of cells per millilitre.

When counting the cells under a microscope equipped with × 10 objective lens, only 4 squares in the corners were taken into account due to the uniformity of cell distribution and error reduction. The number of cells was calculated using the following equation

$$Num = Sum/4 \times 10^4$$

Where Num, is the cell number per millilitre; Sum, is the total number of cells in the four corners.

2.3.5 Cell freezing

Cell were detached with trypsin according to section 2.3.3, followed by centrifugation at 1700rpm for 5 minutes. The cells were resuspended in complete cell culture medium with 10% dimethyl sulfoxide (DMSO).

One millilitre pre-labelled CRYO.STM tubes (Greiner Bio-One, Germany) were used to harbour 1ml cell suspension. The cryotubes were first stored at -80℃, then transferred to a liquid nitrogen tank for long term storage.

2.3.6 Cell resuscitation

The stored CRYO.STM tube was taken out of the -80 ℃ freezer or liquid nitrogen tank, then thawed in a 37℃-water bath. The cell suspension was transferred to a 30ml universal containing 5ml prewarmed complete cell culture medium. After centrifugation at 1700rpm for 5 minutes, the supernatant was aspirated, and the cell pellet was resuspended in 5ml medium. This cell suspension was transferred to 25cm^2 flasks (Greiner Bio-One Ltd, Gloucestershire, UK) and stored in an incubator.

2.4 RNA detection

2.4.1 RNA isolation

Prior to RNA isolation, culture medium from the respective cells was aspirated and 1ml Tri Reagent kit (Sigma-Aldrich, Inc., Poole, Dorset, England, UK) was added to the cells to produce cell lysis. The cell lysate was transferred to a sterile 1.5ml microfuge and thoroughly mixed with 0.2ml chloroform (Sigma-Aldrich, Inc., Poole, Dorset, England, UK). After a 5-minute-incubation at room temperature, this homogenate was centrifuged at 12000rpm for 15 minutes. The top aqueous fraction containing RNA was then transferred to another sterile microfuge with 0.5ml pre-aliquoted 2-propanol (Sigma-Aldrich, Inc., Poole, Dorset, England, UK). This sample was shaken for 10 seconds and incubated on ice for 15mins, followed by centrifugation at 12000rpm for 10 minutes to allow the RNA to form a pellet on the bottom. After the supernatant was aspirated, the RNA pellet was washed twice using 1ml of 75% ethanol by vortex and centrifugation at 7500rpm for 5 minutes. The remaining ethanol was entirely removed by drying the RNA pellet at 55℃ for

5-10minutes. Once dried, the RNA pellet was resuspended in DEPC water to produce an RNA solution for quantification.

2.4.2 RNA quantification

The isolated RNA was quantified using a UV 1101 Biotech spectrophotometer (WPA, Cambridge, UK). After quantification, the RNA sample was diluted with TBE buffer to the desired concentration. This solution was stored in a -80℃ freezer or immediately used for further experiments.

2.4.3 Reverse transcription reaction

The RT reaction was conducted using an RT kit purchased from Promega. The quantified RNA was diluted with nuclease-free water in a 200µl PCR tube (ABgene) until a solution of 9µl at the concentration of 500ng/µl was constituted. 1µl of Oligo dT primer (Promega) and 10µl of RT mix were added to this solution sequentially. Reverse transcription reaction was carried out in an ABI2720 thermocycler (Applied Biosystems, Loughborough, Leicestershire, England, UK) which sequentially heated the sample at 65℃ for 5 minutes, 42℃ for 20 minutes and 75℃ for 10 minutes.

2.4.4 Polymerase chain reaction (PCR)

After the reverse transcription reaction, the cDNA template was formed and diluted with DEPC water at 1:4 ratio. PCR was performed in a 200µl PCR tube (ABgene, Surrey UK) and the PCR sample components are listed in Table 2.15.

Table 2.15 PCR components and volume

Components	**Volume per reaction/µl**
2 × GoTaq Green Master Mix	8.0
Forward primer (1µM)	1.0
Reverse primer (1µM)	1.0
Nuclease-free water	4.0
cDNA template	2.0
In total	**16.0**

The reaction was performed by mixing all the components followed by centrifugation. A negative control was required in case of any contamination in the PCR sample, which contained the same components as set out in Table 2.16 but with the cDNA template replaced by nuclease-free water. The prepared PCR tube was placed in an ABI2720 Thermo Cycler (Applied Biosystems) and PCR was run under the following procedure detailed in Table 2.16:

Table 2.16 PCR procedure and conditions

Procedure	Temperature	Time	Cycles
Initialisation	94℃	5mins	1
Denaturation	94℃	20secs	
Annealing	55℃	20 secs	32
Extension	72℃	30secs	
Final extension	72℃	10mins	1
Final hold	4℃	∞	1

2.4.5 Agarose gel electrophoresis and DNA visualization

Agarose gels with agarose ranging from 0.8% - 2%, depending on the size of the PCR products, was produced by mixing the required amount of agarose in 100ml TBE buffer before completely dissolving under microwave heating. The agarose solution, after cooling, was poured into a DNA resolution cassette, preassembled with a suitable gel comb. This was allowed to cool and set. The cassette was placed into a gel electrophoresis tank (Life Technologies Ltd, Paisley, UK), the electrophoresis cassettes were immersed in 1 × TBE buffer, and the gel comb was subsequently removed. SYBR®Safe DNA gel stain (Scie-Plas Ltd, Cambridge, UK) was then added to the solution.

Once the agarose gel was generated, an 8µl DNA ladder (GenScript®, Piscataway, USA) was added to the first well and DNA samples were added to the following wells. The electrophoresis was performed using a dedicated power supply (Gibco BRL, Life Technologies Inc.) set at 120V, 100mA and 50Watts for approximately 30-50 minutes. Gels were visualised and saved automatically by Syngene U: Genius3 fluorescence UV transilluminator (Synoptics Ltd, Cambridge, UK).

2.4.6 Real Time Quantitative RT-PCR (Q-PCR)

The Real-time quantitative PCR was set up as listed in Table 2.17:

Table 2.17 The components of Q-PCR and their volume

Component	Volume
2x iQ™ Supermix	5µl
Forward primer (10pmol/µl)	0.3µl
Reverse primer (1pmol/µl)	0.3µl
Amplifluor™ probe (10pmol/µl)	0.3µl
cDNA	1µL
PCR H_2O	3µl
Total volume per reaction	10µl

After the qPCR samples were added, the qPCR plate was covered with MicroAmp® Optical Adhesive film (ThermoFisher Scientific, Life Technologies Ltd, Paisley, UK). The PDPL (podoplanin) gene was run as a reference control gene with a known transcript number to generate a standard curve. After centrifugation, the 96-well plate was placed in a StepOne Plus™ Thermal Cycler (Applied Biosystems), and the reaction temperature was set up as listed in Table 2.18.

Table 2.18 The reaction temperature of Q-PCR for each step

Step	Temperature	Time (minutes:seconds)	Number of cycles
Initial denaturation	94°C	05:00	50-70 cycles
Denaturation	94°C	00:10	
Annealing	55°C	00:35	
Extension	72°C	00:20	

The instrument was programmed to capture the fluorescence signal at the annealing step. The transcript copy number of each sample was normalised against the detection of β-actin or GAPDH copy numbers, and at least three repeats for each sample was carried out.

2.5 Protein detection

2.5.1 Protein extraction and cell lysate preparation

When cells reached the required confluence in the culture flasks, the medium was removed, and the cells were twice washed with PBS buffer and then were scraped with a cell scraper in 5ml PBS. The cell solution was centrifuged in a universal tube at 1700 rpm for 10 minutes., to obtain a cell pellet. The cell pellet was then resuspended in 200-300µl (depending on pellet size) protein lysis buffer and the cell suspension was transferred to a 1.5ml microfuge tube. The sample was then placed on a spinner programmed at 20rpm and kept at 4℃ for 1 hour. After centrifugation at 13,000 rpm for 15 minutes the supernatant containing proteins was removed and transferred to a new microfuge tube. The protein sample was used for quantification for Western Blot or stored at -20℃ until future use.

2.5.2 Protein quantification

In order to standardise the concentration of protein samples for running Western Blotting, the protein samples were quantified using the Bio-Rad DC Protein Assay kit (Bio-Rad Laboratories, Hemel-Hempstead, UK). The kit contains alkaline copper tartrate solution (Reagent A) and Folin reagent (Reagent B) for the determination of protein concentration underlying this colorimetric assay. Bovine serum albumin (BSA) was used as a standard control with known concentration. In this reaction, the protein with copper in the alkaline medium lead to the subsequent reduction of the Folin reagent and the production of a characteristic blue colour. The reaction products were read under absorbance between 405-750nm).

In a 96 well plate, a standard curve was established by diluting 50mg/ml BSA standard (Sigma-Aldrich, Poole, Dorset, UK) with lysis buffer from 50 mg/ml to 0.78mg/ml to determine the concentration of target proteins.

The quantification procedure was carried out according to manufacturer's instructions. Briefly, 5µl of either protein samples or standards were added in each well on a 96-well plate, and 25µl of Reagent A (prepared by adding 20µl of reagent S to every 1ml of reagent A) and 200µl of Reagent B were added into each well.

After the sample was mixed, the plate was left at room temperature on the shaker for 30 minutes for the colorimetric reaction to occur. The absorbance was measured at a wavelength of 630nm using the EL×800 plate reading spectrophotometer (Bio-Tek, Wolf Laboratories, York, UK).

After reading the plate, the standard curve was set up and the protein concentration of the samples was determined using the standard curve. Appropriate amounts of lysis buffer were used to standardise the protein samples to the same concentration based on the protein samples with lowest protein concentrations. These samples were finally diluted with 2 × Laemmli sample buffer (Sigma-Aldrich, Poole, Dorset, UK) and then denatured by boiling at 100℃ for 10 minutes. The boiled samples were either used immediately for Western Blot or stored at -20℃ until future use.

2.5.3 Western Blot

2.5.3.1 Sodium Dodecyl Sulphate Polyacrylamide Gel Electrophoresis (SDS-PAGE)

The system used in this study was a Bio-Rad Western Blot system. The resolving gel was added after the setup of two glass plates on a casting stand. The percentage of resolving gel was prepared according to the molecular weight of target proteins. A mixture of 15ml was prepared by adding all the reagents listed in Table 2.19 and Table 2.20.

Table 2.19 The components of 8% resolving gel

8% Resolving gel (protein size over 100 kD)	
Distilled water	6.9ml
30% acrylamide mix (Sigma-Aldrich, Poole, Dorset, UK)	4.0ml
1.5 M Tris (pH8.8)	3.8ml
10% SDS	0.15ml
10% Ammonium persulphate	0.15ml
TEMED (Sigma-Aldrich, Poole, Dorset, UK)	9.0µl

Table 2.20 The components of 10% Resolving gel

10% Resolving gel (protein size less than 100 kD)	
Distilled water	5.9ml
30% acrylamide mix (Sigma-Aldrich, Poole, Dorset, UK)	5.0ml
1.5 M Tris (pH8.8)	3.8ml
10% SDS	0.15ml
10% Ammonium persulphate	0.15ml
TEMED (Sigma-Aldrich, Poole, Dorset, UK)	6.0µl

7µl resolving gel mix was added into the space between two glass plates, and methanol was then added to cover the gel to prevent gel oxidation. After the gel had completely set, the methanol overlay was removed and the stacking gel was prepared as listed in Table 2.21 and added on the top of resolving gel, meanwhile, a comb was inserted immediately after adding the stacking gel, and the gel was left to set at room temperature for around 20 minutes.

Table 2.21 The components of stacking gel

Component	Stacking gel
Distilled water	3.4ml
30% acrylamide mix (Sigma-Aldrich, Poole, Dorset, UK)	0.83ml
1.0M Tris (PH 6.8)	0.63ml
10% SDS	0.05ml
10% Ammonium persulphate	0.05ml
TEMED (Sigma-Aldrich, Poole, Dorset, UK)	0.005ml

After the stacking gel had set, the running cassette was set up and covered with 1 × running buffer. The comb was removed and 10µl of Broad range marker (Santa Cruz Biotechnology, UK) was loaded into the first well of the gel. In the subsequent wells, target protein samples were loaded. These experimental sample sets, corrected to the same protein concentration, were loaded onto the same gel, with replicates separated by spare wells, to allow multiple probing of different proteins under the same condition. The proteins were run and separated at 100-120V, 50mA, and 50W for a period up to 2-3 hours until the target protein was separated properly.

2.5.3.2 Transferring proteins from gel to PVDF membrane

After SDS-PAGE electrophoresis, the gel cassettes were disassembled and the gels were taken out from between the glass plates, and the stacking gel was cut off. The filter paper (Whatman International Ltd., Maidstone, UK) was soaked in transfer buffer and the PVDF membrane was activated in methanol before use. The sandwich was made of two squares of filter paper, PVDF membrane, resolving gel, and two further filter paper squares (Figure 2.1). Electroblotting was then conducted at 15V, 500mA, and 8W for 40-60 minutes using an SD20 SemiDry Maxi System blotting unit (SemiDRY, Wolf Laboratories, York, UK) according to the protein size. On completion, the PVDF membrane was carefully removed and briefly rinsed in TBS buffer, before soaked in a Ponsea S solution, to stain the protein on the membrane. The membrane was then carefully cut into stripes at the spare well with a scalpel. Each stripe was labelled with the protein to be probed, one of which was the house keeping protein, β-actin or GAPDH.

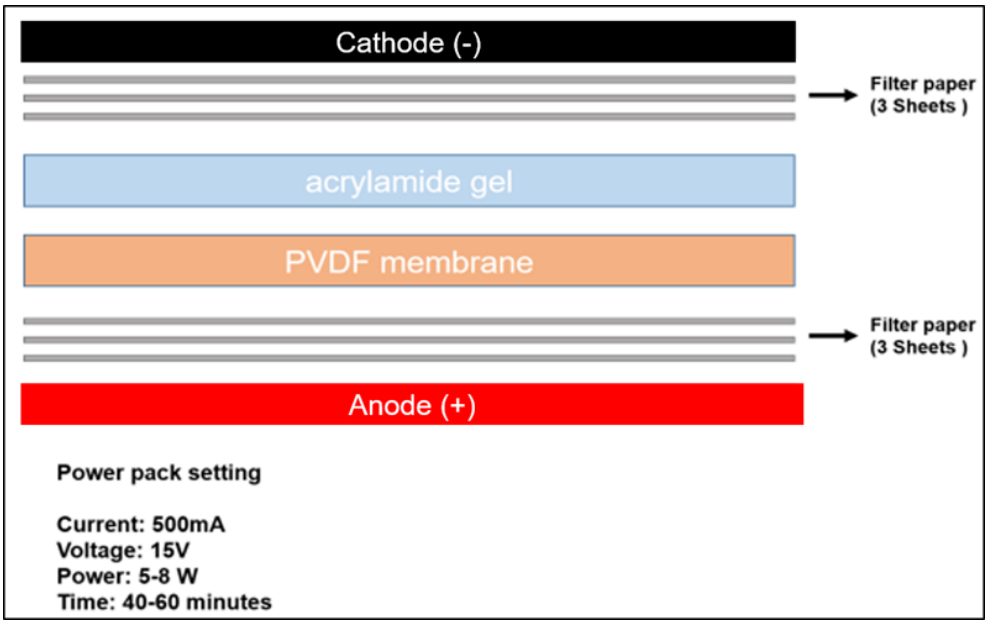

Figure 2.1 Diagram depicting the process of Western Blotting; the transferring of proteins onto a PVDF membrane.

In order to reduce the background, the membrane was blocked with 10% milk solution (10% skimmed milk powder and 0.1% polyoxyethylene (20) sorbitan monolaurate (Tween 20) in TBS for at least one hour at room temperature once the proteins had been transferred sufficiently.

2.5.4 Protein detection using specific immuno-probing

When blocking was completed, the membrane was transferred into an incubation tray with the membrane surface upwards. The membrane was incubated overnight with primary antibody at a predetermined suitable dilution in 5% milk at 4°C. The membrane was washed with TBST (TBS with 0.2% Tween 20) three times the next day to remove the remaining unbound antibodies. The membrane was subsequently incubated with relevant secondary antibody (1:1000) in 3% milk for one hour at room temperature and the membrane was then washed three times (10 mins each) with 5ml TBST before undertaking chemiluminescent detection. The house keeping protein, namely β-actin or GAPDH, was probed in each and every experiment, to allow normalisation of the respective protein sets.

2.5.5 Chemiluminescent protein detection

Chemiluminescent protein detection was conducted using the Luminate Forta Western HRP substrate (Cat. No. WBLUF0500, Merck-Millipore, Hertfordshire, UK), which consists of a highly sensitive chemiluminescent substrate and is used to detect the HRP for visualising the probed protein bands. The reagent was added to cover the surface of the membrane and excess solution on the membrane was removed. The chemiluminescent signal was detected using a G:Boxtm Imager (Syngene, Cambridge, UK) which contains an illuminator and a camera linked to a computer. The exposure time for the membrane was adjusted until the protein bands were visible and the image was captured and analysed using ImageJ for the purpose of band quantification.

2.6 Kidins220 knockdown using lentivirus shRNA

RNA interference (RNAi) is a widely used method to regulate specific gene expression. It has also been considered as a possible approach in targeting specific genes as a therapeutic tool by controlling gene expressions that are linked to certain

conditions including cancer. In the current study, the constructed shRNA was delivered based on lentivirus vector with a Kidins220 shRNA (GGCCTGCAAGATCCAATTATA) construct with three selective markers including a green fluorescent protein (GFP) and resistance genes to ampicillin for prokaryotes and Neomycin/G418 for mammalian cells (Figure 2.2). The lentivirus vector is able to deliver genetic materials into cells and can integrate shRNAs into cells, resulting in long term expression of the transgene, which in turn targets the specific gene(s).

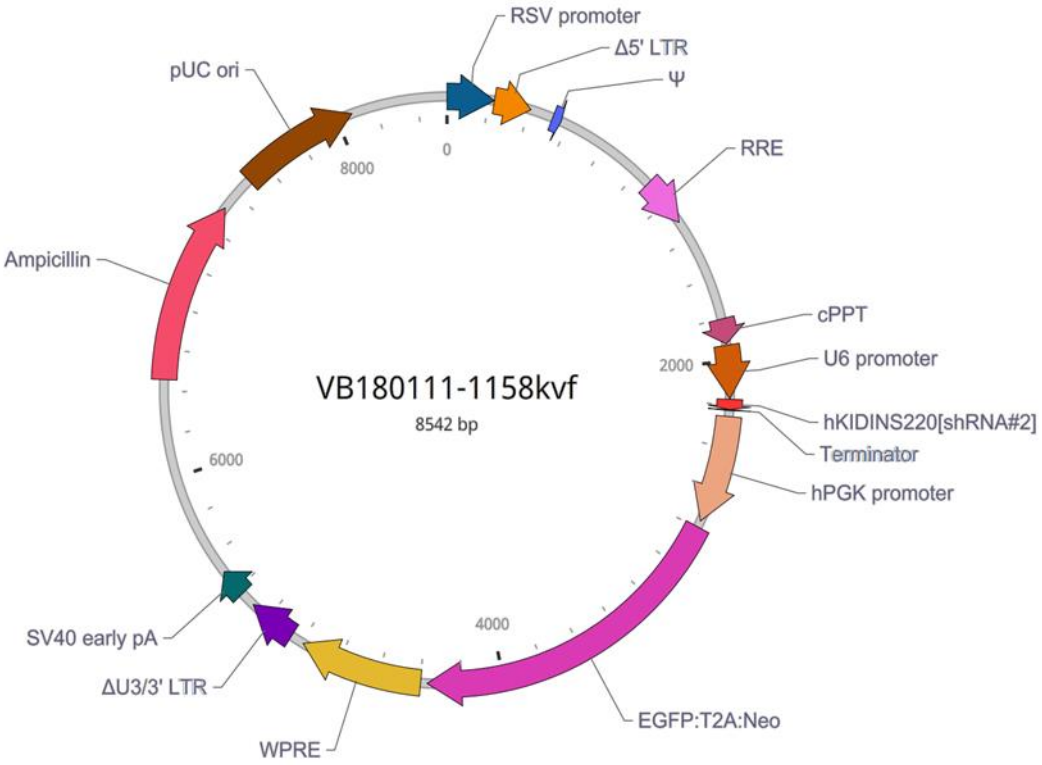

Figure 2.2 Schematic presentation of the pLV lentivirus plasmid. The lentivirus plasmid containing shRNA was generated using the online vector designing tool. (https://www.Vectorbuilder.com).

2.6.1 Plasmid amplification and purification

A stock of *Escherichia coli (E.coli),* which was transformed by Kidins220 shRNA plasmid, was thawed and a portion of the stock was added to 10ml LB medium containing 100µg/ml ampicillin in a Falcon tube. The tube was incubated at 37°C

overnight with constant agitation on a Stuart orbital shaker (Cole-Parmer Scientific, St Neots, England, UK). The *E. coli* stock was centrifuged at 4°C for 15 minutes at 6,000rpm in order to obtain a stock pellet for subsequent plasmid extraction.

The plasmid extraction was conducted using the Sigma GenElute Plasmid MiniPrep kit (Sigma-Aldrich, Poole, Dorset, UK) according to the protocol supplied by the manufacturer. Briefly, the *E. Coli* pellet was resuspended in 200µl of resuspension solution and the mix was then transferred into 2ml collection tubes. An additional 200µl lysis solution was added and gently mixed by inverting the tubes 5-6 times, and this was allowed to stand at room temperature for 5 minutes before adding 350µl of neutralisation buffer. The tube was subsequently inverted several times, and centrifuged at 12,000rpm (4°C) for 10 minutes.

The supernatant was carefully removed, without disturbing the protein layer on the bottom and then transferred into the upper chamber of a fresh collection tube. The upper chamber is separated by a Mini Spin resin column from the bottom chamber. This was centrifuged at 12,000rpm for 1 minute.

The flow through in the bottom chamber was discarded and the column was washed three times with 700µl of wash solution (containing 70% ethanol) and centrifuged at 12,000rpm for 1 minute. The flow through was discarded once more before the column was dried by further centrifugation for one minute.

The column was then transferred into a fresh collection tube for elution. This was carried out by adding 100µl of elution solution and centrifugation at 12,000rpm for 1 minute. The resulting flow through containing the purified plasmid was collected.

2.6.2 Production of lentivirus particles

A human kidney epithelial cell line, expressing a mutant SV40 large T antigen used for virus packaging, was seeded in a 6cm^2 tissue culture plate. The cells were grown until they reached 50-80% confluency and ready for plasmid transfection. The transfection reagent (Insight Biotechnology, UK) was mixed and added to polypropylene microfuge tubes and 20µl serum-free OPTI-MEM as listed in Table 2.22.

Table 2.22 The components of the transfection reagent

1μg	pLV shRNA plasmid
750ng	psPAX2 packing plasmid
250ng	pMD2.G envelope plasmid

The transfection mixture was added into HEK-293T cells and the cells were incubated at 37℃, 5% CO_2 for 12-15 hours. The medium, which contained packaged lentivirus particles, was collected and stored in Falcon tubes in the fridge, and the cells were replenished with fresh medium for another 24 hours. The medium was harvested from cells the next day and pooled together with the previously collected medium. The viral containing medium thus harvested from the HEK-293T cells was centrifuged at 1,250 rpm for 5 minutes, in order to remove any cell debris and residual HEK-293T cells. The lentiviral particles were stored at -80℃ for future use.

2.6.3 Infecting target cells

Targeted breast cancer cells were seeded in 24-well plates and grown at 37℃ and 5% CO_2 overnight. When cells were approximately 70% confluent, 8μg/ml polybrene was added to the medium to increase the transfection efficiency. Following this 100μl Lentiviral particles was added to the target plate and the cells were incubated at 37℃ and 5% CO_2 overnight.

2.6.4 Establishment of stable expression in mammalian cell lines

In order to obtain a stable cell line, cells were selected with G418 following infection. The pLV vector containing a resistance gene against G418 was used for the selection in mammalian cells. The cells were cultured in selection medium containing 500μg/ml G418 for 1-2 weeks. During this period, cells that failed to pick up the plasmid from the lentivirus were killed by G418. Only the infected cells that contained the plasmid would survive. The cells were subsequently cultured in maintenance medium containing 100μg/ml G418. The knockdown of Kidins220 was verified using RT-PCR and Western Blotting at both gene and protein levels. Once the cells had been verified, the cells were subject to use in *in vitro* function assays to investigate any changes in the biological functions of the cells due to altering expression of the target gene.

2.7 MTT assay

The cell viability was evaluated using an MTT assay. After the PEFE treatments, 20µl 5mg/ml MTT was added into each well in a 96-well plate. The cells were subsequently incubated at 37°C for 4 hours. After incubation, the medium was removed and 100µl DMSO was added to resolve the MTT. The plate was wrapped with foil and shaken for 15min, to allow crystals formed within the cells to dissolve. The absorbance was then read at 560nm wavelength using GloMax®-Multi Detection System (Promega, UK).

2.8 Metabolic assays

2.8.1 Glucose-Glo™ Assay

This bioluminescent assay can achieve rapid, selective and sensitive detection of glucose in biological samples. The assay couples glucose oxidation and NADH (nicotinamide adenine dinucleotide (NAD)+hydrogen (H)) production with a bioluminescent NADH detection system, illustrated in Figure 2.3. Glucose dehydrogenase uses glucose and NAD+ to produce NADH. In the presence of NADH a pro-luciferin Reductase Substrate is converted by Reductase to luciferin that is then used by Ultra-Glo™ Recombinant Luciferase to produce light. When Glucose Detection Reagent, containing glucose dehydrogenase, NAD+, Reductase, Reductase Substrate and Luciferase, is added to a sample containing glucose at a 1:1 ratio, the enzyme-coupled reactions start and run simultaneously. The luminescent signal is proportional to the amount of glucose in the sample.

Cancer cells were seeded at the number of 5×10^4 per well and placed in designated wells in a 96-well plate. After incubation overnight, PEFE treatments were performed at designated times. Two microlitres of cell culture medium from each well was transferred to the spare wells in the same plate and diluted with 98µl of PBS buffer. The prepared samples were further diluted 2-fold in PBS buffer, after which 50µl of the diluted samples were transferred to another 96 well plate containing 50µl of Glucose Detection Reagent (refer to section 2.2.5.1) in each well. After mixing thoroughly, the plate was incubated at room temperature for 60

minutes. The glucose in the samples was quantified by luminescence recording using GloMax®-Multi Detection System (Promega, UK).

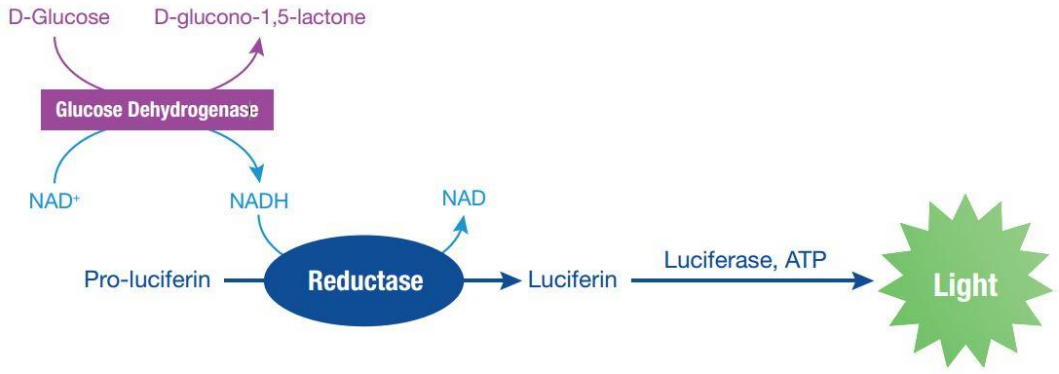

Figure 2.3 Schematic diagram of the Glucose-Glo™ Assay principle. Source: Promega UK Available: https://www.promega.co.uk/-/media/files/resources/protocols/technical-manuals/101/glucose-glo-assay.pdf?la=en

2.8.2 Lactate-Glo™ Assay

This bioluminescent assay can achieve rapid, selective and sensitive detection of L-Lactate in biological samples. Lactate is produced by glycolysis, a major metabolic pathway responsible for glucose homeostasis and energy production. This assay couples lactate oxidation and NADH production with a bioluminescent NADH detection system, illustrated in Figure 2.4. Lactate dehydrogenase uses lactate and NAD+ to produce pyruvate and NADH. In the presence of NADH a pro-luciferin Reductase Substrate is converted by Reductase to luciferin, which is then used in a luciferase reaction to produce light. When Lactate Detection Reagent, containing lactate dehydrogenase, NAD+, Reductase, Reductase Substrate and Luciferase, is added to a sample containing lactate at a 1:1 ratio, the enzyme-coupled reactions start and run simultaneously. The luminescent signal is proportional to the amount of lactate in the sample.

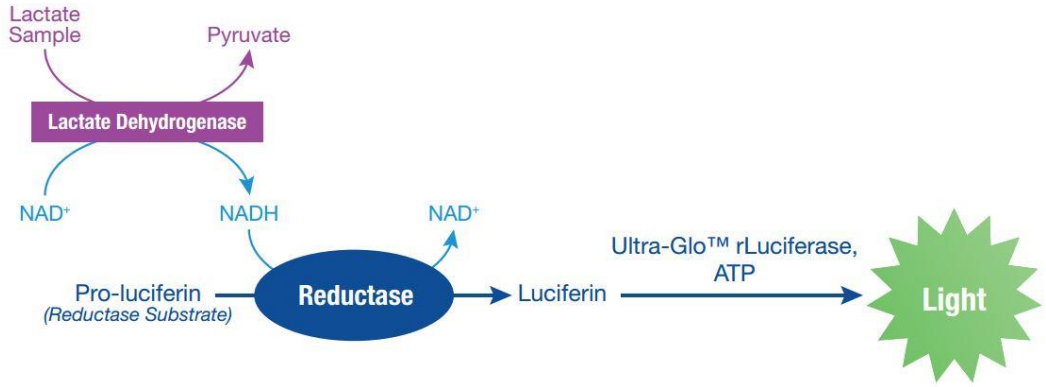

Figure 2.4 Schematic diagram of the Lactate-Glo™ Assay principle. Source: Promega UK Available: https://www.promega.co.uk/-/media/files/resources/protocols/technical-manuals/101/lactate-glo-assay-protocol.pdf?la=en

The cancer cells were seeded at the number of 5×10^4 per well and placed in designated wells in a 96-well plate. After incubation overnight, PEFE treatments were performed at designated times. Two microlitres of cell culture medium from each well was transferred to the spare wells in the same plate and diluted with 98µl of PBS buffer. Fifty microlitres of the prepared samples were transferred to another 96 well plate containing 50µl of Lactate Detection Reagent (refer to section 2.2.5.2) at each well. After mixing thoroughly, the plate was incubated in room temperature for 60 minutes. The lactate in the samples was quantified by luminescence recording using GloMax®-Multi Detection System (Promega, UK).

2.8.3 Glutamine/Glutamate-Glo™ Assay

This bioluminescent assay can achieve rapid, selective and sensitive detection of glutamine and glutamate in biological samples. The assay is based on the conversion of glutamine to glutamate by Glutaminase enzyme. Next, glutamate oxidation and NADH production are coupled with a bioluminescent NADH detection system, illustrated in Figure 2.5. Glutamate dehydrogenase uses glutamate and NAD+ to produce α-ketoglutarate and NADH. In the presence of NADH, a pro-luciferin Reductase Substrate is converted by Reductase to luciferin that is then used by Ultra-Glo™ Recombinant Luciferase to produce light.

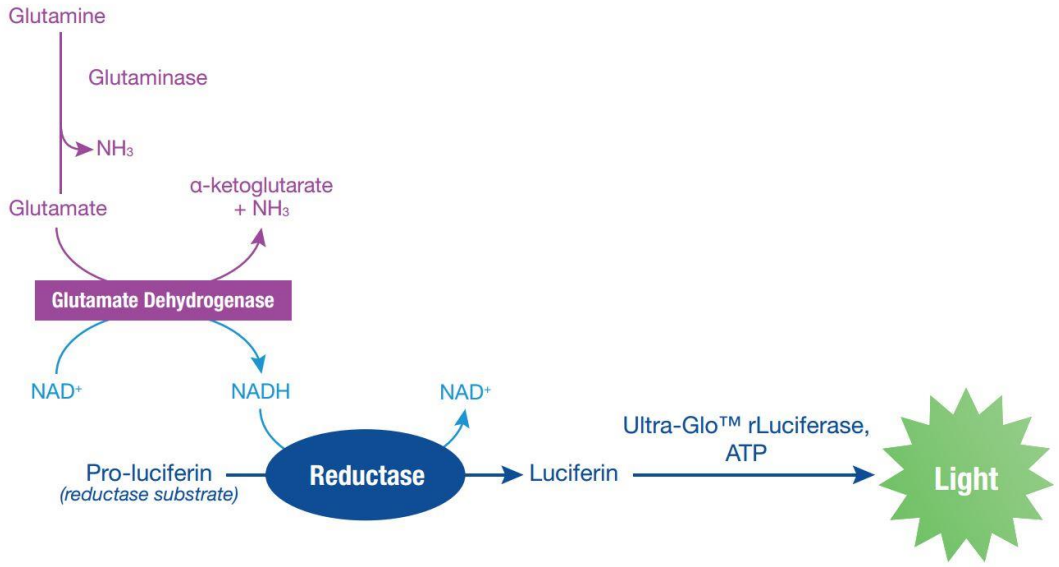

Figure 2.5 Schematic diagram of the Glutamine/Glutamate-Glo™ Assay principle. Source: Promega UK Available: https://www.promega.co.uk/-/media/files/resources/protocols/technical-manuals/101/glutamine-glutamate-glo-protocol.pdf?la=en

This assay uses two steps: 1) glutamine conversion to glutamate by Glutaminase; and 2) glutamate detection with the Glutamate Detection Reagent. When Glutamate Detection Reagent, containing glutamate dehydrogenase, NAD+, Reductase, Reductase Substrate and Luciferase is added to a sample containing glutamate at a 1:1 ratio, the enzyme-coupled reactions start and run simultaneously. The luminescent signal is proportional to the amount of glutamate.

When using this assay, both glutamine and glutamate will be measured. For samples that contain both glutamate and glutamine, the light signal will be proportional to the starting concentration of total glutamine plus glutamate. Therefore, a second reaction without the Glutaminase enzyme is needed to measure the glutamate-only concentration. Measurement of total glutamine plus glutamate, and glutamate-only are performed in separate wells simultaneously. Glutamine levels are calculated by subtracting the glutamate-only signal from the total glutamine plus glutamate signal. The assay can also be used to measure only glutamate from a sample by omitting the Glutaminase step.

MDA-MB-231 cells were seeded at a concentration of1x 10^4 per well and allowed enough time to attach. PEFE treatments were performed at designated time points. Two microlitres of cell culture medium from each well was transferred to a spare well in the same 96-well plate and diluted with 98µl of PBS buffer. Two 25µl aliquots from each prepared sample were transferred into two wells in another 96-well plate. These two wells were used to decide total glutamine plus glutamate and glutamate only, respectively. In the first set of wells 25µl of Glutaminase in Glutaminase Buffer was dispensed, while 25µl of Glutaminase Buffer was added to the second set of wells. The samples were mixed thoroughly then incubated at room temperature for 30-40 minutes, following which 50µl of Glutamate Detection Reagent (refer to section 2.2.5.3) was dispensed to each well and mixed thoroughly. After 60-minute incubation at room temperature, total glutamine plus glutamate and glutamate only were respectively quantified by luminescence using GloMax®-Multi Detection System (Promega, UK).

2.8.4 Griess Reagent System

Nitric oxide (NO) is an important physiological messenger and effector molecule in many biological systems, including immunological, neuronal and cardiovascular tissues. One means to investigate nitric oxide formation is to measure nitrite (NO_2^-), which is one of two primary, stable and non-volatile breakdown products of NO. The Griess Reagent System is based on the chemical reaction shown in Figure 2.6, which uses sulfanilamide and N-1-napthylethylenediamine dihydrochloride (NED) under acidic (phosphoric acid) conditions. This system detects NO_2^- in a variety of biological and experimental liquid matrices such as plasma, serum, urine and tissue culture medium.

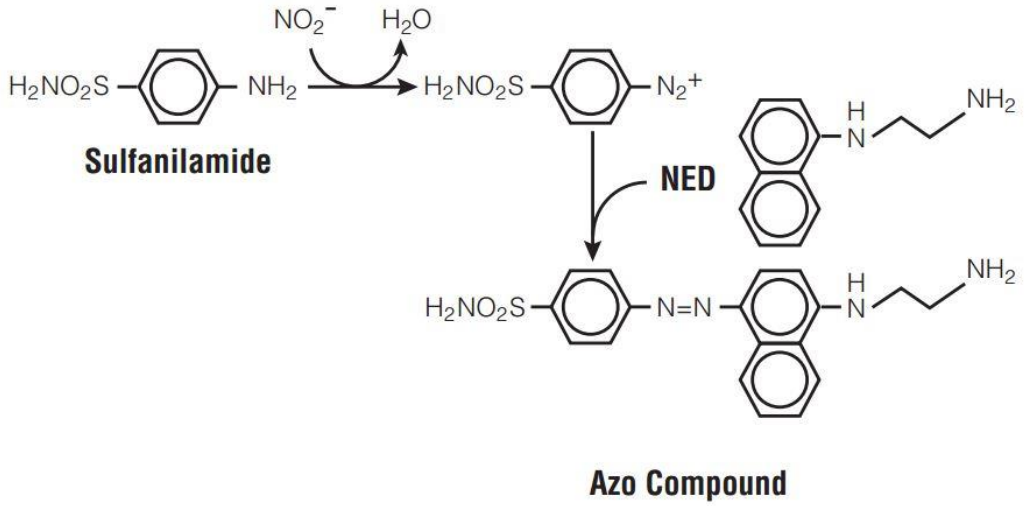

Figure 2.6 Chemical reactions involved in the measurement of NO_2^- using the Griess Reagent System. Source: Promega UK Available: https://www.promega.co.uk/-/media/files/resources/protocols/technical-bulletins/0/griess-reagent-system-protocol.pdf?la=en

MDA-MB-231 cells were seeded at 5×10^4 per well for both experimental samples and control samples and placed in specified wells in a 96-well plate with triple replicates. PEFE treatments started after overnight incubation. Before Nitrite level measurements, 50µl of Sulfanilamide Solution was dispensed to all of the wells including those used for the Nitrite standard curve, followed by incubation at room temperature for 5-10 minutes, protected from light. Then, 50µl of NED Solution was dispensed to all wells and these wells were incubated in room temperature for another 5-10 minutes, protected from light. The Nitrite levels were quantified by absorbance measurements performed by GloMax®-Multi Detection System (Promega, UK) using 560nm filter.

2.8.5 NAD(P)H-Glo™ Detection System

This homogeneous bioluminescent assay can generate a light signal from biochemical reactions that contain reduced nicotinamide adenine dinucleotide (NADH) or nicotinamide adenine dinucleotide phosphate (NADPH). This assay quantitatively monitors the concentration of the reduced forms, NADH and NADPH, and does not discriminate between them. NADH and NADPH are

collectively referred to as NAD(P)H throughout this assay. The oxidized forms, NAD+ and NADP+, are not detected and do not interfere with quantitation.

In the presence of NAD(P)H, the enzyme Reductase reduces a proluciferin reductase substrate to form luciferin. Luciferin is then quantified using Ultra-Glo™ Recombinant Luciferase (rLuciferase), and the light signal produced is proportional to the amount of NAD(P)H in the sample, illustrated in Figure 2.7. Both reactions occur with the addition of a single reagent. The reductase and luciferase reactions are initiated by adding an equal volume of NAD(P)H-Glo™ Detection Reagent, which contains Reductase, Reductase Substrate and Ultra-Glo™ rLuciferase, to a NAD(P)H-containing sample. Luminescence is proportional to NAD(P)H concentrations and is specific for the reduced forms.

The cancer cells were seeded at 5×10^4 per well for both experimental samples and control samples and placed in specified wells in a 96-well plate. PEFE treatments started after overnight incubation. Once all the PEFE treatments were done, 50µl of NAD(P)H-Glo™ Detection Reagent (refer to section 2.2.5.4) was dispensed to each well, followed by shaking gently. After incubation at room temperature for 40-60 minutes, luminescence was recorded using GloMax®-Multi Detection System (Promega, UK).

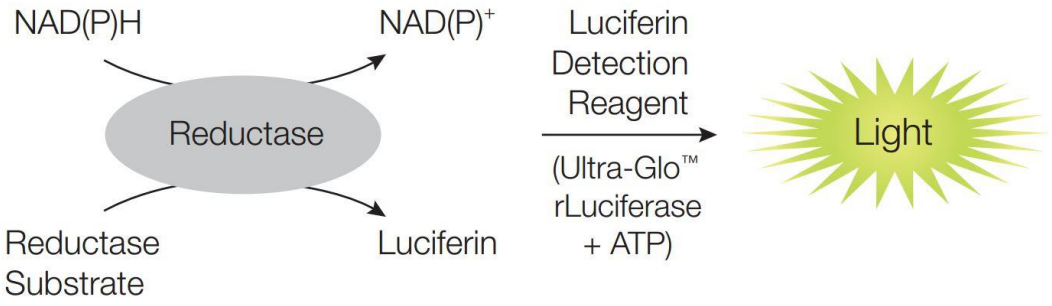

Figure 2.7 Schematic diagram of the NAD(P)H-Glo™ Detection System technology. Source: Promega UK Available: https://www.promega.co.uk/-/media/files/resources/protocols/technical-manuals/101/nadph-glo-detection-system-protocol.pdf?la=en

2.8.6 CellTiter-Glo® 2.0 Assay

This assay provides a homogeneous method to determine the number of viable cells in culture by quantitating the amount of ATP present, which indicates the presence of metabolically active cells. The luciferase reaction for this assay is shown in Figure 2.8. The 'add-mix-measure' format results in cell lysis and generation of a luminescent signal that is proportional to the amount of ATP present. The amount of ATP is directly proportional to the number of cells present in culture. This assay relies on the properties of a proprietary thermostable luciferase (Ultra-Glo™ Recombinant Luciferase), which generates a stable "glow-type" luminescent signal and improves performance across a wide range of assay conditions.

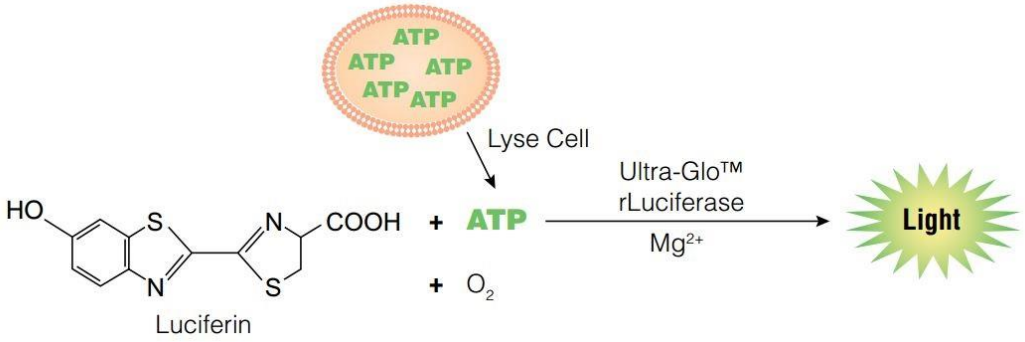

Figure 2.8 Overview of CellTiter-Glo® 2.0 Assay principle. Source: Promega UK Available: https://www.promega.co.uk/-/media/files/resources/protocols/technical-manuals/101/celltiterglo-2-0-assay-protocol.pdf?la=en

The cancer cells were seeded at 8×10^4 per well and placed in specified wells in a 96-well plate. After incubation overnight, PEFE treatments were performed and the plate was equilibrated to room temperature for approximately 30 minutes following which 100µl of CellTiter-Glo 2.0 Reagent (refer to section 2.2.5.5) was dispensed to each well and mixed for 2 minutes on an orbital shaker to induce cells lysis. Once complete, a 10-minute incubation of the plate at room temperature was required for luminescent signal stabilization. The amount of ATP in the samples was then quantified by luminescence measurements using GloMax®-Multi Detection System (Promega, UK).

2.8.7 GSH/GSSG-Glo™ Assay

Most of the glutathione exists in reduced form (GSH) in which the sulfhydryl group of the cysteine is not linked in a disulfide linkage to a second glutathione. Oxidized glutathione (GSSG) is an indicator of cell health and oxidative stress. Certain chemicals react with GSH to form adducts or to increase the GSSG levels, decreasing the ratio of reduced to oxidized glutathione (GSH/GSSG).

This assay is a luminescence-based system to detect and quantify total glutathione (GSH +GSSG), GSSG and GSH/GSSG ratios in cultured cells. The assay provides a simple, rapid multi-well plate format where stable luminescent signals are correlated with either the GSH or GSSG concentration of a sample. Both GSH and GSSG determinations are based on the reaction scheme shown in Figure 2.9 where GSH-dependent conversion of a GSH probe, Luciferin-NT, to luciferin by a glutathione S-transferase enzyme is coupled to a firefly luciferase reaction. Light from luciferase depends on the amount of luciferin formed, which in turn depends on the amount of GSH present. Thus, the luminescent signal is proportional to the amount of GSH.

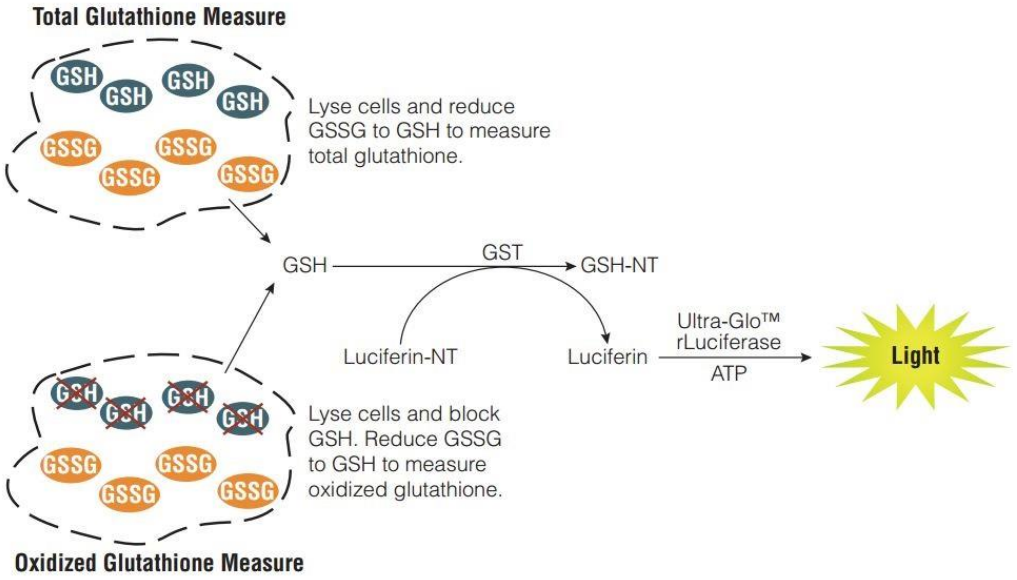

Figure 2.9 GSH-dependent conversion of a GSH probe, Luciferin-NT, to luciferin by a glutathione S-transferase enzyme is coupled to a firefly luciferase reaction. Source: Promega UK Available: https://www.promega.co.uk/-/media/files/resources/protocols/technical-manuals/101/gsh-gssg-glo-assay-protocol.pdf?la=en

Firstly, 1×10^4 per well of cancer cells were seeded and allowed enough time to attach, followed by PEFE treatments at designated time points. The cell culture medium was aspirated, and the remaining medium was removed by washing with PBS twice. Then 50µl of Total Glutathione Lysis Reagent was dispensed to the wells containing cells and those used for Glutathione standard curve. The plate was placed on a plate shaker for mixing at room temperature for 5 minutes, following which 50µl of Luciferin Generation Reagent was dispensed to all wells followed by shaking briefly and 30-minute incubation at room temperature. Subsequently 100µl of Luciferin Detection Reagent was added to each well followed by another incubation at room temperature for 15 minutes. The total Glutathione concentration was quantified by luminescence recording using GloMax®-Multi Detection System (Promega, UK).

2.8.8 ROS-Glo™ H_2O_2 Assay

This assay is a homogeneous, rapid and sensitive luminescent assay that measures the level of hydrogen peroxide (H_2O_2), a reactive oxygen species (ROS), directly in cell culture or in defined enzyme reactions. The scalable multi-well format couples a stable luminescent signal to the level of H_2O_2 in a sample.

The mechanism for H_2O_2 measurement is shown in Figure 2.10. An H_2O_2 Substrate is employed that reacts directly with H_2O_2 to generate a luciferin precursor. Upon addition of ROS-Glo™ Detection Reagent containing Ultra-Glo™ Recombinant Luciferase and d-Cysteine, the precursor is converted to luciferin by the d-Cysteine, and the produced luciferin reacts with Ultra-Glo™ Recombinant Luciferase to generate a luminescent signal that is proportional to H_2O_2 concentration.

The cancer cells were seeded at 1×10^4 per well and placed in specified wells in a 96-well plate. PEFE treatments were performed after incubation overnight. Once PEFE was completed, 120µl of medium in each well was aspirated with 80µl of medium remaining. A volume of 20µl of H_2O_2 Substrate solution was dispensed to each well and mixed thoroughly. The plate was then incubated at 37°C in a CO_2 incubator for 6 hours. Following incubation, 100µl of ROS-Glo™ Detection Solution (refer to section 2.2.5.7) was added to each well followed by a 20-minute-

incubation at room temperature. The H_2O_2 concentration was quantified by luminescence recording using GloMax®-Multi Detection System (Promega, UK).

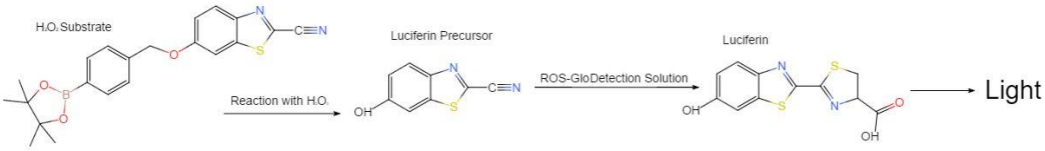

Figure 2.10 ROS-Glo™ H_2O_2 Assay chemistry. Source: Promega UK Available: https://www.promega.co.uk/-/media/files/resources/protocols/technical-manuals/101/ros-glo-h2o2-assay-protocol.pdf?la=en

2.9 Protein extraction for Kinexus™ antibody microarrays

To capture a panoramic view of the intracellular signalling response to PEFE treatment in cancer cells, the study adopted a protein kinase antibody microarray, which detected changes of over 800 key protein kinases. This was the Kinexus 850 microarray platform (Kinexus Inc., Vancouver, Canada).

The Kinexus protein platform is based on the antibody capture technologies with over 850 capture antibodies, which either recognise phosphorylated specific kinases or total kinase proteins, spotted on to each array slide. Upon application of test protein samples, the platform goes through stringent washes, and labelling for detected proteins, see Figure 2.11.

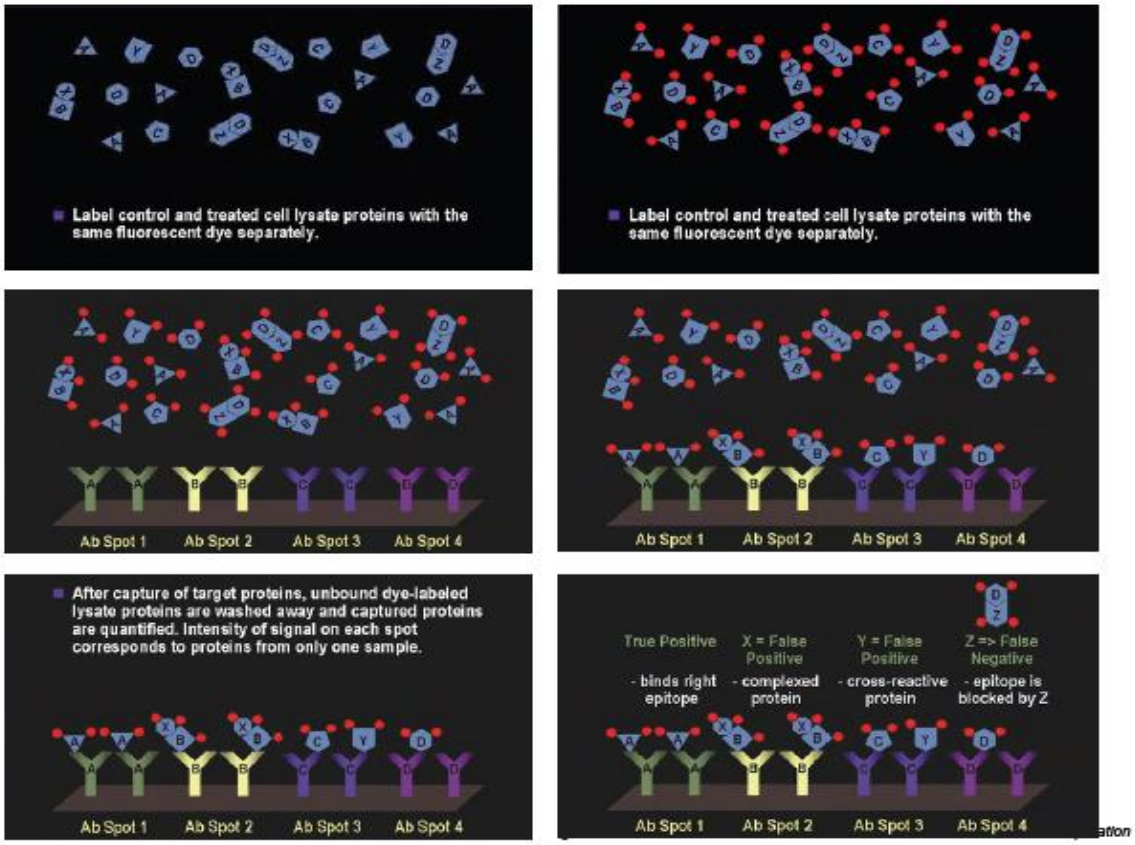

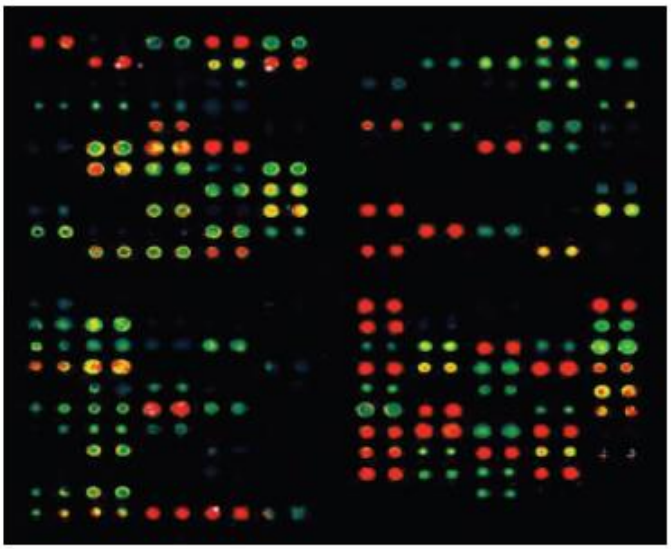

Figure 2.11. Top: Protein recognition and labelling with the Kinexus antibody array platform (www.kinexus.com). Bottom: Image from a sample Kinexus protein array.

After PEFE treatment, both breast cancer cells, control and PEFE treated groups, in 6 well plates were washed twice with PBS and scraped using 5ml sterile PBS. This cell suspension was then centrifuged at 2,500 rpm for 10 minutes to acquire the cell pellet. The cell pellet was lysed in 600µl lysis buffer and was subsequently placed on a Labinoco rotating wheel (Wolf laboratories, York, UK) (25rpm and 4°C) for 40-60 minutes for sufficient extraction. The lysis solution was then centrifuged at 13,000rpm for 15min and the supernatant containing protein lysate was collected. As per section 2.5.2, protein concentrations in the samples were quantified and standardised to 2mg/ml. This was then sent to Kinexus™ antibody microarray platform for analysis (Kinexus Bioinformatics, Vancouver, British Columbia, Canada).

The following key parameters are captures for each sample on the array:

1. ***Globally Normalized Signal Intensity:*** Background corrected intensity values are globally normalized. The Globally Normalized Signal Intensity is calculated by summing the intensities of all the net signal median values for a sample.
2. ***%CFC:*** The percent change of the treated sample in Normalized Intensity from the specified control. This was calculated using the following: Calculation = (Globally Normalized Treated – Globally Normalized Control)/Globally Normalized Control) *100
3. ***Z Scores, Z Score difference and Z ratios:*** Z score transformation corrects data internally within a single sample. ***Z Score Difference*** - The difference between the observed protein Z scores in samples in comparison. **Z Ratios** - Divide the Z Score Differences by the SD of all the differences for the comparison.

2.10 *In vivo* animal study

The *in vivo* PEFE experimentation was conducted in Sun Yat-sen College of Medicine (GuangZhou City, China), via an institutional collaboration between Cardiff University and Sun Yet-sen University. This study was ethically approved by the Sun Yat-sen College of Medicine research ethics committee. The

experiments were conducted at the in vivo Experimental Centre of Sun Yat-sen College of Medicine and in full compliance with the Institutional and Guangdong Provincial Government Regulations for Experimental Use of Animals. The participants of the study received licences from the institution and Guangdong government authority. Initially, 3×10^6 MDA-MB-231 breast cancer cells were subcutaneously injected into each nude mouse. Control group or those treated with PEFE at different conditions were closely monitored until the tumours grew to around 1cm. Anaesthesia (4% chloral hydrate, 100µl per mouse) was carried out for each mouse, prior to and throughout the treatment procedure, to reduce the pain and discomfort caused by microwave treatment. The PEFE was generated at 2.2GHz and the power level was fixed at 50 watts. The pulse period of PEFE was fixed at 1ms. The temperature at the area of treatment was monitored to ensure normothermic conditions. Each group contained 5 nude mice and the experiment was set up as follows:

Group A: Control group

Group B: 40 µs in pulse width. Mice were treated with 40 seconds PEFE followed by 40 seconds power off, repeated 10 times.

Group C: 74 µs in pulse width. Mice were treated with 40 seconds PEFE followed by 40 seconds power off, repeated 4 times.

Tumour size was checked every 3 days for 27 days duration according to different treatment protocols, and the volume of tumours was calculated by using the following formula(Hather et al., 2014):

$$\text{Tumour volume } (mm^3) = 0.5\times \text{Width}^2\times\text{length}$$

At the conclusion of the study, mice were sacrificed and tumours, where visible, and tissues around the initial site of tumours, were dissected and processed for histological and biochemical analysis.

2.11 Investigation on cellular migration after Kidins220 knockdown using Electric Cell-Substrate Impedance Sensing (ECIS)

The 96W1E arrays (ECIS culture ware, Applied Biophysics Inc, NY, USA) were used in this study. Prior to seeding the cells, this array was required to be stabilized with 200µl medium per well in order to clean the electrodes. After stabilization, the medium was aspirated, and the array was ready to use. The cell lines used in this study were MDA-MB-231 scramble and Kidins220 knockdown together with MCF-7 scramble and Kidins220 knockdown. Each cell line was seeded at 10×10^4 cells per well containing 200µl medium for 8 wells in the array. The array was then placed in a dedicated incubator connected with a Theta ECIS controller system (Applied Biophysics Inc, NY, USA), as shown in Figure 2.12. The software was configured with multi-frequencies and the resistance under each frequency was measured to quantify the cell adhesion and migration. The cellular migration measurements were performed within 6 hours.

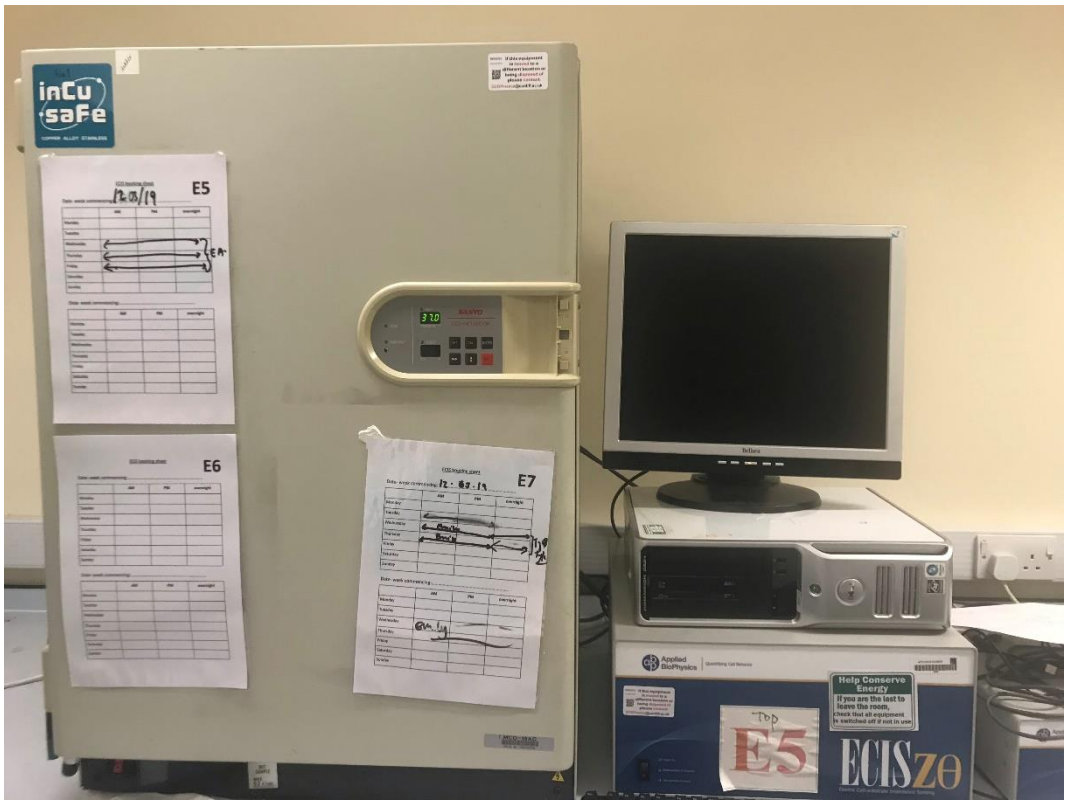

Figure 2.12 Theta ECIS controller system with incubator (Applied Biophysics Inc, NY, USA).

2.12 Immunofluorescence (IFC) Staining

MCF-7 breast cancer cells were seeded into Millicell® EX slide (Merck KGaA, Darmstadt, Germany) and grown to 100% confluency, then treated with PEFE for 5 hours. When the microwave treatment was completed, the cells were fixed with ice cold ethanol and stored at -20℃ until use.

MCF-7 breast cancer cells were first rehydrated with PBS, after removing the ethanol, and 100µl 0.1% Triton was added to permeabilise the cells for 2 minutes. The cells were subsequently washed three times with PBS. Following which 100µl 10% horse serum was added to block the cells for at least 60 minutes. The cells were then washed with 3% horse serum and incubated with ZO-1 primary antibody (1: 500 dilution) and 3% horse serum overnight. The cells were washed with 3% horse serum 6 times the next day, and 100µl 3% horse serum and TRITC secondary antibody (1:2000 dilution) was added into each well and rocked for 40min. The cells were subsequently washed six times with 3% horse serum followed by 6 washes with PBS. The slide was gently removed and was flicked to gently remove excess buffer. Four drops of Fluorsave™ was then added before gently placing the cover slip on. The slide was covered with foil and stored at 4℃ before capturing the images under a fluorescence microscope.

2.13 DAPI staining

The cancer cells underwent PEFE treatments and direct heating at 40℃, were incubated at 37℃ for 6 hours, and then collected for DAPI staining. Two microlitres of DAPI was transferred to those treated cancer cells and directly heated at 40℃ separately. After 1-hour incubation at 37℃, the results were visualised using a fluorescence microscope as demonstrated in section 2.12.

2.14 Transmission electron microscopy (TEM)

This was carried at the Light and Electron Microscopy Unit of the Central Biological Service of Cardiff University and the University Hospital of Wales, Cardiff, UK, assisted by Dr. Christopher von Ruhland. Briefly, cancer cells were seeded over glass cover slips which were placed at the bottom of a petri dish. After

cells adhered to the surface, PEFE experiments were carried out on the cells. Cells were fixed using formaldehyde and processed for transmission microscopy.

2.15 Trypan blue exclusion test

Trypan blue exclusion test was used for cancer cell viability assessment. Prior to adding trypan blue, cultured cancer cells were detached using trypsin (50µl per well) which is illustrated in section 2.3.3. Once detached, 150µl of cell culture medium was added to each well to neutralise the trypsin and form a cell suspension. Following this 10µl of cell suspension was transferred to a 0.5ml microfuge tube containing 10µl of trypan blue, followed by gently mixing with 10µl of that mixture, then transferred to a dedicated cell counting chamber slide (Fisher Scientific UK Ltd) and cell viability was evaluated using a Countess™ II Automated Cell Counter (Thermo Fisher Scientific Inc.), shown in Figure 2.13 and Figure 2.14.

Figure 2.13 Cell counting chamber slide. Source: Fisher Scientific UK Ltd. Available: https://www.fishersci.co.uk/shop/products/invitrogen-countess-cell-counting-chamber-slides-5/10399053

Figure 2.14 Countess™ II Automated Cell Counter. Source: Thermo Fisher Scientific Inc. Available: https://assets.thermofisher.com/TFS-Assets/LSG/brochures/countess-II-automated-cell-counters-brochure.pdf

Chapter 3 Pulsed Electromagnetic Field Exposure (PEFE) System Introduction and Instrumentation

3.1 Pulsed electric field exposure (PEFE) system introduction

PEFE used in this research was based on continuous microwave signals, modulated by DC signals at desired repetitive frequencies, generating a synthetic signal with adjustable duty cycle determining a ratio of how much the signal is on and off, shown in Figure 3.1. The choice of the duty cycle allowed control of the amount of power into the sample and therefore the induced heat, while still ensuring the exposure to the electro-magnetic fields was at controllable levels. The generated signal was then amplified to desired levels and transferred to biological samples through coaxial cables and a manufactured open-ended probe; while the incident and reflected power were monitored by two dedicated power sensors, capable of detecting pulsed signals. A precise temperature fibre optic sensor that is not impacted by the electro-magnetic fields, was applied to monitor the temperature locally. The PEFE system overview is shown in Figure 3.2, this system consists of a serial of dedicated instruments and devices, operating at microwave frequencies.

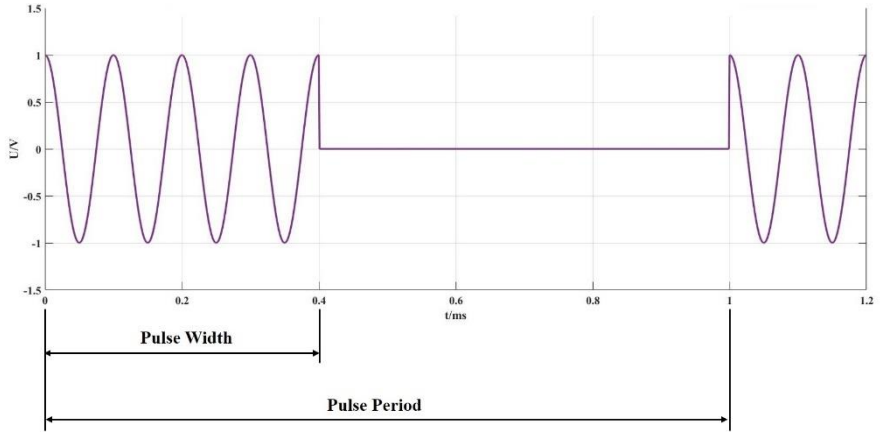

Figure 3.1 An example of PEFE signals used in this research, which was synthesized by continuous microwave and DC signals.

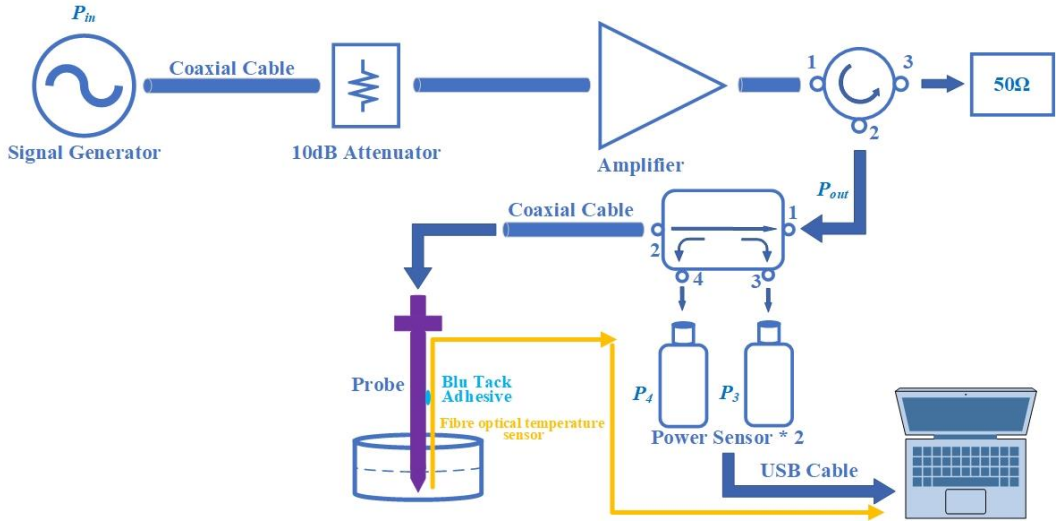

Figure 3.2 PEFE system constructed by a series of microwave devices. The main components of this system include signal generator, amplifier, and power sensors.

3.1.1 Components in PEFE system

The main components of the PEFE system includes a signal generator, power amplifier, power sensors, temperature sensor and some passive devices such as circulator and coupler. The details of each component are discussed in the following sections.

3.1.1.1 Signal generator

The signal source used in this research for PEFE generation was N5181B MXG X-Series RF Analog Signal Generator (Keysight Technologies UK Limited), shown in Figure 3.3. This broadband signal generator can allow users to accurately adjust output frequency. Continuous wave mode and other modulation schemes including pulse modulation are supported for varied applications. Since the entire measurement system was a scalar system and the phase of the signal was not necessary, this analogue signal generator was able to meet all the requirements for this research. The main parameters in the specification are listed in Table 3.1. The maximum output of this generator is +19*dBm* (approximately 0.0794 watts), which is much lower than the minimum power required in this research (20 watts).

Therefore, a high-power amplifier was necessary for this research to increase the input signals to the desired value.

Figure 3.3 N5181B MXG X-Series RF Analog Signal Generator. Source: https://www.keysight.com/en/pdx-x201911-pn-N5181B/mxg-x-series-rf-analog-signal-generator-9-khz-to-6-ghz?nid=-32490.1150486.00&cc=GB&lc=eng

Table 3.1 Main parameters of signal generator used in research

Specification	
Frequency range	9kHz-6GHz
Frequency resolution	0.001Hz
Amplitude settable range	+19 *dBm* to -144 *dBm*
Amplitude resolution	0.01 *dB*
Minimum pulse width ALC on/off	>2μs/ >20ns
Repetition frequency ALC on/off	10Hz to 500kHz/DC to 10MHz
Pulse overshoot	<15%

3.1.1.2 High power amplifier

An AS1860 solid state power amplifier from MILMEGA was used to boost the input signals to the required levels. The maximum input power for this amplifier was +15*dBm*, and for protection, one 10*dB* attenuator was attached to its input port to ensure that it would not be overdriven by the signal generator. This GaN based amplifier was developed to cover frequency band 1.8 – 6.0 GHz and produced high power with excellent linearity and low harmonics. Fans were integrated to this compact amplifier to make the entire system air-cooled to prevent overheating. The main parameters of this amplifier are listed in Table 3.2.

A drift in gain was observed when this amplifier was initially switched on and the output power was decreased continuously if measured by the power sensor. The circuits inside the amplifier were allowed sufficient time to reach a thermal stable state, leading to an accurate power output and delivery. Typically, 40 minutes to 1 hour, depending on environmental temperature, was required for the drift in performance to stabilise.

Table 3.2 Main parameters of AS1860 power amplifier

Specification	
Frequency range	1.8 to 6.0 GHz
Psat (min)	125 watts
P1dB (min)	100 watts
Gain (min)	46 *dB*
Gain Variation (max)	+/- 3.0 *dB*
Third order intercept point IP3	10 *dB* > P1dB
Input power (no damage)	+15 *dBm*
Output VSWR	2 : 1 (Typical)
Input VSWR	2 : 1
Noise figure	8.0 *dB*

3.1.1.3 Microwave circulator

When conducting experiments, an open-ended coaxial cable was used as a microwave probe to inject a high frequency electric field into the biological sample. Reflected signals will propagate from the end of the probe to the amplifier due to the equivalent impedance mismatch between the biological sample and the coaxial cable. These reflected signals can induce amplifier output power decrease, and waveform distortion, leading to inaccurate measurements. A microwave circulator, placed immediately after the amplifier directly addresses this problem.

The microwave circulator consisted of a Y-junction strip line coupled to a magnetically biased ferrite material, operating at microwave frequency. The circulator (AltanTecRF AS7122) used in this research consisted of 3 ports of which port 3 was inherently terminated with a standard 50Ω load, shown in Figure 3.4, to minimise any reflections. The power flow becomes unidirectional, the input signals inserted into port 1, will exit at port 2. While any signals propagate into port 2, they will exit at port 3, where they will be terminated by the 50Ω load to prevent reflected signal. Consequently, there is no signal propagation from port 3 back to port 1.

The circulator acts here as an isolator between incident signals at port 1and reflected signals at port 3 so that no signals will be inserted back into the amplifier. This ensures a safe and more stable amplifier operation.

Due to the resonance effects of ferrite materials, the circulators are manufactured and operated at specific frequencies. Most circulators are designed with a narrow frequency band. The loss will increase, and isolation will decrease outside this frequency band. The frequency bands of microwave circulators used in this research were 2.0-2.2GHz and 5.4-6.6GHz, respectively.

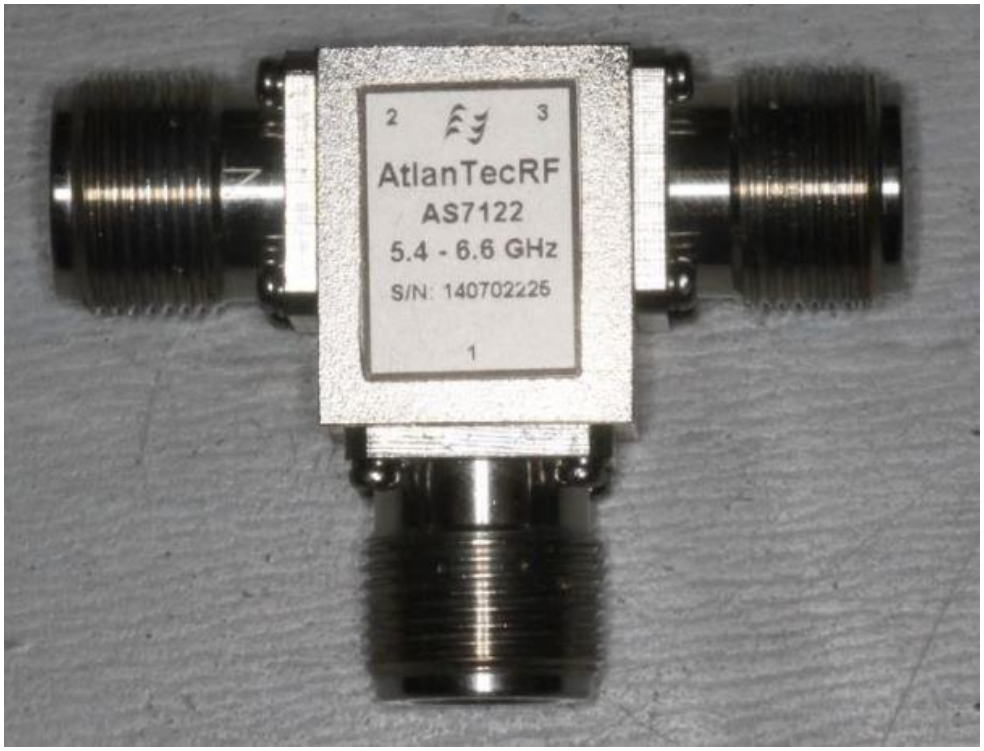

Figure 3.4 AltanTecRF AS7122 microwave circulator(Ehtaiba, 2017).

3.1.1.4 Microwave directional coupler

As discussed in section 3.1.1.3, the equivalent impedance of biological samples was never matched to the impedance of the coaxial cable giving rise to both incident signals and reflected signals within the measurement system. Both signals are relevant for the monitoring of the experiments and further analysis of acquired data.

Thus, a microwave directional coupler, which can separate the incident wave and reflected wave, is included within measurement set-up.

A directional coupler is made of two transmission lines, the main line and the coupled line, as shown in Figure 3.5. The directional coupler properties can be understood by inspecting its scattering parameter matrix, *i.e.* its *S*-parameter matrix:

$$\begin{bmatrix} S_{11} & S_{12} & S_{13} & S_{14} \\ S_{21} & S_{22} & S_{23} & S_{24} \\ S_{31} & S_{32} & S_{33} & S_{34} \\ S_{41} & S_{42} & S_{43} & S_{44} \end{bmatrix} = \begin{bmatrix} \rho_1 & l_1 & k & \tau \\ l_1 & \rho_1 & \tau & k \\ k & \tau & \rho_2 & l_2 \\ \tau & k & l_2 & \rho_2 \end{bmatrix}$$

It is typically assumed that the device is passive (reciprocal) and symmetrical, thus the return loss of the main line and coupled line are $S_{11}=S_{22}=\rho_1$, and $S_{33}=S_{44}=\rho_2$. If the device is well matched to the reference impedance, then $\rho_1 \approx \rho_2 \approx 0$. The terms l_1 and l_2 represent the losses of the two transmission lines.

The term *k* in the *S*-matrix is the coupling factor. When a signal source is connected to port 1 of the coupler and port 2 is connected to a non-matched load with a reflection coefficient ΓL, in case, port 3 and port 4 are well matched, we have:

$$b_3 = ka_1 + \tau a_2$$
$$b_4 = \tau a_1 + ka_2$$

where a_i and b_i are the incident and reflected waves respectively, at each *i*-port of the coupler. As long as τ, the isolation factor, is kept small, b_3 is proportional to a_1 and also b_4 is proportional to a_2, through the same factor *k*.

The microwave directional coupler used in this research was a four-port bidirectional coupler with a rated coupling factor of 30*dB* over a broad frequency range, shown in Figure 3.6. System calibration was necessary to determine the actual coupling factor and obtain a quantitative measure of the actual signal that is injected into the sample.

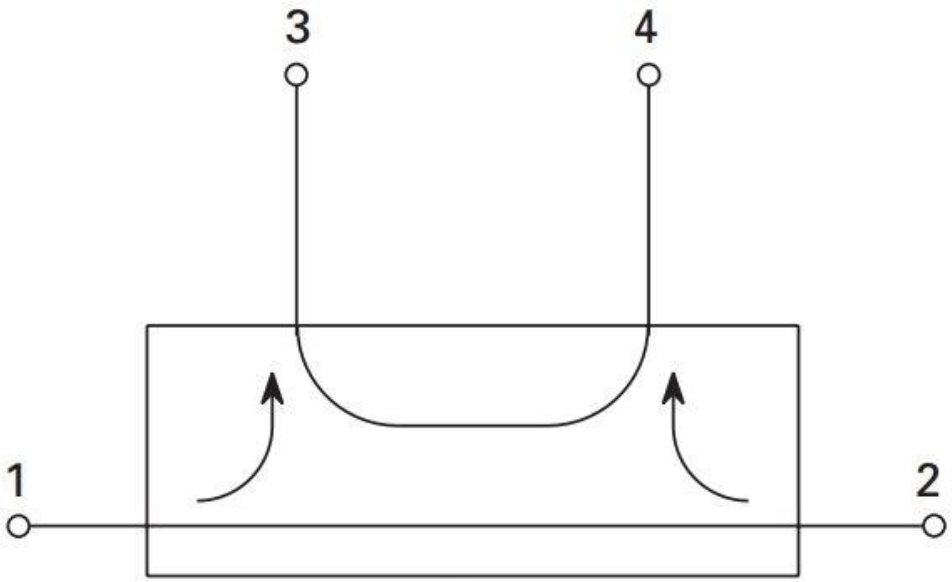

Figure 3.5 Typology of microwave directional coupler(Teppati et al., 2013).

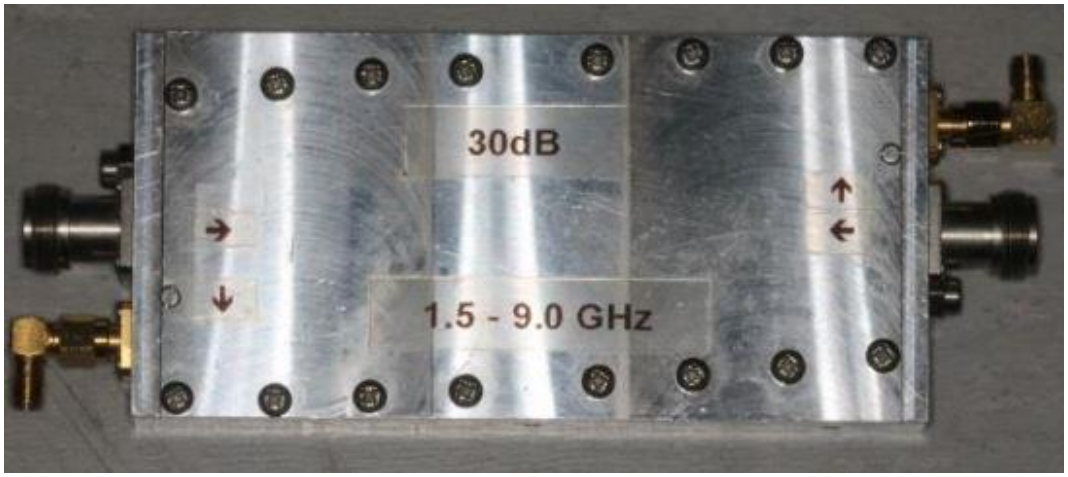

Figure 3.6 Microwave directional coupler used in this research(Ehtaiba, 2017).

3.1.1.5 Power sensors

In lumped circuits, electric currents and voltages are measured by ampere meters and voltmeters, respectively. In high frequency circuits, electric currents and voltages keep changing with the location of the cables and power is measured instead, to describe the characteristic of the circuits. Thus, two power sensors were used to measure the incident power and reflected power separately.

The power sensors used in this research were the U2021XA Peak power and Average power sensor (Keysight Technologies UK Limited), shown in Figure 3.7. This power sensor can measure continuous wave and pulsed signals over a broad band of frequencies with a high accuracy. Other important parameters of the specification are listed in Table 3.3. This power sensor draws power from a USB port and does not need additional triggering modules to operate, making it portable and lightweight. When used, dedicated software was required to drive the power sensor. In this research, Labview2017 was selected to run the power sensor and achieve data collection.

Labview2017 is a graphical programming language developed by Nation Instruments. Its concept is based on data flow and uses Virtual Instruments ('VIs') to control the data flow and perform data analysis. Each VI has a front panel and a block diagram. The block diagram is used for the programming while the front panel is for user interface. Keysight provides specific manuals and dedicate VIs to allow users to generate codes for the power sensors in different applications. The flowchart utilised in this research is shown in Figure 3.8.

Figure 3.7 U2021XA Peak power and Average power sensor. Source: https://www.keysight.com/gb/en/assets/7018-03449/data-sheets/5991-0310.pdf

Table 3.3 Main parameters of power sensor used in this research

Specification	
Frequency range	50 MHz to 18 GHz
Dynamic range	-30*dBm* to +20*dBm* (peak/gated) -45*dBm* to +20*dBm* (average only)
Rise/fall time	⩽13ns
Minimum pulse width	50ns
Minimum pulse repetition rate	10 MHz

It can be seen from Figure 3.8 that the operation of power sensors contains four stages, including initiate, configuration, data acquisition and analysis, and close. In the first stage, the power sensors were identified by the software and relevant memory space designated within the computer. Then, the required configurations for power units, working frequency and measurement types were assigned to power sensors. Next, a loop was constructed for continuous data acquisition and analysis. Finally, the power sensors were closed and their memory space was released when measurements were completed.

Notably, the power sensors were set-up to work selectively in two different modes depending on the application, the calibration mode and the measurement mode. The calibration mode is used for entire system calibration, which involved the correct settings of the generator, total loss calculation, and the determination of parameters to quantify incident and reflected power signals. The calibration mode is performed at low power levels using a continuous wave signal. The measurement mode is

selected afterwards when performing PEFE treatments. Here, pulsed signals will be generated instead and then injected into biological samples; thus, power sensors will be adjusted to measure the peak power.

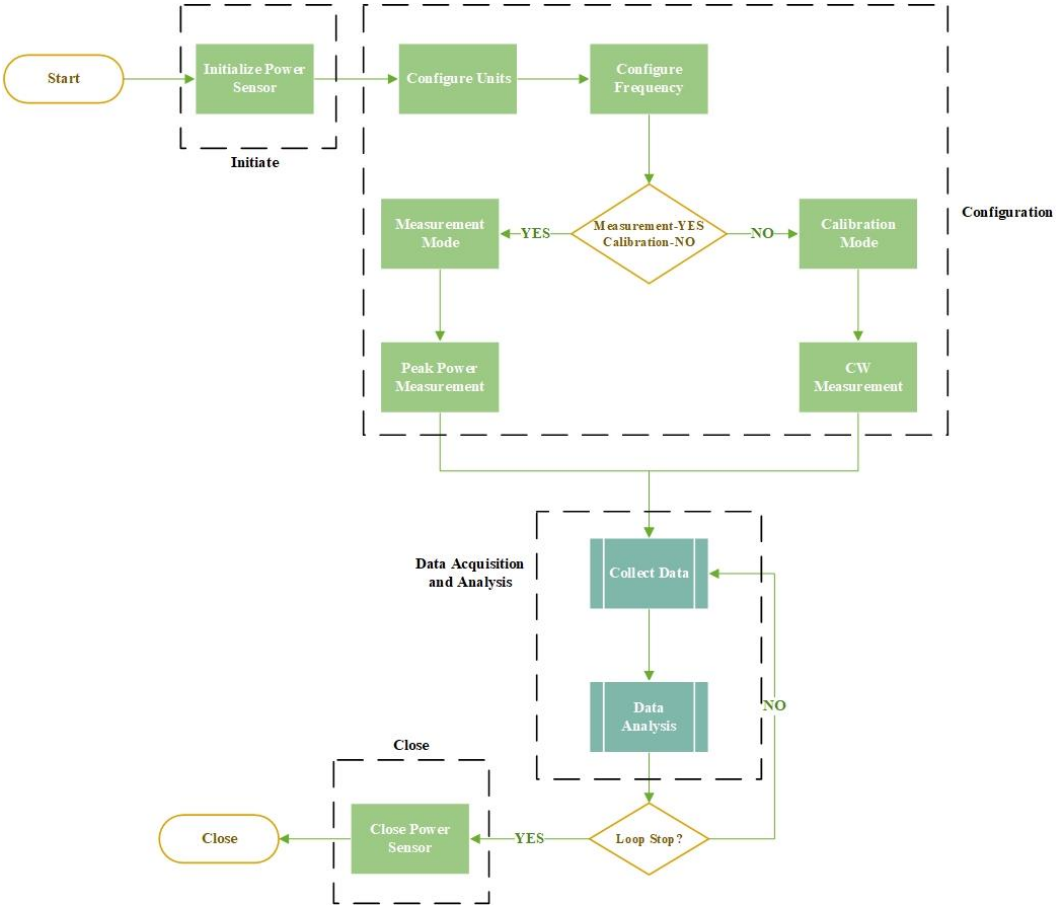

Figure 3.8 Flowchart of PEFE instrumentation. The entire instrumentation can be grouped as four stages, including 'Initiate', 'Configurations', 'Data acquisition and analysis' and 'Close'.

3.1.1.6 Open-ended microwave probe

The probe used in PEFE treatments both *in vitro* and *in vivo* was manufactured from a semi-rugged RG-405 microwave coaxial cable (2.2 mm in outer diameter), shown in Figure 3.9 (a) and (b). This microwave coaxial cable can effectively transmit electromagnetic signals at microwave frequencies and was constituted by inner conductor, dielectric layer, and outer conductor. The inner and outer conductors

were made of copper while the dielectric layer was made of Polytetrafluoroethylene (PTFE), shown in Figure 3.10. One end of this coaxial cable was cut to be pointed, making it easy to be inserted into the nude mice when used *in vivo*. The other end was connected to a microwave directional coupler via soft microwave coaxial cables.

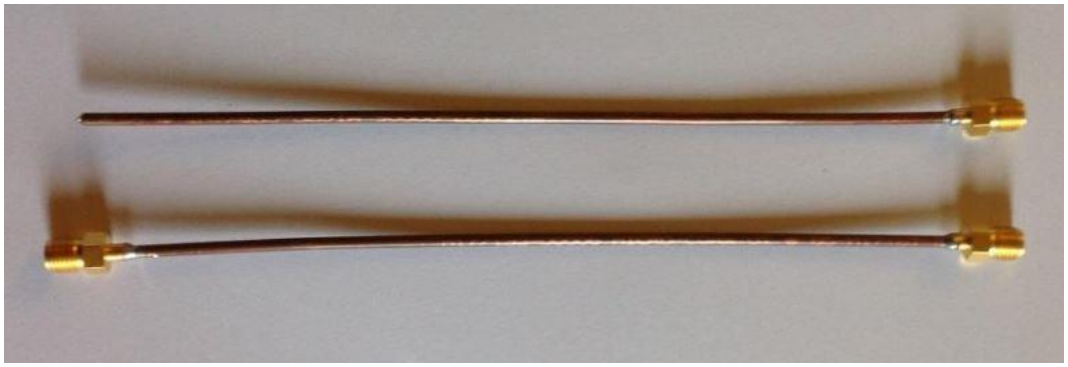

(a) Open-ended probe used in treatments

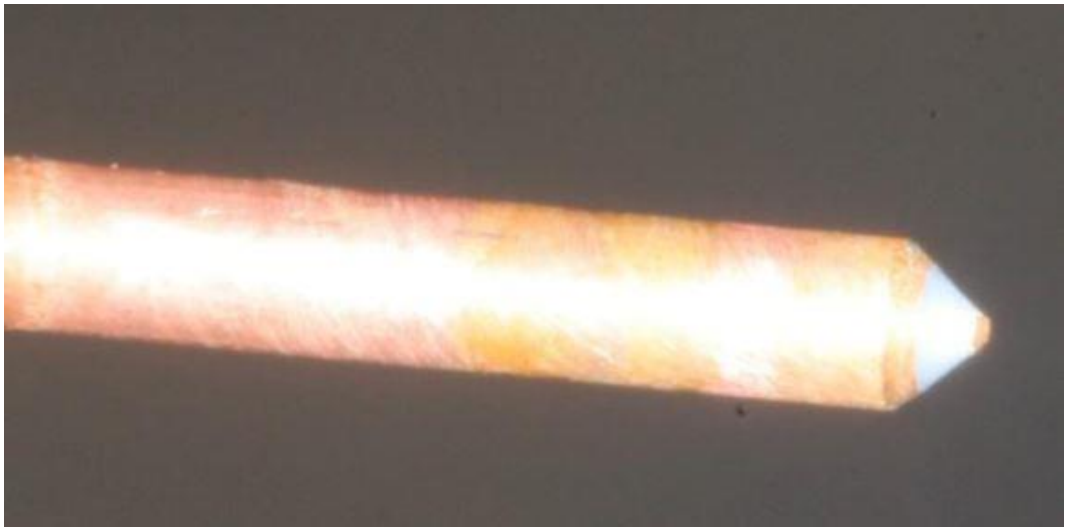

(b) Pointed tip of probe

Figure 3.9 Open-ended probe used in this research and its pointed tip(Ehtaiba, 2017).

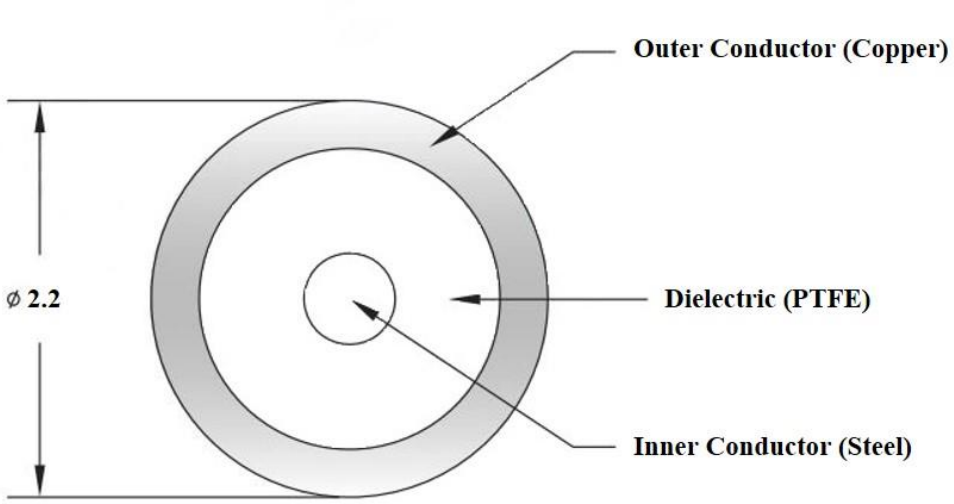

Figure 3.10 The cross sectional dimensions and materials in typical RG405 cable.

3.1.1.7 Fibre optical temperature sensor

PEFE was developed to provide a stable and relatively low temperature during cancer treatments, which is in stark contrast to other thermal therapies, such as RF ablation, microwave ablation, laser ablation. When conducting treatments, the temperature was strictly maintained below 42℃. Thus, a sensitive temperature sensor was required to accurately monitor the temperature around the probe tip.

The temperature sensor used in this research was Luxtron812 Industrial Temperature Monitor, from LumaSense Technologies Inc, shown in Figure 3.11. This sensor is an industrial grade fibre optic temperature monitoring system designed with two measurement channels and an easy-to-read LED display. It can monitor the temperature over a very wide range, typically from -100℃ to 330℃. Further details of this sensor are listed in Table 3.4. When used in treatments, this temperature sensor was placed very close to the probe tip and adhere to the probe by Blu Tack adhesive to fix its location, shown in Figure 3.2.

Figure 3.11 Luxtron812 Industrial Temperature Monitor. Source: http://www.asras.com/images/sub_1369197268/Luxtron-812_datasheet.pdf

Table 3.4 Luxtron812 Industrial Temperature Monitor Specification

Specification	
Measurement Range	-100 to 330 °C, probe dependent
Accuracy (calibrated)	+/- 0.5 °C RMS @ 8 samples per measurement
Output Format	℃, °F, °K
Storage Temperature	-30 to 75 °C
Operating Environment	10 °C to 50 °C

3.2 PEFE system calibration

The signal source used for PEFE generation is an analogue signal generator. The power sensors used for the detection of the incident power and reflected power, can only measure the total amplitude of the signals and do not provide any information of their phase. As a result, the calibration of the PEFE system is only concerned with the correction of the power amplitudes at a specific frequency. It is assumed here that only one dominant frequency is present within the detected power signal. To ensure this condition, the amplifier is used only within its linear input power range with all the remaining components being passive and a power range in line

with the utilised signals. Once the frequency is changed, the calibration should be performed again. The calibration procedure can be divided into 5 steps and the details are illustrated as follow:

3.2.1 Generator calibration

The generator calibration was applied to inspect whether the generator was working normally, generating correct power levels at the desired frequency. When calibrating the generator, typically a frequency of 2.2 GHz was selected, and two power sensors used to carry out this calibration procedure. A set of power levels (*PG*) ranging from -30*dBm* to 12*dBm*, was set to the generator sequentially. The generated powers were directly measured by two power sensors separately (*Pm1*, *Pm2*). This procedure is illustrated in Figure 3.12 and a typical calibration result is listed in Table 3.5.

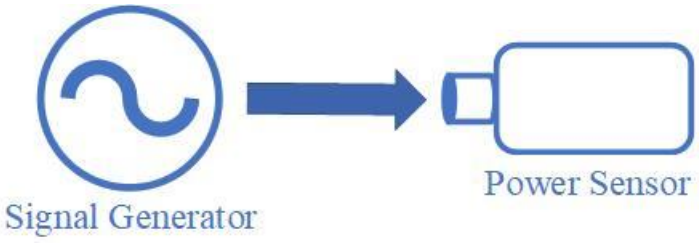

Figure 3.12 Generator calibration. One power sensor was directly attached to the signal generator. A series of power levels were generated then measured.

Table 3.5 Generator calibration at 2.2GHz

PG	***Pm1***	**Error1%**	***Pm2***	**Error2%**
-30	-29.87	0.13	-29.83	0.17
-20	-19.88	0.12	-19.85	0.15
-10	-9.85	0.15	-9.87	0.13
0	0.18	0.18	0.17	0.17
3	3.17	0.17	3.16	0.16
6	6.14	0.14	6.16	0.16
9	9.13	0.13	9.14	0.14
10	10.14	0.14	10.13	0.13
11	11.14	0.14	11.12	0.12
12	12.13	0.13	12.11	0.11

3.2.2 Gain calibration

The purpose of the generator calibration is to determine whether both the generator and power sensors are working correctly. During a gain calibration, only one power sensor was required. Prior to calibration measurements, the generator was connected to the power amplifier using a coaxial cable and the circulator was connected to the output of the amplifier. Within the set-up, the generated signal is injected in port 1 of the circulator and forwarded to port 2 with port 3 of the circulator being terminated by a 50Ω load. Then, the power sensor is attached to port 2 of the circulator.

During PEFE treatments, one 10 *dB* attenuator was required at the input port of the amplifier to ensure that the inserted signal stayed below the specified maximum value for the input. To maintain the validity of the calibration, the same attenuator was also required when calibrating the gain of the set-up. Based on this connection, the gain immediately before the directional coupler was calculated instead of the gain of the amplifier itself to account for any connection and transmission losses. According to the specification of the amplifier listed in Table 3.2, the P1dB is 100 watts which is much higher than the maximum power (50 watts) used in this research. As a result, the amplifier was operating within its linear region during PEFE treatments, leading to a constant gain, shown in Figure 3.13. Since the gain of the set-up was kept constant, the gain calibration could be performed at a much lower power level to protect the power sensors at port 2 of the circulator.

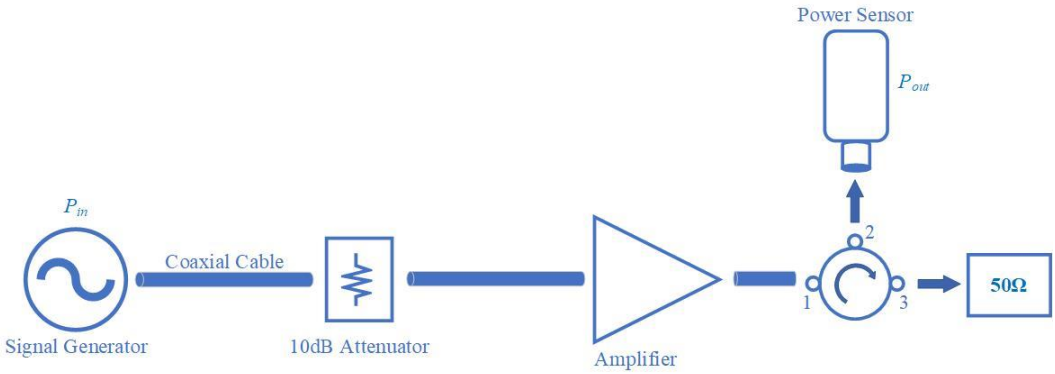

Figure 3.13 Gain calibration. The generator was connected to the amplifier via an attenuator. The power was directed to the power sensor through a circulator.

When performing the calibration, a set of low power levels, ranging from -40*dBm* to -19*dBm*, was set to the generator and the output power was measured using the power sensor. Due to the maximum input power of the power sensor (+20*dBm*), the maximum input power was limited to -19*dBm*. Once the output powers were measured, the gain was calculated by the following equation:

$$Gain = Pout - Pin$$

where *Pin* is the set input power at the signal generator in *dBm* and *Pout* the measured power at the power sensor in *dBm*. The calibration results are listed in Table 3.6.

Table 3.6 Measured gain at different input power levels

Input power/*dBm*	Output power/*dBm*	Calculated gain/*dB*
-40	-3.74	36.26
-35	1.23	36.23
-30	6.23	36.23
-27	9.25	36.25
-24	12.22	36.22
-21	15.24	36.24
-20	16.24	36.24
-19	17.25	36.25

The amplifier can be significantly affected by the temperature, leading to a drift in the gain. Such a performance drift can be readily observed shortly after the amplifier is switched on. The amplifier needs time to become thermally stable. Therefore, when calibrating the system enough time should be given for the amplifier to reach a thermally stable state.

3.2.3 Loss calculation

During gain calibration, the loss of circulator and coaxial cables was already taken into consideration when measuring Pout. In this section, only the loss of the directional coupler, an additional coaxial cable and the probe is calculated.

Based on the circuit connection during the gain calibration, the directional coupler was connected to the output port of the circulator using a coaxial cable of suitable length. During this calibration step, ports 3 and 4 of the directional coupler are terminated by two 50Ω loads to minimise any signal reflections. The double ended

probe, shown in Figure 3.9(a) was then connected to the coaxial cable and linked to a power sensor, as illustrated in Figure 3.14. The double ended probe was of the same length and coaxial cable type as the actual probe used during the PEFE experiments. The double-ended probe allows for the inclusion of the loss of the probe itself which end cannot be connected to the power sensor.

The loss can then be calculated by the following equation:

$$Loss = Pout - Pend$$

where, *Loss* is the total loss between port 2 of the circulator and the end of the probe in *dB*, *Pout* are the power sensor readouts from the previous gain calibration stage in *dBm*, and *Pend* is the power measured by the power sensor in *dBm*.

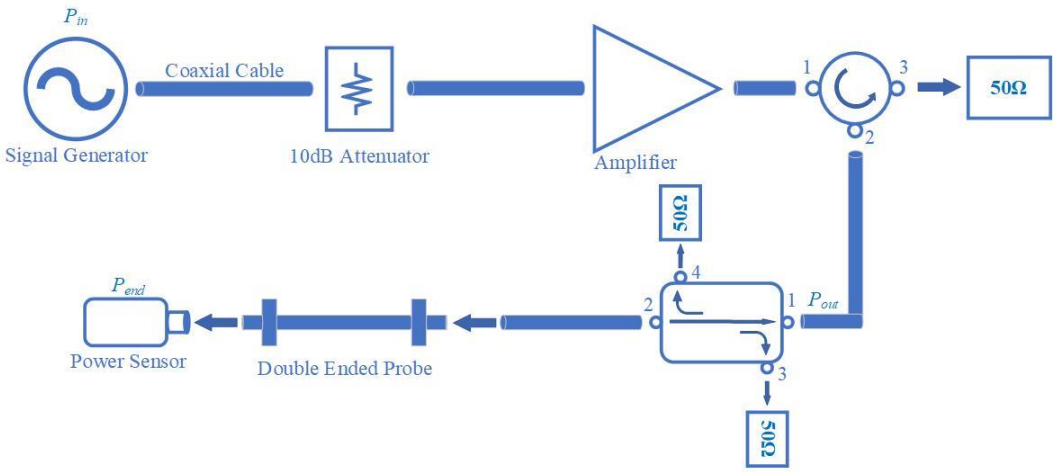

Figure 3.14 Loss calculation. Based on the circuit connection in section 3.2.2, the coupler and the double ended probe were added between the power sensor and port 2 of the circulator through coaxial cables.

3.2.4 Incident power calibration

During the treatments, the generated PEFE signals were injected into port 1 of the directional coupler and output at port 2 with the proportional coupled power appearing at port 3. To determine the relationship between the injected signal and coupled signal, the calibration factor *K1* was calculated.

First, the second power sensor was attached to port 3 of the coupler replacing one previously utilised 50Ω load to detect the incident power P_3 shown in Figure 3.15 The other 50Ω load was kept at port 4 to maintain isolation between ports 3 and 4. The *K1* factor was calculated form the following equation:

$$K1 = \left| P_3 - Pend \right|$$

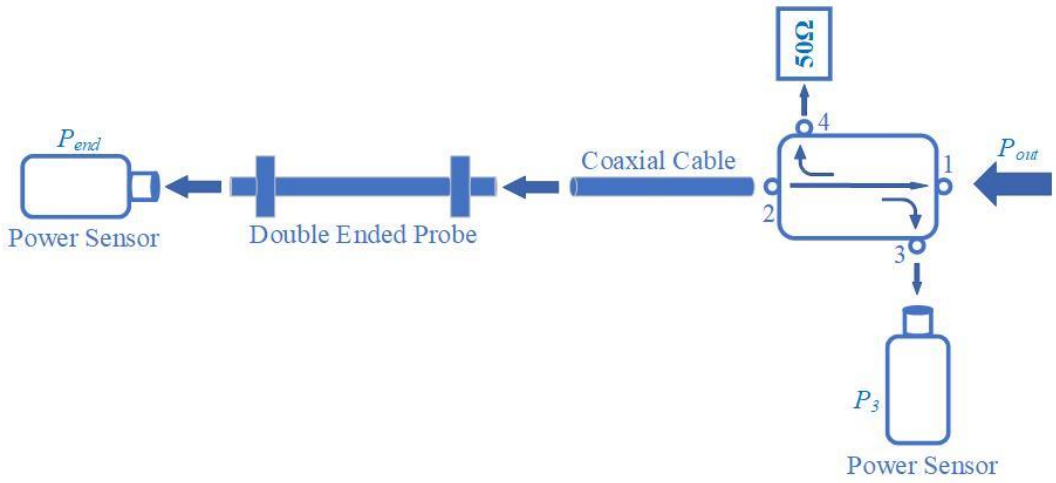

Figure 3.15 Calibration factor *K1* calculation. The power was injected from port 1 of the coupler then measured as *Pend*. The coupled power was measured as P_3.

3.2.5 Reflected power calibration

The reflected signals coming from the probe entered at port 2 of the directional coupler and was output at port 1 with the proportional coupled reflected power determined at port 4. The calibration factor *K2* took into account the differences between the two signals at port 2 and 4.

To perform this calibration, *Pout* was injected into port 2 of the coupler. This was achieved by connecting the free end of the double-ended probe to the reference plane at which *Pout* was recorded during a previous calibration step. Only one power sensor was required at port 4 to measure the reflected power, P_4 in *dBm* and two 50Ω loads were attached at port 3 and 1 as illustrated in Figure 3.16. The *K2* was then calculated as follows:

$$K2 = \left| P_4 - Pout \right|$$

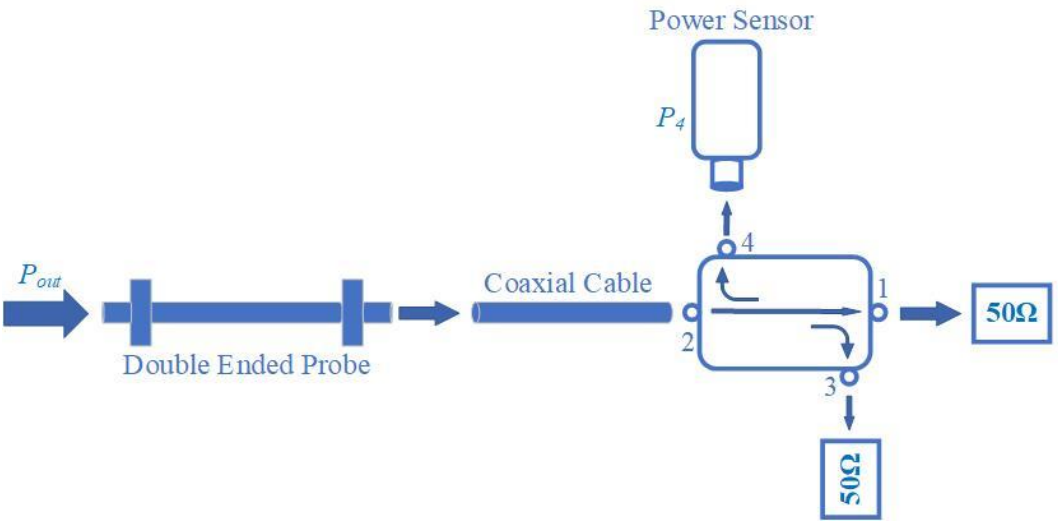

Figure 3.16 Calibration factor *K2* calculation. The power was injected from one end of the probe. The coupled power was measured as P_4.

3.3 PEFE treatments instrumentation

Once all calibration steps were completed, the input power set by the generator for a given power to be inserted into a biological sample at the end of the probe was be worked out as follows:

$$PG = Ps + Loss - Gain$$

where, *PG* was the input power set by the generator in *dBm*; and *Ps* as the power needed at the end of the probe in *dBm*. The required connections for the PEFE treatments are depicted in Figure 3.2. The two power sensors were attached at port 3 and port 4 of the directional coupler, respectively. The single ended probe was attached to the end of the entire set-up with the pointed tip inserted into a single well within a 96-well plate. The probe was placed at the centre of the well and fully immersed into the cell culture medium. The temperature sensor was attached next to the probe, measuring the local temperature. The desired pulse parameters including frequency, pulse period and pulse width, were set at the generator. When everything was completed, the PEFE treatments could be performed by manually switching on/off the generator.

3.4 Experimental data collection and analysis

The experimental data included incident power, reflected power, power dissipated in the sample, and the magnitude of the reflection at the probe tip, referred here as the $|S11|$ parameter. These data were automatically collected analysed and displayed using Labview2017.

The coupled power, measured by two power sensors, designated as P_3 and P_4, was used to calculate the incident power, *Pin*:

$$Pin = P_3 + K1$$

While the reflected power, *Pref* is calculated by the following equation:

$$Pref = P_4 + K2$$

Both values are also automatically converted to watts:

$$P_{in}^{'} = 10^{\frac{P_{in}}{10}} \Big/ 1000$$

$$P_{ref}^{'} = 10^{\frac{P_{ref}}{10}} \Big/ 1000$$

The power dissipated within the sample, *PD*, watts, can be calculated by equation:

$$P_D = P_{in}^{'} - P_{ref}^{'}$$

The $/S11/$ parameter is then obtained from the following equation:

$$|S_{11}| = \sqrt{\frac{P_{ref}^{'}}{P_{in}^{'}}}$$

3.5 Irradiation pattern simulation of *in vitro* treatments

When a pulsed electromagnetic field is generated and delivered to a biological medium containing cancer cells, both electric field and magnetic field will penetrate inside the biological medium, interacting with the cancer cells. It has been reported

that this interaction is mainly dependent on electric fields at high frequencies. Thus, the distribution of the electric field on the cancer cells was of main interest during this research. The cancer cell lines used in PEFE treatments have the characteristics of adherent growth *in vitro*, thus the cultured cancer cells adhere to the bottom of a container (96 well plate). Before treatments, simulation should be conducted to investigate and estimate the electromagnetic distribution, especially electric fields inside the container. The electric field distribution on the bottom of a well can represent the field that impacts cancer cells as the thickness of cancer cells is rather small in comparison to the wavelength of the E-field.

The software selected for simulations was COMSOL Multiphysics, which utilises advanced numerical methods for modelling and simulating physics-based problems. COMSOL Multiphysics is based on finite element analysis and simulates physical phenomenon through solving partial differential equations (PDEs), thus has high accuracy and efficiency. Many embedded modules broaden its application to more specialist fields. The 'RF Module' was chosen for the simulation in this study.

The modelling of the PEFE treatments mainly consisted of the probe and a single well within a 96 well plate containing biological medium. Although the biological medium is composed of many components, the majority is water which decides its dielectric properties. Thus, biological medium was replaced by water in this simulation. The dielectric property of water consists of real part (ε') and imaginary part (ε'') which are frequency and temperature dependent (Kaatze, 1989, Kaatze and Uhlendorf, 1981). According to the frequencies used in PEFE treatments, 2.2GHz was selected to be applied for the simulation.

Before PEFE treatments, the cancer cells were cultured in an incubator (37℃). During the treatment, the temperature of the medium was measured to be 25℃ approximately. As a result, the initial temperature for dielectric properties of water was set to 25℃ within the simulator. Since the dielectric properties of water under various conditions have been well established, the value used in this simulation was calculated in previously published work (Peacock, 2009, Liebe et al., 1991) and listed in Table 3.7. Furthermore, the distance between the probe tip and the bottom

of the well was fixed at 3mm. 'RF' module was selected to perform the simulation in the frequency domain.

Table 3.7 Dielectric properties of water under different frequencies at 25℃

NO.	Frequency	Real part of dielectric property (ε')	Imaginary part of dielectric property (ε'')
1	2.2GHz	77.5	8.22

The geometry and materials of the 96 well plate and probe were confirmed from manuals and the set up was simulated as shown in Figure 3.17. The probe was centred in the well and the tip was completely immerged into the medium. The entire set-up was axisymmetric thus the simulation was created from a 2D model. The mesh was automatically generated by software then the electric fields inside the well and at the bottom were calculated and plotted in Figure 3.17 and Figure 3.18.

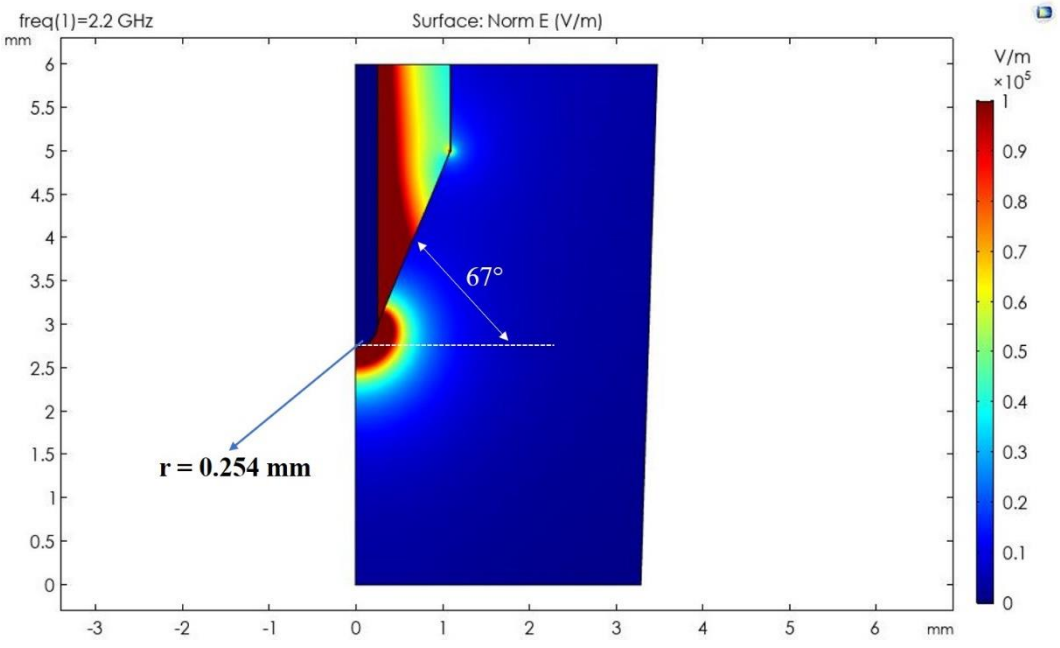

Figure 3.17 Electric field distribution inside the well. The probe was placed in the centre of the well and immerged by the medium. Part of the probe which was outside the medium was ignored in this simulation.

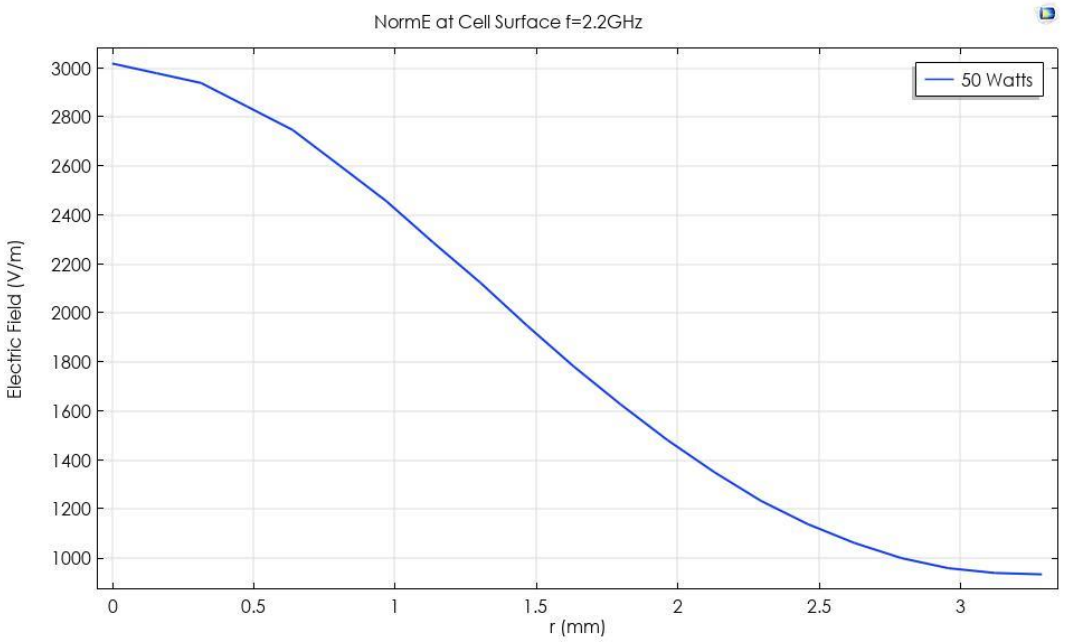

Figure 3.18 Electric field distribution on the bottom of well. This E field was able to represent that on the surface of cancer cells.

According to the simulation, the electromagnetic field was able to penetrate to cultured cancer cells. Due to the mismatched impedance of the probe and medium, part of the incident microwave signal was reflected at the end of the probe producing a reflection coefficient of 0.7 approximately. The electric field at the bottom was also calculated showing a radial pattern with a maximum at the centre and decreasing when moving away with the radius *r*. The highest electric field strength on the bottom was 3000V/m approximately when input power was 50 watts.

3.6 PEFE treatments and improvement

The MDA-MB-231 cells were seeded at 9×10^4 per well containing 200µl biological medium, then sufficient time was allowed to establish an adhesion at the bottom. Once a monolayer was formed, the cells were ready for treatment. With the PEFE system and calibration completed, the initial experiments were conducted at 5.8GHz with a 50-watt input power level. The probe was fully immerged in the medium and the experiments were performed within a Class II laminar flow cabinet (SafeF ST Classic, FASTER) in case of any contamination. The number of viable

cancer cells was calculated using MTT assay before experiments, 24 and 48 hours after experiments, respectively.

3.6.1 Probe handling

The probe was centred in the well and the distance from the tip to the bottom of the well was fixed to approximately 3mm, which allowed the tip to be completely immerged into the medium. To establish repeatable results, the probe handling was required to ensure a coherent performance, including the polishing of the tip and sterilization of the probe.

3.6.1.1 Polishing of probe tip

When the experiments started, many bubbles were produced which attached to the probe tip. Consequently, a thin layer of gas formed between the probe tip and the medium, which significantly reduced the impact of the PEFE treatment. As the reflection coefficient (S_{11}) was monitored during the experiments, a rapid increasing of S_{11} was observed when the gas film formed, shown in Figure 3.19.

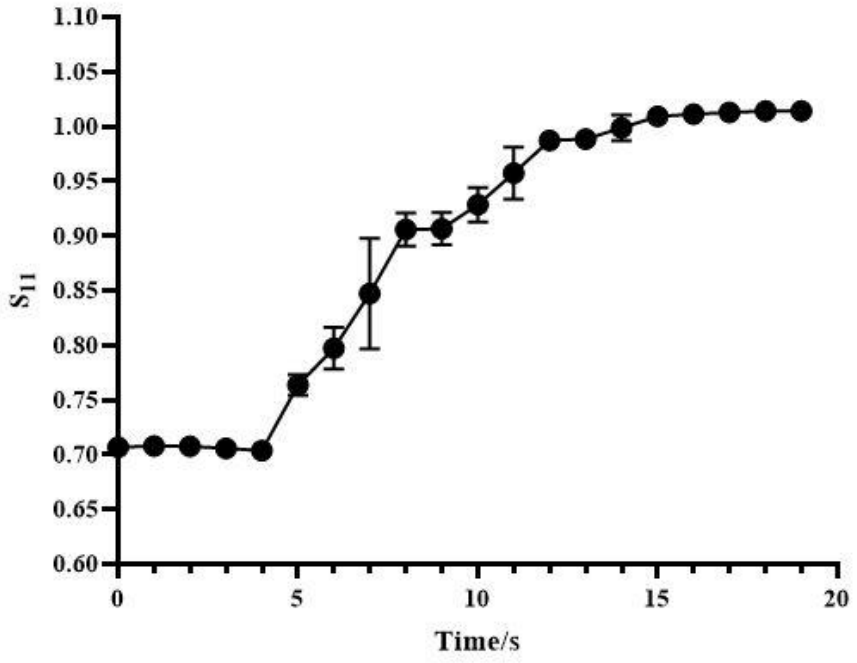

Figure 3.19 The rapidly increasing S_{11} using rough probe. PEFE was generated at 5.8GHz with a 50-watt input power level. Error bar stands for standard error of means.

As shown in Figure 3.19, the magnitude of S_{11} was measured at 0.71 approximately within the first 5 seconds, then started to increase and eventually reaching 1.0 after about 15 seconds. Once the magnitude of S_{11} reached unity, all of the microwave signals returned at the probe tip and no microwaves were penetrating into the biological medium. When this occurred, the experiments had to be stopped and the probe was pulled out and cleaned with PBS buffer to remove any attached residue. Once bubbles were removed, the probe was immerged into the medium and experiments were restarted. Unfortunately, the same formation of a gaseous layer can occur multiple times within a single experiment, making it impractical.

In order to further investigate the source of the bubbles, different liquids in the lab were used and irradiated with the same microwave signals for 30 seconds, the results of the measured S_{11} magnitude and the generation of the gaseous layer are listed in Table 3.8.

Table 3.8 Initial experiments using different liquids

	dH_2O	**PBS Buffer**	**BI[1]**
Bubbles	---	few	few
Temperature Increase	slow	slow	slow
S_{11}	0.98	0.80	0.83

1. BI: Disinfection solution (Pharmacidal™ Sprays and Solution) used for cell culture.

As seen in Table 3.8, when injecting PEFE into dH_2O, no formation of a gaseous layer was observed. The S_{11} magnitude was almost 1.0 from the beginning of the experiment, and therefore nearly no microwave signals propagated into dH_2O. This lead only to an insignificant temperature increase. As for PBS buffer and Br solution, few bubbles were observed, and the temperature increased slowly due to the high S_{11}. Except for dH_2O, biological medium, PBS buffer and BI solution are all dH_2O based and it can be concluded that the gas production likely depends on the components within the liquid.

Another solution was required to polish the probe tip and minimize the bubble adhesion to the probe. When the probe was manufactured, the surface of the probe tip was quite rough, making it easier for the generated bubbles to adhere to the tip.

A sharpening stone with a grit 1000 was used to polish the probe tip. After polishing, the experiments were repeated, almost eliminating any formation of the gaseous layer with a typical measured reflection coefficient over time shown in Figure 3.20.

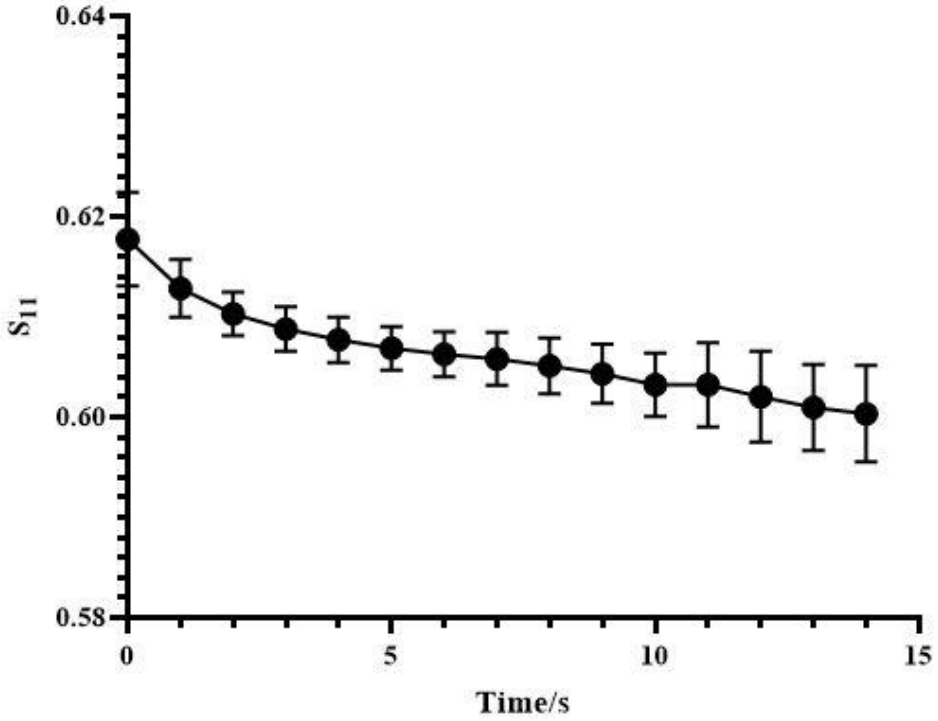

Figure 3.20 Relatively constant S_{11} measured with polished probe. PEFE was generated at 5.8GHz with a 50-watt input power level. Error bar stands for standard error of means.

Figure 3.20 shows the S_{11} was relatively constant, fluctuating at 0.61 during the 15 seconds time interval. Comparing to the results that were obtained with an unpolished probe, a lower reflection coefficient was observed, and its magnitude never increased to values close to unity. Therefore, it can be concluded that the polishing of the probe was an effective solution for establishing coherent and

repeatable PEFE treatments. Within this experiment, the signal generator was switched off after 15 seconds as the temperature had reached 42℃.

3.6.1.2 Sterilization of probe tip

After initial experiments, contamination of cultured cells was observed 24 hours later. The contamination was probably due to bacteria or fungi which originally attached to the probe. The introduced bacteria or fungi would compete with the cultured cells for space and nutrition, eventually leading to cell death. More seriously, it would be able to induce faults when evaluating the number of cells using MTT assays. As a result, sterilization of the probe tip was required to ensure correct experiment results.

One dedicated disinfection solution named 'Pharmacidal™ Sprays and Solution' was used for sterilization of the probe, as shown in Figure 3.21. This disinfection solution is quite effective and widely used in biological labs and incubators. When cancer cells are cultured in 96 well plates, they are isolated from any high concentration of the disinfection solution. However, the cultured cells will be directly exposed to high concentrations of this disinfection solution when inserting the sterilized probe into the 96 well plate. Although the probe can be washed using PBS after sterilization, any residue still needs further investigation on whether it can impact on the viability of cancer cells.

One experiment carried out used a sterilized probe without any injected microwave signal that was immerged into a medium for 15 minutes. Prior to experiments, the probe was washed with PBS to minimize the residual disinfection solution. The cell number was calculated using an MTT assay immediately before experiments ('0h'), 24 hours ('24h') and 48 hours ('48h') post experiments. The results are shown in Figure 3.22.

Figure 3.21 Disinfection solution named 'Pharmacidal™ Sprays and Solution'. Source: https://www.bioind.com/worldwide/pharmacidal-spray-solutions/

No contamination was observed during the period of 48 hours after the experiment. The cells within the control group showed a sustained growth with the number of cells increasing over time. However, a reverse pattern was observed with the cells exposed to the sterilized probe. The number of cells decreased within 48 hours, indicating that this disinfection solution was able to induce cell death and add errors to the experimental PEFE outcomes.

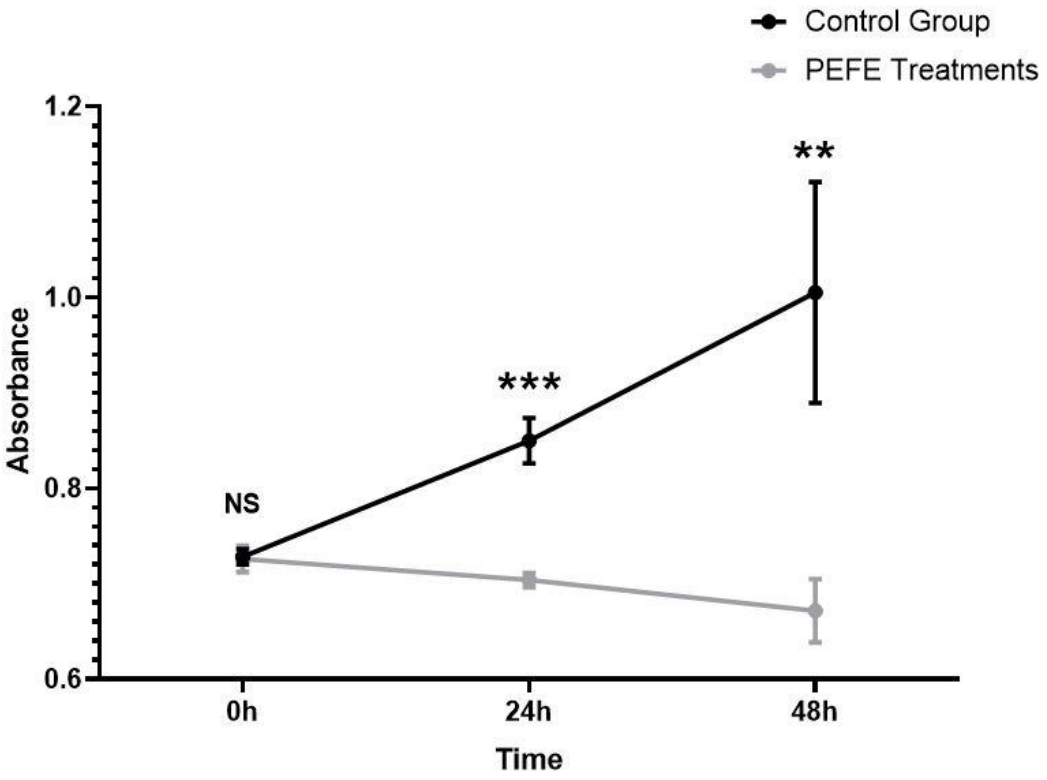

Figure 3.22 Calculated cell number using sterilized probe without any PEFE (n = 3). Error bar stands for standard error of means. **p <0.01, ***p<0.001. No statistical significance ('NS') was observed immediately after experiments ('0h').

Another alternative scheme for sterilization was to expose the probe to UV light for 2 hours then wash it with 70% Ethanol followed by PBS washing. Since the Ethanol is volatile at room temperature, there should be little residual Ethanol on the probe after washing with PBS. To investigate whether this approach could achieve sterilization and eliminate any effect on cell viability, some experiments were conducted using the sterilized probe without any microwave signals and the results are shown in Figure 3.23.

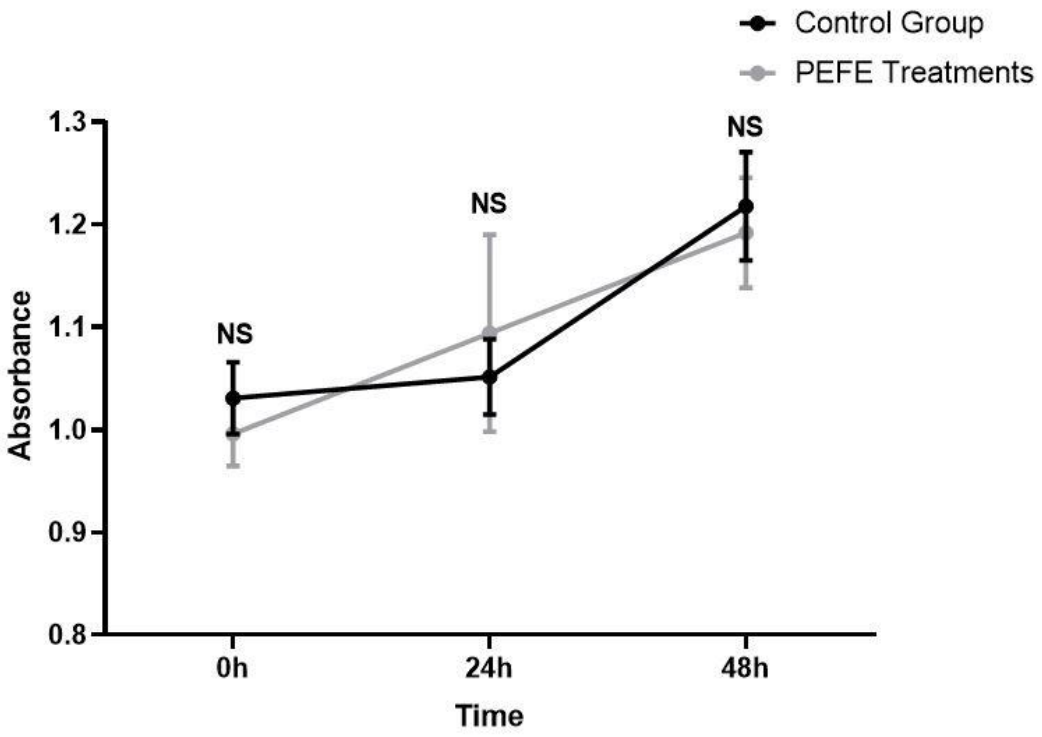

Figure 3.23 Calculated cell number using sterilized probe without any PEFE (n = 3). Error bars stand for standard error of means. No statistical significance ('NS') was observed at each designated time.

No contamination was observed during the period of 48 hours, demonstrating that this alternative approach produced an effective sterilisation method. Furthermore, there were no significant differences between the numbers of cells in the control group over the entire duration of 48hrs after the experiment. As a result, this approach for sterilization was proven to be optimal and could be applied in subsequent PEFE treatments.

3.6.2 Temperature profile during PEFE treatments

When the probe was polished to minimize the formation of a gaseous layer, the resulting temperature profile during PEFE treatments was investigated. The results are shown in Figure 3.24. Before the experiments, the temperature of the biological medium was measured at 25.3℃, then the temperature increased rapidly in the first 16 seconds of the PEFE treatment. When the temperature was very close to 42℃, the generator was switched off to prevent further temperature increase. When the

temperature fell back to 37℃, the PEFE was injected again. This process was controlled and repeated manually during the entire treatments.

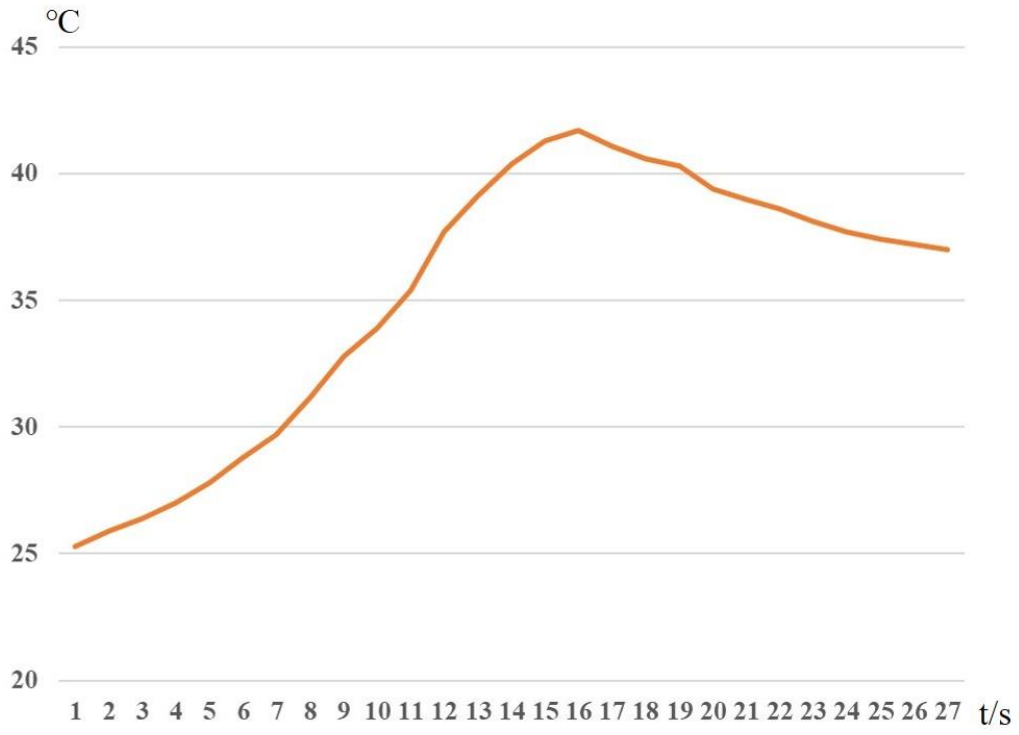

Figure 3.24 Temperature profile during PEFE treatments, observed within first 30 seconds.

3.6.3 Results of initial experiments based on the improvement of probe handling

Once the probe handling was improved, the PEFE treatments were performed and the results are shown in Figure 3.25.

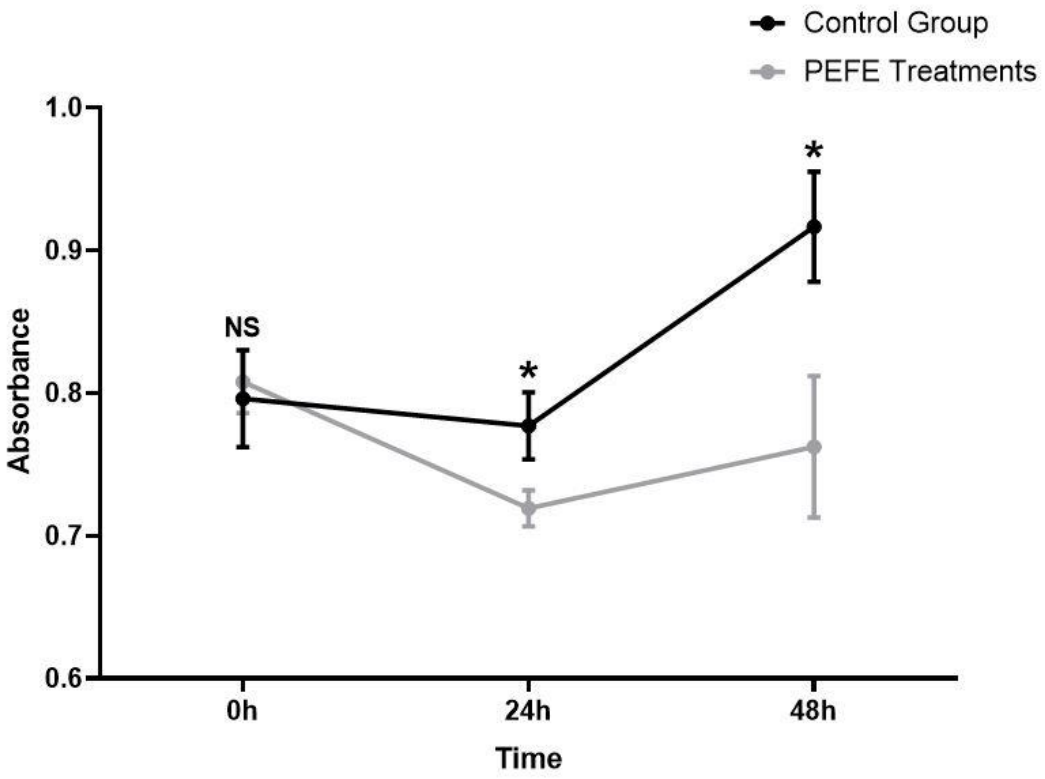

Figure 3.25 The outcome of PEFE treatments based on improved probe handling (n = 3). Error bar stands for standard error of means. *p <0.05. No statistical significance ('NS') was observed immediately after experiments ('0h').

Figure 3.25 shows significant differences in cell numbers were observed between the control group and the cells exposed to PEFE 24 and 48 hours after treatments, respectively. The decreased cell number, compared with the control group, indicated a significant cell death induced by PEFE treatments.

3.6.4 Discussion

During the PEFE treatments, it was essential that the injected microwave signals penetrated towards the cancer cells through the biological medium. The medium and the resulting impedance mismatch at the probe tip allowed only part of the microwave to propagate towards the cells with the remainder of the microwave power being reflected back into measurement set-up, Once the microwave power was propagated inside the medium, a high temperature localised at the probe tip

was produced resulting in chemical reactions leading to formation of a gaseous layer. The produced bubbles adhered to the probe tip, preventing microwave signals from propagating into the medium resulting in a rapidly increasing S_{11} magnitude as the experiment progressed. After polishing of the probe tip, much better PEFE performance was observed with the microwave signals able to consistently propagate into the medium and reach the cancer cells.

Although the experiments were conducted inside a Class II laminar flow cabinet (SafeF ST Classic, FASTER), only the bacteria and fungi floating in the air were able to be isolated from the cancer cells. The bacteria and fungi which originally adhered to the probe should be considered and effectively removed to prevent false PEFE results. According to the results of the experiments, described in section 3.6.1.2, it can be concluded that sterilization of the probe through an appropriate approach is crucial when assessing the results of PEFE treatment. Furthermore, the improved scheme for sterilization was proposed to ensure accurate results in the subsequent PEFE treatments.

Based on the entire improvement of probe handling, the PEFE treatments were repeated. The results showed a successful cell-killing effect induced by PEFE treatments. It is well known that MTT is quite accurate in viable cell counting and widely used in proliferation assays. It is still necessary to further investigate whether the use of MTT assay fits well with this research. In this research, the number of viable cells was evaluated immediately before experiments, 24 hours, and 48 hours after experiments respectively. While the PEFE treatments did induce cell death, there was less likelihood of achieving complete cell eradication according to MTT assays, indicating that only some of the treated cells died. The remaining cells sustained normal growth and division over time. Thus, even with the existing dead cells, the number of viable cells was also likely to keep increasing over time, which made it confusing to draw conclusions about the effectiveness of the treatment. As for the control group, the number of cells was not able to significantly increase according to the growth curve for the cell line used, shown in Figure 3.26. The initial number of cells was 9×10^4 per well, which was almost in the stationary phase. As a result, there would not be a significant difference between the measured numbers of treated cells in a well and a well within the control group.

In the subsequent PEFE treatments, the cell viability assessment should be conducted targeting dead cells rather than viable cells. Trypan blue staining has been proven to be an effective approach for viability assessment. As a permselective membrane, intact cellular membrane cannot allow trypan blue to permeate it. Once the cells die, the disrupted membrane structures will allow trypan blue to permeate, hence staining the cells. Therefore, microscopy can distinguish between living and dead cells through varying colourisation. To calculate the number of dead cells, a dedicated cell counting chamber slide (Fisher Scientific UK Ltd) and Countess™ II Automated Cell Counter (Thermo Fisher Scientific Inc.) should be used in future PEFE treatments.

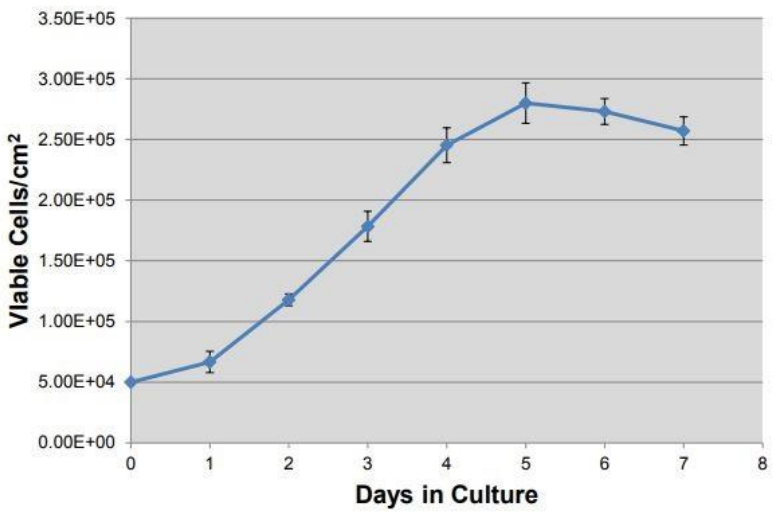

Figure 3.26 Growth curve of MDA-MB-231 cell line. Source: https://physics.cancer.gov/docs/bioresource/breast/NCI-PBCF-HTB26_MDA-MB-231_SOP-508.pdf

Furthermore, it is also worth investigating how soon PEFE treatments can induce cell death. The cell viability assessments should also be performed immediately after treatments. This may provide some indications about the types of cell death being induced by PEFE.

3.5 Summary

In the area of study described in this chapter, a PEFE system was constructed with a series of microwave devices with suitable frequency and input power levels. The details of each component were introduced and studied to ensure microwave signals were correctly delivered. In order to precisely adjust input power levels and achieve accurate data analysis, system calibration was performed. Once system calibration was completed, the PEFE became operational at the desired frequency and power levels. The electric field distribution inside the well was simulated using COMSOL Multiphysics to confirm that the injected PEFE signal was able to penetrate towards the cultured cancer cells.

Establishment of proper probe handling was crucial to minimize experimental failures. The main failure relating to the probe was the formation of a gaseous layer that blocked microwave signals from penetrating into the medium. Also, it was determined that an unsuitable sterilization induced unexpected cell death. The improvement in probe handling and treatment, allowed for repeatable and coherent PEFE investigations.

The approach for assessing the results was examined in terms of its validity. The dead cells were ignored when the MTT assays were selected to assess the results due to targeting of viable cells. If the treatments were only effective in some of the cultured cells, the MTT results might not be able to provide consistent outcomes. Thus, trypan blue staining was established as a better alternative as it targets dead cells and allows for separate counts of viable and dead cells when using a dedicated cell counting chamber and instrument. The outcomes of the improved PEFE treatments will be presented and discussed in the following chapters.

Chapter-4

The Usage of PEFE in Treating Breast Cancer Cells *In vitro* and *In vivo* with the Involvement of Potential Protein Regulators

4.1 Introduction

For the past few decades, microwave technologies have been used in medical fields for the diagnosis and treatment of human disease, including cancer. In addition to its relatively low-cost, microwave diagnostic techniques are non-ionic thus enjoying, to some degree, the advantage of an innocuous nature compared with some of the other traditional diagnostic techniques, such as CT. Importantly, microwave diagnostic techniques might have other advantages that are yet to be further interrogated including width of frequency, that may deliver better resolution in diagnosing the disease.

The introduction of microwave technologies to medical treatments has been established for some time. A particular area in this case is in cancer treatment, namely application of microwave ablation (MWA) or combined with other therapies such as chemotherapies and radiotherapies, as an adjuvant treatment. Microwave ablation is usually operated at a high-power level to achieve rapid local high temperatures in excess of 60℃ to ensure complete destruction of cancer tissues. When operated as an adjuvant treatment to assist chemotherapies or radiotherapies, microwaves can be injected at a relatively low power level to supply mild hyperthermia and enhance the efficacy of the conventional therapies. Although there have been success stories, these applications tend to be on large tumours and in solid organs, namely cancers of the liver and kidneys. A key reason for the choice has been the high temperature induced collateral injury to the surrounding normal tissues and adjacent organs. The collateral thermal injuries tend to result in severe and lasting side effects, which are likely to be intolerable to the patients. The thermal based ablation thus makes it an unlikely choice for small tumours and for tumours in tissues/organs with fine tissue structure and vital surroundings.

As presented in the previous chapter, pulsed electromagnetic fields exposure (PEFE) operated microwaves at high power levels such as 30 watts, 40 watts, and 50 watts, meanwhile, while strictly limiting the temperature increase through pulsing the delivered energy. Temperature monitoring was performed during the treatments to ensure local temperature did not exceed 42℃. This technique has the advantage of injecting high levels of electromagnetic fields and maintaining much

lower temperatures during the treatments in comparison with MWA, and we considered the technologies a novel technique to treat breast cancer cells and conducted series *in vitro* and *in vivo* investigation.

The impact of PEFE on cell death, cell permeability, and expression of various genes in breast cancer cells under PEFE treatment was examined in the current study. We also aimed to discover if an apoptosis and neural-related scaffold protein named Kidins220 has a role in regulating PEFE induced apoptosis of breast cancer cells. Furthermore, the hypothesis of whether Kidins220 expression could act as an indicator to predict the PEFE treatment efficiency of breast cancer patients, or to evaluate its role as a potential biomarker to select patients who are better candidates for PEFE treatments was also tested.

4.2 Methodology

4.2.1 Cells preparation

Cells used in this study included breast cancer cells and primary cultured breast cells. For each cell line involved in treatments, 8×10^4 cells were seeded per well in both treatment and control groups in 96-well plates in triplicate. The layout of this experiment is shown in Figure 4.1.

The cells were allowed sufficient time to settle down and attached to the surface of the culture ware. Cell confluency was inspected to ensure seeded cancer cells formed a monolayer prior to treatment. Once confluency was reached, the cell culture medium was refreshed with 200µl complete cell culture medium, which was sufficient to completely immerge the probe and temperature sensor.

4.2.2 Viability assessment

In this research, cell viability assessment was performed using trypan blue exclusion tests. The tests were carried out prior to PEFE treatments, immediately after PEFE treatments, and 24 hours and 48 hours after treatments, respectively. Cell death rate was calculated using a cell counting chamber slide (Fisher Scientific UK Ltd) and Countess™ II Automated Cell Counter (Thermo Fisher Scientific Inc.).

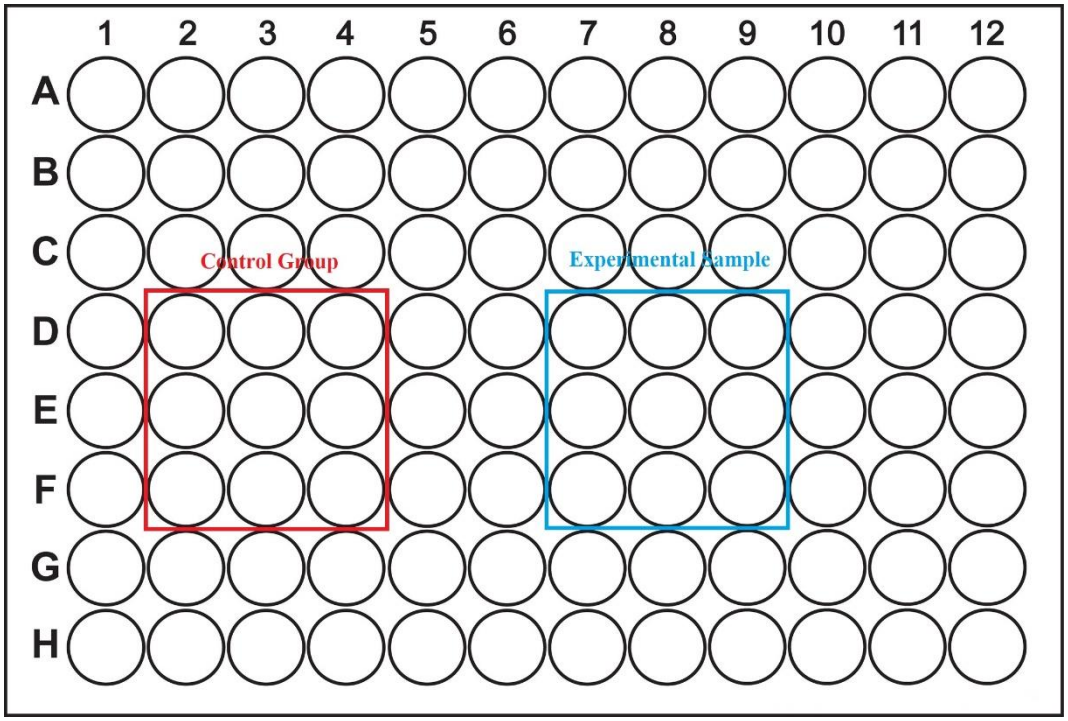

Figure 4.1 Cancer cells seeded in a 96 well plate

4.2.3 Effects of temperature only on cancer cells

When electromagnetic fields (EMFs) were injected into cancer cells cultured *in vitro*, most of the EMFs propagated back to the circuits and were then absorbed by attenuation. The small part of the EMFs which dissipated in the cell culture medium might be able to elicit a significant temperature increase. Campbell, 1990 has reported that cell death started when the temperature exceeded 42°C(Campbell, 1990). Thus, pulsed EMFs which were also within the range of PEFE, were used in this research to limit the temperature during the treatment of cancer cells. In order to confirm that the induced cell death was indeed due to PEFE itself instead of high temperatures, the initial experiments were conducted with high temperatures only, in order to investigate how this high temperature might affect the death of cancer cells.

A dedicated heating pad was used to heat the cultured cancer cells. The cancer cells attached to the bottom of a 96 well plate and this plate was placed directly on the heating pad in the incubator when conducting experiments. The temperature was

set at 40℃ and 45℃ sequentially, limited by heating pad configuration. When heating was completed, the heating pad was removed, and the heated cancer cells were then cultured for subsequent viability assessments.

4.2.4 PEFE treatment instrumentation

The microwave devices required in PEFE treatments were connected as illustrated in section 3.1. System calibration was performed immediately prior to use as shown in section 3.2. Notably, system calibration had to be performed again when some of the microwave devices were changed or system frequency was changed. Furthermore, system calibration was also required when the PEFE system was idle a for long time. Once calibrated, the desired power level was calculated and set in the generator side, illustrated in section 3.3. PEFE treatments were performed with triple replicates for each condition, and each PEFE treatment lasted 15 minutes.

A dedicated holder was manufactured to hold the 96 well plate containing the cancer cells. This holder not only fixed and centralised the probe and temperature sensor in the well, not reaching the bottom where the cells were attached, but also adjusted the distance from the probe tip to the bottom of the well. In this research, two distances were selected to investigate how PEFE affected cancer cells, including 1mm and 3mm.

4.2.5 Transmission electron microscopy (TEM)

As demonstrated in section 2.14, cancer cells and primary cultured breast cells were treated with PEFE respectively. The PEFE was generated at 2.2GHz with 50 watts power level. The distance between the probe tip and the bottom of petri dish was fixed at 1mm. The results were visualised through TEM.

4.2.6 Frequency influence on cancer cell death

In this study, how different frequencies affected cancer cells was investigated. Two separate frequencies were selected which were 2.2GHz and 5.8GHz. The 5.8GHz frequency has been widely applied in the industrial field, such as in wireless communication, in scientific research and medical applications. The other frequency, 2.2GHz was also chosen because of the practicality, in that the current

microwave devices in the laboratory such as the circulator, could only be operated at this frequency.

For each experimental setting, two 96 well plates containing cancer cells were prepared and cultured in an incubator until monolayers were formed. The PEFE system was first calibrated at 2.2GHz then PEFE treatments were performed with the first 96 well plate. When treatments were completed, cancer cells were returned to the incubator. The PEFE system was then calibrated at 5.8GHz. Once calibrated, the second 96 well plate containing cancer cells was treated with PEFE. When treatments were completed, cancer cells were returned to the incubator. The conditions of PEFE treatments are listed in Table 4.1.

Table 4.1 Configurations of PEFE treatments in this study

NO.	Frequency	Input Power	Pulse Width	Pulse Period	Distance
1	2.2GHz	30 watts	50μs	1ms	1mm
2		50 watts			
3	5.8GHz	30 watts			
4		50 watts			

4.2.7 Electric field strength influence on cancer cell death

In this research, electric field strength was adjusted by two means. One method was to change the input power level while maintaining the distance from the probe tip to the bottom of the 96 well plate. The other method was to change the distance while maintaining the same input power level.

In this study, frequency was fixed at 2.2GHz and likewise, the pulse width was fixed at 50μs while the pulse period was kept at 1ms.

4.2.7.1 Power level change

The distance from the probe tip to the bottom of the 96 well plate was fixed at 1mm. The input power level was increased from 20 watts to 50 watts, the exposure scheme is listed in Table 4.2.

Table 4.2 PEFE treatment scheme

NO.	Input Power	Pulse Width	Pulse Period	Time
1	20 watts	50μs	1ms	15 mins
2	30 watts			
3	40 watts			
4	50 watts			

When the cultured cancer cells were ready for use and the PEFE system was calibrated at 2.2GHz, PEFE treatments were conducted with each input power level at designated time. Cell viability was assessed at the end of the entire experiments.

4.2.7.2 Distance change

The input power level in this study was selected at 50 watts, and the distances ('D') from probe tip to the bottom of the 96 well plate was fixed at 1mm and 3mm (Table 4.3). Two 96 well plates containing cancer cells in monolayers were prepared before treatments. When the PEFE system was calibrated, the first 96 well plate with cancer cells was placed in the holder and the distance was adjusted to 1mm. The cancer cells were treated with PEFE then returned to an incubator. The second 96 well plate with cancer cells was placed on the holder and the distance was adjusted to 3mm. After PEFE treatments, the cancer cells were cultured in the incubator for subsequent experiments.

Table 4.3 Configurations of PEFE treatments in this study

NO.	D	Input Power	Pulse Width	Pulse Period	Frequency
1	1mm	30 watts	50μs	1ms	2.2GHz
2		50 watts			
3	3mm	30 watts			
4		50 watts			

4.2.8 Pulse parameters influence on cancer cell death

In this study, the frequency of PEFE was selected at both 2.2GHz and 5.8GHz respectively, and the distance from probe tip to the bottom of the 96 well plate was fixed at 1mm, meanwhile, the input power level was maintained at 50 watts. The pulse parameters of PEFE were changed and listed in Table 4.4.

Table 4.4 Pulse parameters applied in this study

NO.	Pulse Width	Pulse Period	Duty Cycle
D1	200µs	4ms	5%
D2	10µs	200µs	
D3	5µs	100µs	
D4	200µs	1ms	20%
D5	10 µs		1%
D6	5µs		0.5%

When cultured cancer cells were ready and the PEFE system calibration was completed, PEFE treatments were conducted with each combination of pulse parameters. The treated cancer cells were then returned to the incubator for viability assessment.

4.2.9 Cancer cell lines influence on cancer cell death

In this study, four different kinds of cell lines were treated in order to investigate whether PEFE treatments affected cancer cells was cell line specific. The four cell lines were all from human breast cancer, details listed in section 2.1. These cell lines, with varying hormone receptor status and invasiveness, were cultured individually in four 96 well plates until a monolayer was formed. The configurations of PEFE is listed in Table 4.5.

Table 4.5 The configurations of PEFE treatments in this study

Frequency	Input Power	Pulse Width	Pulse Period	Distance
2.2GHz	20-50 watts	50µs	1ms	1mm

When cultured cancer cells were ready and the PEFE system calibration was completed, PEFE treatments were conducted with each cell line. The treated cancer cells were then returned to the incubator for future experiments.

4.2.10 Further analysis on cell viability for PEFE treatments

In order to further analyse how PEFE treatments interacted with cultured cancer cells, the cell viability assessment was performed in a different fashion. The cell line used in this study was MDA-MB-231. The PEFE treatments was conducted at 2.2GHz with 50 watts input power with triple replicates. The distance from the

probe tip to cells was fixed at 1mm, which produced the highest electric fields on cells. Cell viability was assessed before treatment ('BE'), immediately after treatment ('IE'), and 24 hours and 48 hours post treatment, and presented here as the number of dead cells and death rate.

When performing the cell counting of dead cells, those floating in the medium (*Nf*) and those still on the bottom of the well (*Nb*) were calculated separately. The total number of dead cells (*Nd*) at each time was calculated using the following equation:

$$Nd = Nf + Nb$$

When calculating the number of dead cells, the total cells (*NT*) including dead and alive cells were calculated accordingly, the death rate (*R*) at each designated time was calculated using the equation below:

$$R = Nd / NT * 100\%$$

The cell morphology was inspected before and immediately after treatment. Furthermore, Transmission electron microscopy (TEM) was used to investigate how PEFE treatments affected the cell membrane and cellular organelles.

4.2.11 *In vivo* animal study

The *in vivo* PEFE treatments were conducted using a nude mice model with MDA-MB-231 breast cancer cells injected subcutaneously. When the size of tumour reached an approximate size of 1cm in diameter, the mice were treated. Anaesthesia (4% chloral hydrate, 100µl per mouse) was carried out for each mouse to alleviate pain prior to treatment. The temperature of the treated area was monitored throughout the treatment. Tumour sizes were measured every 3 days for a total 36 days' duration. The treatment protocol is illustrated in section 2.10.

4.2.12 Cell model establishment using MDA-MB-231 and MCF-7 with Kidnis220 knockdown

MDA-MB-231 and MCF-7 cell lines were used to knockdown Kidins220 by lentivirus shRNA, detailed in section 2.6. The Kidins220 knockdown after transfection was verified by qPCR and Western Blot (n = 3), detailed in section 2.4

and 2.5 respectively. The genetically modified cells were tested in their response to PEFE and were compared to the control cells.

4.2.13 Cellular migration quantification using ECIS

The cell lines used in this study were MDA-MB-231 scramble (SC) and Kidins220 knockdown (KD) together with MCF-7 scramble (SC) and Kidins220 knockdown (KD). Each cell line was seeded at 1×10^5 per well containing 200µl medium for 8 wells in the 96W1E array (Applied Biophysics Inc, NY, USA). The array was then placed in the Theta ECIS controller system (Applied Biophysics Inc, NY, USA) and the cellular migration measurements continued for 6 hours.

4.2.14 PEFE treatments using MDA-MB-231 and MCF-7 cell lines losing Kidins220

Cell models of Kidins220 knockdown (KD) and scramble control (SC) were established using MDA-MB-231 and MCF-7 cell lines, according to section 2.6. Cell migration assays were conducted using Electric Cell-Substrate Impedance Sensing (ECIS) in the established cell models, detailed in section 2.11. Prior to PEFE treatments, 9×10^4 cells from each cell line were seeded with 200µl biological medium and allowed sufficient time to adhere. Each treatment included 3 replicates and the entire treatments were repeated 3 times for each cell line. Cell viability was assessed using trypan blue staining, detailed in section 2.15.

4.3 Results

4.3.1 Investigation on heat only affecting cancer cells

In this study, the heating pad was allowed sufficient time to reach the assigned temperature. The heating lasted for 20mins in order to ensure the cells were heated at the designated temperature for 15 mins, taking the temperature dissipation in the incubator and the efficiency of energy transportation into consideration. The results are shown in Figure 4.2 and Figure 4.3.

When the cultured cancer cells were heated at 45℃ directly, a significantly rapid cell death (78.87%) was observed immediately after the experiments compared to that before the experiments (11.79%). In the following 48 hours, the death rate did

not change significantly, indicating that direct heating at 45℃ for 20mins was able to induce significant cell death.

As for direct heating at 40℃, cell viability was evaluated before experiments and only 15.79% of the cultured cells died. After experiments, no significant changes in the death rate was observed until 48 hours later (24.33%). This increase in the death rate after 48 hours was thought to be largely due to normal cell senescence rather than cell death, indicating that direct heating at 40℃ was safe for cell viability.

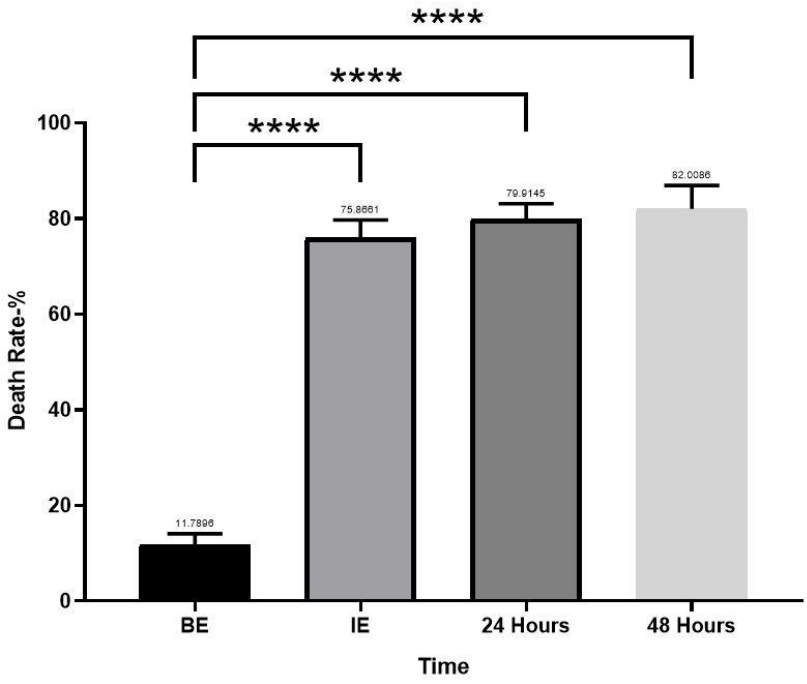

Figure 4.2 Death rate of the cancer cells that underwent direct heating only at 45℃ for 20 mins (n = 3). The death rate was calculated before experiments ('BE'), immediately after experiments ('IE'), and 24 and 48 hours after experiments. Error bar stands for standard error of means (SEM). *******p*<0.001.

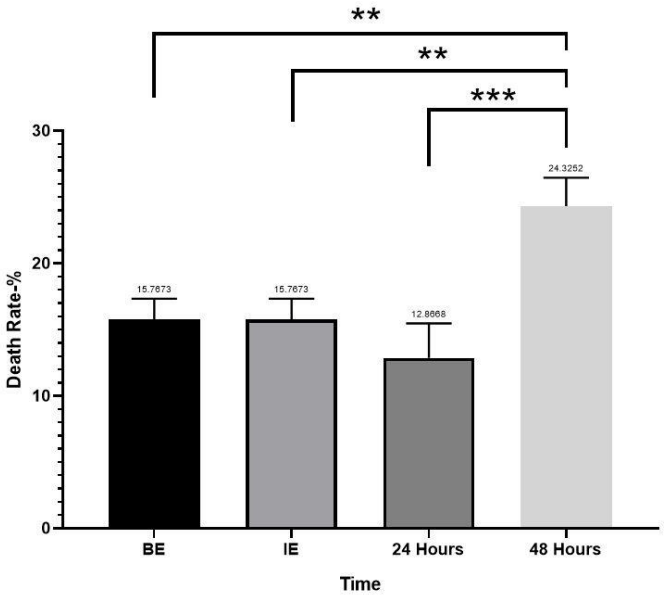

Figure 4.3 Death rate of the cancer cells that underwent direct heating only at 40°C for 20 mins (n = 3). The death rate was calculated before experiments ('BE'), immediately after experiments ('IE'), and 24 and 48 hours after experiments. Error bar stands for SEM. *p<0.05, **p <0.01, ***p<0.001.

Following these observations, an optical fibre sensor was used. The sensor was injected into the wells of a 96 plate together with the PEFE probe and was located very close to the probe tip without reaching the bottom of the culture wells. When performing PEFE treatments, the temperature was constantly monitored by the sensor to keep the temperature of cancer cells below 40°C. This was a fundamental aspect of the current study in order to confirm that any of the changes that occurred in the cancer cells were triggered by the PEFE rather than the temperature.

4.3.2 Investigations on different frequencies affecting cancer cell death

When the frequency of PEFE was set at 2.2GHz, PEFE treatments were performed at 30 watts and 50 watts input power, with shared control groups. Cell death rate was calculated and shown in Figure 4.4 and 4.5, respectively.

In Figure 4.4, cell viability was checked prior to the experiment, and showed only 8.07% of the cultured cells died. Immediately after treatment, the death rate of treated cells significantly increased to 15.93% while no changes were observed in the control group. Twenty-four hours post treatment, a much higher death rate (38.97%) was significantly exhibited compared to the control group (16.67%). Forty-eight hours after treatment, the evaluated death rate of treated cells (43.28%) was significantly higher than that of the control group (13.19%). Furthermore, the increased death rate of the treated cells at 48 hours post treatment was not significant compared to that evaluated at 24 hours post treatment, indicating the PEFE treatment induced approximately 30% of cell death.

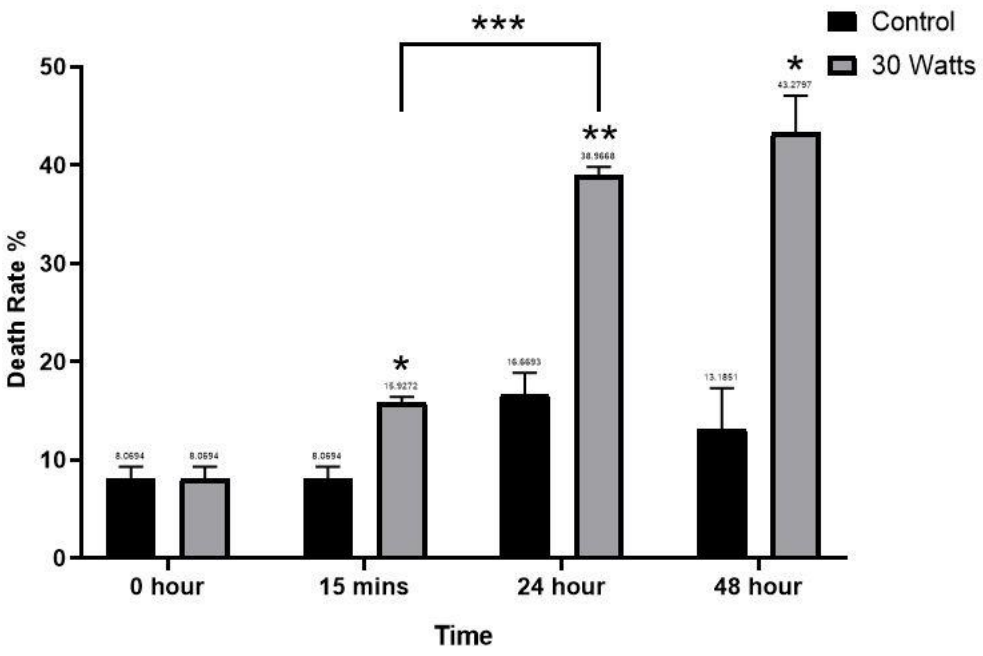

Figure 4.4 Death rate of cultured cancer cells that underwent PEFE treatments and control group at 2.2GHz and 30watts (n = 3). The probe was placed at 1mm from the bottom of the well. Cell viability was assessed before treatments ('0 hour'), immediately after treatments ('15 mins'), and 24 and 48 hours after treatments. Error bar stands for SEM. *p<0.05, **p <0.01, ***p<0.001.

When the power level was altered to 50 watts (Figure 4.5), a significant increase in the death rate was seen immediately after treatment (30.39%) compared to the control group (8.07%). This death rate continued to rise significantly after 24 hours (47.88%) and 48 hours (56.57%). The control group only showed a marginal and insignificant rise, 16.67% and 13.19% after 24 and 48 hours, respectively. The PEFE treatments with 50 watts input power was able to induce approximately 40% of cell death.

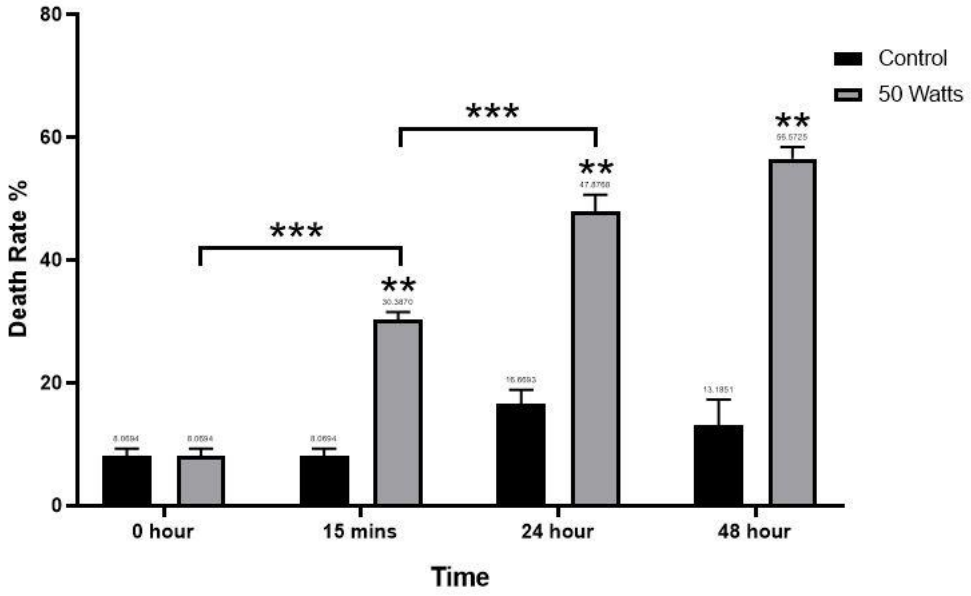

Figure 4.5 Death rate of cultured cancer cells that underwent PEFE treatments and control group at 2.2GHz and 50watts (n = 3). The probe was placed at 1mm from the bottom of the well. Cell viability was assessed before treatments ('0 hour'), immediately after treatments ('15 mins'), and 24 and 48 hours after treatments. Error bar stands for SEM. *****p* **<0.01, ******p*****<0.001.**

When the frequency of PEFE was altered to 5.8GHz, PEFE treatments were also performed with input power of 30 watts and 50 watts with shared control groups. The results are shown in Figure 4.6 and 4.7, respectively.

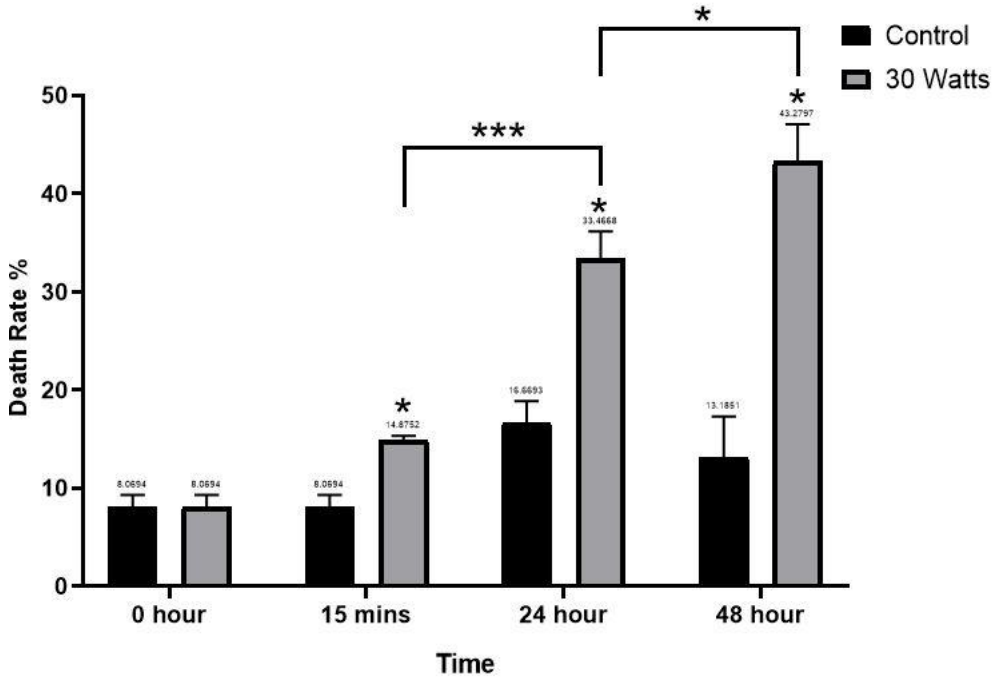

Figure 4.6 Death rate of cultured cancer cells that underwent PEFE treatments and control group at 5.8GHz and 30watts (n = 3). The probe was placed at 1mm from the bottom of the well. Cell viability was assessed before treatments ('0 hour'), immediately after treatments ('15 mins'), and 24 and 48 hours after treatments. Error bar stands for SEM. *p<0.05, **p <0.01, ***p<0.001.

When PEFE at 30 watts was applied, 14.88% of the treated cancer cells died immediately after treatment while only 8.07% of cancer cells died in the control group. The death rate significantly increased to 33.47% and 43.28%, 24 and 48 hours after the treatment (Figure 4.6). In contrast, the death rate in the control group was approximately at 14% during the 48 hours period. When the input power level increased to 50 watts, the death rate in the treated cells (22.89%, 40.88%, 48.57%) were significantly higher than that in the control group (8.07%, 16.67%, 13.19%) at each of the three time points (Figure 4.7). Furthermore, a significantly increased

death rate in the treated cells (from 22.89% to 40.88%) was observed within the first 24 hours after treatment.

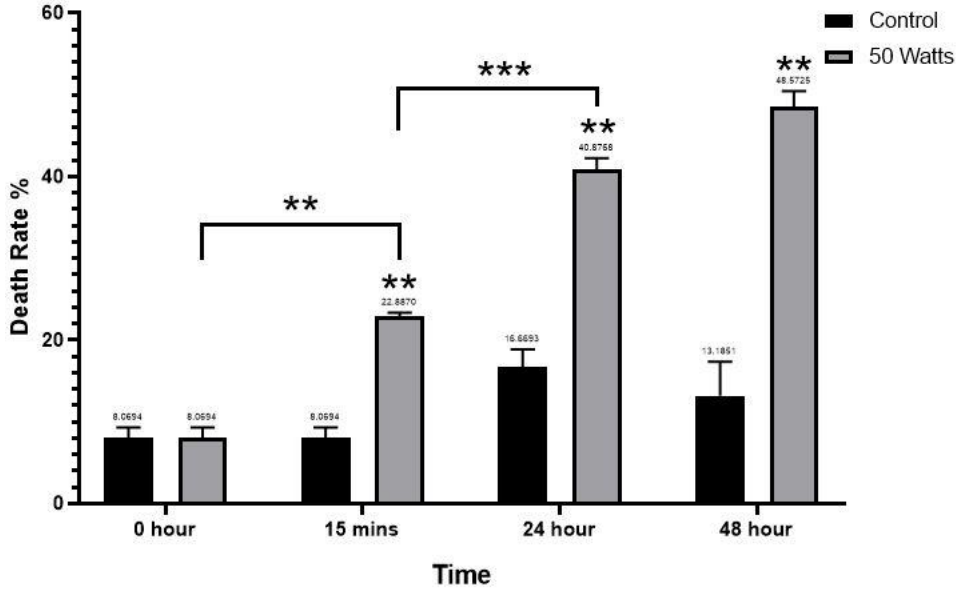

Figure 4.7 Death rate of cultured cancer cells that underwent PEFE treatments and control group at 5.8GHz and 50watts (n = 3). The probe was placed at 1mm from the bottom of the well. Cell viability was assessed before treatments ('0 hour'), immediately after treatments ('15 mins'), and 24 and 48 hours after treatments. Shown in the figure are mean and SEM. *****p* **<0.01, ******p*****<0.001.**

4.3.3 Investigation on different electric field strength impacting cancer cells

4.3.3.1 Varied electric field strength by adjusting input power levels

In this study, the control group was shared by each PEFE treated sample. The death rate of the control group at each time was 3.05%, 30.5%, 7.62% and 18.72% respectively. In Figure 4.8, each power level was able to induce a significant increased death rate compared to the control group, indicating that the PEFE treatment under each power level was capable of achieving cell-killing to cultured cancer cells. For the cells which underwent PEFE treatment, the death rate under different power levels were compared and statistically analysed. The results are

illustrated in Table 4.6. Furthermore, the death rate at different times under each power level was also compared and the results are listed in Table 4.7 to Table 4.10.

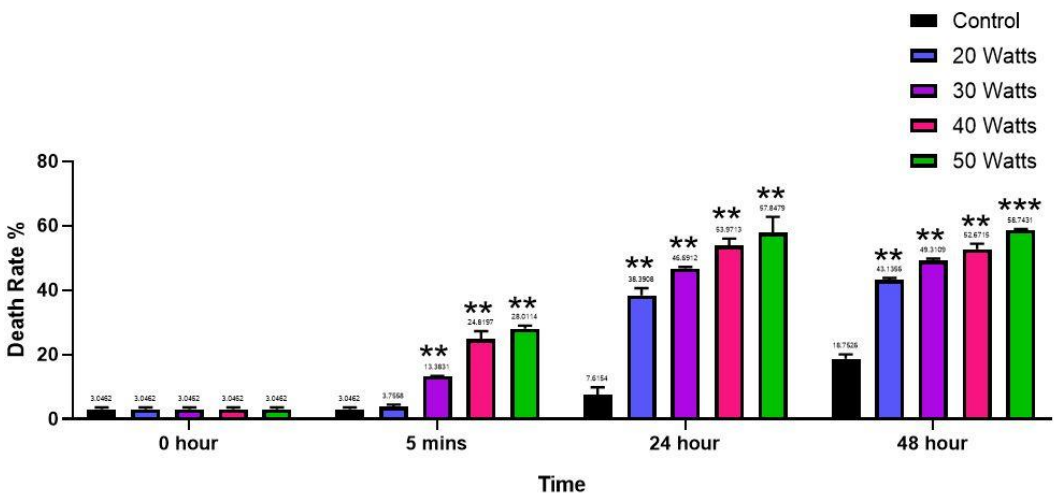

Figure 4.8 Cell death rate for cells that underwent PEFE treatments and control group evaluated before treatments ('0hour'), immediately after treatments ('15mins'), and 24 and 48 hours after treatments, respectively (n = 3). PEFE was generated at 2.2GHz, with input power level ranging from 20 watts to 50 watts. The probe was fixed at 1mm from bottom of the well. Shown in the figure are mean and SEM. *****p* **<0.01, ******p*****<0.001.**

Table 4.6 Statistical significance when comparing results under varied power levels (**p*****<0.05, *****p*** **<0.01, ******p*** **and *******p*****<0.001, NS--'Not Statistical', W--'watts')**

	0 Hour	15 mins	24 Hours	48 Hours
20 W *vs* 30W	--	**	*	**
20 W *vs* 40W	--	**	*	**
20 W *vs* 50W	--	**	*	**
30 W *vs* 40W	--	*	*	*
30 W *vs* 50W	--	**	**	NS
40 W *vs* 50W	--	NS	NS	*

Table 4.7 Statistical significance when comparing results at varied time using 20W (*p<0.05, ****p<0.001)

0 Hours	15 mins	24 Hours	48 Hours
15 mins	--	****	****
24 Hours		--	*
48 Hours			--

Table 4.8 Statistical significance when comparing results at varied time using 30W (**p<0.001, NS--'Not Statistical')**

0 Hours	15 mins	24 Hours	48 Hours
15 mins	--	****	****
24 Hours		--	NS
48 Hours			--

Table 4.9 Statistical significance when comparing results at varied time using 40W (**p<0.001, NS--'Not Statistical')**

0 Hours	15 mins	24 Hours	48 Hours
15 mins	--	****	****
24 Hours		--	NS
48 Hours			--

Table 4.10 Statistical significance when comparing results at varied time using 50W (*p<0.05, ****p<0.001)

0 Hours	15 mins	24 Hours	48 Hours
15 mins	--	****	****
24 Hours		--	*
48 Hours			--

It is clear from Table 4.6 that a higher input power level resulted in an increased death rate in treated cancer cells, especially in the first 24 hours after PEFE treatment. However, the significantly increased death rate only existed at 48 hours post treatment when comparing input power level at 40 watts and 50 watts.

In Table 4.7 and Table 4.10, a significant increase in death rate was observed over time when input power level was selected at 20 watts and 50 watts. Interestingly, when 30 watts or 40 watts input power was injected, significantly increased death rate was observed in the first 24 hours post treatment, but not at 48 hours after treatment.

4.3.3.2 Varied Electric field strength by adjusting the height of probe

In this part of the study, the impact of the distance between the probe and cells on the death rate of breast cancer cells was investigated. The probe was located at 3mm and 1mm from the bottom of the 96 well plate respectively. The death rate of cancer cells is shown in Figure 4.9 (3mm) and Figure 4.10 (1mm).

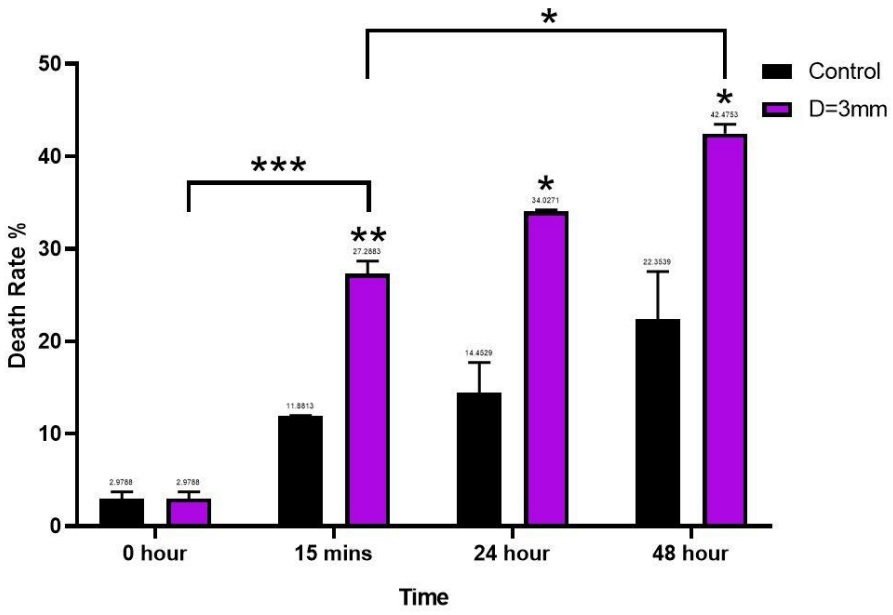

Figure 4.9 Cell death rate for cells that underwent PEFE treatments and control group evaluated before treatments ('0hour'), immediately after treatments ('15mins'), and 24 and 48 hours after treatments, respectively (n = 3). PEFE was generated at 2.2GHz, with input power level at 50 watts. The probe was fixed at 3mm from bottom of the well. Error bar stands for standard error of means. *p<0.05, **p <0.01, ***p<0.001.

In Figure 4.9, an increased death rate of treated cells was seen and this death rate was significantly higher than that observed in the control group at each time point post treatment (27.29% *vs* 11.88% at 15mins, 34.03% *vs* 14.45% at 24 hours, and 42.48% *vs* 22.35% at 48 hours, respectively).

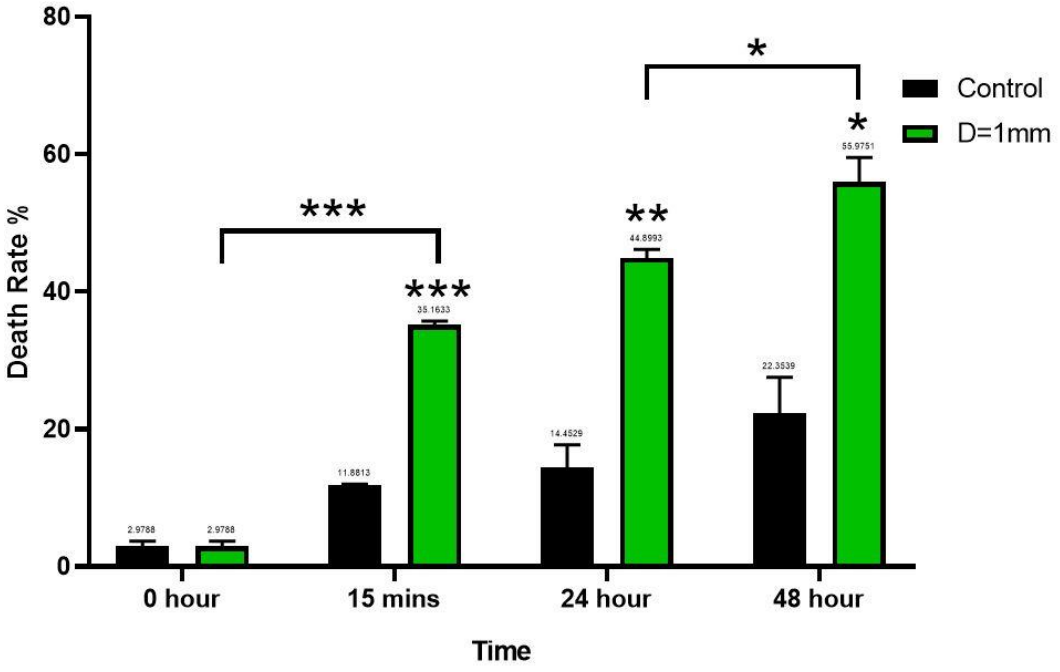

Figure 4.10 Cell death rate for cells that underwent PEFE treatments and control group evaluated before treatments ('0hour'), immediately after treatments ('15mins'), and 24 and 48 hours after treatments, respectively (n = 3). PEFE was generated at 2.2GHz, with input power level at 50 watts. The probe was fixed at 1mm from bottom of the well. Error bar stands for standard error of means. *p<0.05, **p <0.01, ***p<0.001.

In Figure 4.10, an increased pattern of death rate of treated cells was observed and this death rate was significantly higher than that of the control group at each time point post treatment (35.16% *vs* 11.88% at 15mins, 44.90% *vs* 14.45% at 24 hours, and 55.98% *vs* 22.35% at 48 hours, respectively).

It is clear that the PEFE treatments were able to significantly induce cancer cell death at each Electric field strength. A direct comparison for the impact of different distances was made and is shown in Figure 4.11.

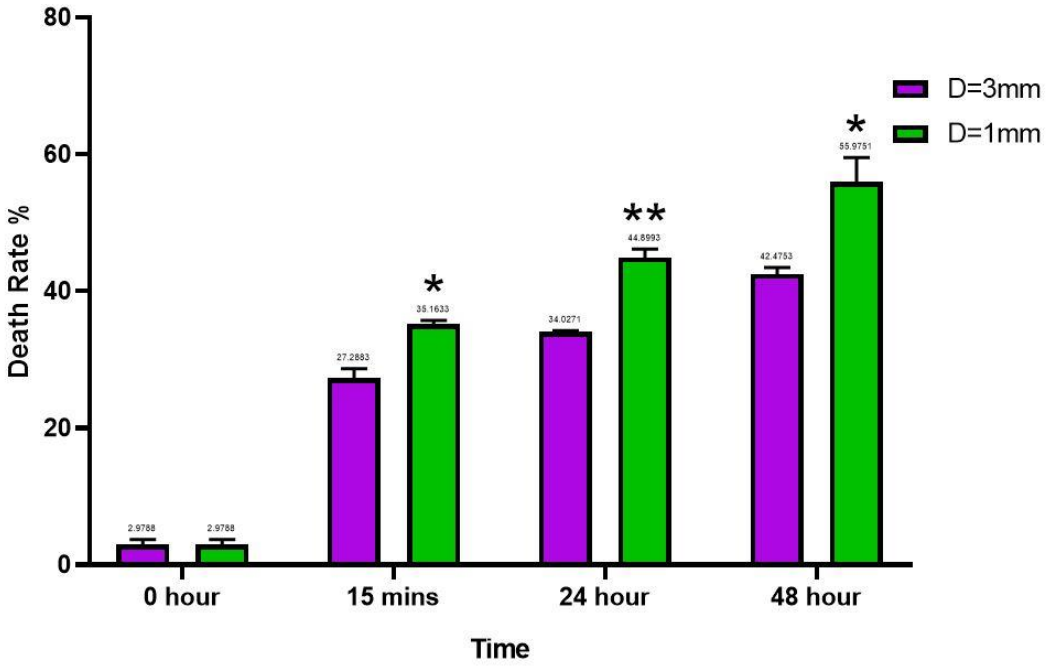

Figure 4.11 Cell death rate comparison for PEFE treatments with different Electric field strength (n = 3). The death rate was evaluated before treatments ('0hour'), immediately after treatments ('15mins'), and 24 and 48 hours after treatments, respectively. PEFE was generated at 2.2GHz, with input power level at 50 watts. The probe was fixed at 3mm ('D=3mm') and 1mm ('D=1mm') from bottom of the well sequentially. Error bar stands for standard error of means. *p<0.05, **p <0.01.

The closer the probe tip was to the cells, the higher the Electric field was distributed on the cells. Thus, higher Electric fields were generated when the probe tip was 1mm from the bottom of the well compared to 3mm. This higher Electric field distribution contributed to a significantly higher death rate evaluated post PEFE treatment as shown in Figure 4.11 (35.16% *vs* 27.29% at 15mins, 44.90% *vs* 34.03% at 24 hours, and 55.98% *vs* 42.48% at 48 hours, respectively).

4.3.4 Investigation on pulse parameters impacting cancer cell death

In this study, pulse parameters were reconfigured as listed in Table 4.4. The frequency of the PEFE was 2.2GHz, and the experimental results are illustrated in Figure 4.12 and 4.13.

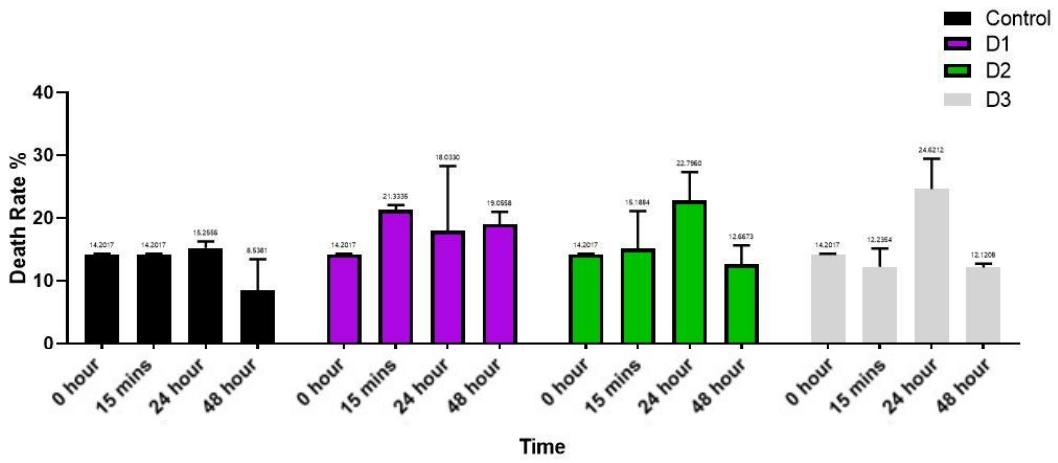

Figure 4.12 Cell death rate comparison for PEFE treatments with different Electric field strength (n = 3). The death rate was evaluated before treatments ('0hour'), immediately after treatments ('15mins'), and 24 and 48 hours after treatments, respectively. PEFE was generated at 2.2GHz, with input power level at 50 watts. The probe was fixed at 1mm from the bottom of the well. Pulse parameter was set as listed in Table 4.4 (D1 being 200 µs pulse width, 4ms pulse period and 5% duty cycle, D2 being 10µs, 200 µs, 5% and D3 being 5µs, 100 µs, 5% respectively). Error bar stands for standard error of means. No statistical significance was exhibited in all groups.

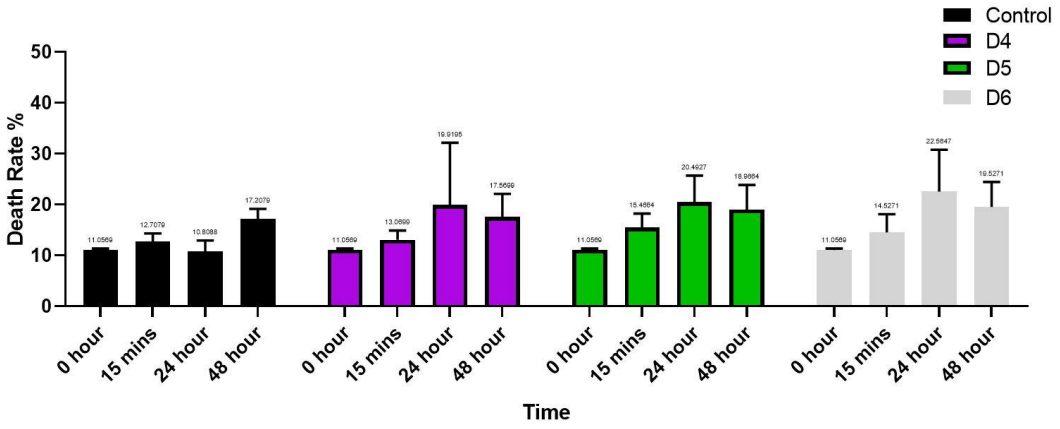

Figure 4.13 Cell death rate comparison for PEFE treatments with different Electric field strength (n = 3). The death rate was evaluated before treatments ('0hour'), immediately after treatments ('15mins'), and 24 and 48 hours after treatments, respectively. PEFE was generated at 2.2GHz, with input power level at 50 watts. The probe was fixed at 1mm from the bottom of the well. Pulse parameter was set as listed in Table 4.4 (D4 being 200 µs pulse width, 1ms pulse period and 20% duty cycle, D5 being 10µs, 1msµs, 1% and D6 being 5µs, 1ms, 0.5% respectively). Error bar stands for standard error of means. No statistical significance was exhibited in all groups.

In Figure 4.12 and Figure 4.13, the death rate of the cells that underwent PEFE treatment did not show any significant differences compared to the control groups, indicating that these treatments failed to induce any significant cancer cell death. Importantly, even if the pulse parameters were changed in each treatment, there was no difference exhibited in the death rate amongst the different treatments.

Another series of experiments were conducted at 5.8Ghz, and the results were shown in Figure 4.14 and 4.15.

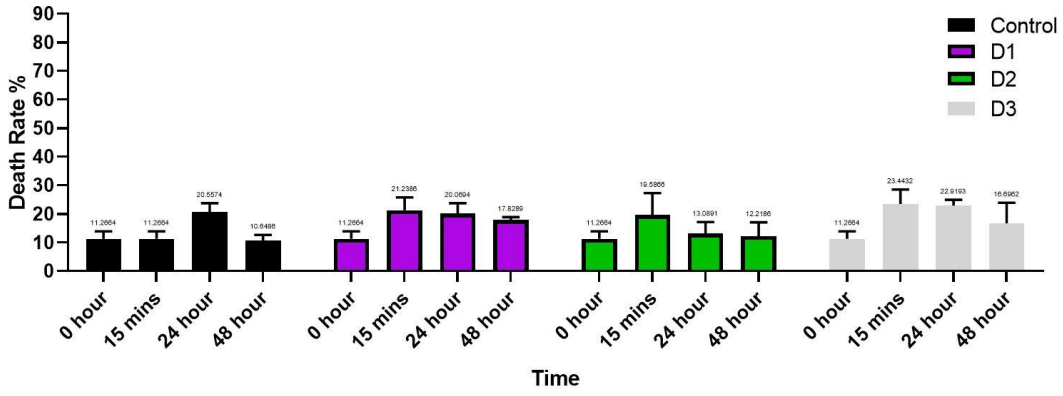

Figure 4.14 Cell death rate comparison for PEFE treatments with different Electric field strength (n = 3). The death rate was evaluated before treatments ('0hour'), immediately after treatments ('15mins'), and 24 and 48 hours after treatments, respectively. PEFE was generated at 5.8GHz, with input power level at 50 watts. The probe was fixed at 1mm from the bottom of the well. Pulse parameter was set as listed in Table 4.4 (D1 being 200 µs pulse width, 4ms pulse period and 5% duty cycle, D2 being 10µs, 200 µs, 5% and D3 being 5µs, 100 µs, 5% respectively). Error bar stands for standard error of means. No statistical significance was exhibited in all groups.

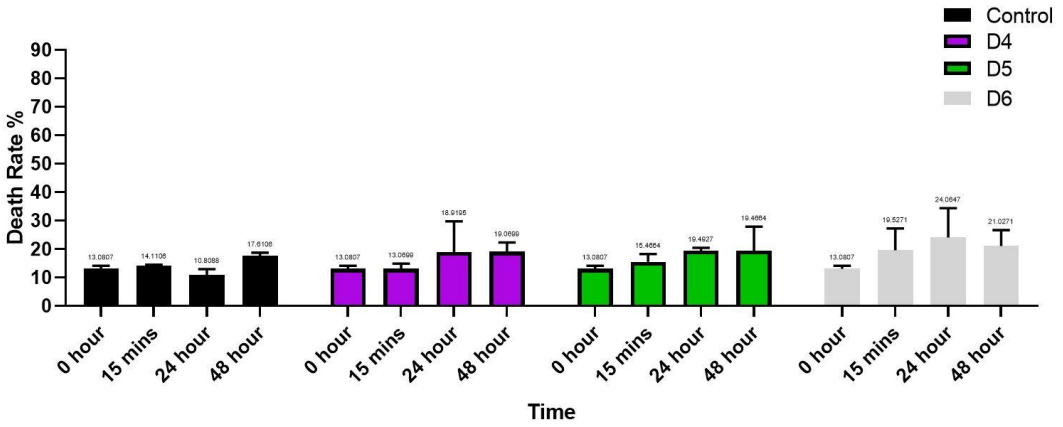

Figure 4.15 Cell death rate comparison for PEFE treatments with different Electric field strength (n = 3). The death rate was evaluated before treatments ('0hour'), immediately after treatments ('15mins'), and 24 and 48 hours after treatments, respectively. PEFE was generated at 5.8GHz, with input power level at 50 watts. The probe was fixed at 1mm from the bottom of the well. Pulse parameter was set as listed in Table 4.4 (D4 being 200 µs pulse width, 1ms pulse period and 20% duty cycle, D5 being 10µs, 1msµs, 1% and D6 being 5µs, 1ms, 0.5% respectively). Error bar stands for standard error of means. No statistical significance was exhibited in all groups.

Similarly, when the frequency of PEFE was altered to 5.8GHz, the treatment under each condition failed to induce significant cell death compared to the control group. Additionally, the changed pulsed parameters were not able to yield significant differences in the death rate of treated cells. In summary, even if the various frequencies were applied, no effective cell killing effects was observed and no significant differences were exhibited in death rate when varied combinations of pulse width and pulse period were applied.

4.3.5 Investigation on different cancer cell lines impacting cell death

In this study, four different cancer cell lines from breast cancer tissues were treated with PEFE, including MDA-MB-231, MCF-7, BT549 and T47D. The results are shown in Figure 4.16 to 4.19.

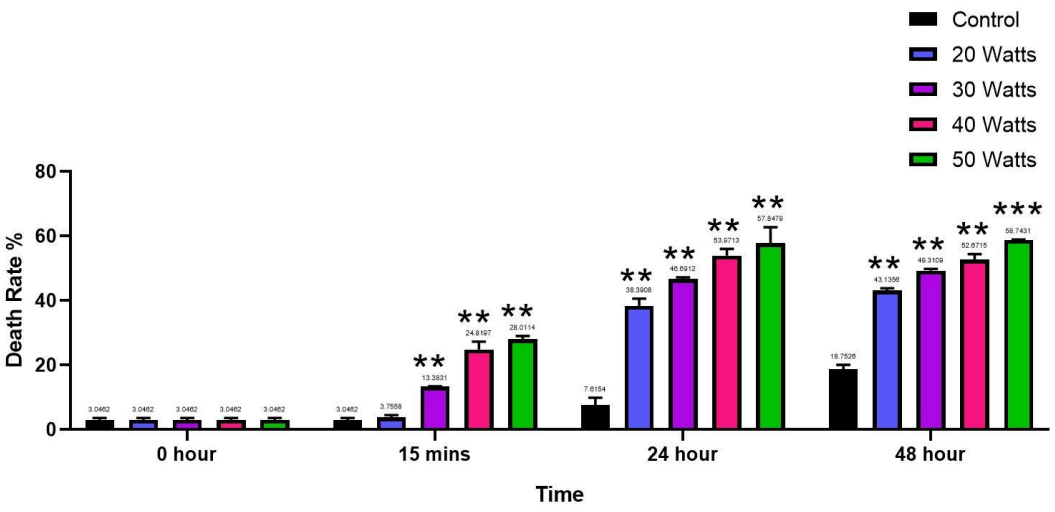

Figure 4.16 The cell line used in these treatments was MDA-MB-231 (n = 3). The cell death rate was evaluated for cells that underwent PEFE treatments and for the control group before treatments ('0hour'), immediately after treatments ('15mins'), and 24 and 48 hours after treatments, respectively. PEFE was generated at 2.2GHz, with input power levels ranging from 20 watts to 50 watts. The probe was fixed at 1mm from the bottom of the well. Error bar stands for standard error of means (SEM). **p <0.01, ***p<0.001.

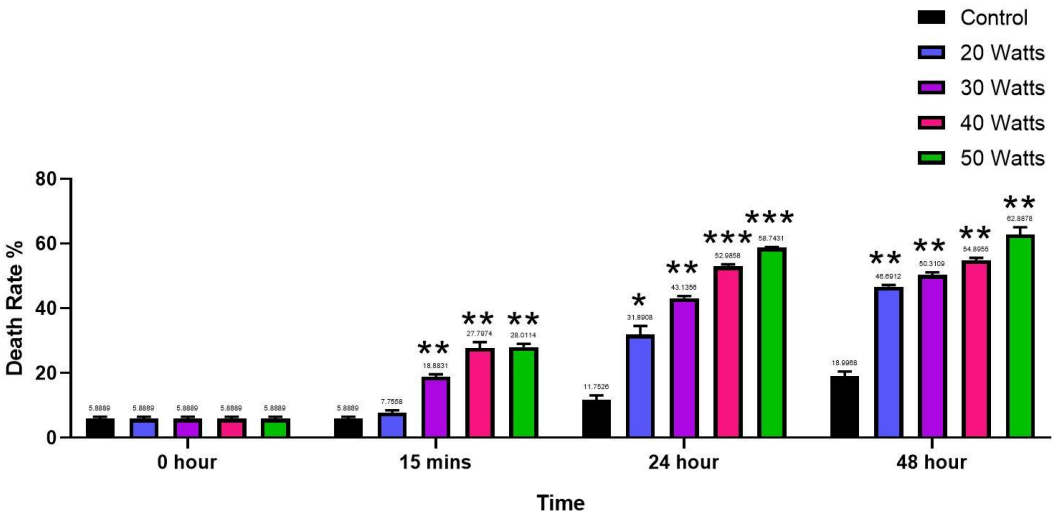

Figure 4.17 The cell line used in these treatments was MCF-7 (n = 3). The cell death rate was evaluated for cells that underwent PEFE treatments and for the control group before treatments ('0hour'), immediately after treatments ('15mins'), and 24 and 48 hours after treatments, respectively. PEFE was generated at 2.2GHz, with input power levels ranging from 20 watts to 50 watts. The probe was fixed at 1mm from the bottom of the well. Error bar stands for standard error of means (SEM). *p<0.05, **p <0.01, ***p<0.001.

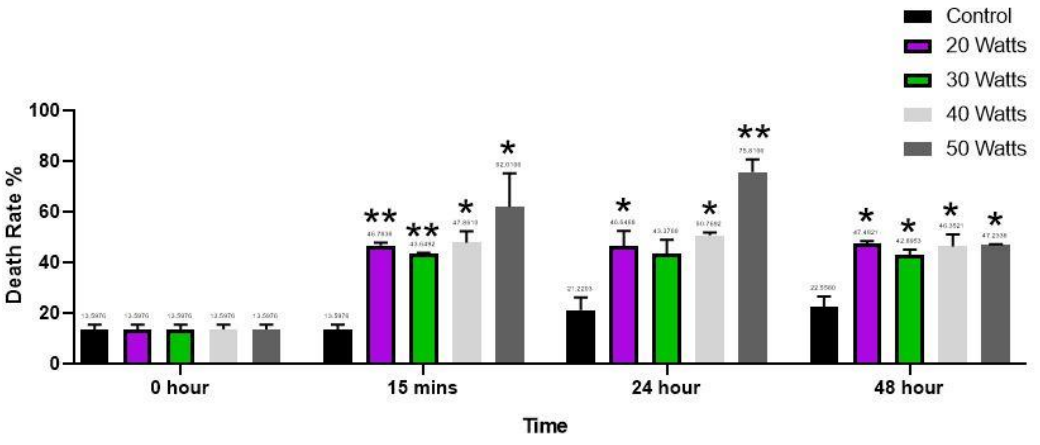

Figure 4.18 The cell line used in these treatments was BT549 (n = 3). The cell death rate was evaluated for cells that underwent PEFE treatments and for the control group before treatments ('0hour'), immediately after treatments ('15mins'), and 24 and 48 hours after treatments, respectively. PEFE was generated at 2.2GHz, with input power levels ranging from 20 watts to 50 watts. The probe was fixed at 1mm from the bottom of the well. Error bar stands for standard error of means (SEM). *p<0.05, **p <0.01.

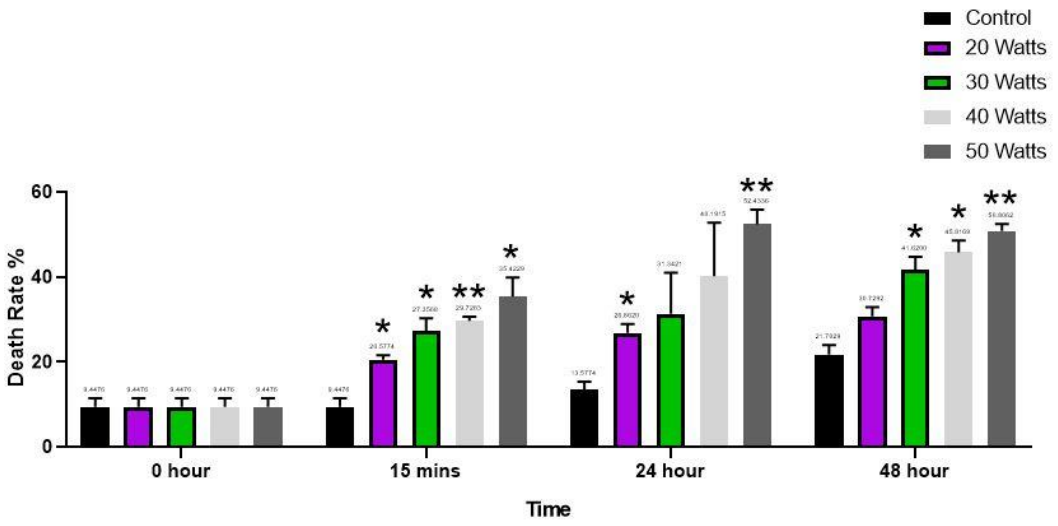

Figure 4.19 The cell line used in these treatments was T47D (n = 3). The cell death rate was evaluated for cells that underwent PEFE treatments and for the control group before treatments ('0hour'), immediately after treatments ('15mins'), and 24 and 48 hours after treatments, respectively. PEFE was generated at 2.2GHz, with input power levels ranging from 20 watts to 50 watts. The probe was fixed at 1mm from the bottom of the well. Error bar stands for standard error of means (SEM). *p<0.05, **p <0.01, ***p<0.001.

The tests clearly demonstrated that PEFE was able to induce significant cell death in the four cell lines, which are widely used in biological and medical research. This was despite the fact that hormone receptor status and invasiveness are different, namely MDA-MB-231 cells are triple negative and highly invasive, whereas T47D/MCF7 cells are receptor positive and less invasive. Importantly, the induced cell death was not limited to the different cell lines and phenotypes, indicating that PEFE has the potential to be a significant clinical treatment for breast cancers of different types, independent of their histological or hormone receptor status.

4.3.6 Cell viability, cell morphology and ultra structure of breast cancer cells in response to PEFE treatments

4.3.6.1 Cell viability assessment targeted at the number of dead cells over time

The number of dead cells and the death rate were calculated separately, and the results are illustrated in Figure 4.20.

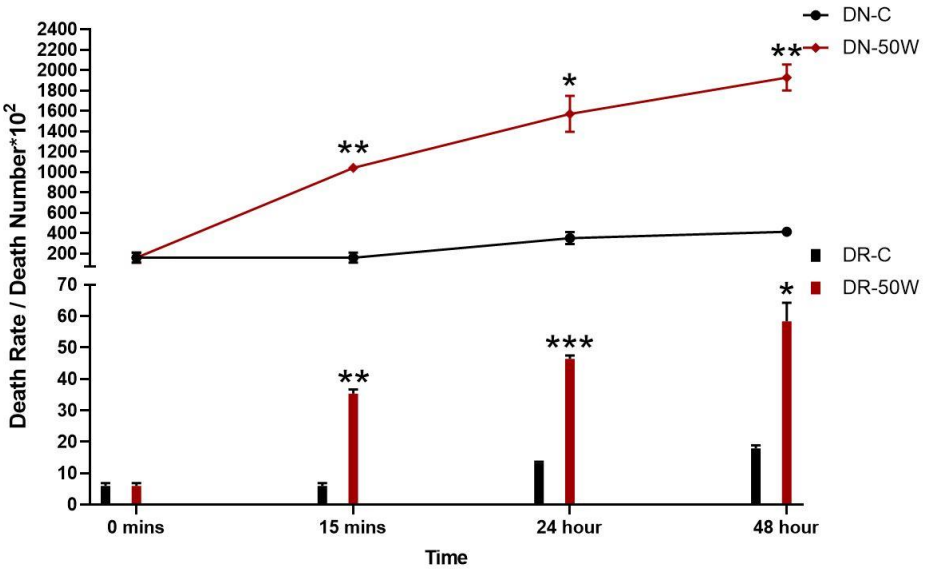

Figure 4.20 Calculation on cell death number (line graph, control group: 'DN-C', treated sample: 'DN-50W') and death rate (bar graph, control group: 'DR-C', treated sample: 'DR-50W') of PEFE treatments (n = 3). The PEFE was generated at 2.2GHz with 50-watt input power level. The probe was placed at 1mm to the cultured cancer cells. Cell viability was assessed before treatments ('0hour'), immediately after treatments ('15mins'), and 24 and 48 hours after treatments, respectively. Error bar stands for standard error of means. *p<0.05, **p <0.01, ***p<0.001.

The number of dead cells in the PEFE treatments was significantly higher than that in the control group at each designated time. Similarly, a significantly higher death rate was observed in the treated cells at each designated time point compared to the control groups. More detailed comparisons are given in Figure 4.21.

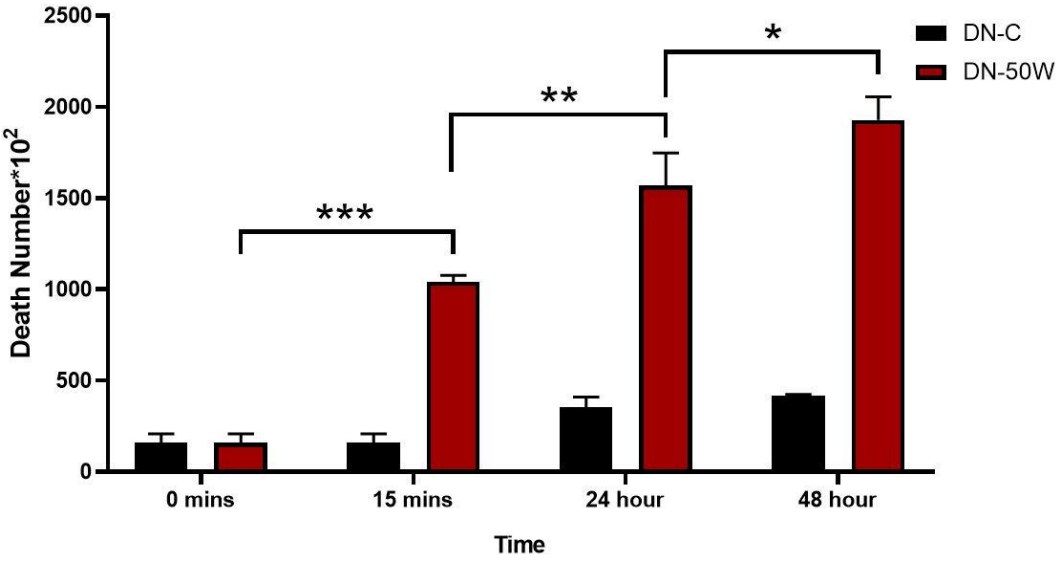

Figure 4.21 Statistical analysis on the number of dead cells in the control group and cells that underwent PEFE treatments (n = 3). The data was in accordance with that in line graph from Figure 4.20. Error bar stands for standard error of means. *p<0.05, **p<0.01, ***p<0.001. No Statistical significance was exhibited in control group.

In Figure 4.21, the number of dead cells in the control groups did not change significantly over time. In contrast, the number of dead cells induced by PEFE treatments significantly increased over time. It can be extrapolated that some cell death occurred during PEFE treatments and that this induction of cell death was sustained over time, at least over 48 hours.

4.3.6.2 PEFE had an impact on the morphology of breast cancer cells

The cultured cells (MDA-MB-231) were inspected under the microscope before the treatments were applied, and images are shown in Figure 4.22. The cultured cells exhibited normal cellular morphology for that cell line and no alterations were observed in the cells.

Immediately after PEFE treatments, the control group and cancer cells undergoing PEFE were checked again under the microscope, and images of the cell morphology are shown in Figure 4.23 and Figure 4.24. In the control groups, no changes were observed before and immediately after treatments. However, a cell-free zone was

produced on the bottom of the 96 well plate after the PEFE treatments. This cell-free zone was exactly under the probe tip indicating that the previously adhesive cancer cells were detached during PEFE treatments.

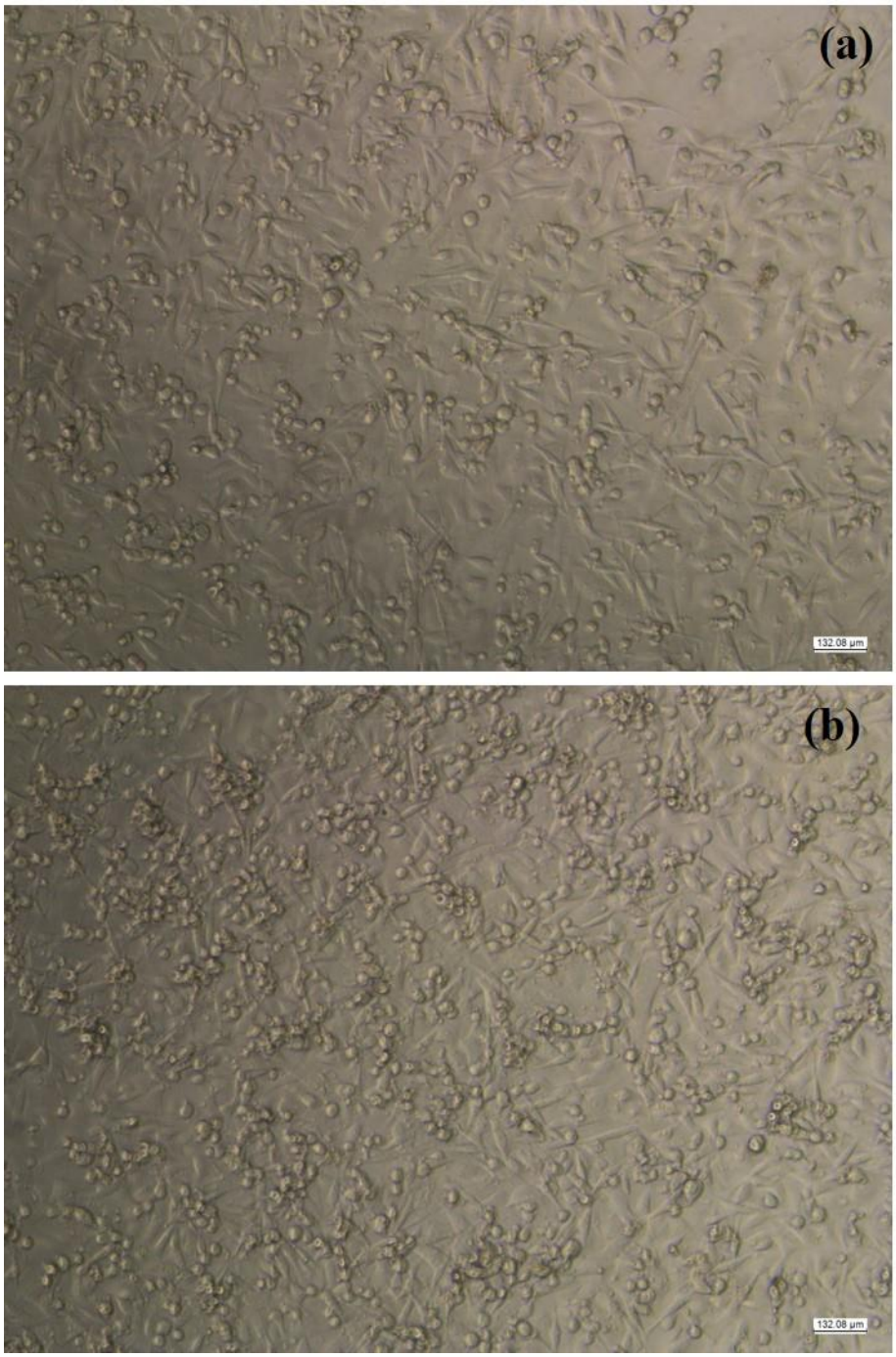

Figure 4.22 Visualization of cultured cancer cells (MDA-MB-231) using microscopy before PEFE treatments. (a) control group. (b) cells to be treated by PEFE. Scale bar: 132.08µm. Magnification:10X

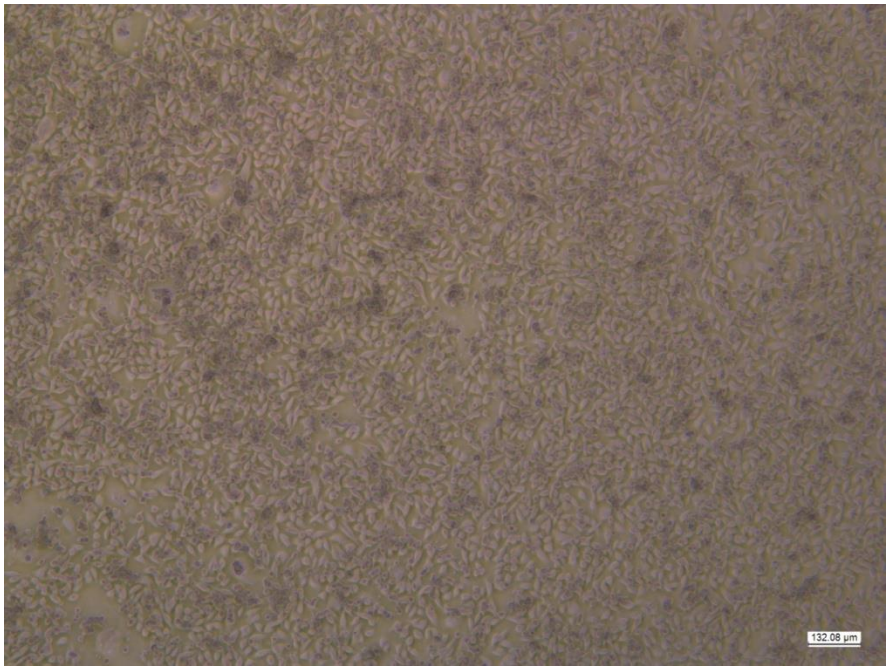

Figure 4.23 Visualization of cultured cancer cells (MDA-MB-231) of control group using microscopy immediately after PEFE treatments. Scale bar: 132.08µm. Magnification:10X

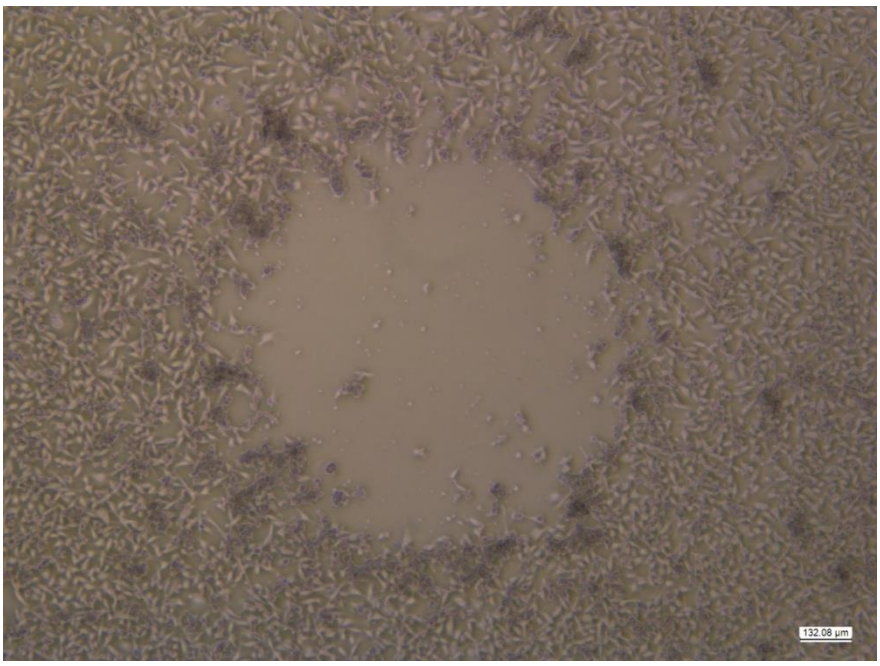

Figure 4.24 Cell-free zone formed on the bottom of well, near probe tip, during the PEFE treatments using MDA-MB-231 cell line. Scale bar: 132.08µm. Magnification:10X

4.3.6.3 PEFE treatment resulted in marked changes in the integrity of cell membrane and cellular organelle

In order to further explore the nature and extent of cell morphological response after PEFE treatment, we employed transmission electron microscopy (TEM) technology with a particular reference to the alterations in the cellular membrane, intracellular organelle and inter-cellular space.

For the cells in the control group, normal cellular organelles were observed as indicated by yellow arrows and intact membrane structure and tightly closed intercellular junctions were also exhibited as indicated by red arrows on the top of Figure 4.25. For the cells undergoing PEFE treatments, disrupted cellular organelles were observed, as indicated by yellow arrows, and the breakdown of membrane structure together with intercellular junctions was exhibited, as indicated by red arrows on the bottom of Figure 4.25. The rapid disruption of cellular organelle resulted in cell death, whilst the breakdown of the membrane structure and intercellular junctions can contribute to dysregulated cell-cell adhesion and increased paracellular permeability.

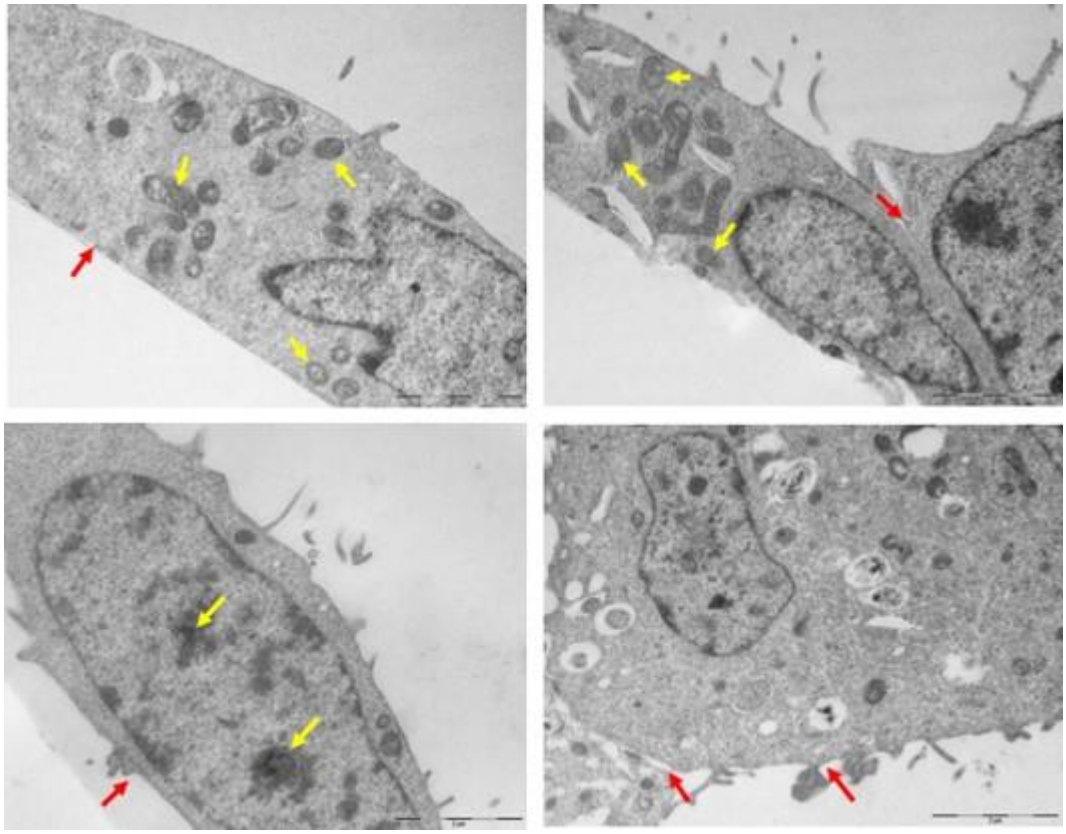

Figure 4.25 Morphological alterations of cultured breast cancer cells in response to PEFE treatments under SEM. Top: Control group of MDA-MB-231 cells. Top left showing a cell with normal organelles and top right showing two cancer cells with normal intercellular junctions. Bottom: MDA-MB-231 treated by PEFE. Bottom Left showing the breakdown of membrane structure and intracellular organelles. Bottom Right: disintegrated intercellular junctions following PEFE treatment (4 hours). Yellow arrows indicate intracellular organelles. Red arrows indicate intercellular junctions.

Interestingly, no alternations were observed in primary cultured breast cancer cells after PEFE treatments, in regards to the cell membrane structure, organelles and the integrity of the intercellular junctions, as shown in Figure 4.26 (desmosome clearly visible).

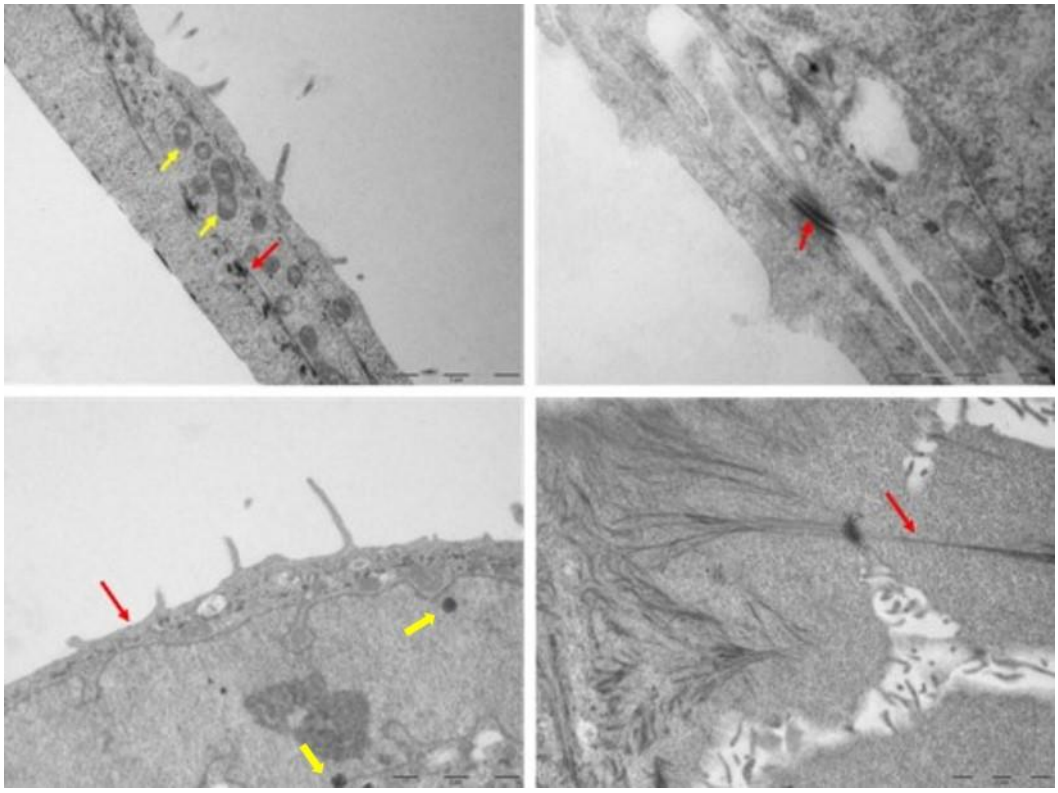

Figure 4.26 Morphological alterations of primary cultured breast cells in response to PEFE treatments under SEM. Top: Control group. Top left showing a cell with normal organelles and top right showing two cells with normal intercellular junctions. Bottom: cells treated by PEFE. Bottom left showing the intact membrane structure and intracellular organelles. Bottom right showing integrated intercellular junctions following PEFE treatment (4 hours). Yellow arrows indicate intracellular organelles. Red arrows indicate intercellular junctions.

4.3.7 *In vivo* animal study

A xenograft mouse model was established by subcutaneously injecting 3×10^6 MDA-MB-231 cancer cells into each nude mouse (n = 5 mice per group), shown in Figure 4.27. Tumour size were checked and measured every 3 days, and the mice were terminated under Schedule 1 at 4 weeks. The microwave treatment commenced on the 15th day after the tumour size had reached approximately 1cm in diameter. The mice in group B were treated with 40μs in pulse width for 40 seconds power on, followed by 40 seconds power off, and the treatments were repeated 10 times. The Group C mice were treated with 74μs in pulse width for 40 seconds power on, followed by 40 seconds power off, and the treatments were

repeated 4 times for each mouse. The results showed the tumour volume decreased after the PEFE treatment in both treated groups (Group B and Group C), but the tumours kept growing in the control group (Group A). Interestingly, breast tumours in Group B had the lowest tumour volume at day 24, and tumours in Group C had the lowest tumour volume on day 21. This result predicted that the breast cancer cells may have different reactions under different times and pulse width of treatment (Figure 4.28). It is also noteworthy that during the study period of 27 days, there were no side effects observed, including negative effects on the skin, site of probe insertion, and general wellbeing of the experimental subjects. There were no deaths due to cancer related incidence nor due to any other reasons.

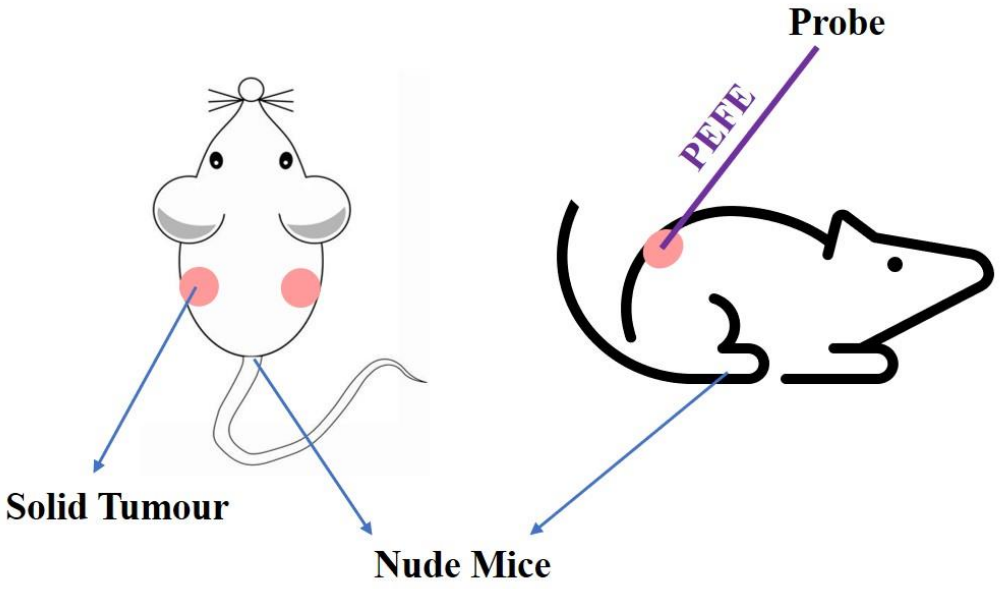

Figure 4.27 A schematic diagram showing the locations of solid tumours and position of the probe inside the tumour.

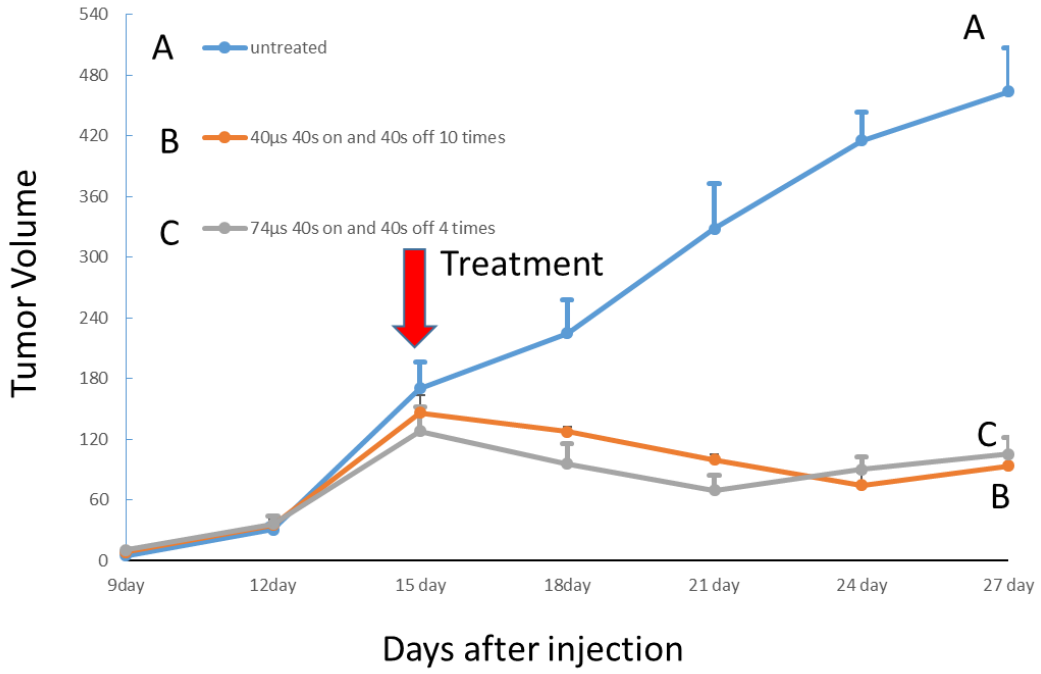

Figure 4.28 The impact of PEFE microwave treatment on the tumour volume of a xenograft mouse model developed by MDA-MB-231 breast cancer cells. The length and width of the tumours were measured every three days and the tumour volume (mm^3) was calculated according to the equation (length × $width^2$)/2.

4.3.8 The role of Kidins220 as a biomarker in predicting the efficiency of PEFE treatments

The role of Kidins220 in tumorigenesis has been indicated in several cancer types and its connection to neuronal and endocrine related cell functions have also been reported (Chapter-1). Given the intimate connection between microwaves, cancer, neuronal signalling and cell growth and death, we explored the possible connection between Kidins220 and PEFE mediated cell behaviours.

The *in vitro* Kidins220 knockdown cell model was established using lentivirus particle and was confirmed at both the RNA level and protein level, as shown in Figure 4.29 and Figure 4.30 respectively. A significant decrease in the expression of Kidins220 was exhibited in both cell lines

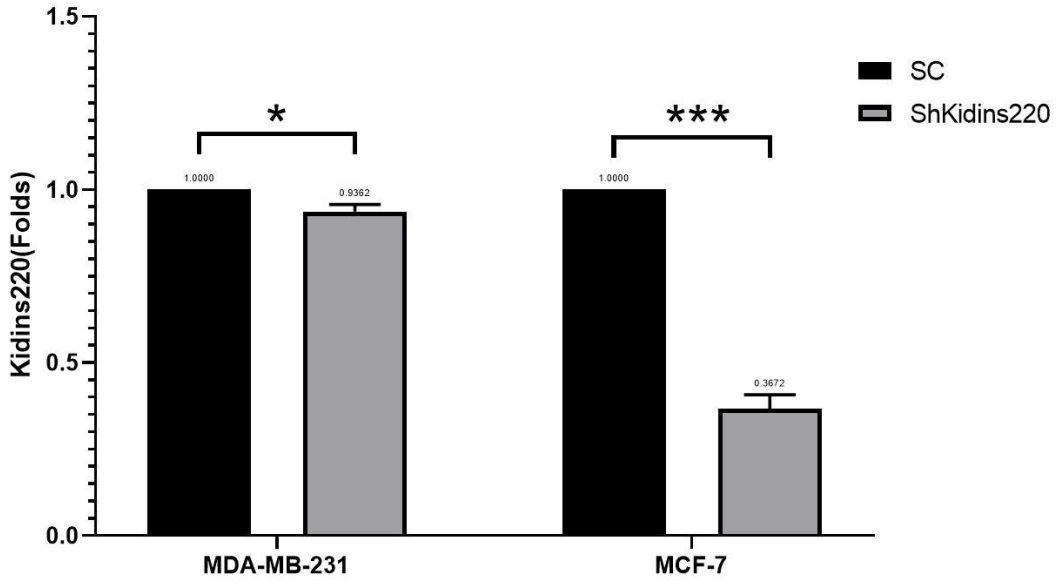

Figure 4.29 Verification of Kidins220 knockdown in MDA-MB-231 and MCF-7 cell lines (n = 3). The RNA expression of Kidins220 knockdown model ('ShKidins220') was normalised using the expression of Kidins220 Scramble ('SC'). Error bar stands for standard error of means. *p<0.05, ***p<0.001.

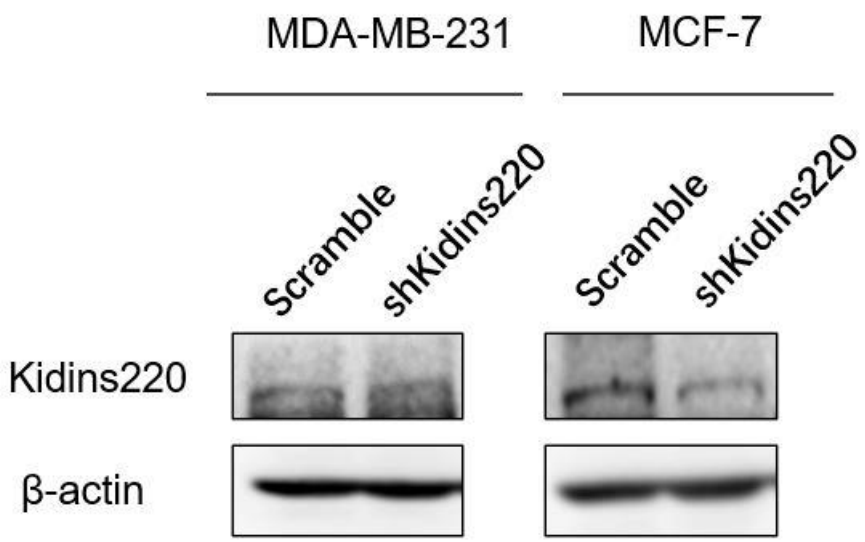

Figure 4.30 An example showing Western Blot result for the expression of Kidins220 extracted from Kidins220 Scramble ('Scramble') and Kidins220 knockdown ('ShKidins220') cell models in MDA-MB-231 and MCF-7 cell lines respectively.

In order to investigate the role of Kidins220 in regulating cellular function in human breast cancer cells, the ECIS system (Applied Biophysics Inc, NY, USA) was used to identify the possible impact of Kidins220 knockdown on cell migration. The results obtained showed that breast cancer cells, after losing Kidins220 by way of knockdown, displayed increased cellular migration in comparison with scramble control cells in both MDA-MB-231 and MCF-7 cells (Figure 4.31 and Figure 4.32).

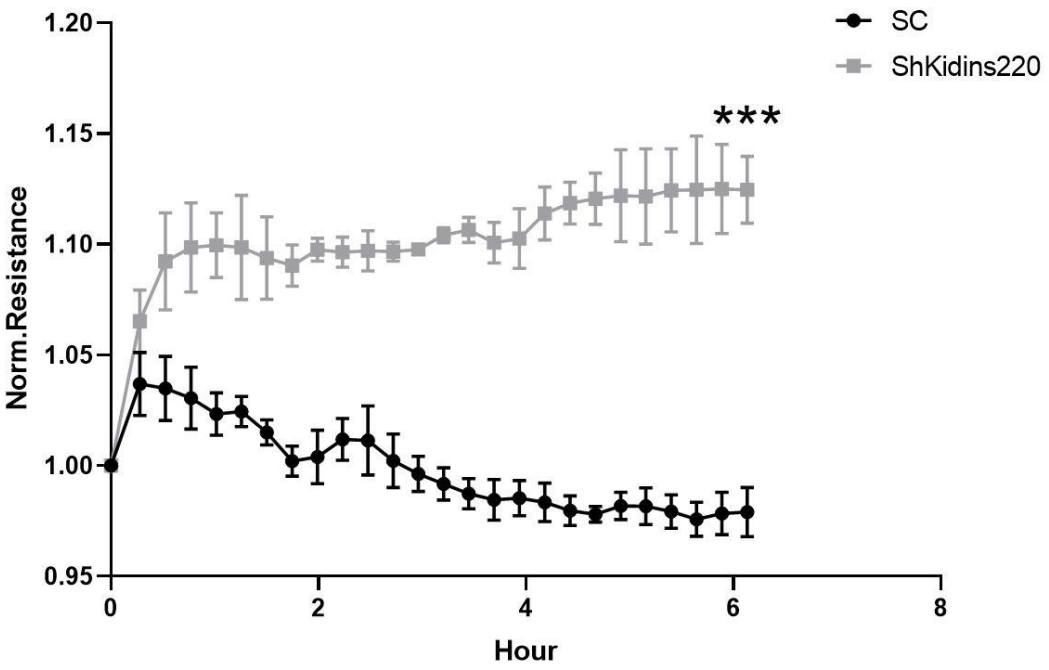

Figure 4.31 ECIS based migration assay on MDA-MB-231 breast cancer cells of Kidins220 knockdown ('ShKidins220') and scramble control ('SC') (n = 3). The image presented the first five hours resistance following the wounding. Eight repeats were included for the cell line in the experiment. The measured resistance was normalised ('Norm.Resistance'). Error bars represent standard deviation (SD). ***p<0.001.

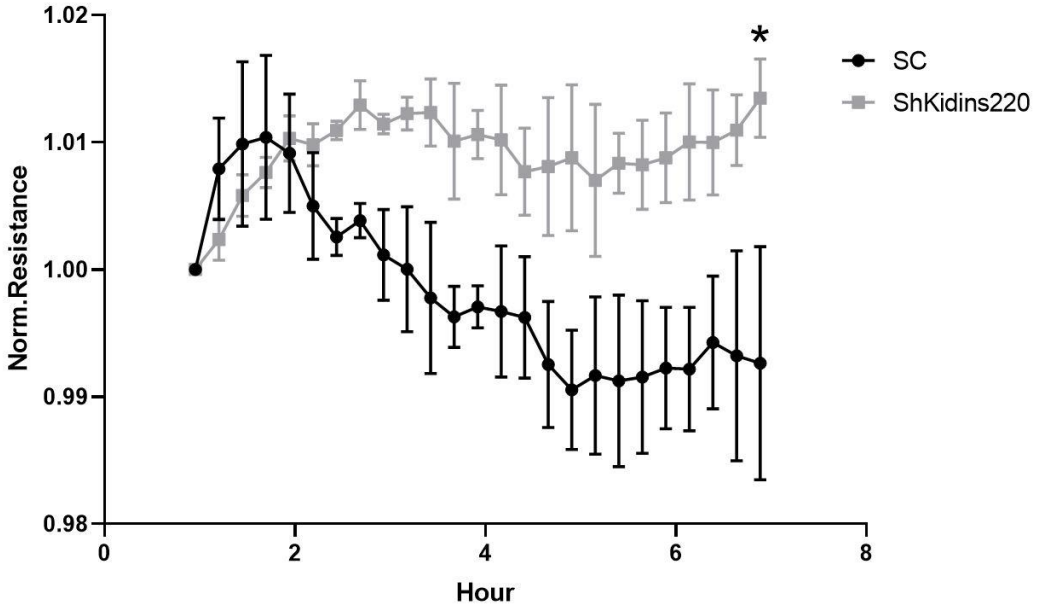

Figure 4.32 ECIS based migration assay on MCF-7 breast cancer cells of Kidins220 knockdown ('ShKidins220') and scramble control ('SC') (n = 3). The image presented the first six hours resistance following the wounding. Eight repeats were included for the cell line in the experiment. The measured resistance was normalised ('Norm.Resistance'). Error bars represent standard deviation (SD). * p<0.05.

Subsequently, PEFE was used to treat scramble control and Kidins220 knockdown cells in both cell lines to evaluate whether this molecule mediated cell death. The result showed a significant increase in the number of cells undergoing cell death after Kidins220 knockdown 48 hours post PEFE treatment in MDA-MB-231 (***p<0.001) and MCF-7 (**p<0.01) breast cancer cells (Figure 4.33 and Figure 4.34).

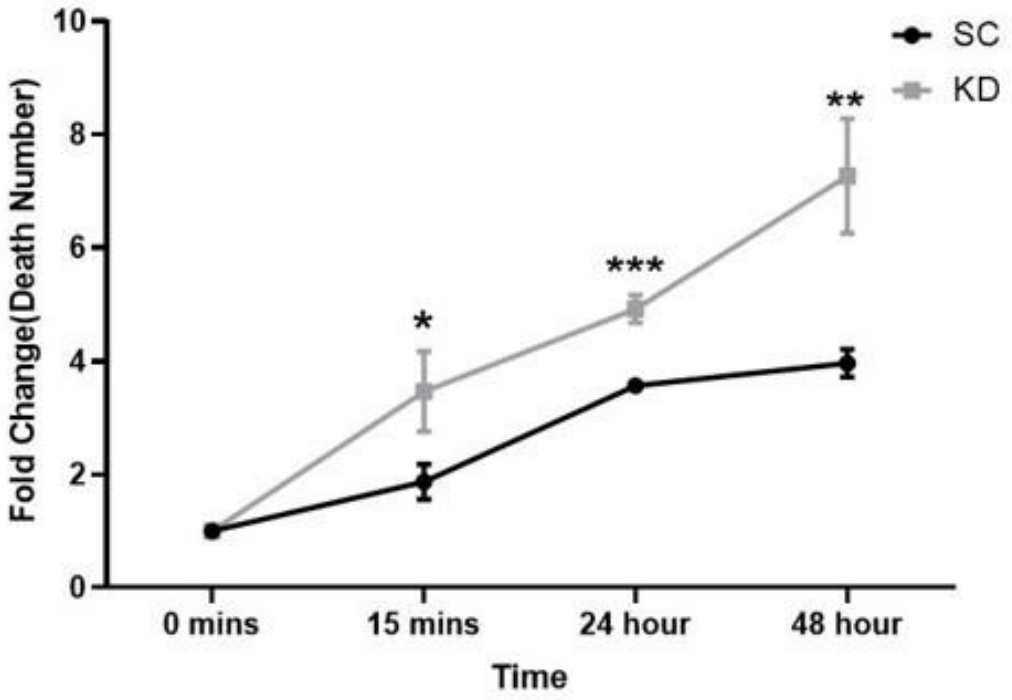

Figure 4.33 PEFE treatments using MDA-MB-231 cancer cells of Kidins220 knockdown ('KD') and scramble control ('SC') (n = 3). PEFE treatments were conducted at 2.2GHz and 50 watts input power level. The distance between probe tip and cells was fixed at 1mm. The number of PEFE induced dead cells was measured before treatments ('0mins'), immediately after treatments ('15mins'), and 24 and 48 hours after treatments. The results were exhibited by fold change. Error bars represent standard deviation (SD). *p<0.05, **p<0.01, ***p<0.001.

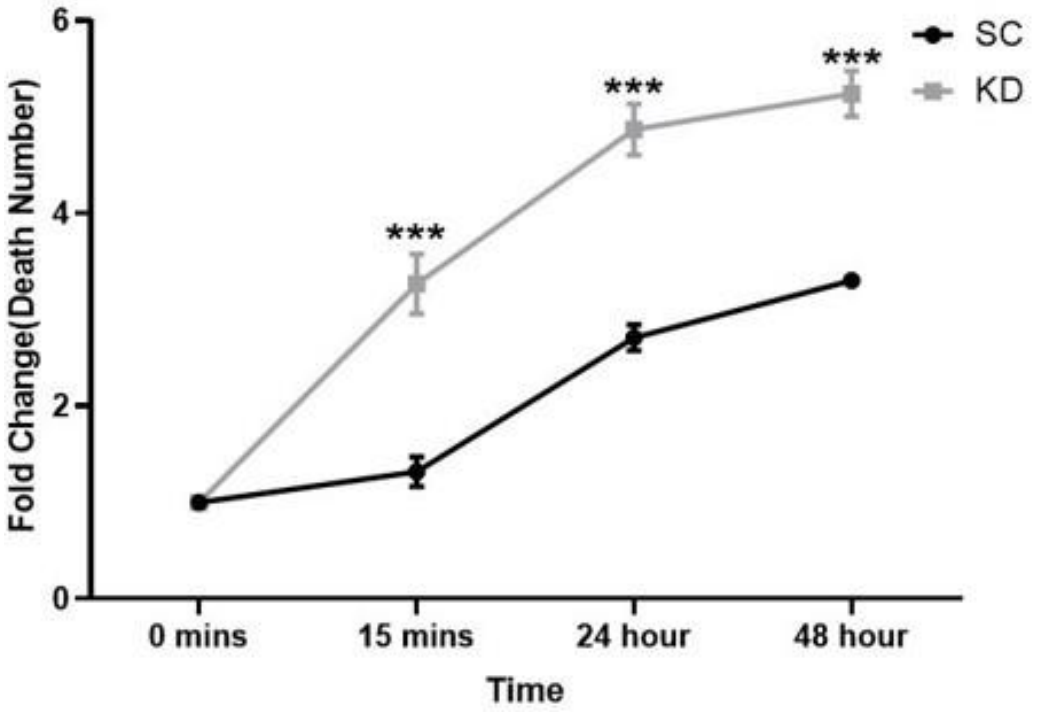

Figure 4.34 PEFE treatments using MCF-7 cancer cells of Kidins220 knockdown ('KD') and scramble control ('SC') (n = 3). PEFE treatments were conducted at 2.2GHz and 50 watts input power level. The distance between probe tip and cells was fixed at 1mm. The number of PEFE induced dead cells was measured before treatments ('0mins'), immediately after treatments ('15mins'), and 24 and 48 hours after treatments. The results were exhibited by fold change. Error bars represent standard deviation (SD). ***p<0.001.

4.4 Discussion

Microwave as an ablation technique in clinical treatments has been well established for decades. Microwave ablation (MWA) produces high local temperature which achieves rapid damage to tissues and leads to necrosis of tumours. MWA has been used to treat certain solid cancers, primarily in liver, kidney and lung cancers. With the early and existing MWA technologies, heat is central to the anticipated beneficial effects of cancer treatment. As discussed in Chapter-1, it is this thermal effect of MWA generated within the tissues that causes the side effects and collateral damage, and this has limited its wider use in medical treatments, particularly in cancer. As presented in Chapter-3, our research has produced a new ablation technique using pulsed electromagnetic exposure at the microwave range.

The most significant advantage of the new PEFE technology is that it produces little heat in the conditions used in this current study.

From the experiments presented in this chapter, and supported by the literature, temperatures higher than 42℃ result in marked cell death, in this case in breast cancer cells. The data shown here further confirms that the PEFE technique does not utilise the heat delivered by microwaves as the temperature was maintained below 42℃ throughout the treatments. This approach, compared with traditional ablation such as MWA, has significant advantages. There is no requirement for a cooling system during PEFE treatments which would alleviate any pain that otherwise would have been caused by the MWA systems. Another advantage of PEFE treatment is that it does not need a complicated design or manufacture for the PEFE probe. The probe used in PEFE treatments is a standard coaxial cable with only a simple pointed tip. Thus, the manufacture of the probe and any other costs involved can be further minimised. In addition, it would be anticipated that PEFE treatment would be carried out under non-surgical conditions, *i.e.* under local anaesthetic, thus saving costs to the healthcare service and providing a far less invasive and gruelling procedure for the patient.

4.4.1 PEFE treatment efficacy under different conditions

The frequency for use was the first parameter to be investigated for its efficacy in PEFE induced cell death. Limited by the bandwidth requirement of some microwave devices, the present study was able to generate two frequencies including 2.2GHz and 5.8GHz for the experimental purpose. This strategy, although with limitation, proved a successful formula: the PEFE generated at these two frequencies were both able to effectively elicit cancer cell death. Moreover, no significant difference between the two frequencies was observed in the efficacy of cancer cell-killing, indicating that frequency was less likely to affect PEFE treatments.

In the investigation of how electric field strength impacted on cell death, two separate groups of experiments were conducted with varied input power levels and height of probe, respectively. According to the results in section 4.3.3, it can be

concluded that higher electric field strength was able to yield higher death rate. Thus, intensive electric fields on cells were required to ensure efficacy.

When pulse parameters were reconfigured, the waveform of PEFE was changed. Nevertheless, these different combinations of pulse width and pulse period failed to affect the death rate significantly, as discussed in section 4.3.4. More significant death rate was achieved using current pulse parameters, which were 50μs for pulse width and 1ms for pulse period. It appears that cell death was waveform specific, indicating that there are optimal pulse parameters for achieving maximum cell death.

4.4.2 Potential application in managing breast tumor growth

The current study chose four breast cancer cell lines with different hormonal and aggressive characteristics. For example, MDA-MB-231 is an adenocarcinoma cell type and is triple hormone receptor negative (TNB, namely ER, PR and Her2 negative), whereas the other cell lines originated from ductal carcinoma of the breast, *i.e*. T47D cells, and these tend to be ER and PR positive. Our data has shown that the PEFE treatments were effective on all four cell lines (section 4.3.5), indicating that PEFE technology would have a broad spectrum of application with regard to cell types and cancer types. The present study tested only breast cancer. Future studies will expand to other solid tumour types to assess efficacy.

In vivo experiments using a xenograft mouse model provided evidence that PEFE treatments were a promising technology for the treatment of breast cancer. An additional observation was that the *in vivo* procedure did not generate any side effects, further supporting the concept that PEFE is a safe procedure, at least in the *in vivo* models employed here.

4.4.3 Different types of cell death induced by PEFE treatments

There are two main types of cells death including necrosis and apoptosis, induced by PEFE treatments. They both lead to the death of a cell, albeit via different mechanisms and different cellular processes and are manifested differently (to a large degree). Necrosis is premature death, normally triggered by external factors, it takes place quickly, with membrane disruption, ATP depletion and metabolic

collapse. Apoptosis on the other hand is programmed, triggered by internal and/or physiological factors, taking place via a programmed process and thus requiring a longer time to complete, with characteristic changes in both the membrane and nucleus. Apoptosis requires energy input to complete the suicide process, whereas necrosis does not.

During the PEFE treatments, rapid cell death, as exhibited microscopically, was confirmed by viability assessment immediately after treatment. This rapid cell death was initially thought to be due to necrosis. Moreover, the number of dead cells increased over time even after PEFE treatments were completed, as confirmed by the results in Figure 4.20. This prolonged cell death revealed a different type of cell death, which was thought to very likely be apoptosis. Collectively, it is likely that PEFE treatment could result in both necrosis and apoptosis of breast cancer cells, although from the rate of cell death at each time point, apoptotic death appeared to be the more significant mode of killing. Further investigations were conducted and are presented in the next chapter.

4.4.4 Cell membrane and intracellular organelles were destroyed by intensive electric field delivered by PEFE

During the PEFE treatments, pulsed microwave signals were generated at source and propagated into samples via a probe, then penetrated and reflected at the bottom of the wells. This pulsed electric field on the surface of the attached cancer cells was fairly strong so that it was likely to induce cellular structures to breakdown.

Generally, mammalian cell membranes are composed of approximately 50% lipids and 50% proteins by mass, with the most common lipid being a phospholipid. This phospholipid is composed of a hydrophilic head and hydrophobic tail, shown in Figure 4.35. The hydrophilic head is a polar molecule, meaning that under an applied electric field it will subject a force that will cause it to align in the direction of the field. It is assumed that the energy provided by the electric field is sufficiently high enough to overcome the bonding energy holding these molecules together, resulting in the structure breaking down.

To confirm this hypothesis, transmission electron microscopy (TEM) was used to assess the cellular and intracellular organelles in response to PEFE. The results demonstrated an obvious disruption of cellular organelles and breakdown of membrane structure and intercellular junctions in the cancer cells that underwent PEFE treatments. As for the control group, no alterations or damage were observed by visual inspection, and the cells maintained normal morphology, as shown in Figure 4.25. The breakdown of the membrane structure and cellular organelles can directly contribute to rapid cell death. The loss of intercellular junctions can potentially lead to subsequent cell apoptosis. Furthermore, no alterations were exhibited in the results of TEM for primary cultured breast cells, whether or not they were the control group or PEFE treated cells. This can be a potential indicator that PEFE can kill cells selectively, inducing cancer cell death while not affecting normal cells.

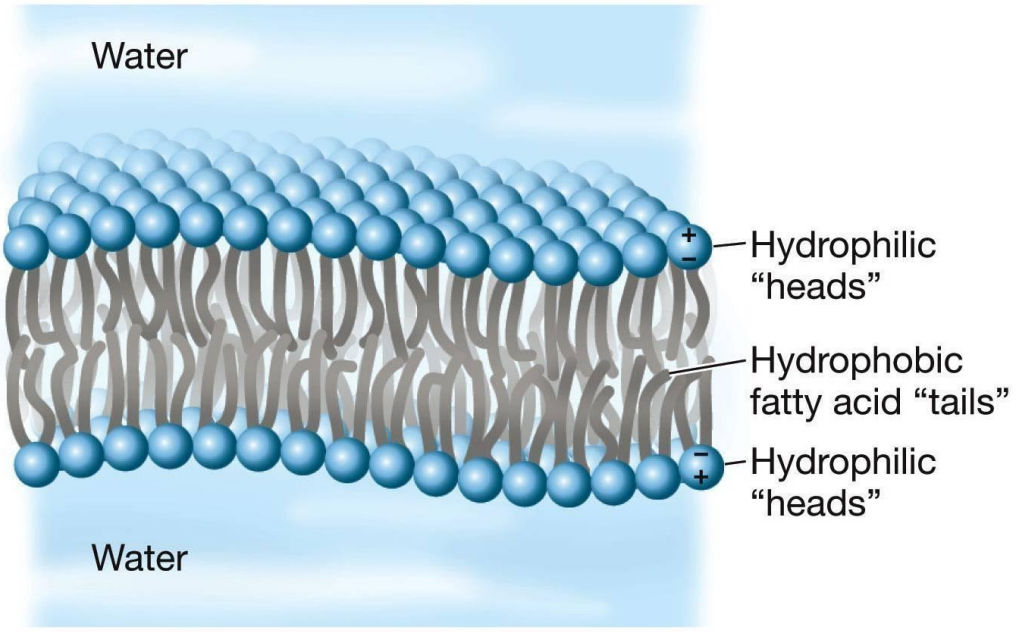

Figure 4.35 Components of phospholipid, including hydrophilic and hydrophobic. Source: https://s3.amazonaws.com/test.classconnection/823/flashcards/391823/jpg/phospholipid-bylayer.jpg

4.4.5 The role of Kidins220 as a potential biomarker in PEFE treatments

Kidins220 has undergone study by our research group and the role of Kidins220 involved in tumorigenesis has been indicated in several cancer types. In breast cancer, Kidins220 played a role in regulating cellular migration, as confirmed in section 4.3.9. Thus, Kidins220 might potentially impact intercellular junctions in breast cancer cells. The study has provided clear evidence for the first time that low levels of Kidins200 in breast cancer cells (by way of genetic knockdown) sensitises the cells response to PEFE treatments. This was reproducibly demonstrated in both MDA-MB-231 and MCF-7 cell lines. This has important clinical implications in that it suggests that assessing the level of Kidins200 expression in breast cancer may allow identification of a subset of patients who are more responsive to PEFE treatment. This exciting observation is preliminary at this stage and requires more and extensive research to validate and most importantly, a suitable large clinical study to contest the validity of Kindins220 as a suitable biomarker.

4.4.6 Limitations of this study

When investigating how direct heating impacted cancer cells, it was challenging to measure the real temperature of cultured cancer cells using an optical fibre temperature sensor. One possible method is to use a thermal camera to measure the temperature from the bottom of a 96 well plate. In this study, the temperature of cells was assumed to reach that designated by means of allowing much longer heating time.

The primary cultured breast cells were only used for the transmission electric microscopy to investigate how PEFE impact membrane structure, intracellular organelles and intercellular junctions. This was limited by a limited number of the primary cultured breast cells. As a normal cell line from breast, it exhibits low proliferation and thus had a limited use in this part of the study.

The apoptosis-related proteins such as Caspase3 and Caspase9 can be examined for their expression in order to confirm that PEFE treatments induced cell apoptosis. These are two of the most important intracellular apoptosis signalling pathways, namely the intrinsic and extrinsic pathways. However, these pathways have cross-

talk with other signalling pathways, indicating that the change in expression of some signalling proteins related to cell apoptosis might not successfully induce changed expression of apoptosis-related proteins. To disentangle this cross-talk, we employed additional technologies, as presented in the next chapter.

According to Figure 3.18, highly non-uniform the electric field was produced during the PEFE treatments. This electric field acted on the inhomogeneous cellular membrane structure inside the medium (an electrolyte with relatively high permittivity), potentially leading to local high temperature within the cancer cells. This produced local high temperature was very likely to be much higher than the global temperature. Further investigations should be done to confirm whether this local higher temperature can exist and whether it can impact the cancer cells.

4.5 Summary

In this chapter, the efficacy of PEFE in killing cancer cells was first examined *in vitro*, then further confirmed *in vivo*. PEFE under different conditions was generated and many regimens were conducted to progress to increased efficacy. In order to uncover the potential mechanism of how PEFE induces cancer cell death at the molecular level, a multi-technique approach was applied including studying cellular morphology, organelles, and signalling proteins. Furthermore, Kidins220 was considered as a potential biomarker in PEFE treatments using two different cell lines *in vitro*.

5 Biological Effects of PEFE on Apoptosis of Cancer Cells

5.1 Introduction

With the rapid development in economy and technologies throughout the globe in recent decades, electromagnetic field exposure has become more prevalent in daily life for almost everyone(Bhangari et al., 2019). Initially, electromagnetic field exposure was mainly concentrated in regions along the power lines and near base stations. In recent years, microwave technology has been dramatically expanded, owing to a much wider range of applications of wireless technologies from mobile phones, Bluetooth to Wi-Fi apparatus in every home(Parmar et al., 2019b). As a consequence, the exposure to electromagnetic fields has grown, from only those places near power lines and mobile towers, right through to almost all homes, workplaces and the wider society via these devices. Today, 5G millimetre wave technology is upon us, expanding and enabling an increase in 'smart homes' and 'smart cities'(Lynggaard and Skouby, 2015). It is anticipated that 5G technology will increase electromagnetic irradiation by 30%-100% near to and inside homes(Stein, 2019). The increased exposure of electromagnetic field especially that at the microwave range has raised concerns as to how biological tissues might respond to high frequency electromagnetic field and whether or not it is harmful to our health.

The studies on how electromagnetic field exposure at the microwave range may impact biological process in laboratories and on human health have been investigated for decades, with highly controversial and sometimes contradictory results. Using different biological models, a significant number of publications have reported alterations in biological tissues when exposed to microwave irradiation under different conditions(Del Re et al., 2019). However, there are almost as many studies that have reported that there are not any changes in biological samples induced by microwave irradiation. Some researchers have reported alterations elicited by microwave exposure, but these are not consistent results and therefore cannot support conclusions that such exposure is harmful. Taken together, the biological effects of microwave on biological samples remain controversial and further investigation is still required.

Another important aspect is that most of the previous studies on the effects of microwaves on biological samples focus on whether microwave exposure without hyperthermia can exert adverse effects. The experiments were conducted with normal tissues or normal cells from human or other animals. Only a few researchers conducted experiments using cancer cells to investigate how microwave irradiation under normothermic conditions may impact cancer cells.

Mounting studies have revealed that microwave exposure can result in genotoxicity in biological samples under certain circumstances, such as DNA damage, changes to chromosomal conformation and the formation of micronuclei, likely the outcome of thermal injuries. Some other studies have also reported alterations in oxidative stress using different models, possibly without contribution from the anticipated thermal damage to cells and tissues(Del Re et al., 2019). These alterations could potentially induce cell death. If the same adverse effects could be triggered in cancer cells or tumour tissues, this would become a new cancer treatment and potentially extend the area of cancer therapy.

5.1.1 Heat shock protein (HSP)

The expression of heat shock proteins was originally observed in cells exposed to increased temperature. Subsequent studies have revealed increased expression of these proteins when cells are exposed to environmental stress such as high temperature, irradiation, hypoxia, and chemicals (Stankiewicz and Mayer Matthias, 2012). The role of heat shock proteins in eukaryotes has been gradually uncovered, indicating that they are molecular chaperones to protect cells from damage and maintain cellular functions, through assisting protein folding and preventing nonspecific aggregation of misfolded or unfolded proteins (Stankiewicz and Mayer Matthias, 2012).

The 90 kDa HSP (HSP90) protein is the most abundant chaperone and particularly important to the survival of cells (Picard, 2002). In this research, the expression of HSP90 was quantified after microwave irradiation, as an effective method to confirm that no thermal effects were induced.

5.1.2 Cell death

Cell death is broadly divided into three types, necrosis, apoptosis and autophagy. Apoptosis is a slowly progressing and highly regulated, programmed cell death due to internal and external stimuli. The morphological changes include nuclear fragmentation, membrane blebbing and the formation of apoptotic bodies (Hacker, 2000). Conversely, necrosis is an acute cell death process and the morphological features are organelle swelling, mitochondrial dysfunction, massive oxidative stress and rapid plasma membrane permeabilization (Zhivotovsky, 2004). Similarly to apoptosis, autophagy is also a programmed process that relies on *de novo* formation of cytosolic double-membrane vesicles, autophagosomes, to sequester and transport cargo to the lysosome (Martin and Henry, 2013). Data presented in the previous chapter indicated certain features of apoptosis post-PEFE treatment. In the present chapter, the results of investigations focused on certain key proteins that regulate apoptosis are discussed.

Caspases, a family of cysteine proteases, are the central regulators of apoptosis (Budihardjo et al., 1999). Initiator Caspases (including Caspase-2, -8, -9, -10, -11, and -12) are closely coupled to pro-apoptosis signals. Once activated, these Caspases cleave and activate downstream effector Caspases (including Caspase-3, -6, -7) (Budihardjo et al., 1999).

5.1.3 Tight junctions

The tight junction was initially regarded as an inert solute barrier to prevent leaking of transported solutes and water, whilst sealing the paracellular pathway (Furuse et al., 1998). The tight junction complex in epithelial and endothelial cells is broadly made up of three groups of proteins, including membrane integral (transmembrane) proteins, membrane subcoat proteins and other associated proteins. Two critical transmembrane proteins are occludin (a member of the TAMP – tight junction associated transmembrane protein - family) and claudins. Occludin, the very first transmembrane integral protein of tight junction to be identified, exerts its potent effect in regulating paracellular permeability and plays an important role in cellular structure and barrier function (Furuse et al., 1998) it is also believed to be responsible for a number of other cellular functions but evidence remains scanty,

though it is suggested that it is involved in cell polarity and partitioning. The claudins are a large group of transmembrane proteins that are structurally related and bear similarities to occludin and appear to be tissue specific in origin (Oliveira and Morgado-Diaz, 2007). Both occludins and claudins, via homotypic and heterotypic interactions with the same group proteins on another cell, form an intercellular 'sealing' structure and control the paracellular permeability of macromolecules and cells. The membrane integral proteins are linked to the cytoskeleton by a group of subcoat proteins, namely the Zonula Occluden (ZO) family proteins, which include ZO-1, ZO-2 and ZO-3. ZO-1 was the very first tight junctional protein to be discovered. In addition to membrane integral proteins and subcoat proteins, a long list of other proteins are also important components of the tight junction including those that assist cytoplasmic actin-binding and regulating intracellular signalling of tight junctions.

ZO-1 (220 kD), also known as Tight Junction Protein-1 (*TJP1*), is encoded by the *TJP1* gene of the zona occludens proteins family. This protein is known to be involved in signal transduction at cell – cell junctions (Mohandas et al., 1995).

The outcome of the experimental work detailed in the previous chapter found morphological changes and resistance to electric current (ECIS based assays), indicating that PEFE induces changes in the barrier function of breast cancer cells. In this chapter, investigation of the effect of chronic pulsed electromagnetic fields exposure (PEFE), at 2.2GHz under non-thermal conditions on cancer cells *in vitro*, is discussed. Non-thermal conditions were ensured by temperature monitoring and confirmed by examining the expression of heat shock proteins, as presented in Chapters 3 and 4. After exposure, cancer cell death was observed visually and verified through quantification of the expression of important proteins in cell death signalling pathways such as caspase3. Furthermore, cellular tight junction markers such as ZO-1 were examined in order to uncover the mechanism of how PEFE interacted with cancer cells, leading to cell death.

5.2 Method

5.2.1 Cell preparation for PEFE treatments

The cell line used in this investigation was MDA-MB-231 and 8×10^4 cells per well were seeded in two separate wells in one 96 well plate while another 5×10^5 cells per well were seeded in two wells of one 24 well plate. The seeded cancer cells were incubated at 37℃ and were allowed sufficient time to adhere to culture ware. The cells were cultured until a monolayer was formed. Prior to PEFE treatments, cell culture medium was refreshed with 200µl and 1.5ml for 96 well plate and 24 well plate respectively, meanwhile, removing any remaining dead cells. In these experiments, triplicate settings were prepared and tested to ensure consistency.

5.2.2 PEFE treatment instrumentation

In this study, the frequency of the PEFE system was fixed at 2.2GHz, as per conditions obtained from prior tests (presented in Chapters 3 and 4). The peak input power level was set as 2 watts, which was fairly similar to the output power of cellular phones. When the calibration of the PEFE system was completed, the circuit connection was adjusted to inject PEFE signals into biological samples. The probe was inserted into the incubator where the cancer cells were cultured, then immerged into wells containing cancer cells. The distance between the probe tip and the bottom of well was fixed at 1mm, as per prior tests (Chapter 4). For the cancer cells cultured in the 96 well plate, the PEFE treatments lasted 7 hours, while the duration of PEFE treatments for cells cultured in the 24 well plate, was 12 hours. Temperature monitoring was conducted throughout the entire procedure of PEFE treatments.

5.2.3 Heat only experiments

Similarly to conditions presented in Chapter 4, the control samples were treated with heat only using a dedicated heat pad, which was able to heat the bottom of the 96 or 24 well plates directly. The heating lasted 7 hours for the cells cultured in 96 well plates and 12 hours for 24 well plates, respectively **(n = 3)**. The temperature for heating was set at 40℃, 45℃ and 50℃. These experiments were replicated three times in order to achieve consistent results and enable statistical testing.

5.2.4 Viability assessment

Cell viability was first inspected visually before PEFE treatments and direct heating A second cell viability assessment was performed immediately after PEFE treatments and direct heating, under microscopy and using trypan blue staining. The final cell viability assessment was completed at 24 hours after PEFE treatments and direct heating, under microscopy and using trypan blue staining.

When performing trypan blue staining, the cultured cancer cells were detached first using EDTA-trypsin buffer. Cell culture medium was aspirated then 20µl and 100µl of EDTA-trypsin solution was added to 96 well plate and 24 well plates respectively, followed by 5-minute incubation. The cancer cells were then inspected under microscopy to confirm all of the cells were detached. Once detached, 80µl and 900µl cell culture medium was added into the wells to neutralize the trypsin and 10µl of cell suspension was transferred to a 0.5ml microfuge containing 10µl trypan blue, followed by gently mixing. Subsequently, 10µl of the mixture was transferred to cell counting chamber slides (Fisher Scientific UK Ltd) and the death rate of the treated cells calculated using a Countess™ II Automated Cell Counter (Thermo Fisher Scientific Inc.).

5.2.5 Protein extraction, SDS-PAGE, and Western blot analysis

The protein was extracted from the cells treated by PEFE and quantified using DC Protein Assay Kit (BIO-RAD, USA). After SDS-PAGE, the protein was transferred onto PVDF membranes then probed with anti-HSP90, anti-Caspase3, anti-Caspase9 and anti-ZO-1 primary antibody and corresponding peroxidise-conjugated secondary antibodies. The protein bands were visualised using a chemiluminescence detection kit.

5.2.6 DAPI staining

The cancer cells underwent PEFE treatments and direct heating at 40℃. These were incubated at 37℃ for 6 hours, then collected for DAPI staining, where 2µl of DAPI was transferred to those treated cancer cells and directly heated at 40℃ separately. After one hour of incubation at 37℃, the results were visualised using an EVOS Auto imaging system (Thermo Fisher Scientific, Waltham, MA USA).

5.2.7 Immunofluorescence (IFC) Staining

MCF-7 breast cancer cells were seeded into Millicell® EZ slide (Merck KGaA, Darmstadt, Germany) and grew until 100% confluence, then were treated with PEFE for 5 hours. After treatments, the cells were collected and stained using IFC, please refer to section 2.12.

5.2.8 Protein extraction for Kinexus™ antibody microarrays

To expand the investigation of the effect of PEFE on cancer cells and PEFE influence on molecular signalling, a protein kinase array - Kinexus845 platform was employed. Proteins extracted from cancer cells underwent PEFE treatments and together with the untreated control group, were sent for Kinexus™ antibody microarray analysis (Kinexus Bioinformatics, Vancouver, British Columbia, Canada).

5.3 Results

5.3.1 Heat only experiments

5.3.1.1 Direct heating of cancer cells cultured in 96 well plates

The cultured cells in 96 well plates from control groups were heated directly at 40℃, 45℃ and 50℃ separately in triplicate **(n = 3)**. The results of viability assessment were conducted before the experiment commenced (‘0h’) and immediately after the conclusion of the experiment (‘7h’), as shown in Figure 5.1.

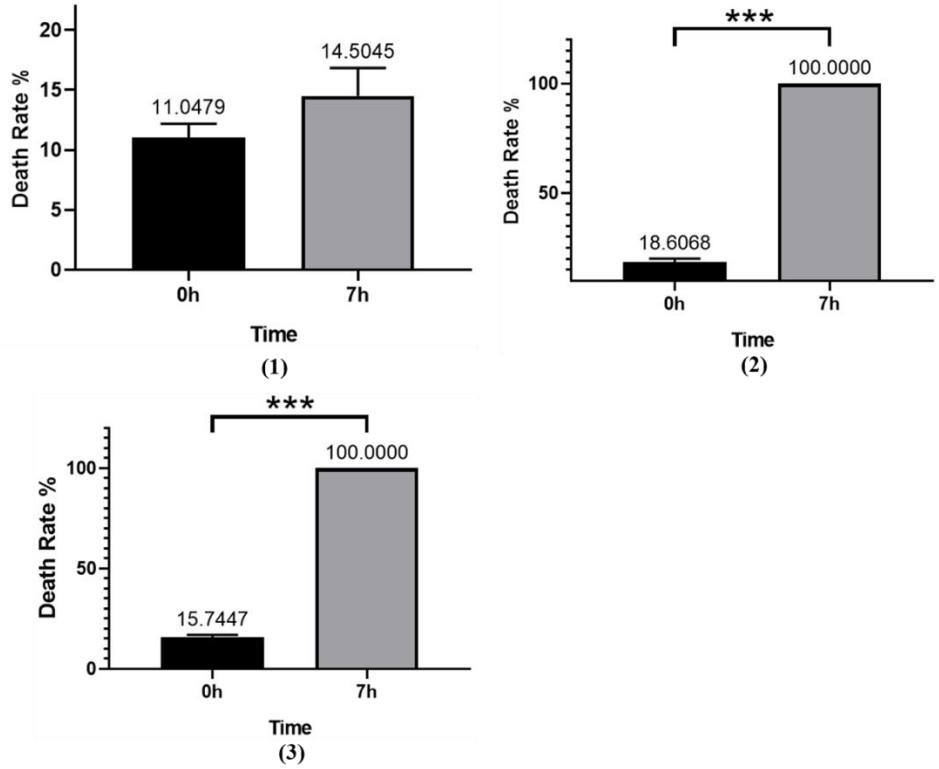

Figure 5.1 Direct heating of cultured cancer cells in 96 well plate. Cell viability was accessed before experiments ('0h') and immediately after experiments ('7h'). (1) Direct heating at 40℃. (2) Direct heating at 45℃. (3) Direct heating at 50℃. Error bar stands for standard error of means. ***p<0.001. No statistical significance was observed in graph (1).

When heating at 45℃ and 50℃ for 7 hours, all of the cultured cancer cells died, confirmed in Figure 5.1 (2) and (3). As for 40℃, no significant cell death was observed; this was checked immediately after the 7-hour experiment, as shown in Figure 5.1(1).

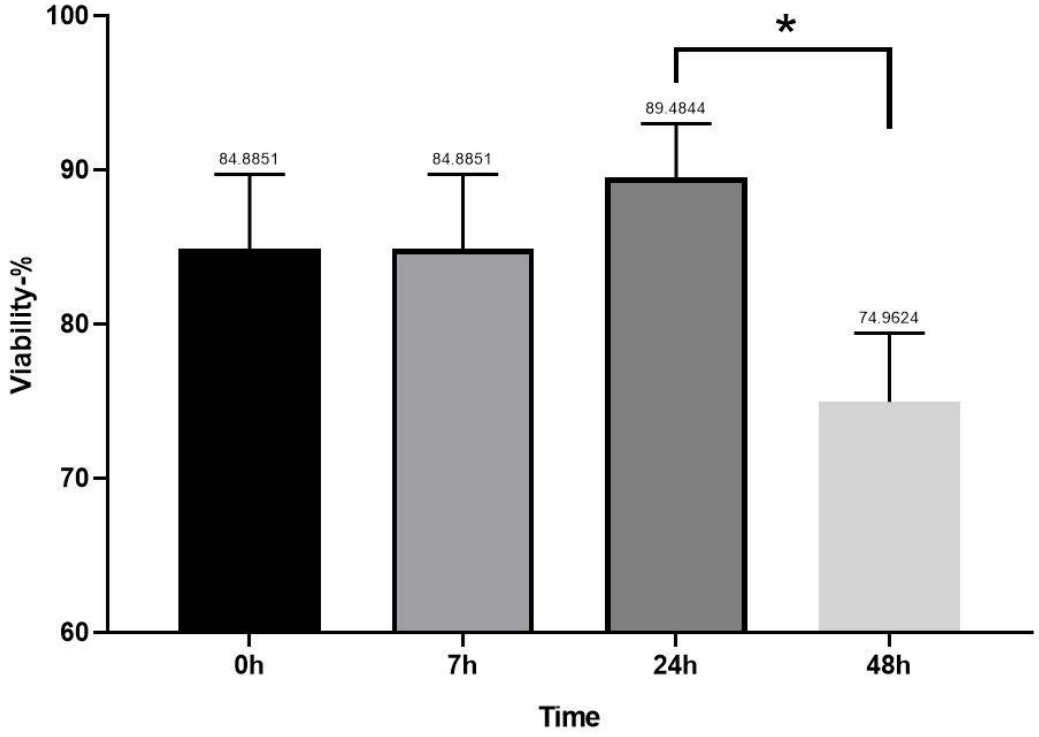

Figure 5.2 Direct heating of cultured cancer cells in 96 well plate at 40℃ for 7 hours. Cell viability was accessed before experiments ('0h') and immediately after experiments ('7h'), 24 ('24h') and 48 ('48h') hours after experiments. Error bar stands for standard error of means. *p<0.05.

Cell treated at 40℃ were continuously monitored for their death for 24 and 48 hours after experimentation. As shown in Figure 5.2, the results did not show any significant differences in viability until 48 hours post experiment. Regarding the decreased viability at 48 hours after experiments, this was due to normal cell senescence and death, partly due to over confluency, rather than direct heating. Taking the results in Figure 5.1 and 5.2 together, it can be concluded that cellular temperature at approximately 40℃ was safe for cultured cancer cells.

5.3.1.2 Direct heating on cancer cells cultured in 24 well plates

When heating the cells in a 24 well plate, a further 5 more hours were required due to the larger volume compared to a 96 well plate. Cell viability was checked before the experiment, immediately after the experiment and then, 24 hours and 48 hours after the experiment. The results are shown in Figure 5.3.

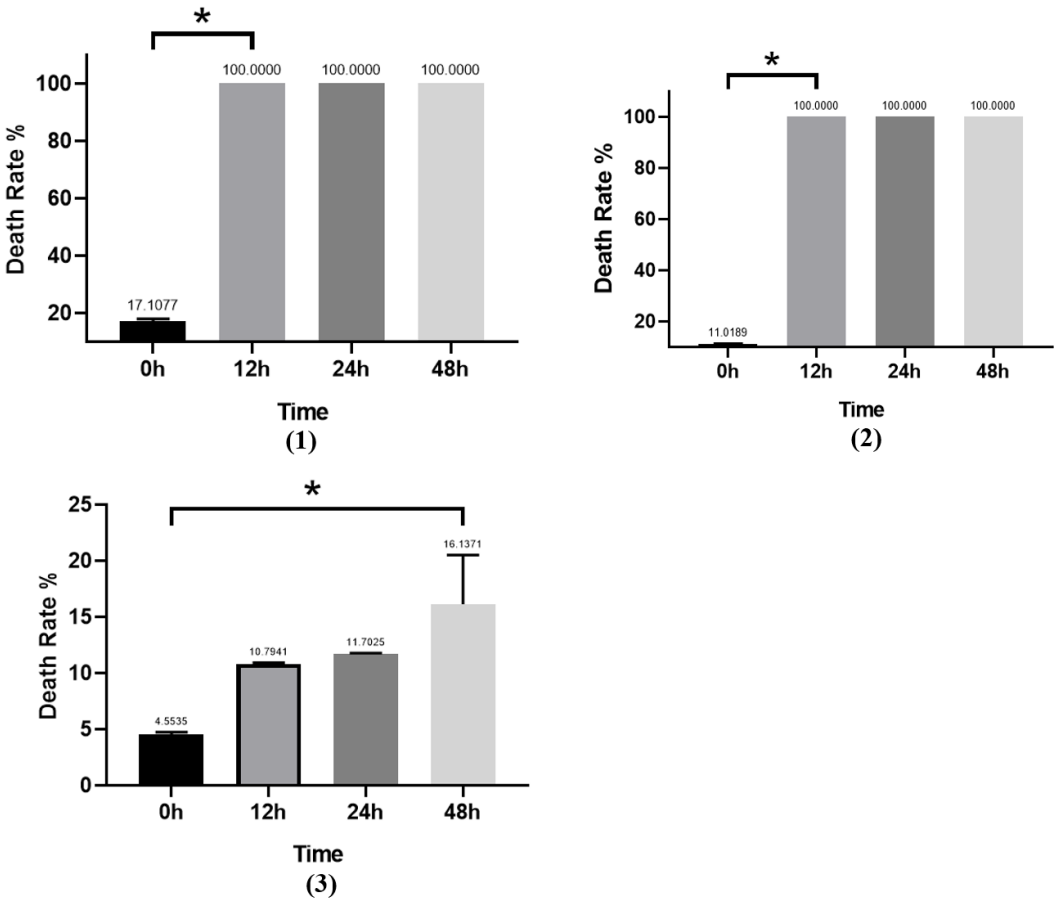

Figure 5.3 Direct heating of cultured cancer cells in 24 well plate. Cell viability was accessed before experiments ('0h'), immediately after experiments ('7h'), 24 hours ('24h') and 48 ('48h') hours after experiments. (1) Direct heating at 45℃. (2) Direct heating at 50℃. (3) Direct heating at 40℃. Error bar stands for standard error of means. *p<0.05.

It is clear from Figure 5.3 (1) and (2) that 100% of cultured cells died after direct heating if the temperature was set at 45℃ or 50℃. When the temperature was 40℃, direct heating seemed to not induce significant cell death until 48 hours after experimentation, shown in Figure 5.3 (3). Considering normal cell death and calculation errors, this slightly increased number of dead cells was less likely due to direct heating, indicating that cellular temperature at approximately 40℃ was safe for cultured cancer cells in a 24 well plate. Collectively, the cell responses to heat in the two culture wares, namely 96 well and 24 well plates which were used in subsequent experiments, were similar.

5.3.2 Cell death after PEFE treatments

Cancer cells cultured in 24 well and 96 well plates were treated with PEFE for 12 hours and 7 hours respectively. The temperature was monitored throughout the entire treatment. The maximum temperature recorded was 40.6℃, which was the area immediately under the probe tip. The maximum temperature of cells beyond the probe tip was near or below 40℃.

The viability and morphology of the cells were initially inspected visually, immediately after treatments and 24 hours post treatment, shown in Figure 5.4 and 5.5. Immediately after the treatment, cultured cancer cells maintained normal morphology and stayed healthy. However, treated cancer cells exhibited altered morphology after 24 hours, when cells became individual and round, which are classic signs of cell stress and apoptosis (Hacker, 2000).

In order to confirm the rate of induced cell death, cell viability was assessed using trypan blue staining. Cell death rate was also calculated using a Countess™ II Automated Cell Counter (Thermo Fisher Scientific Inc.). The results revealed that the cells treated with PEFE were completely eradicated in both 24 well and 96 well plates.

In a clear contrast, the control group was treated by direct heating at 40℃ and failed to show any significant cell death. It can be concluded that the elicited cell death after treatments was under the influence of PEFE, instead of temperature.

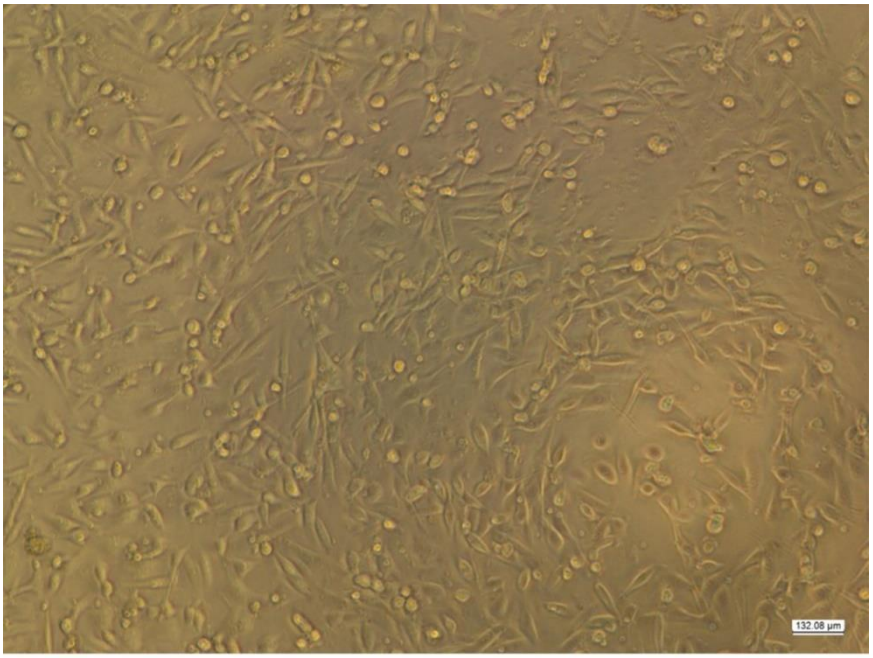

(1)

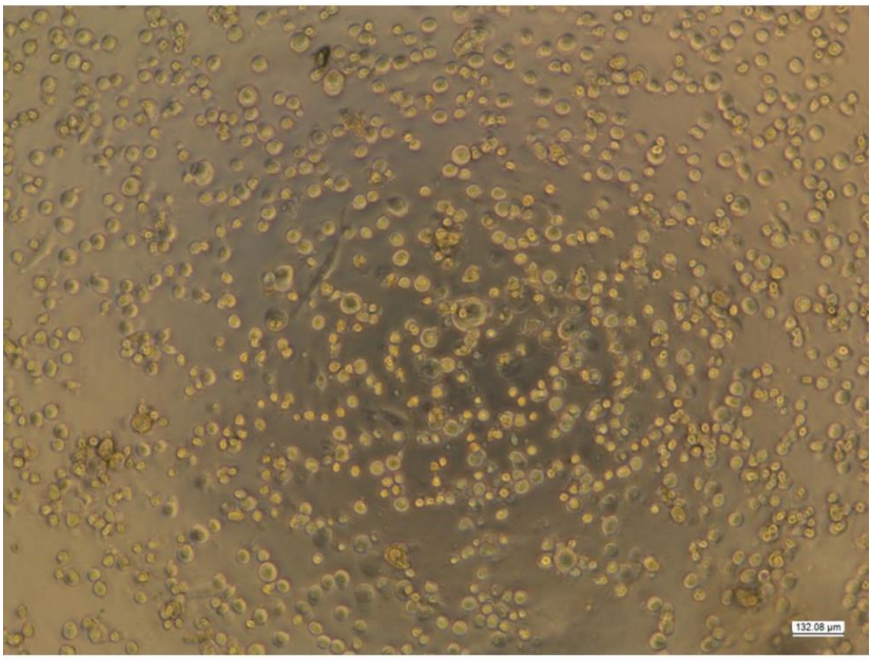

(2)

Figure 5.4 Cell morphology assessment of the treated cancer cells in 24 well plate. (1) Cell morphology observed immediately after PEFE treatments. (2) Altered morphology observed 24 hours after PEFE treatments. Scale bar: 132.08µm. Magnification:10X

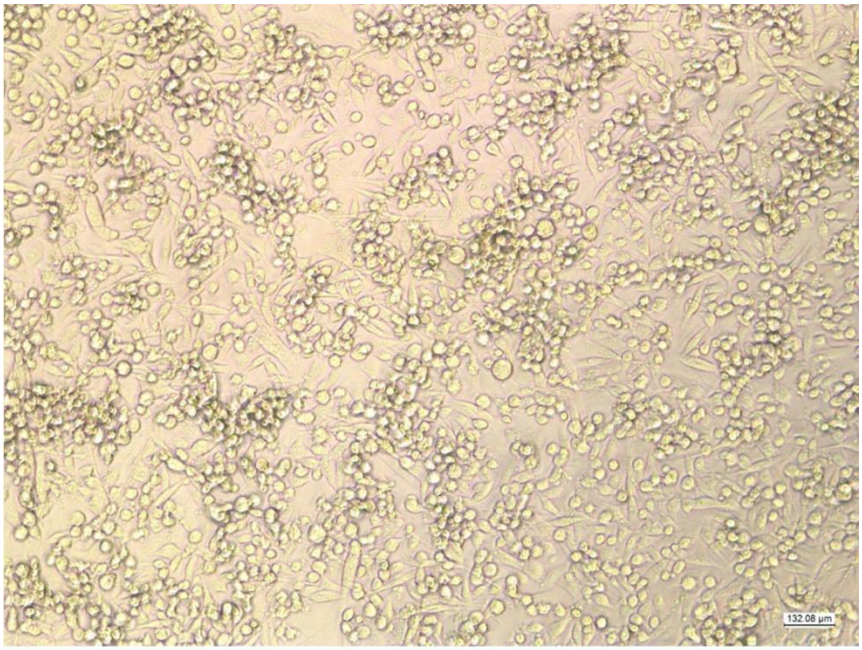

(1)

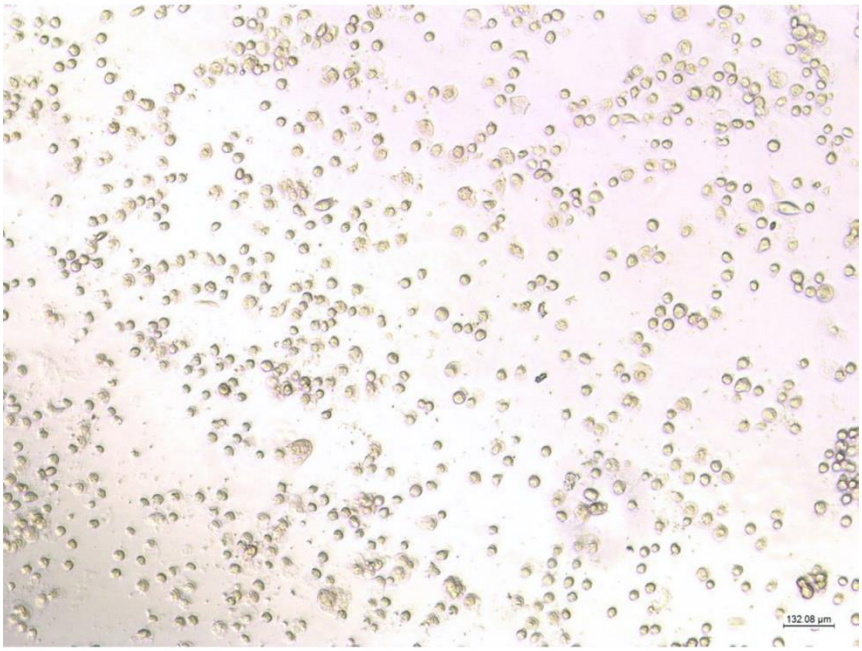

(2)

Figure 5.5 Cell morphology assessment of the treated cancer cells in 96 well plate. (1) Cell morphology observed immediately after PEFE treatments. (2) Altered morphology observed 24 hours after PEFE treatments. Scale bar: 132.08µm. Magnification:10X

5.3.3 Confirmation of cell apoptosis using DAPI staining

DAPI staining was conducted to see changes in nuclear morphology following PEFE treatment. The results showed that breast cancer cells after PEFE treatment had blebbing and condensed nuclear DNA (Figure 5.6b) in comparison to the heathy nuclei in the control group (Figure 5.6a).

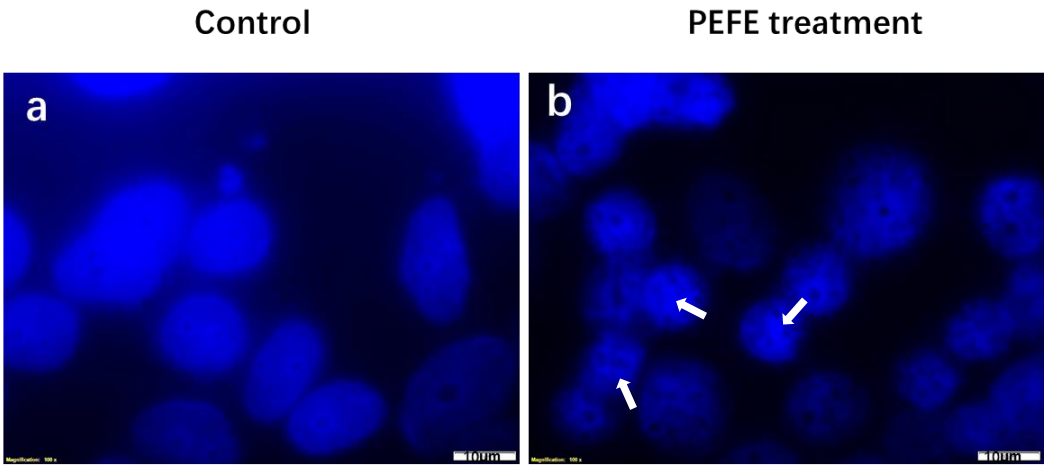

Figure 5.6 DAPI staining of cell nuclear on MCF-7 breast cancer cells. a: nuclear of MCF-7 control cells. b: nuclear of MCF-7 breast cancer cells with PEFE treatment for 5 hours. Arrow indicates condensed nuclear DNA. Scale bar: 10um. Magnification:100X.

5.3.4 The impact of PEFE in regulating cellular functions with involvement of cell signalling in breast cancer cells

In order to investigate the potential response of signalling pathways caused by PEFE treatment of breast cancer cells, a screening of proteins and protein phosphorylation affected by PEFE treatment in MDA-MB-231 breast cancer cells was performed using a protein microarray (Kinexus™ antibody microarray, Kinexus, British Columbia, Canada). The following images (Figure 5.7) are representative of the samples.

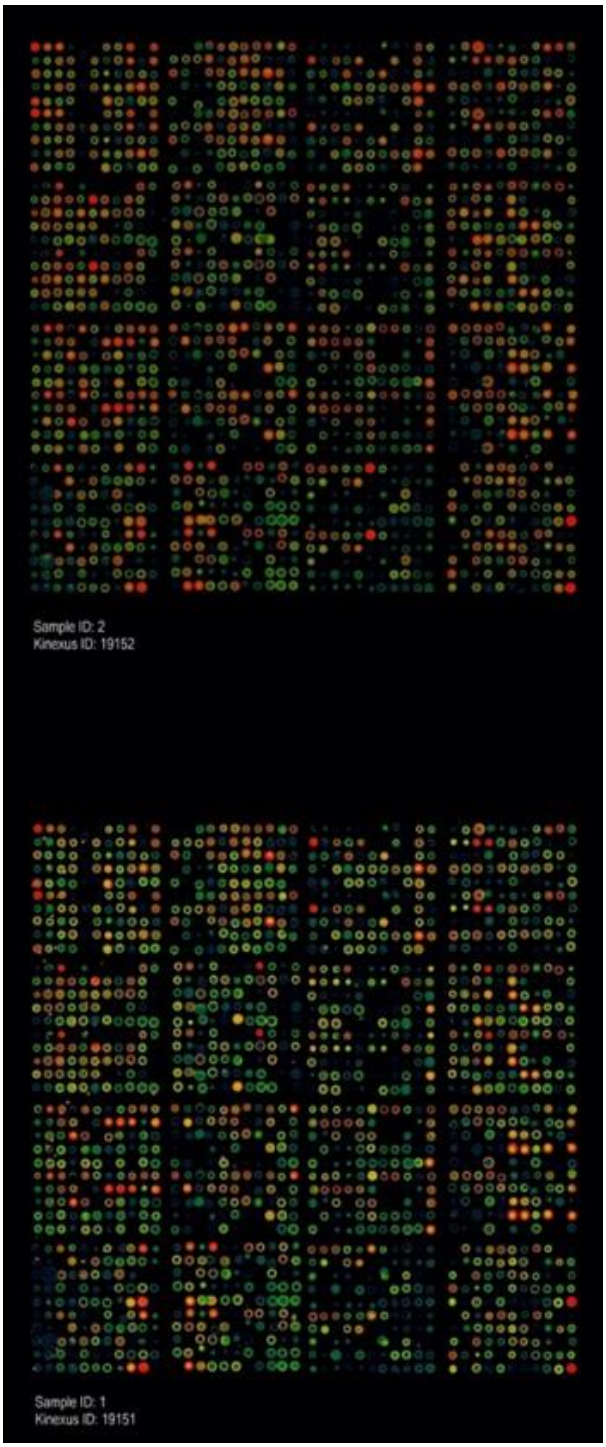

Figure 5.7 Images from Kinexus protein microarray. Array-1 (on the top, Kinexus ID:19152) is from control group and array-2 (on the bottom, Kinexus ID:19151) is from the cells underwent PEFE treatments. The signal intensity represents the different expression level of examined target protein.

The platform produced comprehensive information on the changes in kinases following PEFE treatment. These changes encompass signalling events for a number of pathways regulating cellular biological behavior. It was found that molecules related to cell motility and cell apoptosis were amongst those with the most significant changes after PEFE treatment and that these reflected the function and morphological alterations reported in the previous sections of this thesis. A decreased level of motility-related proteins including FAK (focal adhesion kinase) Vimentin, PAK1 (Serine/threonine-protein kinase, encoded by the *PAK1* gene), PAK4 (Serine/threonine-protein kinase, encoded by the *PAK4* gene), VAV1 (Proto-oncogene vav, encoded by the *VAV1* gene), and an increased level of WASP (Wiskott–Aldrich Syndrome protein) and Ezrin (cytovillin or villin-2, encoded by the *EZR* gene) was found in PEFE treated cells in comparison to the control group (Table 5.1). Furthermore, an enhanced expression of STATs (Signal transducer and activator of transcription) and JAKs (Janus kinase), which are associated with cell death, were detected in PEFE-treated MDA-MB-231 cells (Table 5.2).

A group of proteins linked to apoptosis, such as HSP90, Src Kinase (Tyrosine-protein kinase CSK), SMAD family protein (main signal transducers for receptors of the transforming growth factor beta superfamily), AKT (serine/threonine-specific protein kinase), JNK1 proteins ((Mitogen-activated protein kinase 8, encoded by the *MAPK8* gene)) and NKkappaB p65 proteins (nuclear factor NF-kappa-B p65 subunit, encoded by the *RELA* gene), also showed a response to PEFE, as illustrated in Figures 5.8 to Figure 5.15. In Figures 5.8 to 5.10, the altered expression of HSP90 proteins in response to PEFE was demonstrated. It is noteworthy that the total amount of HSP90 proteins was reduced after treatment, whilst the phosphorylated proteins (both S255 and Y484) were increased (Figure 5.9). The expression of Src Kinase at total level and at phosphorylation level was elevated compared with the control group (Figure 5.10). The alterations in expression of SMAD family proteins namely SMAD-1/2/3, are shown in Figure 5.11. It can be observed that PEFE resulted in an increase in phospho-SMAD on serine residues. As for the altered expression induced by PEFE in AKT, whilst PEFE had little impact on the phosphorylation of AKT, it markedly reduced the

level of total AKT protein (Figure 5.12). It can be seen that PEFE had little influence on the phosphorylation of p65 (Figure 5.15).

Table 5.1 The altered expression of proteins related to cell mortality with PEFE treatment. %CFC (change from control in percentage). Negative values of %CFC refers to the reduction degree in signal intensity compared with control

Protein Target Name	%CFC Microwave vs control
WASP	19
Vimentin	-39
FAK (PTK2)	-13
FAK (PTK2)	-17
Ezrin	11
PAK1 (PAKa)	-15
PAK4	-15
VAV1	-31

Table 5.2 The altered expression of STAT and JAK protein members in STAT-JAK signalling. %CFC (change from control in percentage). Positive values of %CFC refers to the increased degrees in PEFE treatment cells compared with control.

Protein Target Name	%CFC Microwave vs control
STAT1a/b	30.51891538
STAT2	29.33859052
STAT2	71.43157842
STAT3	50.46224409
STAT3	30.18784382
STAT5A	32.13923127
STAT5A	26.27407797
STAT5A	20.63437503
STAT5B	11.62723337
JAK1	20.25261807
JAK1	11.09616993
JAK3	10.39499032
JAK3	29.16096096

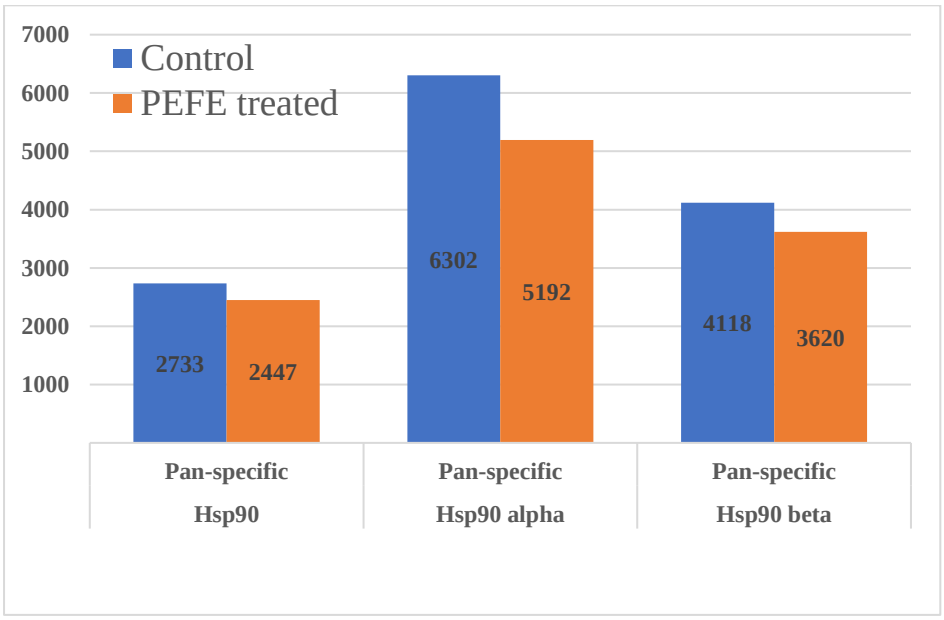

Figure 5.8. Levels of Total HSP90 in MDA MB-231 cells were seen to be reduced after PEFE treatment as demonstrated by the Kinexus platform. 'Control' represented control group and 'PEFE treated' represented the cells underwent PEFE treatments.

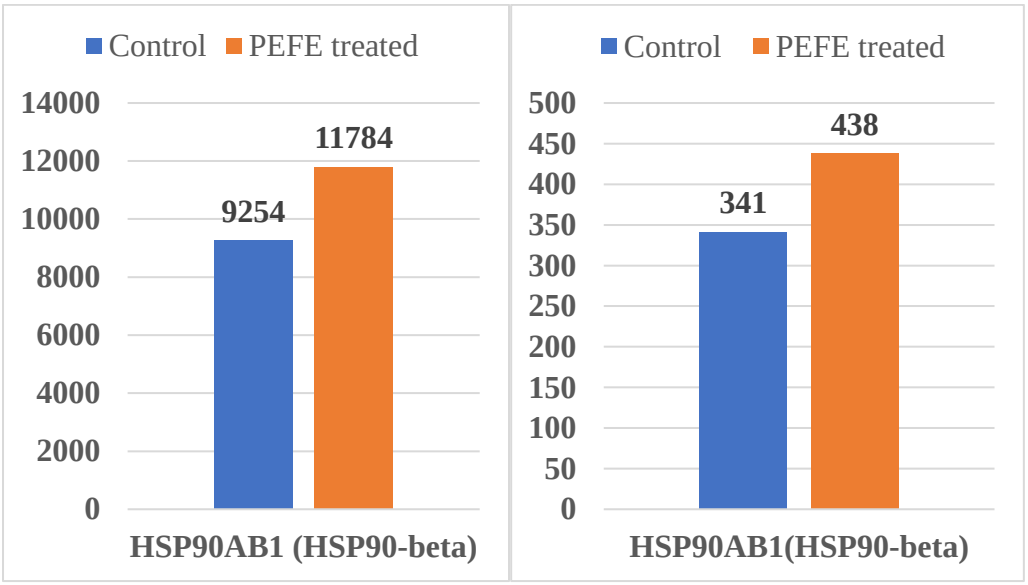

Figure 5.9. Levels of phosphor-HSP90 in MDA MB-231 cells were seen to be increased after PEFE treatment as demonstrated by the Kinexus platform. 'Control' represented control group and 'PEFE treated' represented the cells underwent PEFE treatments. Left: Y484 residual on HSP90; Right S255 residual on HSP90.

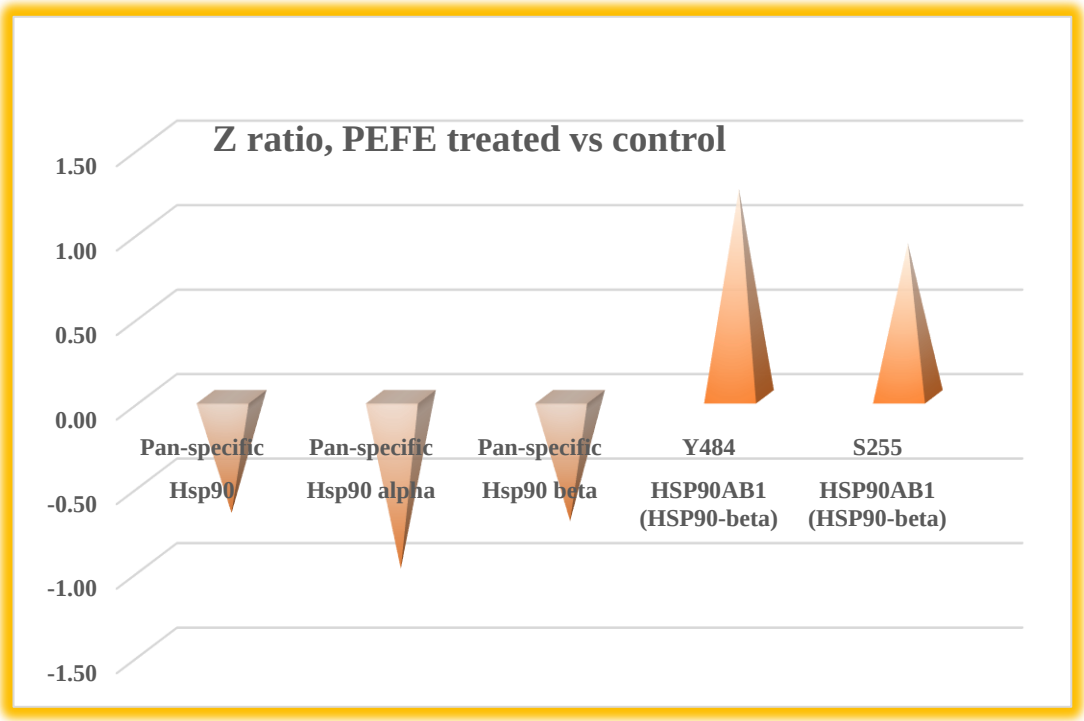

Figure 5.10. Response of HSP90 protein, total level and phosphorylation to PEFE treatment. Shown is Z-ratio.

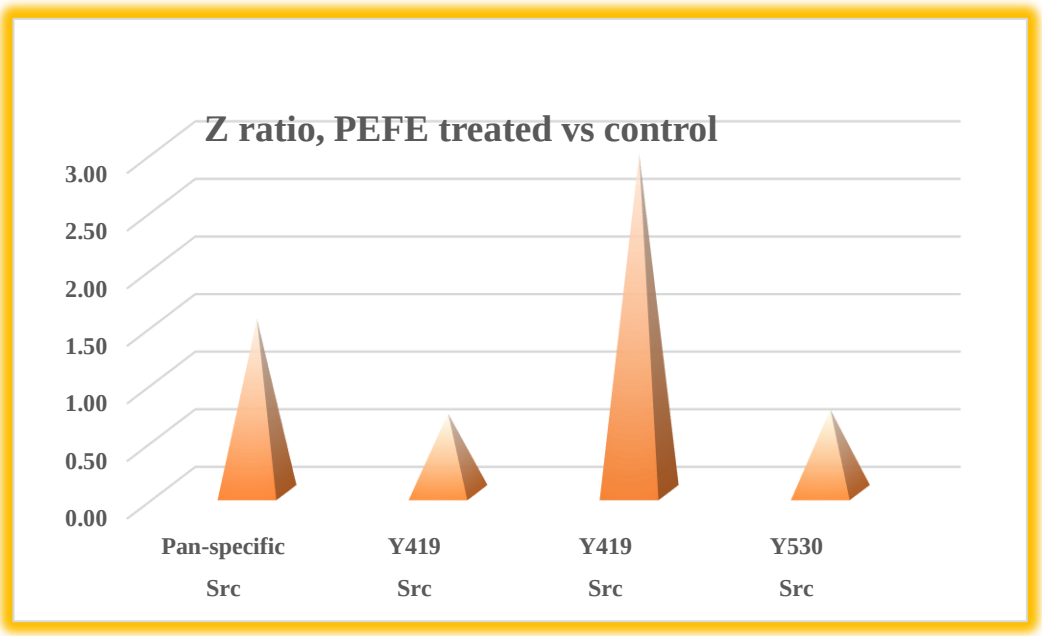

Figure 5.11 Response of Src kinase, total level and phosphorylation to PEFE treatment. Shown are Z-ratio. PEFE treatment resulted in an increase in phosphor-Src.

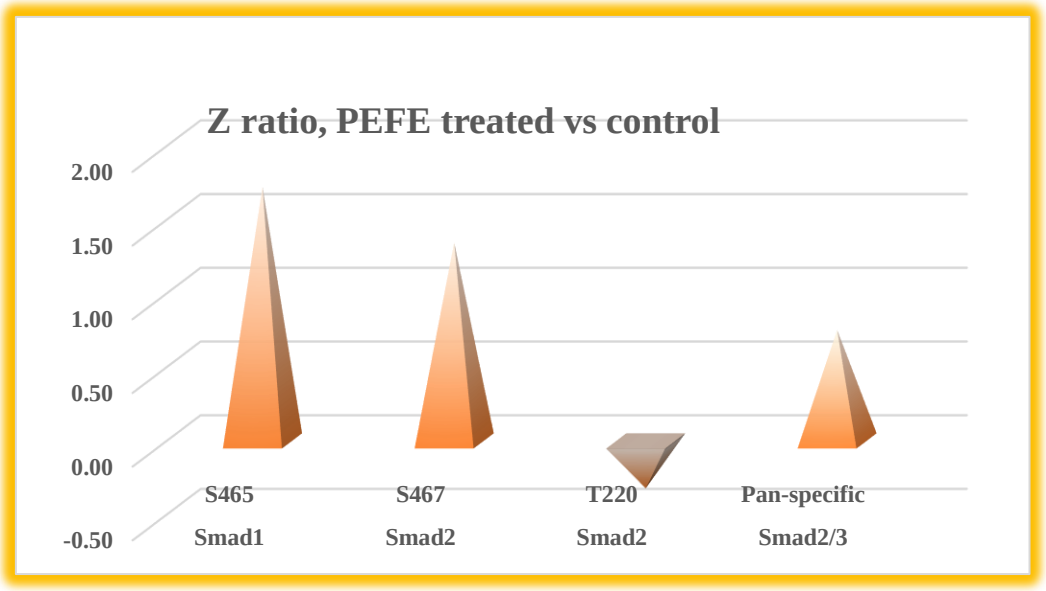

Figure 5.12 Response of the SMAD family protein, SMAD-1/2/3. Shown are Z-ratio. PEFE treatment resulted in an increase in phosphor-SMAD on serine residuals.

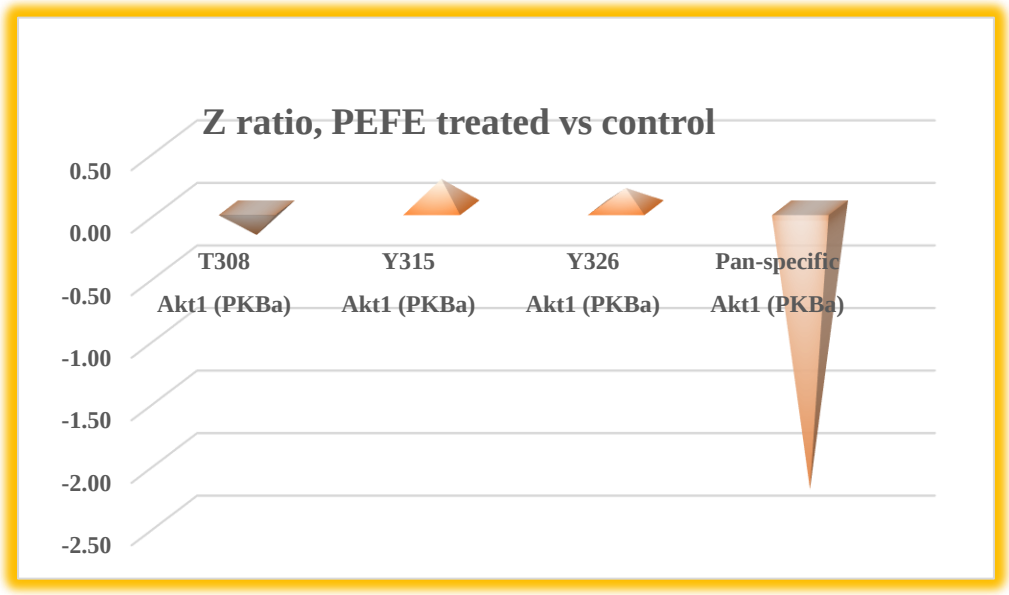

Figure 5.13 Response of the AKT. Whilst PEFE treatment had little impact on the phosphorylation of AKT, it markedly reduced the level of total AKT protein.

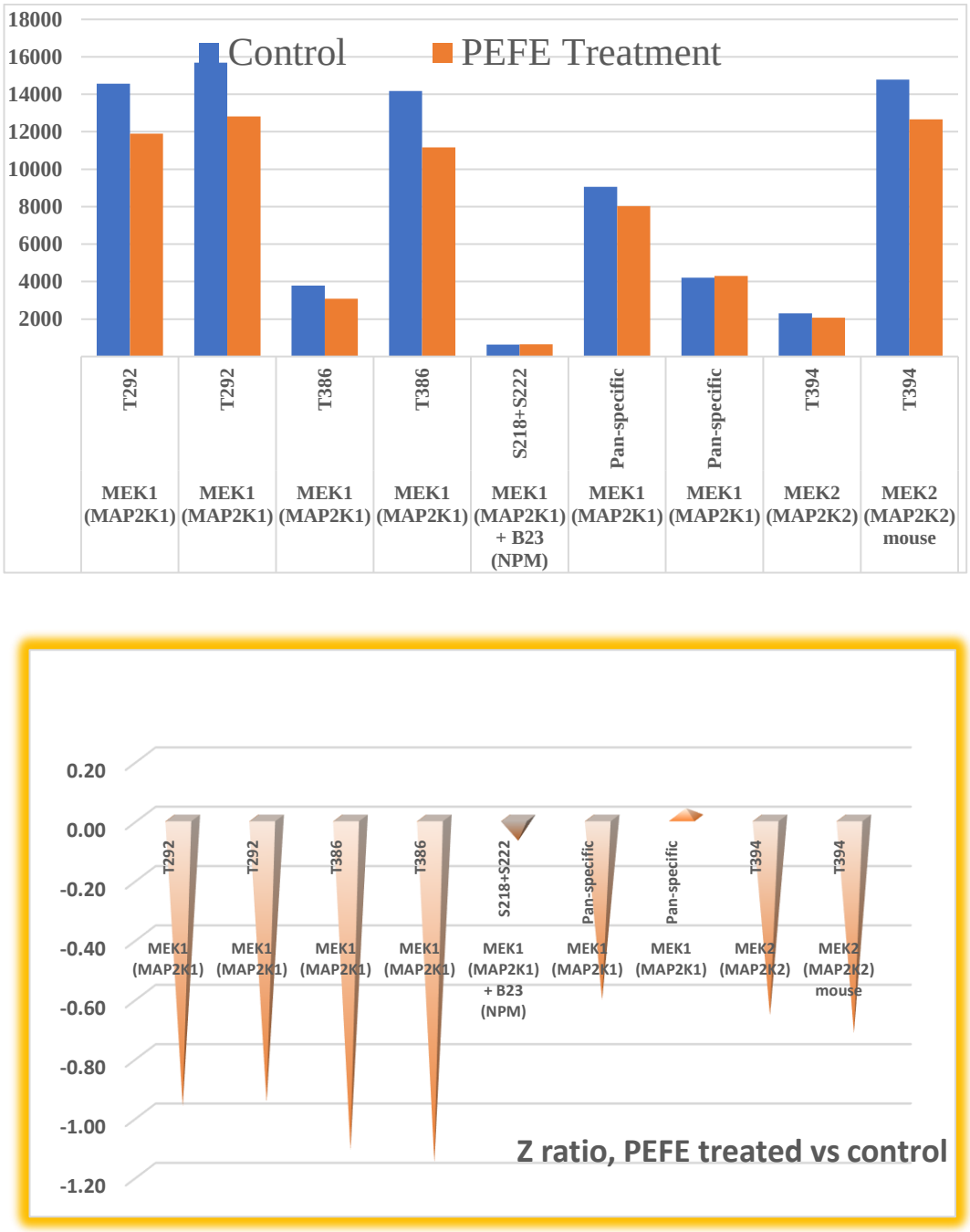

Figure 5.14 Response of MEK1 and MEK2 proteins in MDA BM231 cells, following PEFE treatment. Top: Changes of fluorescence signal in control and PEFE treated cells. Bottom: Z ratio indicating the changes of the respective MEKs in control vs PEFE treatment.

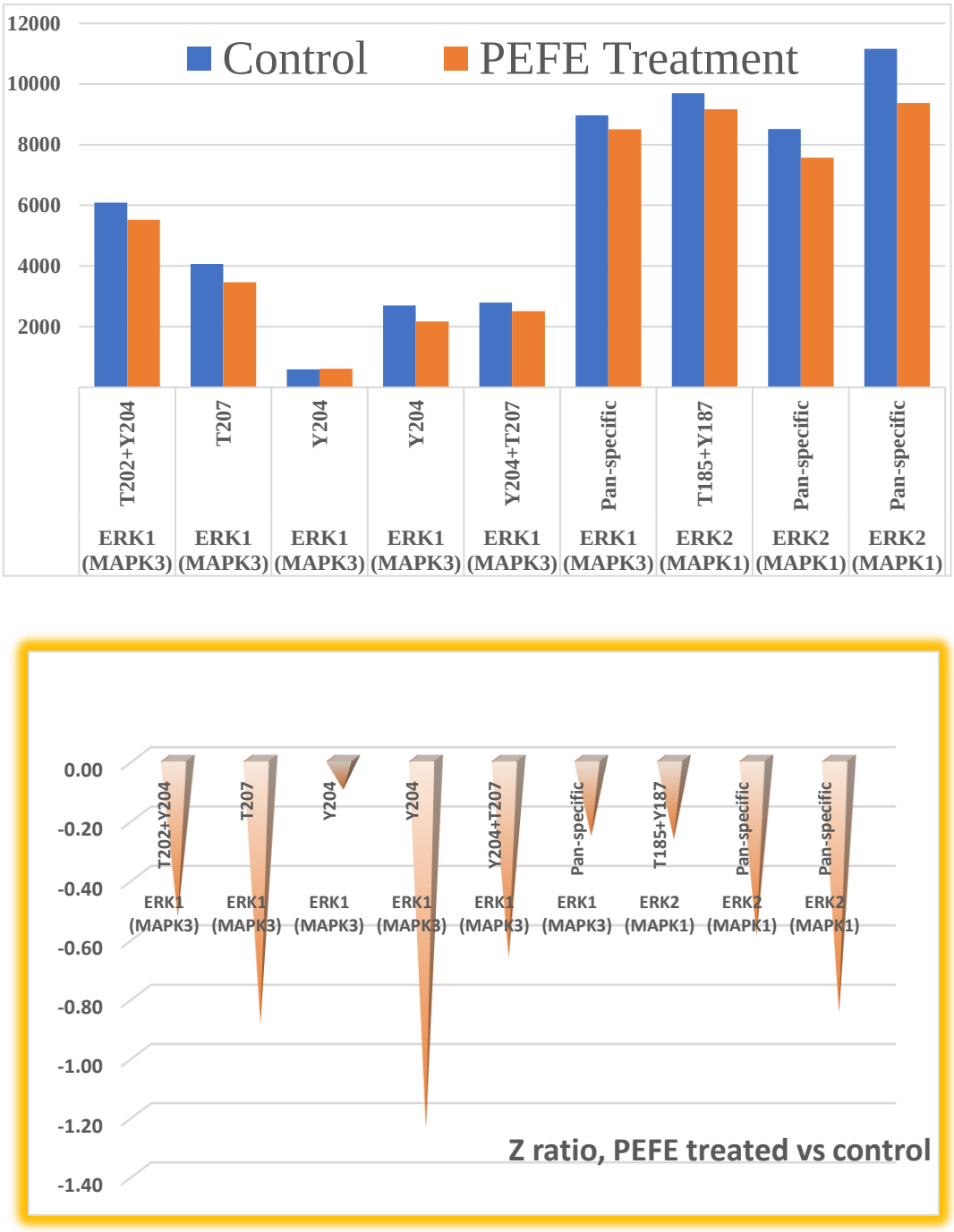

Figure 5.15 Response of ERK1 and ERK2 proteins in MDA BM231 cells, following PEFE treatment. Top: Changes of fluorescence signal in control and PEFE treated cells. Bottom: Z ratio indicating the changes of the respective ERKs in control vs PEFE treatment.

5.3.5 Confirmation of non-thermal effect of PEFE treatment by examining the expression of HSP90

In order to further confirm that cell death after PEFE treatment was caused by PEFE rather than temperature increase, the expression of HSP90 protein was investigated. Changes in HSP90 expression would indicate whether there was any stress response from temperature increase.

Cells were subjected to PEFE treatment for 15 mins, 1 hour, 4 hours and 24 hours, after which proteins were extracted, quantified and standardised to the same concentration. Western blotting was subsequently performed, and one example of the visualised results are illustrated in Figure 5.16 **(n = 3)**. Notably, the treated cells were completely dead after 24 hours, leading to protein degradation. Thus, little protein was extracted and visualised at 24 hours after PEFE treatments, hence no observable bands, Figure 5.17.

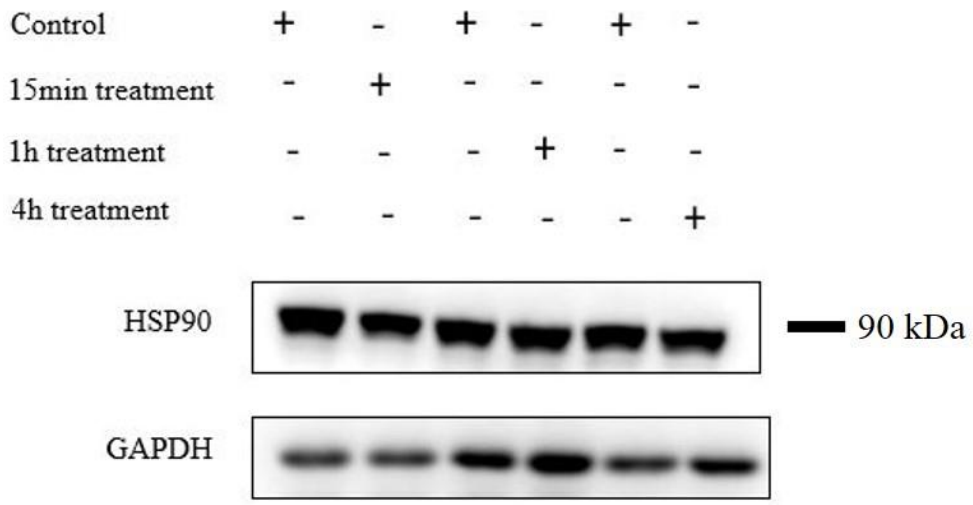

Figure 5.16 Western blot results for the expression of HSP90 extracted from control group ('Control') and cells underwent PEFE treatments ('15min treatment', '1h treatment' and '4h treatment'), indicated by '+'. The expression of HSP90 was examined at 15mins, 1 hour and 4 hours after treatments, respectively. Image shown here is a representative of three replicate of experiments.

The expression of protein was then normalised against the housekeeping control protein, GAPDH, to show any alterations by fold change, shown in Figure 5.17. Fifteen minutes after PEFE treatment, the levels of HSP90 were much lower than that of control cells. This reduction of HSP90 was similar at one hour after PEFE treatment. Four hours after treatment, the degree of reduction of HSP90 was slightly restored, nevertheless, it was still lower than in the untreated control cells.

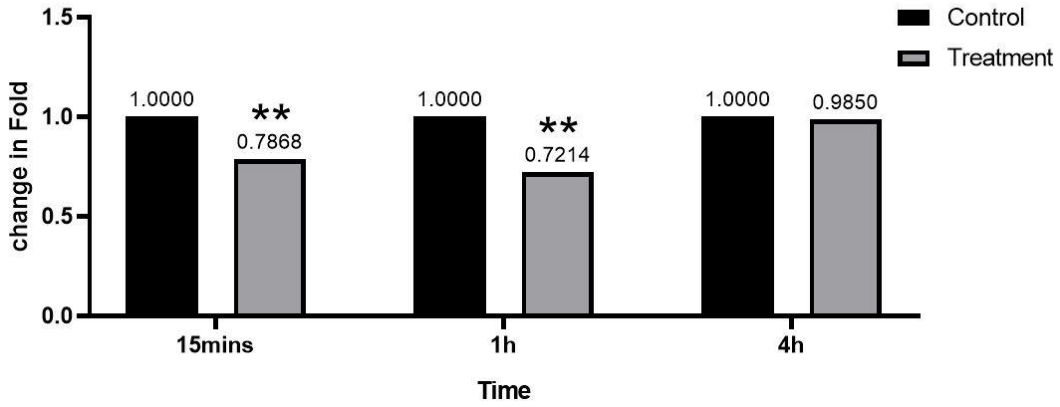

Figure 5.17 The normalised expression of HSP90 in cells underwent PEFE treatments ('Treatment') using the expression of control group ('Control'), examined at 15 mins, 1 hour and 4 hours after PEFE treatments, respectively. Error bar stands for standard error of means. **p <0.01.

5.3.6 Further confirmation of cell apoptosis by examining key proteins in apoptosis signalling pathways

Subsequently, PEFE induced cell apoptosis was further confirmed at the molecular level by examining proteins that are typically involved in cell apoptosis signalling pathways, including Caspase3 and Caspase9. Western blotting was performed to visualise the expression of these two proteins at 15 mins, 1 hour, 4 hours, and 24 hours after treatment. Similarly to HSP90, the protein expression of Caspase3 and Caspase9 at 24 hours after PEFE treatment were not detected due to the degradation of proteins induced by complete cell death. Two examples of the results are shown in Figure 5.18 and Figure 5.19 **(n = 3)**.

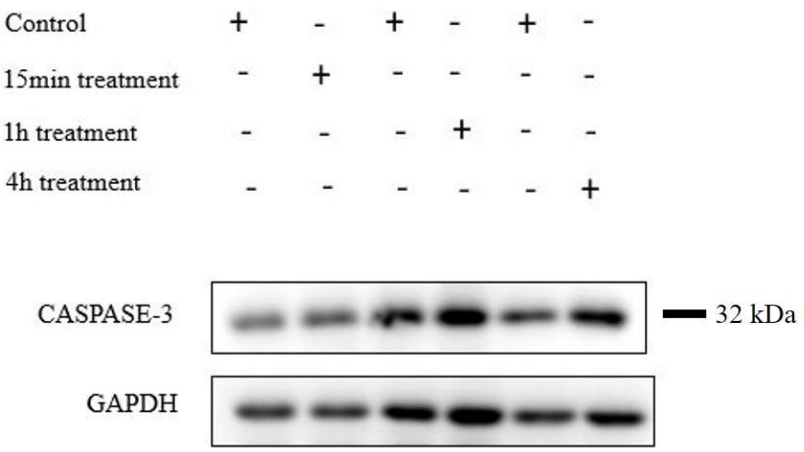

Figure 5.18 Western blot results for the expression of Caspase3 extracted from control group ('Control') and cells underwent PEFE treatments ('15min treatment', '1h treatment' and '4h treatment'), indicated by '+'. The expression of Caspase3 was examined at 15mins, 1 hour and 4 hours after treatments, respectively. Image shown here is a representative of three repeats and is from the same setting as in Figure 5.16. The housekeeping protein image was from the same sample gel cohort of the same experiment as om Figure 5.16.

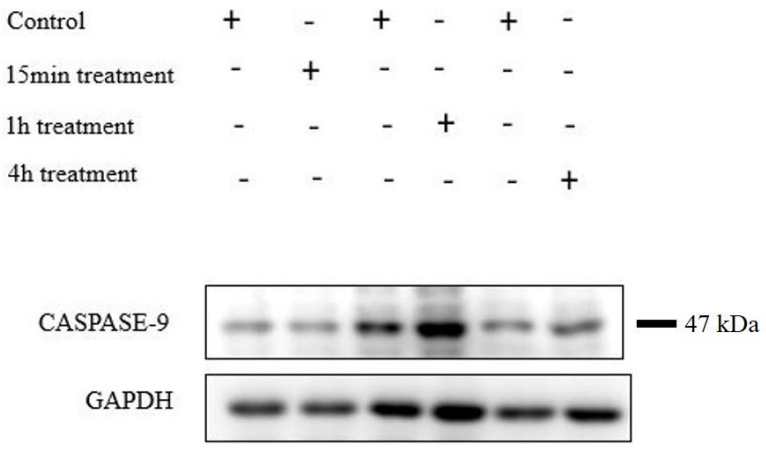

Figure 5.19 Western blot results for the expression of Caspase9 extracted from control group ('Control') and cells underwent PEFE treatments ('15min treatment', '1h treatment' and '4h treatment'), indicated by '+'. The expression of Caspase9 was examined at 15mins, 1 hour and 4 hours after treatments, respectively. Image shown here is a representative of three repeats and is from the same setting as in Figure 5.16. The housekeeping protein image was from the same sample gel cohort of the same experiment as om Figure 5.16.

The alterations in the expression of Caspase3 and Caspase9 were normalised by fold change using the expression levels of the untreated control group. The results are shown in Figure 5.20 and Figure 5.21 respectively.

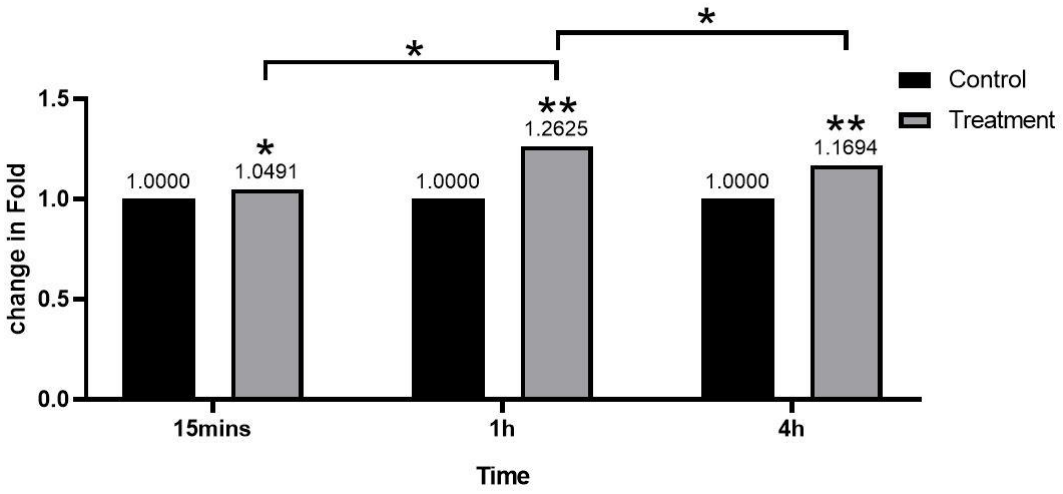

Figure 5.20 The normalised expression of Caspase3 in cells underwent PEFE treatments ('Treatment') using the expression of control group ('Control'), examined at 15 mins, 1 hour and 4 hours after PEFE treatments, respectively. Error bar stands for standard error of means. *p<0.05, **p <0.01.

The expression of Caspase3 increased after PEFE treatments. When considering 15 minutes post treatment, the expression level was only increased slightly compared to the control group. This expression continued to increase at 1 hour before decreasing. The maximum expression of Caspase3 occurred at 1 hour after treatment.

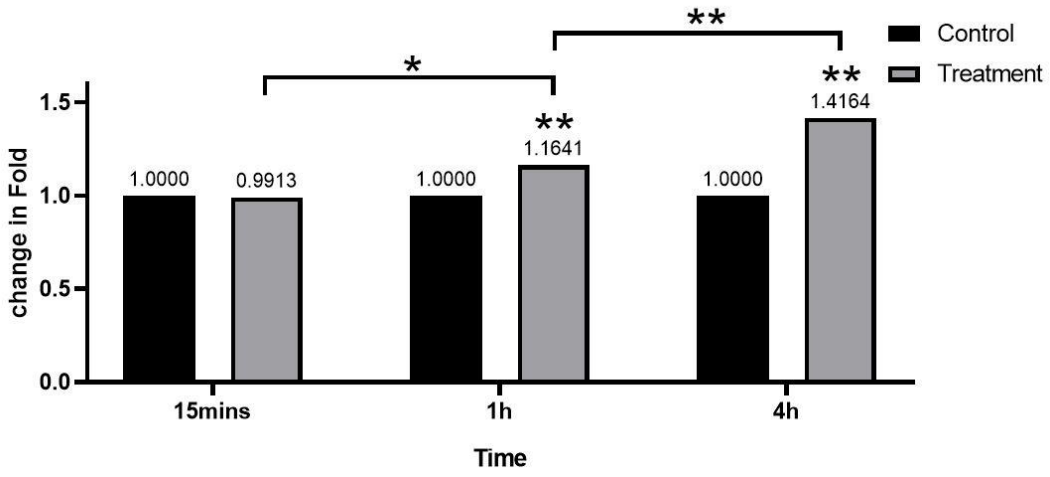

Figure 5.21 The normalised expression of Caspase9 in cells underwent PEFE treatments ('Treatment') using the expression of control group ('Control'), examined at 15 mins, 1 hour and 4 hours after PEFE treatments, respectively. Error bar stands for standard error of means. *p<0.05, **p <0.01.

With Caspase9, the expression at 15 minutes after treatment did not change significantly. However, the expression of Caspase9 went up consistently after 1hour.

The overexpression of Caspase3 and Caspase9 indicated that alterations induced by PEFE treatment occurred in key proteins involved in apoptosis signalling pathways. It is highly likely that some signalling pathways related to cell apoptosis were activated, leading to apoptosis of cancer cells.

5.3.7 Investigation on how PEFE interacted with cellular tight junction (TJ)

In this study, the mechanism of how PEFE exerts its non-thermal effects on cancer cell death was investigated. It is hypothesized here that PEFE initially induced apoptosis only in a small number of cells, *i.e*, those around the probe tip. Following this, the signalling for cell death was transferred through the cell membrane to other cells further away from the probe tip. To investigate this, the expression of ZO-1 was examined and quantified to show any changes in signal transduction at cell – cell junctions (Figure 5.22).

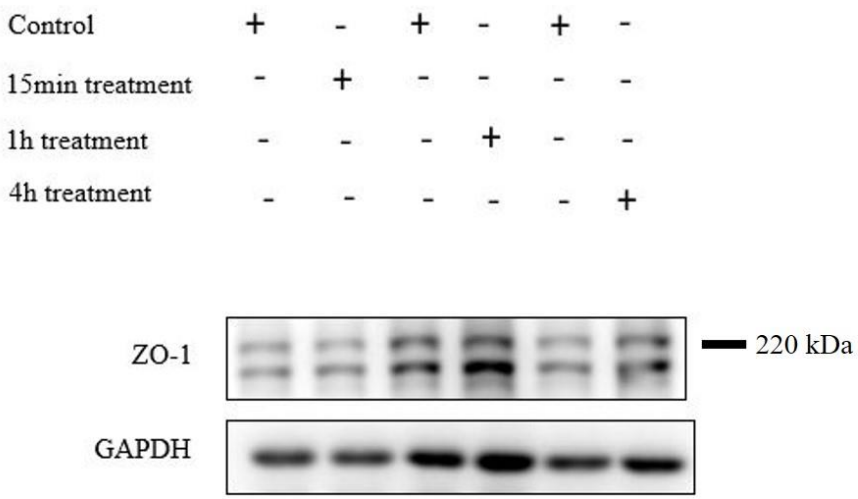

Figure 5.22 An example of Western blot result for the expression of ZO-1 extracted from control group ('Control') and cells underwent PEFE treatments ('15min treatment', '1h treatment' and '4h treatment'), indicated by '+' (n = 3). The expression of HSP90 was examined at 15mins, 1 hour and 4 hours after treatments, respectively. Image shown here is a representative of three repeats and is from the same setting as in Figure 5.16. The housekeeping protein image was from the same sample gel cohort of the same experiment as om Figure 5.16.

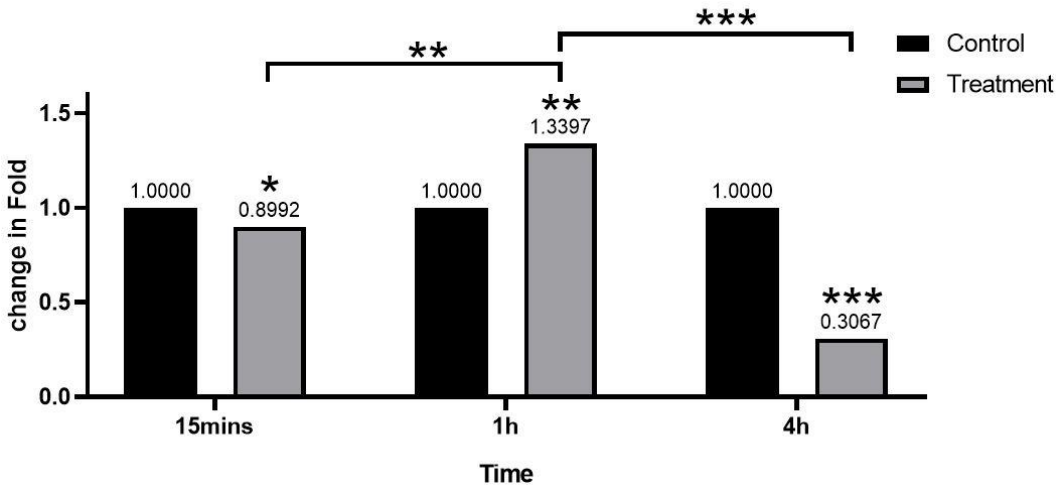

Figure 5.23 The normalised expression of ZO-1 in cells underwent PEFE treatments ('Treatment') using the expression of control group ('Control'), examined at 15 mins, 1 hour and 4 hours after PEFE treatments, respectively. Error bar stands for standard error of means. *p<0.05, **p <0.01, ***p<0.001.

Due to the complete loss of cells after 24 hours, no protein was extracted and quantified in the PEFE treated cells. Thus, there were no bands for 24 hours after treatment, Figure 5.22. The alteration in expression of ZO-1 was quantified by fold change, shown in Figure 5.23.

It can be seen from Figure 5.23 that the expression of ZO-1 in PEFE treated cells was inhibited at 15 minutes after treatment compare to the control group. There was a transient rise in expression at 1 hour after treatment. Three hours later, the expression dramatically decreased when compared with the control group. It can be concluded that the most active signal transduction occurred at 1 hour after PEFE treatment.

5.3.8 Further confirmation on how PEFE interacted with cancer cells by IFC staining

An immunofluorescence assay was conducted on MCF-7 breast cancer cells undergoing PEFE treatment for 5 hours. The cells were stained with ZO-1 primary antibody and a TRITC conjugated secondary antibody. The choice of this cell type was based on the previous studies from the host laboratory showing that it forms stronger and continuous tight junctions and would allow for a clean and fair assessment of any changes. The intact staining of ZO-1 was indeed shown in the present study. Figure 5.24(a) and (b) demonstrate the location of ZO-1 protein which is continuously distributed beneath the intercellular space between the cells. However, following PEFE treatment, the tight junctions, as indicated by ZO-1 staining, were breached as seen by the discontinued and interrupted distribution of ZO-1 ((Figure 5.24(c) and Figure 5.24(d)). ZO-1 is an excellent marker for intact tight junctions. We can observe from the IFC staining that PEFE treatment resulted in reduced expression of ZO-1 at the cell membrane and increased sequestration to the cell nucleus. This is a characteristic of dismantled tight junctions and known to be an indicator of apoptosis.

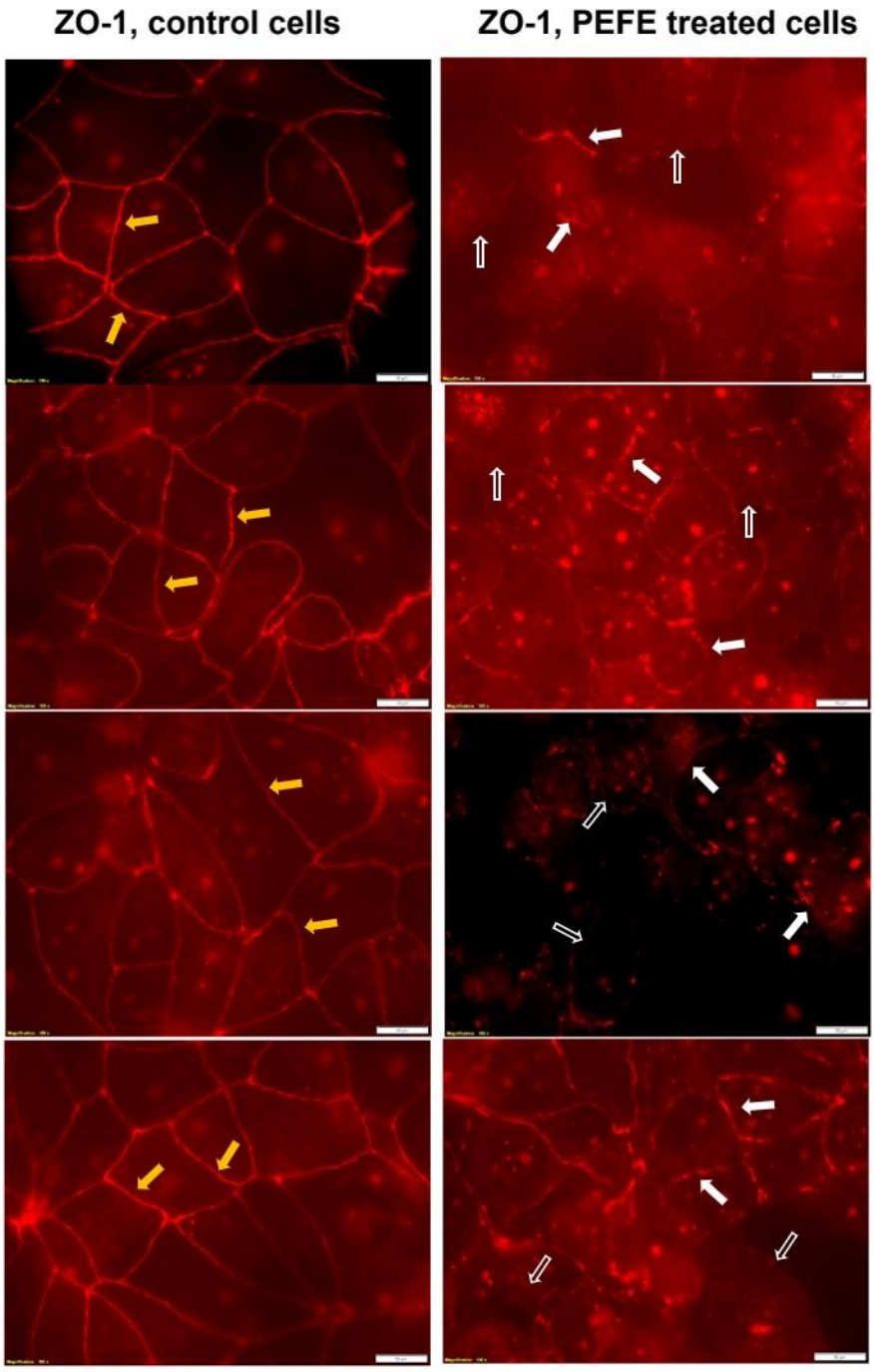

Figure 5.24: Immunofluorescence staining of ZO-1 in MCF-7 breast cancer cells. Left: ZO-1 expression on control cells stained with TRITC secondary antibody. Right: MCF-7 breast cancer cells with PEFE treatment for 5 hours and stained with TRITC secondary antibody. Yellow arrows point to the intact ZO-1 on cell membrane. White solid arrows point to the remaining ZO-1 expression after treatments. White hollow arrows point to the disrupted ZO-1 expression on cell membrane. Scale bar: 10μm. Magnification:100X.

5.4 Discussion

5.4.1 PEFE and non-thermal effects

When PEFE is propagated into biological samples, could the dissipated microwave energy induce temperature increase? In order to investigate the non-thermal effects of PEFE, it is crucial to exclude effects on biological samples induced by temperature increases. It is well known that cell death can be triggered when cellular temperature exceeds 41℃ (Fiorentini and Szasz, 2006). It would appear that cellular temperature at 40℃ is a "safe" temperature at which experiments may be conducted without significant induction of apoptosis. In this study, directly heating cultured cancer cells to 40℃ did not induce any significant cell death. Furthermore, the stress response of heat was also examined by quantifying the expression of HSP90. As a key heat shock protein in mammalian cells, this protein can be overexpressed to modify misfolded or unfolded proteins when cells are exposed to high temperatures, radiation and other stresses from the environment. If the temperature increase caused by PEFE was able to result in cell death, overexpression of HSP90 would be detected (Kalamida et al., 2015). However, Western blot results for HSP90 did not follow this trend, revealing that no temperature stress was detected in PEFE treated cells. Taken together, the cell death observed after PEFE treatments was due to other interactions between PEFE signals and cancer cells, rather than temperature increase.

5.4.2 Chronic microwave exposure induces waveform specific cancer cell death

The type of induced cell death was initially verified under the microscopy based on typical features of three main types of cell death. Immediately after PEFE treatment, the cells were relatively healthy and maintained normal morphology. Cell death was observed after 24 hours indicating that sufficient time was required for the treated cells to die. Since cell necrosis is a rapid cell death, the cell death in this study was less likely to be necrosis. To further investigate the type of cell death, alterations in nuclear morphology were examined using DAPI staining. The nuclear bleeding and condensation were observed in the cells that received PEFE treatment while this did not occur in the control group. This morphological alteration can be an indication of the induced cell apoptosis.

Previous studies conducted by Asano *et al*., (2017b) also confirmed that microwave exposure caused apoptosis of cancer cells, human promyelomonocytic leukamia cell HL60 in this case, and that this was independent of Caspases. In their studies, key proteases from the Caspase family were investigated including Caspase-3, -7, -9, -8, -12. The results showed loss of Caspase9 expression and decreased expression of Caspase12. Although increased expression of other Caspase proteases was detected, it was not statistically significant. Furthermore, the apoptotic protease-activating factor 1 (Apaf-1) was found to be lost, indicating that Caspase-dependent apoptosis was interrupted (Asano et al., 2017b).

In our study, the same cancer cell lines (MDA-MB-231 and MCF-7) were used. Compared with Asano's studies, the main difference was the applied microwave exposure. In Asano's studies, continuous microwave at 2.45GHz was generated and applied on biological samples, while pulsed microwave signals at 2.2GHz were injected into biological samples in our study. Since the frequency and temperature (37℃ *vs* 40℃) were different, the dielectric properties of the biological samples were slightly different as well, leading to different reflected waves. As a result, both incident wave and reflected wave were different. The two kinds of microwave exposure were therefore essentially different in the waveform. It is thus worthwhile to investigate whether the apoptosis was triggered by microwaves through different signalling pathways.

To explore this prospect, the current study assessed Caspase 3 and Caspase 9 expression and found a statistically significant overexpression of both proteins following PEFE treatment, revealing Caspase-depended apoptosis. Importantly, together with the previous studies, the current study strongly indicates the phenomenon that waveform resulted in non-thermal induced apoptosis of cancer cells via different pathways, namely caspase dependent and caspase independent pathways and that in vitro cell death is potentially waveform specific.

5.4.3 PEFE treatments induce cell apoptosis in a manner of dose

The present study noted that that in a 96 well setting, PEFE treatment for 12 hours resulted in altered morphology (Figure 5.5 (2)) followed by subsequent complete cell death. In order to assess if these results were dependent upon the 'dose' of

power/energy delivered to the cell population, the study also tested another experimental setting, namely the same PEFE conditions in a 24-well setup, within which were larger cell numbers and volume of the container. It was interesting to observe that the cells in this new setting only displayed morphological changes 24-hours post treatment with PEFE (Figure 5.4 (2)). This again was followed by 100% cell death. These results indicate links between cell number and exposure dose. Indeed, this hypothesis received further support from another experimental dataset in that the same cell line, when placed in a 96-well setting and treated for only 3 hours. Morphological changes were displayed 24 hours after treatment followed by complete cell death. Taking all these experimental data together, it is clear that PEFE induced cell apoptosis was dose dependent and extra exposure was able to accelerate the apoptotic process of the cell population.

5.4.4 PEFE, Tight Junctions, and Cell Signalling; Mechanisms of Action by PEFE in Cancer Cells

Protein microarray analysis of PEFE treated cells revealed a large number of significantly altered signalling proteins when compared with untreated cells. These signalling proteins are involved in cell mobility, cell morphology and apoptosis. Further experimental evidence has clearly demonstrated that PEFE induces changes in HSP90. Together, it is evidence that a number of signalling events have responded to PEFE and lead to an apoptotic outcome in treated breast cancer cells.

The study also contemplated which molecular/cellular event is the very first (initial) response leading to the subsequent intracellular apoptotic signalling. Our initial attention was on the cell surface structures, as they are likely the first cell structure to sense/face the PEFE signal. Our initial excitement came when we noted the intercellular changes in EM analyses and cell morphology as presented in Chapter-4. They indicated the possibility of tight junctional changes following PEFE treatment. Here, it was firmly demonstrated that breast cancer cells have widespread interruption of tight junctions, as indicated by ZO-1 staining, after PEFE treatment. Tight junctions, the apical most intercellular structure in epithelial and endothelial cells, play a central role in controlling paracellular permeability, cell and intercellular communications, cell adhesion and cell motility. It is plausible to

suggest, based on the experimental data presented here, that the tight junction is the first responsive cell structure to respond to the PEFE signal.

The relationship between tight junctions and apoptosis has been a focus of scientific investigation for some time. A fascinating study by Sabath *et al*., (2008) has established that tight junctional proteins, namely ZO-1, are able to orchestrate with HSP90 and Src regulation of apoptotic signalling events (Sabath et al., 2008). It is noteworthy that HSP90 seems to play a role in cellular signalling transduction. It has been reported that HSP90 can be recruited to the activated Gα12 complex (QL mutation or thrombin). The activated Gα12 complex then activates Src and eventually leading to disruption of ZO-1-formed subcoat complexes. This breakdown of ZO-1 can result in persistent disassembly of the tight junctions (Sabath et al., 2008). In this study, the disruption of ZO-1 after PEFE treatment was observed and confirmed by Western blot and IFC. The Western blot results showed a decreased expression of ZO-1 after PEFE treatment and this was visualized by IFC staining. Once tight junction disruption is triggered, the cells alter morphology and undergo apoptosis under an as yet unknown mechanism.

5.4.5 Limitation of this study

During PEFE treatments, the maximum temperature was measured at 40.6℃. This temperature stood for the liquid temperature in a very small area close to the probe tip. Since there was a 1mm distance from the probe tip to the cell surface, the cellular temperature should be lower than 40.6℃. It is challenging to accurately measure the cellular temperature; thus, it was assumed that the cellular temperature was around 40℃ at maximum and below this temperature during PEFE treatments. Thermal cameras can be a potentially effective tool to measure the temperature of cells, nevertheless, this may further increase the complexity and cost of the entire PEFE system, as a thermal camera needs to be applied below the cultured cells while PEFE should be injected upon the culture vessels.

Caspase-involved apoptosis was verified by the increased expression of Caspase3 and Caspase9. However, it remains unknown which specific signalling pathways were activated and finally resulted in cell apoptosis. Further investigation is

required to examine the expression of other key proteases in different signalling pathways related to apoptosis.

The proteins used in Western blotting were extracted from those treated in a 24 well plate, as the treated cells in 96 well plates were not sufficient in number to exhibit clear bands. It was assumed that the dose of PEFE treatment was not able to impact the type of induced apoptosis. Possibly, the cancer cells cultured in 96 well plates underwent another type of apoptosis. This apoptosis might be activated by another mechanism. To further confirm the hypothesis that pro-apoptosis signals were transferred through cell to cell junctions, more proteins embedded in the cell membrane need to be examined, such as claudin-1, Occludin, JAMA (Junctional adhesion molecule A) and other subcoat proteins.

5.5 Summary

In this area of the study, the biological effects of PEFE on cancer cell death were investigated. Due to the coupled temperature increase when injecting PEFE into biological samples, direct heating experiments were conducted using the same cancer cell line to confirm that cell death after PEFE treatment was elicited by PEFE rather than increased temperature. This was further confirmed through the significantly decreased expression of heat shock protein-HSP90 after PEFE treatment.

After PEFE treatment, cell death was observed; this cell death was verified to be apoptosis first through morphology inspection, then confirmed by examining key proteases regulating cell apoptosis, including Caspase3 and Caspase9. The results revealed that Caspase-involved cell apoptosis was activated by PEFE.

Protein microarray analysis provided insight as to the potential mechanism of cell apoptosis in response to PEFE treatment. ZO-1 regulating cell-cell junctions was demonstrated to be affected by PEFE and eventually led to cell apoptosis. Some other potential mechanisms through different signalling pathways are thought to contribute to cell apoptosis, under the regulation of HSP90. Further investigations are required to completely uncover the mechanisms whereby PEFE affects cellular signalling and leads to cell death.

6 Investigation on Cancer Cells Metabolic Function after PEFE Treatments

6.1 Introduction

Metabolism is essentially the process of energy production and the synthesis of fundamental cellular building blocks. Metabolism is involved with numerous redox reactions, which are under the control of intracellular redox state, metabolism also plays a crucial role in redox homeostasis. Normal cells are equipped with complex signalling networks that are orchestrated by key control enzymes, sensing environmental cues and operating metabolic machineries to provide sufficient energy for survival in a perfectly controlled manner. However, cancer cells exhibit differences in energy supply, biosynthesis and redox homeostasis.

Cancer cells sustain uncontrolled proliferation and replicative immortality and thus require vast amount of energy and biosynthetic precursors. Glycolysis and glutaminolysis are altered to efficiently generate energy and biomass components, known as the 'Warburg effect' (Vander Heiden et al., 2009). Additionally, some of the energetic substrates have been redirected into specific metabolic routes to maintain a higher steady state of reactive oxygen species (ROS), by which cancer cells evade growth suppressors and resist cell death. As a result, the metabolic pathways in cancer cells, have been reprogrammed to better foster survival.

Since the continued growth of cancer cells relies on rewired intracellular signalling pathways, alterations in metabolic pathways can potentially trigger cell death. Accumulating evidence has shown that inhibition of targeting enzymes in glycolysis, can effectively induce cell death through different mechanisms. Inhibitors have been developed, some of which have completed clinical trials (Xie et al., 2009, Wigfield et al., 2008, Schultz et al., 2008, Rodríguez-Enríquez et al., 2009, Giatromanolaki et al., 2008, Garber, 2010, Földi et al., 2007, Clem et al., 2008, Chen et al., 2009, Catherino et al., 2007). Another method that affects metabolism and achieves cell death is targeting hypoxia-inducible factor (HIF)-1α(Semenza et al., 1994, Carmeliet et al., 1998). HIF-1α inhibition can decrease glycolysis in cancer cells by regulating serval genes involved in the process, leading ultimately to cell death (Olenyuk et al., 2004, Kung et al., 2004, Kong et al., 2005). The degradation of HIF-1α can also be indirectly achieved by respiratory complex inhibition and can in turn contribute to the induction of cell death targeting

oxidative phosphorylation (OXPHOS) enzymes. Inhibition of complex I, II, III, IV and V can elicit mitochondrial bioenergetic failure, including ATP reduction, increased ROS level, accordingly, resulting in cell apoptosis through different signalling pathways. Furthermore, some enzymes, as regulators in fatty acid synthesis pathways, such as ATP citrate lyase (ACL), acetyl-CoA carboxylases (ACC), fatty acid synthase (FAS) play an important role in the formation of lipids. The inhibition of these enzymes can limit proliferation, attenuate growth and induce cell death (Wang et al., 2005, Hatzivassiliou et al., 2005, Beckers et al., 2007).

It has been well established that some chemotherapeutic agents and radiation therapies can effectively upgrade the ROS level in cancer cells *in vitro*, leading to necrosis or apoptosis by a dose-dependent means (Mates and Sanchez-Jimenez, 2000, Cejas et al., 2004). Chemotherapy agents including anthracyclines, platinum coordination complexes, alkylating agents, epipodophyllotoxins, and camptothecins can generate the high levels of ROS intracellularly, resulting in apoptosis through the release of cytochrome c from mitochondria and imbalanced redox(Conklin, 2004). Radiotherapy can produce free radicals, such as superoxide and hydroxyl radicals, causing damage to DNA (Chandra et al., 2000).

There appear to be few studies investigating whether microwaves can induce inhibitions of glycolysis or glutaminolysis pathways without hyperthermia. However, it is well established that microwaves can have an impact on oxidative stress in normal cells through direct or indirect manners; for cancer cells, it remains unclear. In this chapter, we investigated whether PEFE treatments can elicit abnormality in energy consumption or oxidative stress of cancer cells, leading to metabolism dysfunction.

6.2 Method

The MDA-MB-231 breast cancer cell line was used for metabolic assays experimentation. The cells were seeded into a 96-well plate with 200µl medium and allowed enough time to attach before use. The reagents needed in each assay were prepared as described in section 2.2.4. The PEFE system was constituted and calibrated at 2.2GHz as illustrated in section 3.2, prior to use. The output power was set to 50 watts whilst the pulse width was selected as 50µs and pulse period

was 1ms. Each single PEFE treatment last 15 minutes. Each metabolic assay was performed as a time course, including 24hours, 6hours, 3hours, 1.5hour, 1hour post PEFE treatments and immediately after treatments (simplified as '0hour' in each Figure of this chapter). An additional 6 wells seeded with cancer cells (3 wells for control group, 3 wells for experimental samples) without any PEFE treatments were prepared do that we might investigate the initial metabolic condition before PEFE treatments (simplified as 'BE' in each Figure of this chapter). Once all PEFE treatments were completed, the assays were performed following protocols, detailed in section 2.8. Each metabolic assay was repeated at 3 times (n = 3) to get consistent results**.**

As demonstrated in chapter 4, PEFE can achieve cell necrosis during treatment and apoptosis post treatment. In order to investigate the potential signalling pathways involved in PEFE induced metabolism and apoptosis, alterations in metabolism indicators were assayed and visualised from the time that PEFE treatments were immediately completed ('0 hour' in each Figure of this chapter). The data was normalised to reflect the differences between the control group and the treated cancer cells.

The statistical significance in each figure was analysed using 2-way ANOVA in Prism8 (GraphPad Software, San Diego, USA).

6.3 Results

6.3.1 Glucose-Glo™ Assay

In this assay, the concentration of glucose in the cell culture medium for each sample was monitored and quantified by luminescence. The data set are presented in Figure 6.1, which recorded the levels before PEFE treatment began ('BE') and in Figure 6.2 which compares glucose levels at the indicated time points with that of treatment immediately after PEFE ('0h'). Before PEFE treatments, the cell culture medium was refreshed with another 200µl medium in order to ensure that the concentration started to change from the same level, shown in Figure 6.1. The starting points of each curve were nearly the same. Once PEFE treatment started, the concentration of glucose in the control group kept decrease consistently in the

following 24 hours. The experimental group exhibited the same trend in concentration as the control group, decreasing throughout the assay. Although the concentration of glucose for each sample kept reducing, the cancer cells without any treatment exhibited a higher glucose intake compare to treated samples. In Figure 6.2, the extracellular glucose levels are shown to be decreasing over time when compared with that immediately after PEFE treatment. This comparison would allow us to eliminate the potential influence due to the small portion of cells becoming necrotic during PEFE treatment (similar comparisons were made throughout this chapter) However, the concentration from cells undergoing PEFE treatment remained at a significantly higher level, compared with the control group.

6.3.2 Lactate-Glo Assay

The concentration of lactate production in the cell culture medium was monitored and quantified by luminescence, and the results are shown in Figure 6.3. The concentration of lactate normalised to the time point immediately after PEFE treatment as presented in Figure 6.4. The cell culture medium was refreshed for each sample immediately before PEFE treatment, to ensure the initial concentration of lactate was kept at the same level. In Figure 6.3, the concentrations measured for lactate for each sample was at very similar level before PEFE treatment, then varied in the same fashion, which was a consistent increase in the following 24 hours. However, the measured concentration for the control group increased more rapidly and at a higher level compared to the PEFE treated samples. Interestingly, the difference between these two curves was not significant immediately after PEFE treatment but became so over the time course. In Figure 6.4, the extracellular concentration of lactate increased over time. However, a significantly lower level was exhibited in cells undergoing PEFE treatment. Due to persistent apoptotic cells in the treated samples, the number of cells was decreased accordingly, leading to a significantly lower production of lactate.

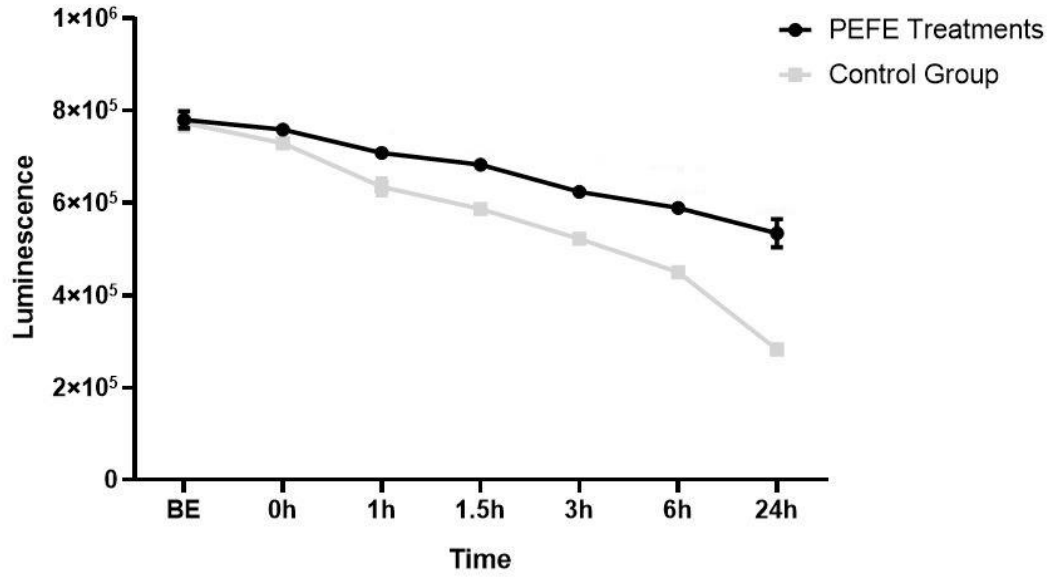

Figure 6.1 Concentration of extracellular glucose in control group and cells underwent PEFE treatments, quantified by luminescence measurement (p<0.01, by two way ANOVA). Error bar stands for standard error of means.

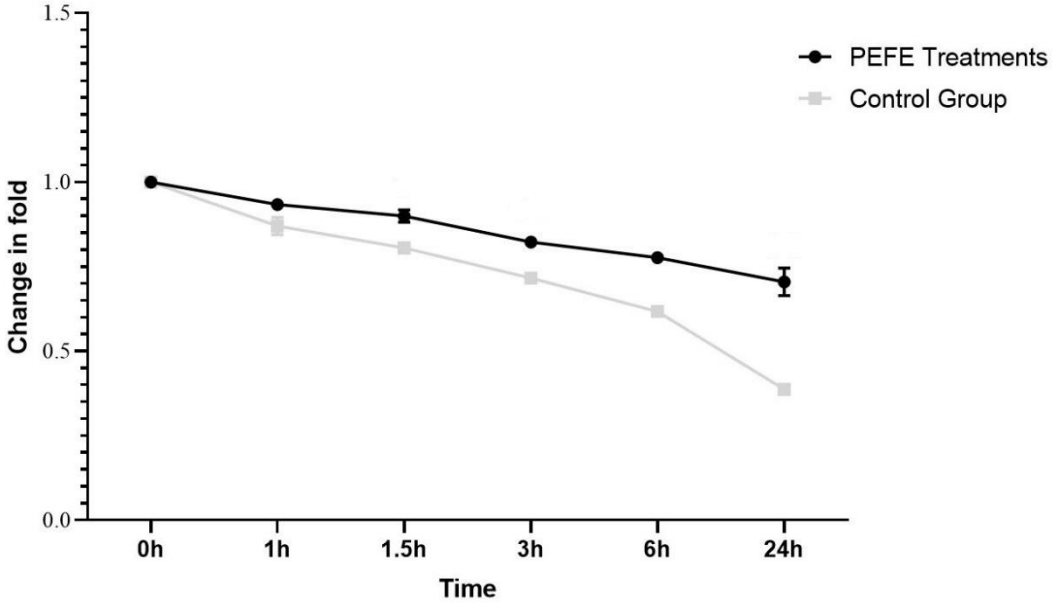

Figure 6.2 Normalised concentration of extracellular glucose in control group and cells underwent PEFE treatments (p<0.01, by two way ANOVA). Error bar stands for standard error of means.

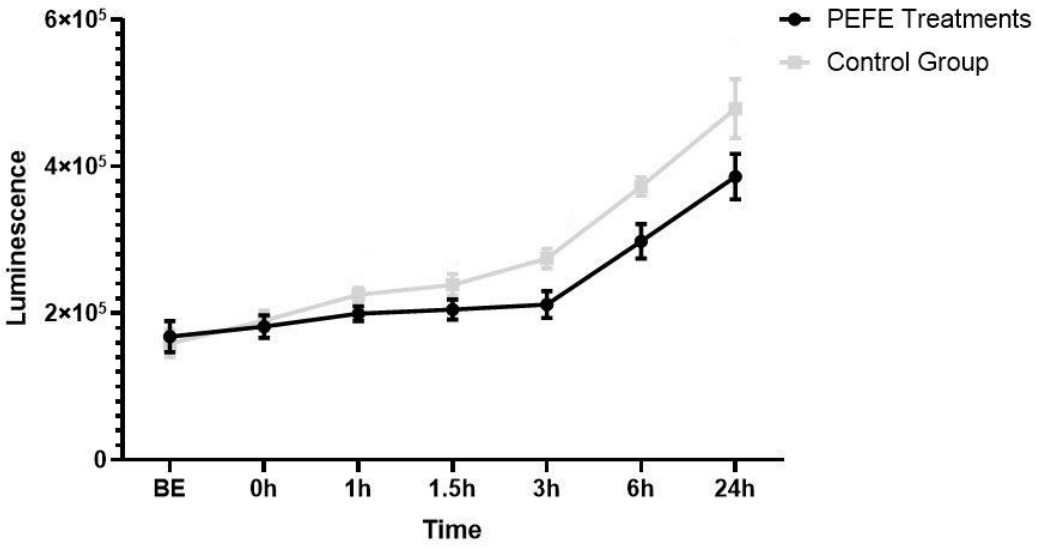

Figure 6.3 Concentration of extracellular lactate in control group and cells underwent PEFE treatments, quantified by luminescence measurement (p<0.05, by two way ANOVA). Error bar stands for standard error of means.

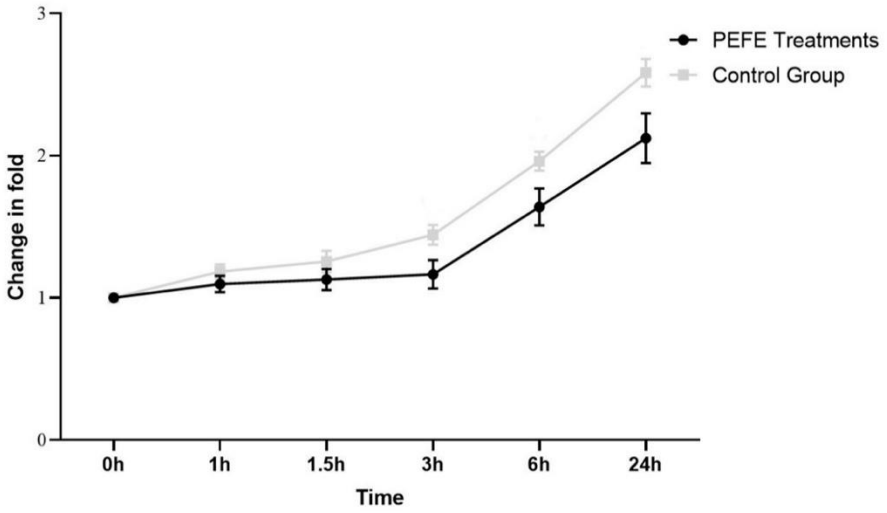

Figure 6.4 Normalised concentration of extracellular lactate in control group and cells underwent PEFE treatments (p<0.05, by two way ANOVA). Error bar stands for standard error of means.

6.3.3 Glutamine/Glutamate-Glo™ Assay

Here, the concentrations of glutamate and glutamine were assessed. Owing to the limitations of the method, we were unable to determine direct measurements of glutamine. Due to this, glutamate was measured first. After adding glutaminase each well to convert all glutamine to glutamate, the total amount of glutamate in each of the corresponding wells was measured. This allowed the glutamine levels to be calculated. The results are shown in Figure 6.5 and Figure 6.6 respectively. The converted glutamine was calculated by subtracting the concentration of glutamate only from the concentration of total glutamate, as plotted in Figure 6.7. The concentration of glutamate only and glutamine normalised to the level immediately after PEFE treatment are shown in Figure 6.8 and Figure 6.9, respectively.

The medium was refreshed for each well, allowing the same starting points for the concentration of the control group and the experimental samples. In Figure 6.5, the concentration of glutamate only for the control group increased due to the consistent conversion from glutamine over time, leading to an accumulation in the cell culture medium. However, the glutamate production of PEFE treated cells increased slightly within the first 6 hours, leading to a much lower concentration compared to the control group. After 6 hours, this production started to increase but was still much lower than that of the control group.

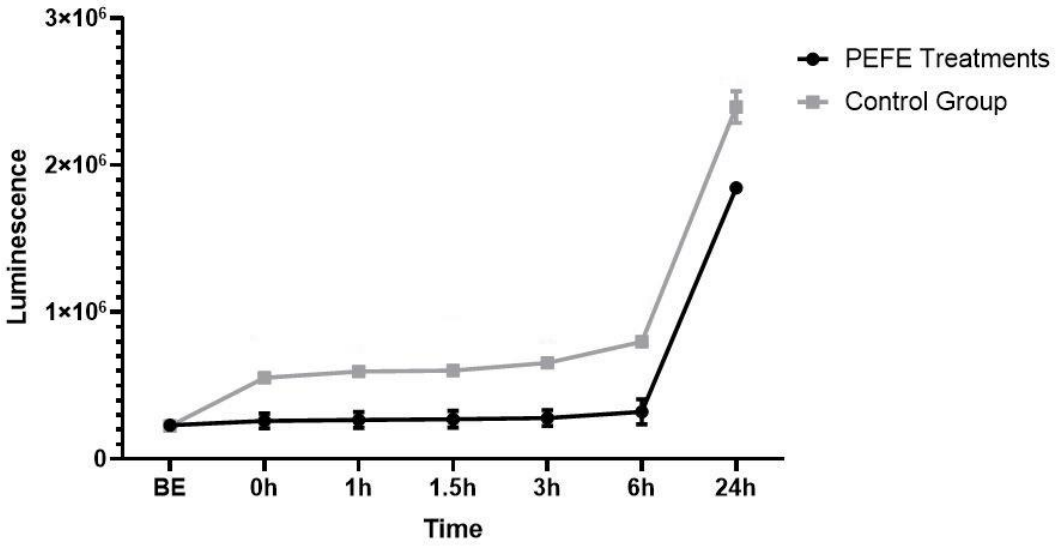

Figure 6.5 Concentration of glutamate only in control group and cells underwent PEFE treatments, quantified by luminescence measurement (p<0.001, by two way ANOVA). Error bar stands for standard error of means.

The total glutamate secretion measurements showed that the concentrations in the control group and experimental samples exhibited a similar trend. They started at similar points and reduced consistently in parallel until 6 hours after PEFE treatment. The total glutamate production then started to increase in the following hours. The difference between the control group and the treated samples did not reach statistical significance.

The calculated glutamine concentration was described in Figure 6.7. The concentration of the control group and treated samples varied initially in the same manner and showed similar trends with consistent reduction. The glutamine consumption of PEFE treated cells exhibited markedly higher levels over time compared to the control group.

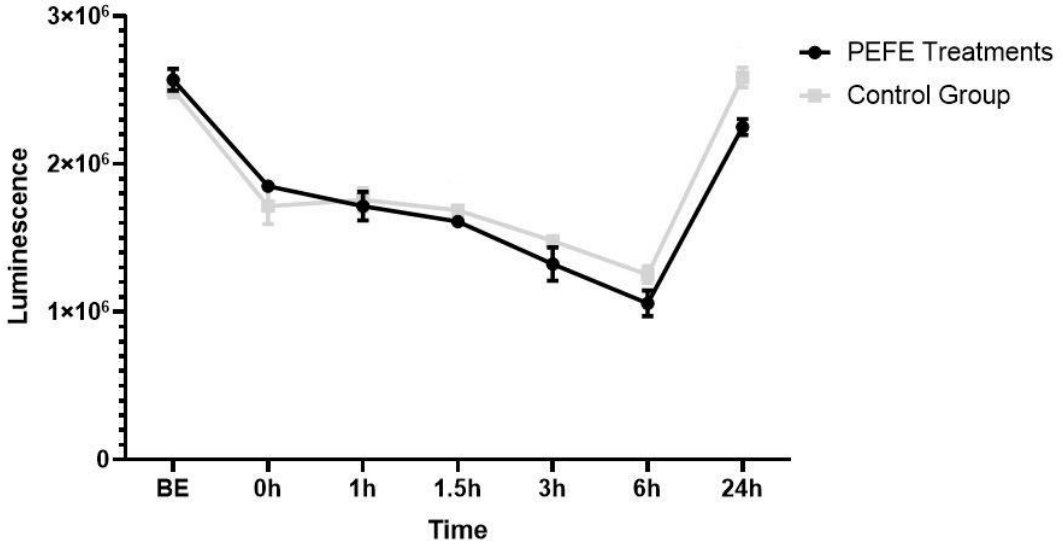

Figure 6.6 Concentration of total produced glutamate in control group and cells underwent PEFE treatments, quantified by luminescence measurement. Error bar stands for standard error of means. No statistical significance was observed between two samples by two way ANOVA.

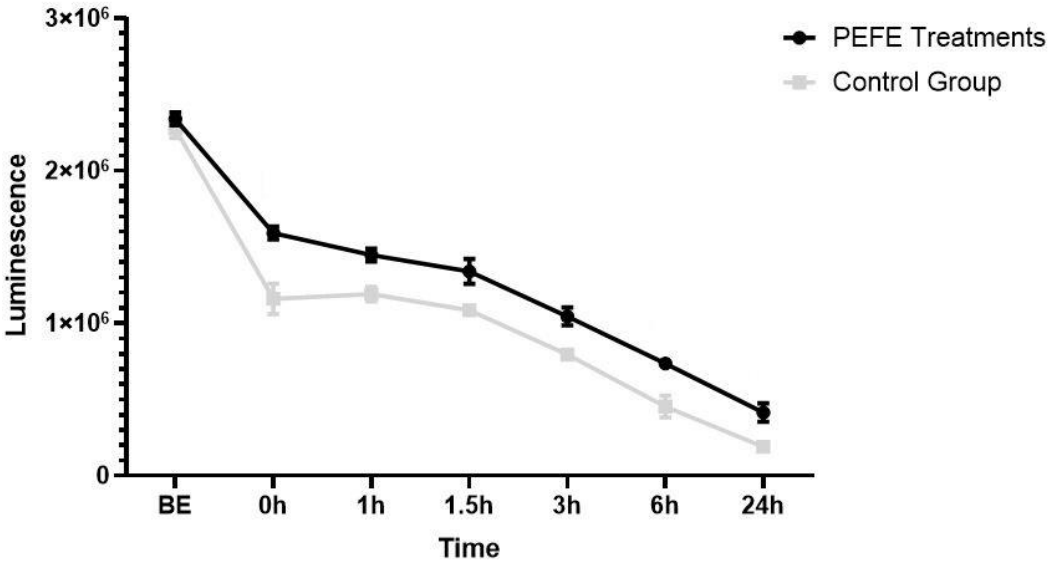

Figure 6.7 Concentration of glutamine in control group and cells underwent PEFE treatments, quantified by luminescence measurement (p<0.05, by two way ANOVA). Error bar stands for standard error of means.

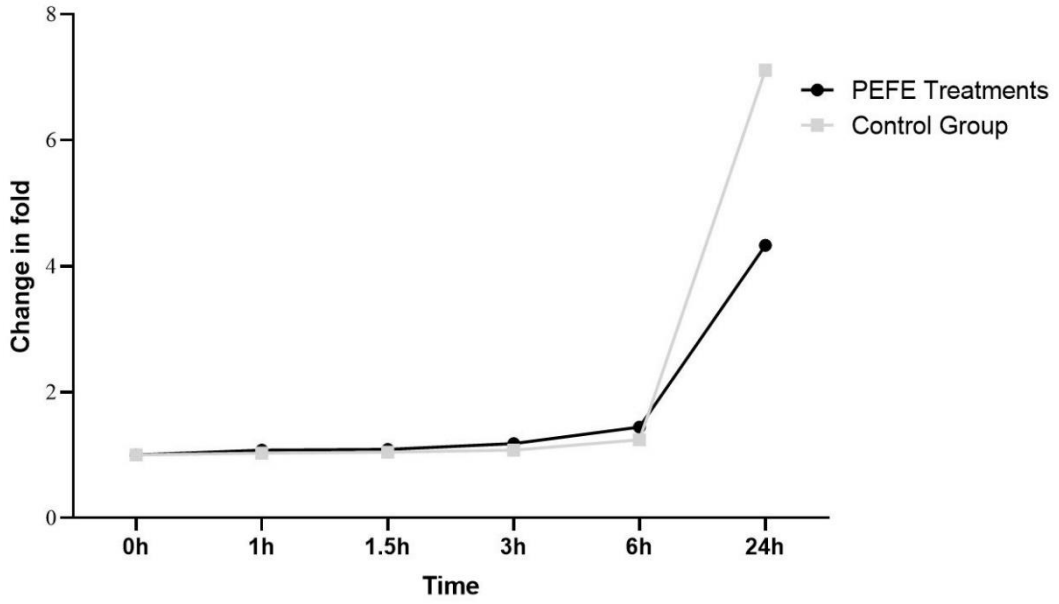

Figure 6.8 Normalised concentration of glutamate only in control group and cells underwent PEFE treatments. Error bar stands for standard error of means. No statistical significance was observed between two samples by two way ANOVA.

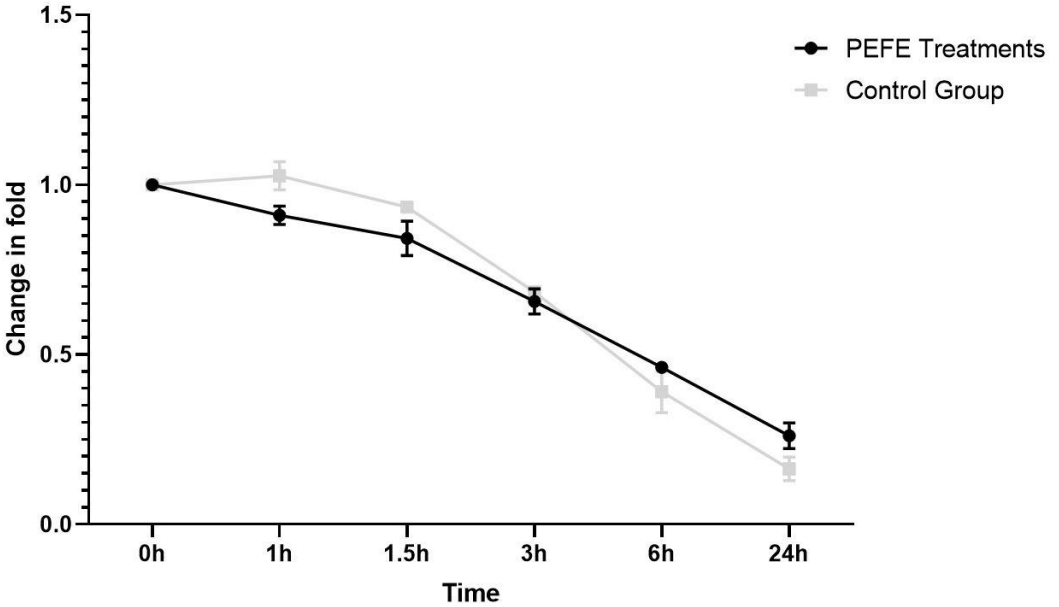

Figure 6.9 Normalised concentration of glutamine in control group and cells underwent PEFE treatments. Error bar stands for standard error of means. No statistical significance was observed between two samples by two way ANOVA.

In Figure 6.8, no significant difference was found in the secreted glutamate levels in the control group and cells undergoing PEFE treatment. This was in contrast to the data presented in Figure 6.6, where all the time points were compared with cells prior to PEFE treatment. It was anticipated that the significant change prior to PEFE treatment and immediately after PEFE treatment (namely time 0), was due to the small portion of cells that had died of necrosis during this period. The secretion of glutamate increased rapidly in both samples from 6 hours and a significantly lower level of glutamate concentration in cells undergoing PEFE treatment was observed at 24 hours post treatment.

Likewise, the extracellular glutamine concentration immediately after treatment, shown in Figure 6.9, demonstrated a continuously decreasing trend and was observed in both samples. However, no significant difference was exhibited between the control group and those cells undergoing PEFE treatment over time.

6.3.4 Griess Reagent System

This assay quantified the concentration of NO_2^- by absorbance. As the primary, stable and non-volatile breakdown products of nitrite oxide, NO_2^- measurements are an efficient method to investigate nitrite oxide formation. The NO_2^- levels of the PEFE treated samples E and the control group are shown in Figure 6.10. The normalised data for the absorbance is presented in Figure 6.11.

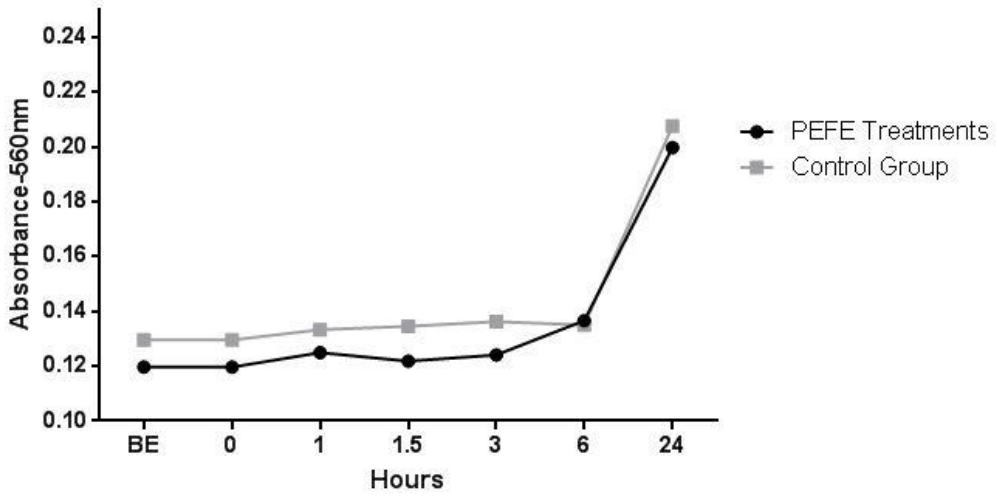

Figure 6.10 Concentration of NO_2^- in PEFE treatments and control group. Error bar stands for standard error of means. No statistical significance was observed in either group by two way ANOVA.

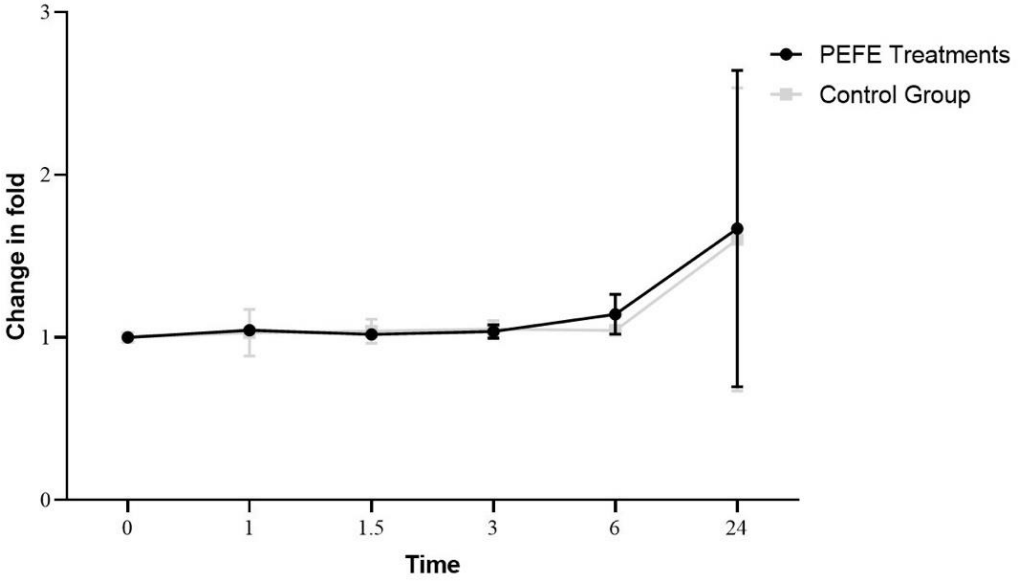

Figure 6.11 Normalised concentration of NO_2^- in PEFE treatments and control group. No statistical significance was observed in either group by two way ANOVA.

It can be seen from Figure 6.11 that higher concentrations of NO_2^- in the sample would lead to higher absorbance measurements. In Figure 6.10, NO_2^- levels of both

PEFE treated cells and the control group kept reasonably constant until 6 hours after treatment. During this period, the absorbance of PEFE treated samples was 0.12 approximately, whilst in the control group it was around 0.13.. After 6 hours, the NO_2- levels increased rapidly and reached 0.2 and 0.21 for PEFE treated cells and the control group respectively, as quantified by absorbance. When all the points were normalised to cells immediately after treatment (Figure 6.11), it is very clear that there was no significant difference in the absorbance of NO_2^- Taking all this data together, PEFE did not induce significant alterations during cell necrosis and apoptosis.

6.3.5 NAD(P)H-Glo™ Detection Assay

We further monitored the concentration of NADH and NADPH, collectively referred to as NAD(P)H. The NAD(P)H in each sample was measured and quantified by luminescence as shown in Figure 6.12. The normalised concentrations of NAD(P)H in the control group and cells undergoing PEFE treatment is shown in Figure 6.13.

Prior to PEFE treatment, the cell culture medium for each well was changed to ensure the initially measured NAD(P)H concentrations were at similar levels. For the control group, the concentration of NAD(P)H fluctuated within the first 6 hours then exhibited significant reduction at 24 hours. In PEFE treated samples, the concentration was different to that of the control group, in that it increased dramatically during PEFE treatment, leading to higher production of NAD(P)H compared to the control group. Immediately after treatment, this concentration decreased to a much lower level than that of the control group at 1 hour and kept consistently decreasing in the following hours. This reduction of NAD(P) when normalised to immediately after PEFE treatment was more evident as shown in Figure 6.13.

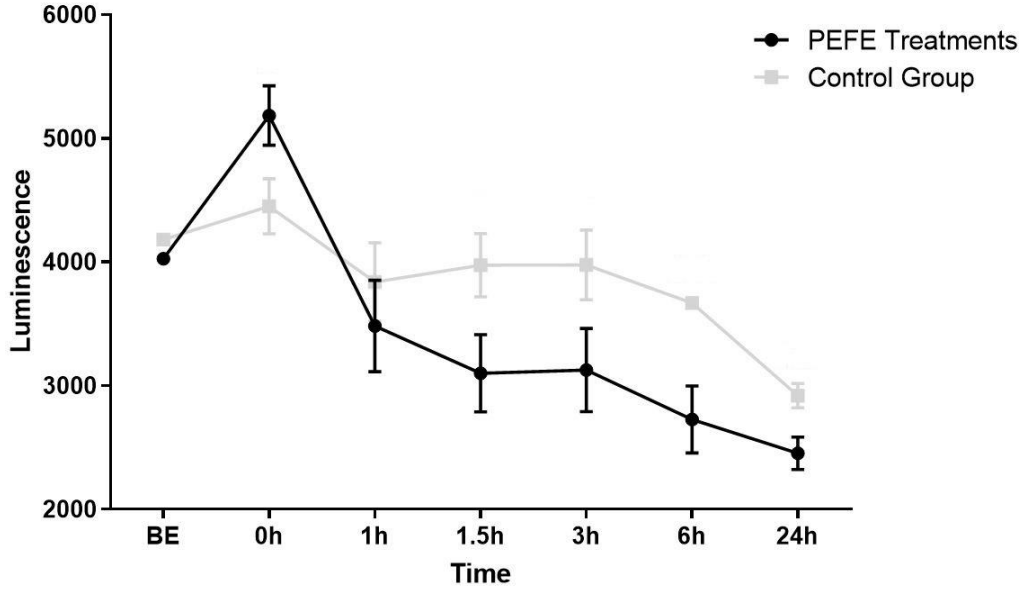

Figure 6.12 NAD(P)H measurements quantified by luminescence of control group and cells underwent PEFE treatments (p<0.01, by two way ANOVA). Error bar stands for standard error of means.

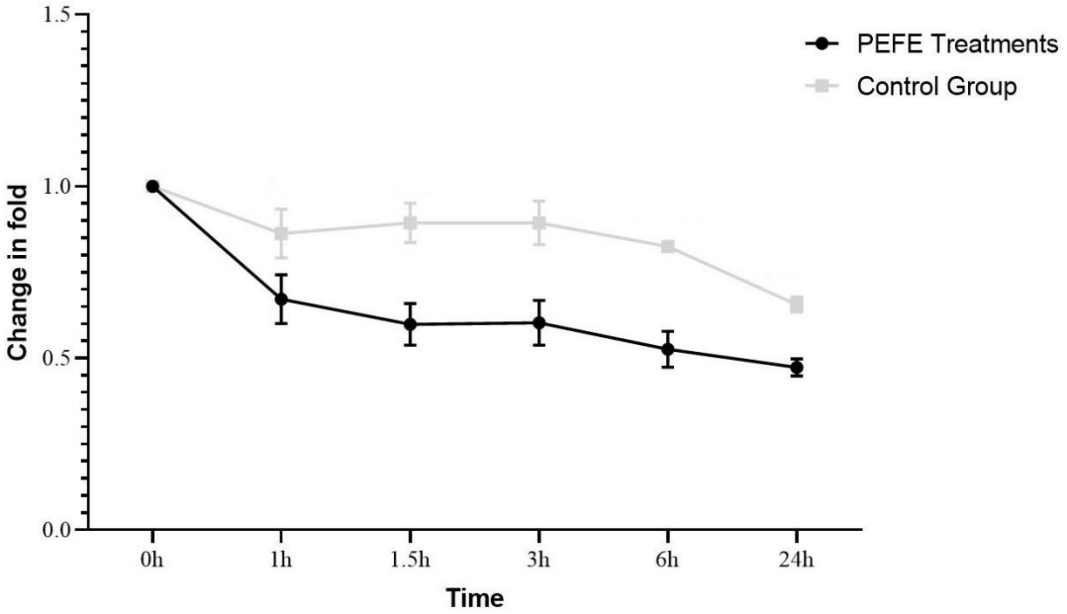

Figure 6.13 Normalised concentration of NAD(P)H in control group and cells underwent PEFE treatments (p<0.01, by two way ANOVA). Error bar stands for standard error of means.

6.3.6 ATP levels assessed by CellTiter-Glo® 2.0 Assay

The amount of ATP is proportional to the number of viable cancer cells which are metabolically active. Since the same number of cancer cells were seeded into each well, the starting points (BE) for the control group and the experimental treated samples in Figure 6.14, were at the same levels. ATP concentration in the control group was largely stable over the 24-hour period. However, when the cells underwent PEFE treatment, there was a marked reduction immediately after (time 0), reflecting a loss of cell number due to necrosis. The levels of ATP otherwise decreased steadily and significantly over the 24 hours period. When the cell necrosis effect was eliminated by normalising all the time points to time 0, a similar significant reduction was seen (Figure 6.15) when compared with the control cells. Collectively, the data set confirmed the findings that there was an immediate reduction in cell number owing to rapid cell necrosis. However, PEFE induced a steady reduction of cellular ATP and hence cell number, coinciding with a potential induction of apoptosis.

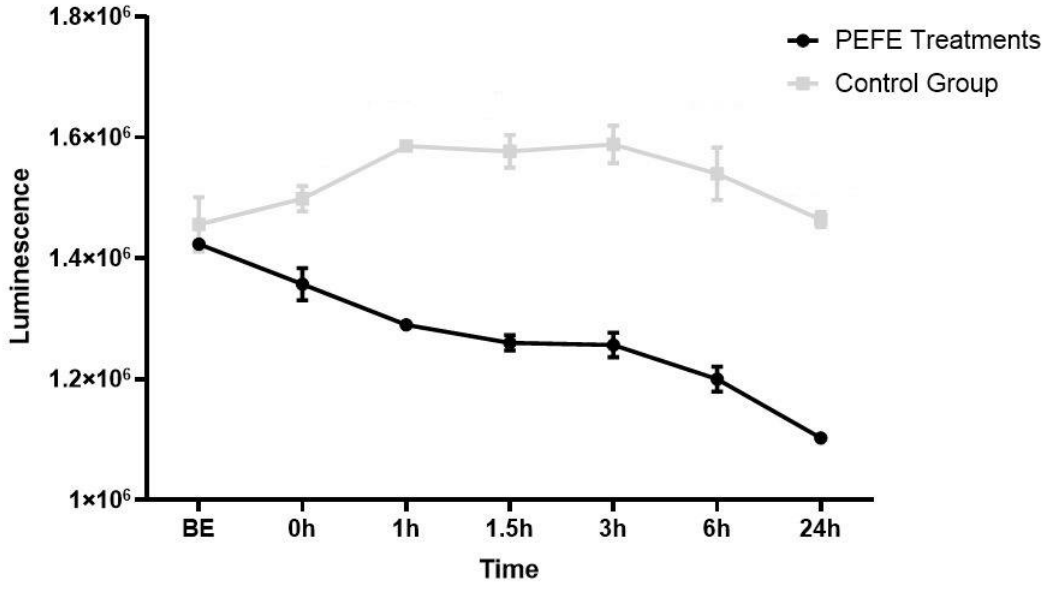

Figure 6.14 Intracellular ATP level measurements of control group and cells underwent PEFE treatments (p<0.001, by two way ANOVA). Error bar stands for standard error of means.

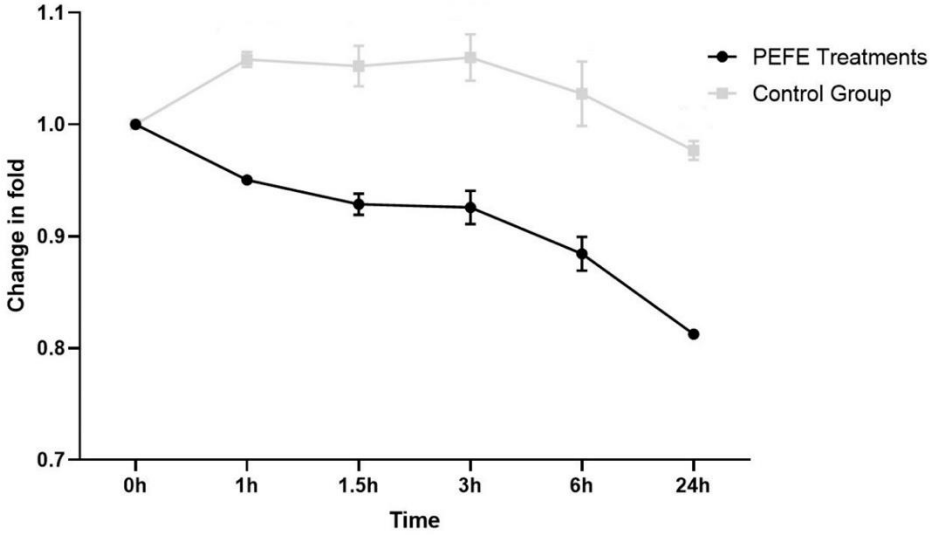

Figure 6.15 Normalised concentration of ATP in control group and cells underwent PEFE treatments (p<0.001, by two way ANOVA). Error bar stands for standard error of means.

6.3.7 GSH/GSSG-Glo™ Assay

The concentration of total GSH and GSSG only were monitored in parallel and quantified by concentration and are shown in Figure 6.16a and Figure 6.17a. After normalisation, the concentration of total GSH and GSSG were plotted, and are shown in Figure 6.16b and Figure 6.17b.

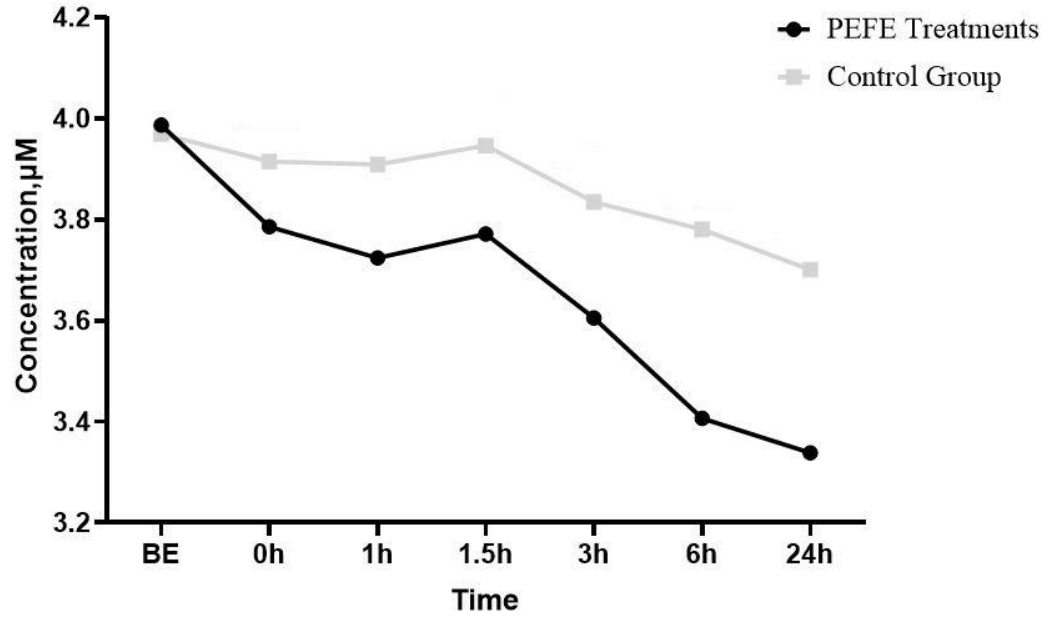

Figure 6.16a Total GSH Concentration of control group and cells underwent PEFE treatments (p<0.01, by two way ANOVA). Error bar stands for standard error of means.

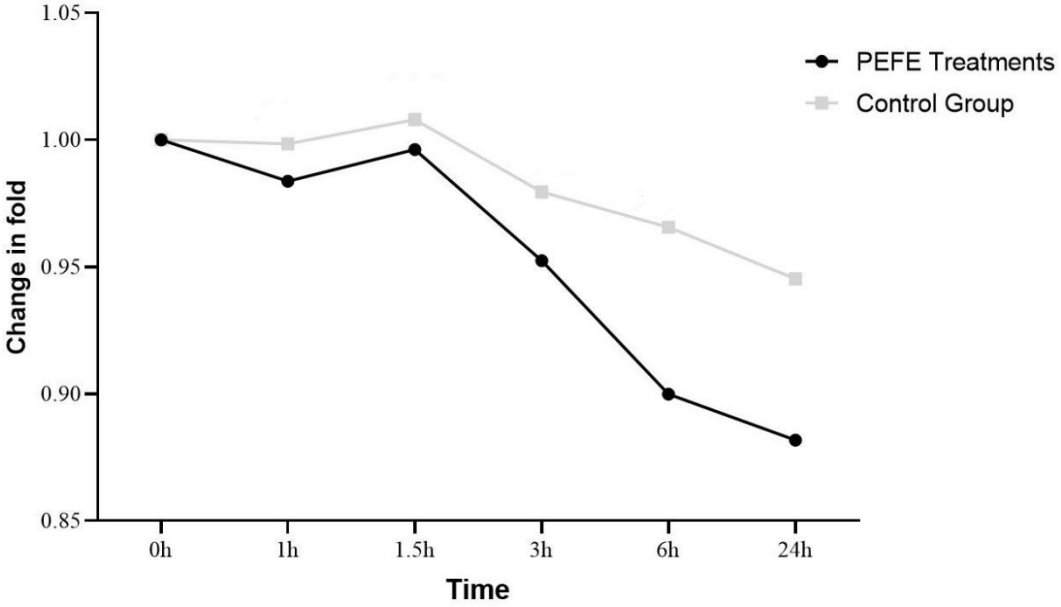

Figure 6.16b Normalised concentration of GSH in control group and cells underwent PEFE treatments (p<0.01, by two way ANOVA). Error bar stands for standard error of means.

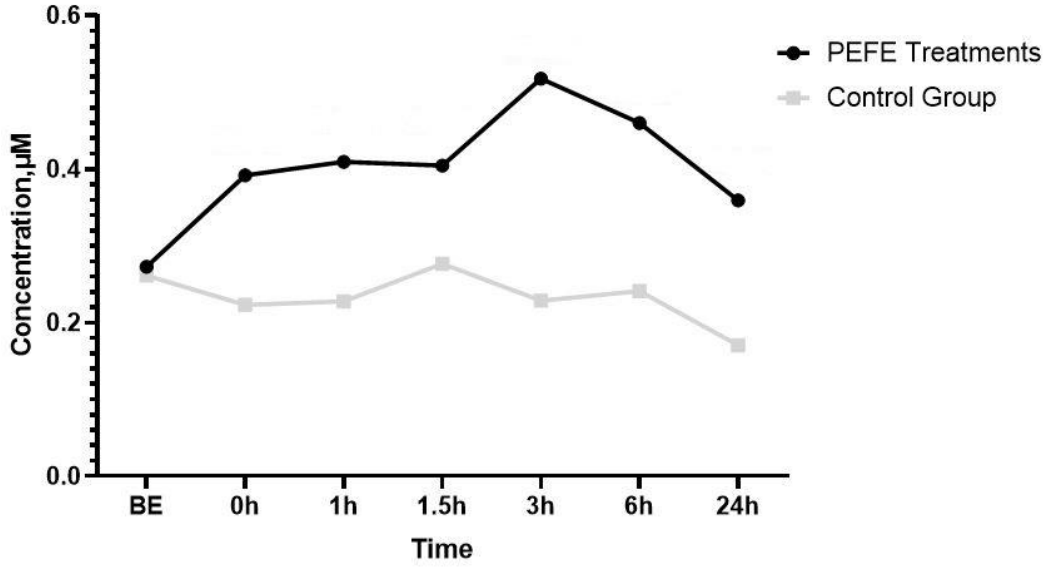

Figure 6.17a GSSG concentration of control group and cells underwent PEFE treatments (p<0.01, by two way ANOVA). Error bar stands for standard error of means.

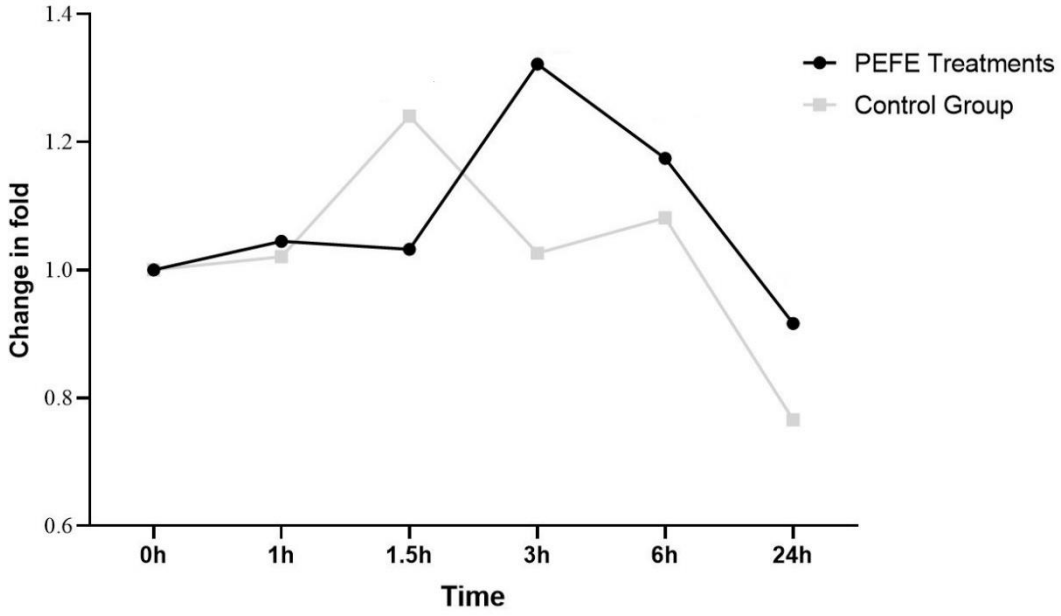

Figure 6.17b Normalised GSSG concentration of control group and cells underwent PEFE treatments. Error bar stands for standard error of means. No statistical significance was observed between two samples by two way ANOVA.

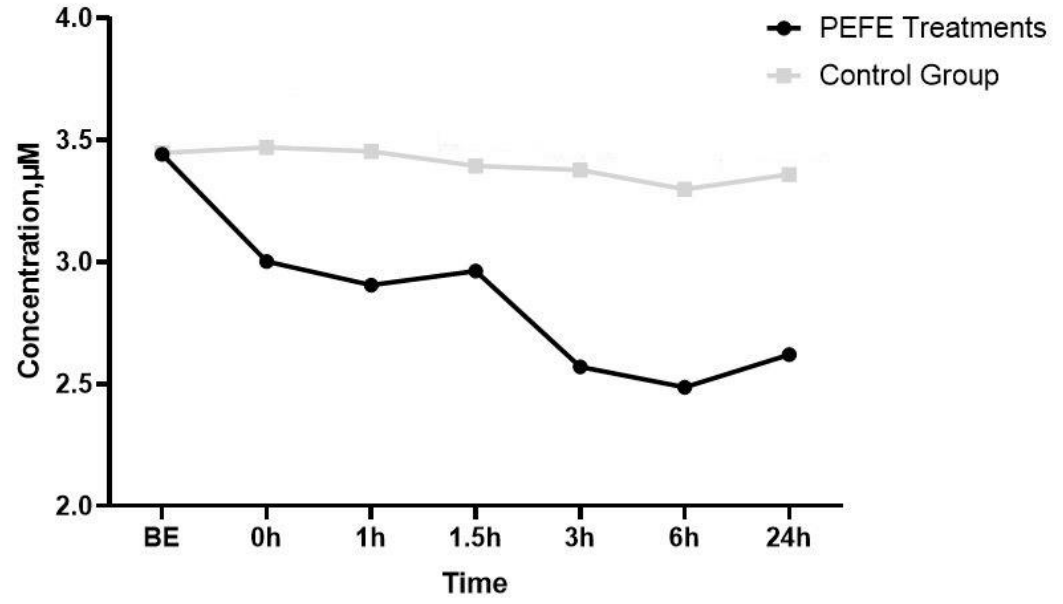

Figure 6.18a Calculated concentration of GSH only of control group and cells underwent PEFE treatments (*p*<0.01, by two way ANOVA). Error bar stands for standard error of means.

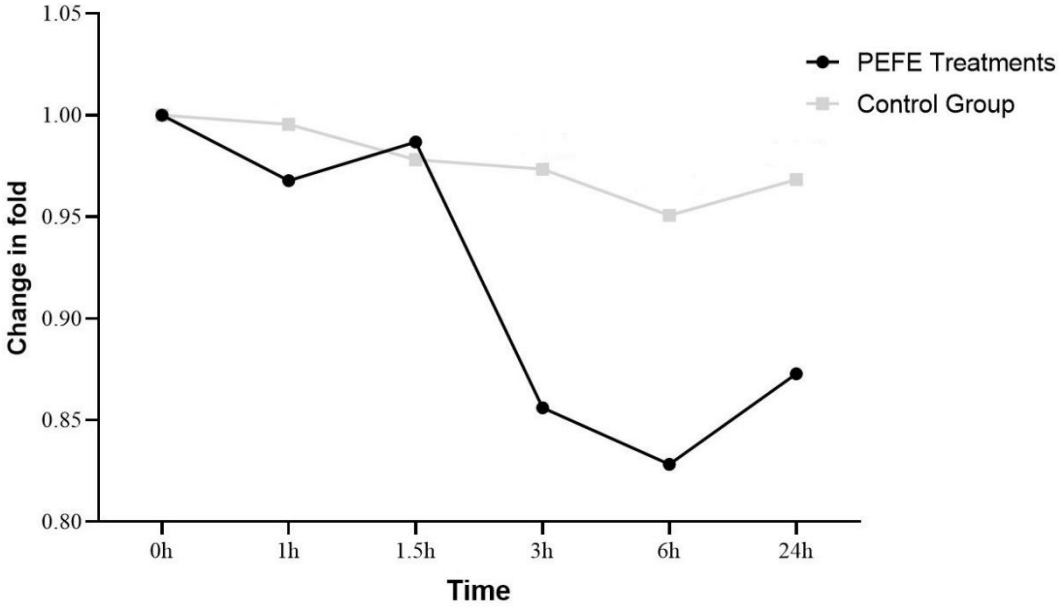

Figure 6.18b Normalised concentration of GSH only in control group and cells underwent PEFE treatments (*p*<0.01, by two way ANOVA). Error bar stands for standard error of means.

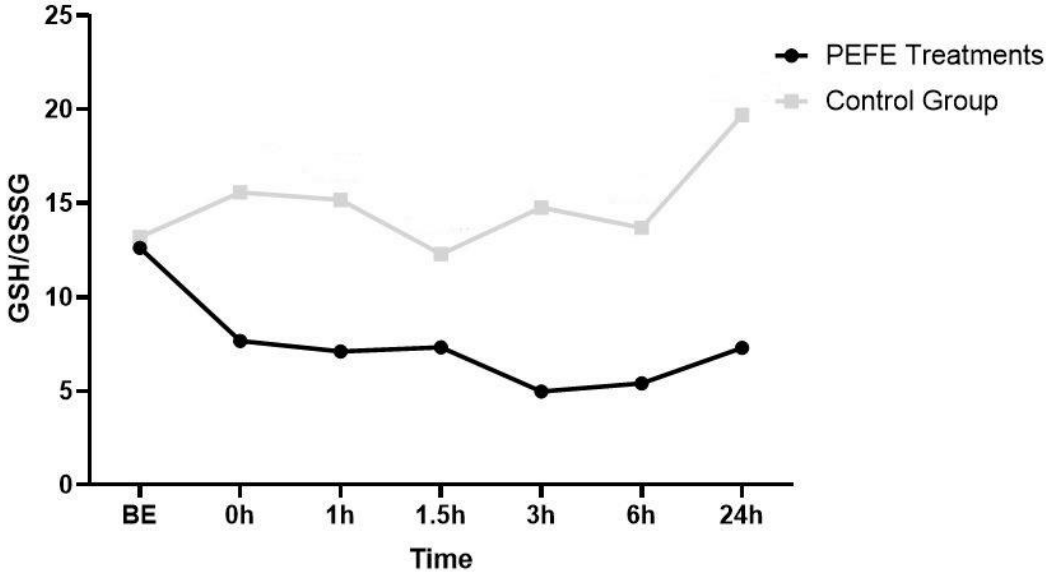

Figure 6.19 Calculated ratio of GSH/GSSG of control group and cells underwent PEFE treatments (p<0.01, by two way ANOVA). Error bar stands for standard error of means.

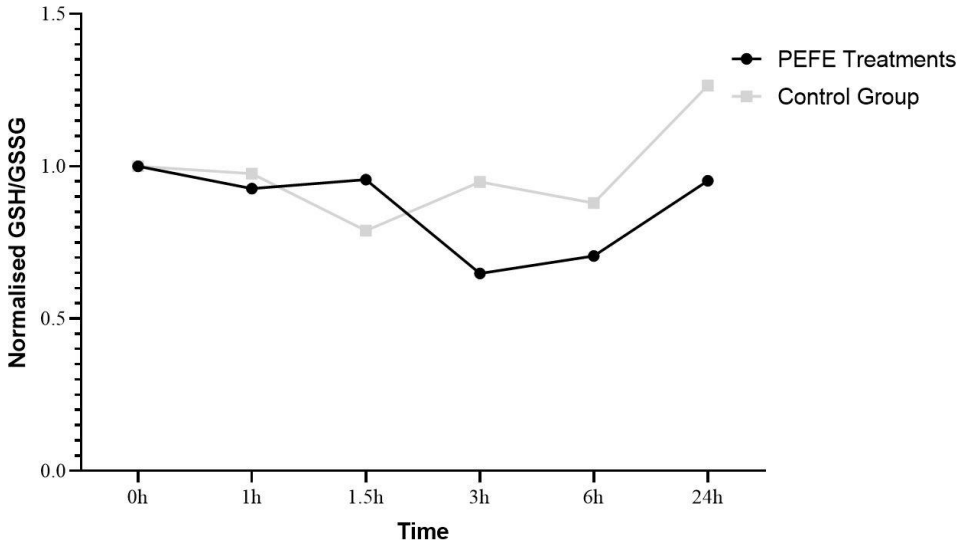

Figure 6.20 Normalised GSH/GSSG in control group and cells underwent PEFE treatments (p<0.05, by two way ANOVA). Error bar stands for standard error of means.

The same number of cancer cells were seeded in each well and the cell culture medium was refreshed immediately before PEFE treatment. The initial concentrations of total GSH and GSSG in both the control group and the experimental group were at similar levels. In Figure 6.16a, the concentration of total GSH can be seen to be fluctuating around 4 μM during the first 1.5 hour. This concentration then started to decrease consistently, reaching 3.7 μM at 24 hours. The concentration of total GSH for experimental samples showed a similar trend as the control group. It decreased from 4 μM approximately, until 1 hour, reaching around 3.7 μM. It then increased by around 0.1 μM and exhibited a second reduction in the following hours. At 24 hours, this concentration decreased to 3.4 μM approximately. The overall concentration of PEFE treated cells was much lower than that of the control group.

In Figure 6.17a, the concentration of GSSG in experimental samples went up from around 0.3 μM to 0.4 μM rapidly during the PEFE treatment. This concentration kept constant in the following 1.5 hour, then showed a second rapid increase to 0.55 μM at 3hours. After 3 hours, it fell back to around 0.35 μM gradually. Starting from the same level, the concentration of the control group showed a fluctuation at around 0.3 μM before 6 hours, then started to decrease by 24 hours.

Since two moles of GSH are generated per 1 mole of GSSG, the concentration of GSH only was calculated by the following equation:

$$Y3 = Y1 – 2 * Y2$$

Where Y3, the concentration of GSH only, μM. The results were plotted and shown in Figure 6.18a. The concentration for the control group nearly kept constant at around 3.5 μM over time. While the concentration of experimental samples showed decreases from 3.5 μM to 3.0 μM at 1 hour. The concentration increased slightly then continued decreasing to around 2.5 μM at 6 hours. Ultimately, this concentration increased slowly to 2.55 μM approximately at 24 hours.

The ratio of GSH/GSSG was calculated by following equation:

$$R = Y3 / Y2$$

The results were plotted and are shown Figure 6.19. Before PEFE treatment, the ratio for each sample was around 13. Within 1.5 hours after treatment, the ratio showed opposing patterns for the control group compared to the treated samples. The ratio of the control group increased to around 15 then fell back to 13 during this period, whilst the ratio decreased to around 7 then increased slightly in the experimental samples. After 1.5 hours, the ratio of the control group gradually increased to around 20. As for the treated samples, levels decreased to around 5 then gradually up to 7 at 24 hours. Furthermore, after normalisation, GSH/GSSG in cells undergoing treatment was significantly lower compared to the control group, except for that at 1.5 hours post treatments, as shown in Figure 6.20.

6.3.8 ROS-Glo™ H_2O_2 Assay

The concentration of H_2O_2 was monitored and measured by luminescence for each sample. The results are shown in Figure 6.21. After normalisation, the H_2O_2 levels in both samples were calculated and are shown in Figure 6.22.

In Figure 6.21, the concentration of H_2O_2 in each sample is shown since it was proportional to the measured luminescence. For the cells without PEFE treatment, the concentration of H_2O_2 kept relatively stable over time. However, the curve of PEFE treated cells showed a different trend; the initial concentration of H_2O_2 was nearly the same as that of the control group; this concentration then increased sharply during the PEFE treatment. After treatment, the concentration kept stable over time and was almost double that in the control group.

As shown in Figure 6.22, no significant difference in the H_2O_2 levels in both samples was observed in the first hour after treatment. At 1.5 hours post treatment, a significantly lower level was observed in cells treated with PEFE, compared to the control group. In the following hours, although H_2O_2 levels were lower in cells exposed to PEFE, no significant difference was observed.

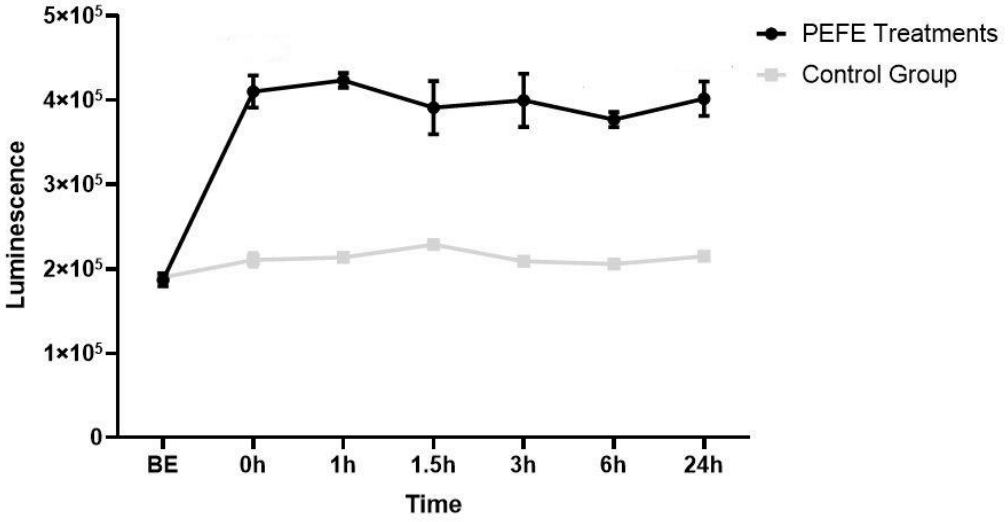

Figure 6.21 H_2O_2 measurements of control group and cells underwent PEFE treatments (p<0.001, by two way ANOVA). Error bar stands for standard error of means.

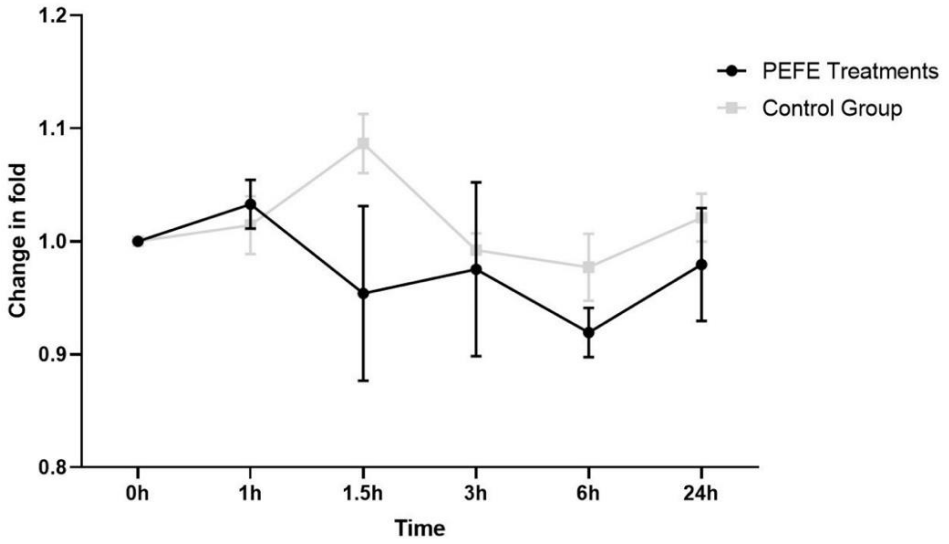

Figure 6.22 Normalised H_2O_2 levels in control group and cells underwent PEFE treatments. Error bar stands for standard error of means. No statistical significance was observed between two samples by two way ANOVA.

6.4 Discussion

The assays described above were chosen as the best available methods to investigate whether PEFE treatment of human breast cancer cells impacted on

metabolic functions intracellularly and were able to determine both aspects of metabolism energetic consumption and synthesis, and redox homeostasis.

6.4.1 Energetic consumption and synthesis

Glucose and glutamine are the main nutritional components for cells to sustain growth and proliferation. Their utilization relies on aerobic glycolysis and glutaminolysis, respectively. Lactate and glutamate are by products of glycolytic and glutaminolytic consumption, by which cancer cells intake glucose and glutamine from cell culture medium then secrete lactate and glutamate into the medium through their membranes. With a sufficient nutrition supply such as in the culture conditions of the present study, the cancer cells continue to grow and divide, which in turn results in increased nutrition consumption. Accordingly, in our study, the intake of glucose and glutamine exhibited showed a consistent increase over time for cancer cells without any treatment, leading to a reduction in the concentration of glucose and glutamine in the cell culture medium. In comparison, the production of lactate and glutamate showed a persistent increase.

As discussed in Chapters 4 and 5, PEFE treatment was able to induce cancer cell necrosis and apoptosis sequentially *in vitro*, leading to a rapid reduction in cell number and prolonged cell death in the hours following treatment, typically a 50% death rate at 24 hours. In the glucose and lactate assays, the same cell death induced by PEFE treatment lowered glucose intake, leading to a much higher concentration of remaining glucose in the cell culture medium compared to that in the control group. Simultaneously, this cell death downgraded lactate secretion in the cell culture medium. Similarly, PEFE treatment induced necrosis led to a significant decrease in secretion of glutamate and consumption of extracellular glutamine compared to the control group. However, in the early stage of subsequent apoptosis, the apoptotic cells were able to sustain a relatively normal metabolism of glutamine and glutamate. At 24 hours post treatment, a dramatic reduction in cell number led to a markedly lower level of glutamate secretion in cells undergoing PEFE treatment.

The consumed glucose and glutamine were mainly converted to ATP through numerous enzyme reactions in metabolic pathways. The synthesized ATP was then

used to maintain cancer cell survival and proliferation. For the cells which remained metabolically active, nutrition was continuously consumed, and the ATP was intracellularly produced over time. As a result, these ATP levels indicated the presence of viable cells. By monitoring the ATP level, the number of viable cells could be estimated. In Figure 6.14, ATP levels was quantified for both the control group and the experimental group separately. Cell culture medium was refreshed for each sample, supplying more nutrition to the cultured cells, prior to PEFE treatment. For the control group, the cancer cells became more metabolically active and produced more ATP, increasing the amount of ATP within the first 1 hour. However, these cells were not able to keep growing as they were already in the stationary phase of the growth curve, as shown in Figure 6.23.

Conversely, the PEFE treated cells demonstrated a markedly lower production of ATP due to consistent cell death. During the first hour, the levels of ATP decreased rapidly, which then slowed. As necrosis is associated with ATP depletion(Chandra et al., 2000), this rapid ATP reduction was confirmed to mainly result from PEFE-inducing necrosis. Meanwhile, the apoptotic cells still sustained metabolism and increased cell death in the following hours, leading to reduction in ATP levels.

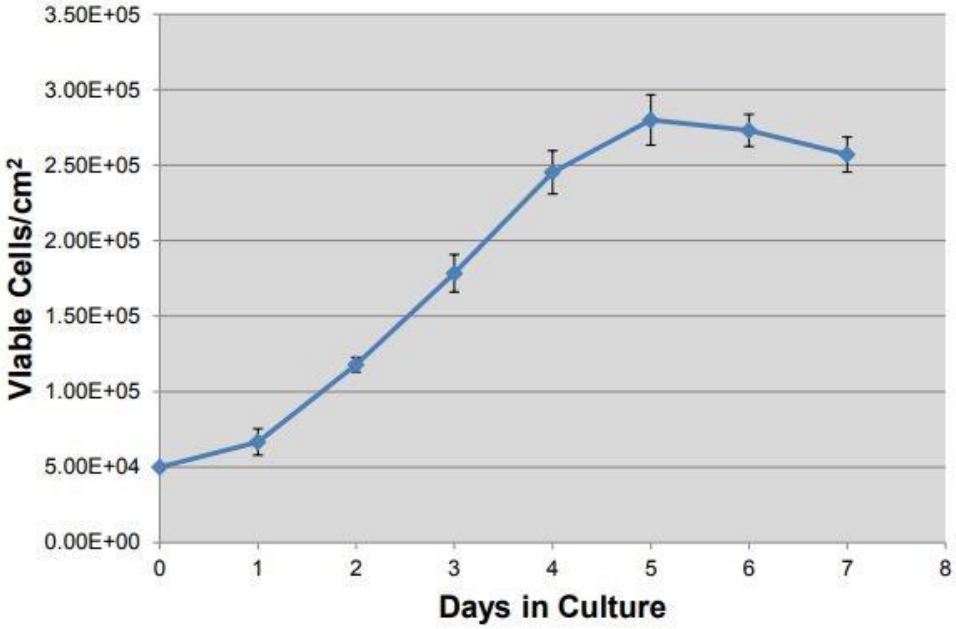

Figure 6.23 Growth curve-MDA-MB-231 cell line. Source: https://physics.cancer.gov/docs/bioresource/breast/NCI-PBCF-HTB26_MDA-MB-231_SOP-508.pdf

6.4.2 Redox homeostasis

The necrosis induced by PEFE treatment was a complicated process inherent involving redox imbalance. During the PEFE treatment, cell necrosis initiated and resulted in a rapid ATP depletion. This ATP depletion increased the intracellular ROS level (H_2O_2), shown in Figure 6.21. The measured amount of H_2O_2 was much higher than in the control group. As a main intracellular antioxidant, GSH plays a role in antagonism of increased H_2O_2 levels. The increased H_2O_2 induced more consumption of GSH. Since the necrosis occurred quickly, the consumed GSH came mainly from that already synthesized. As a result, the GSH level was decreased during PEFE treatment compared to the control group, shown in Figure 6.18a. As two products of this oxidation-reduction reaction, GSSG and NAD(P)H levels were increased accordingly, shown in Figure 6.17a and Figure 6.12.

After cell necrosis, the main cell death mechanism in PEFE treated cells shifted to apoptosis. This apoptosis thus resulted in a consistent reduction in cell number in the following hours.

It is assumed that this apoptosis was directly triggered by increased intracellular ROS. The measured H_2O_2 level would be anticipated to increase continuously. However, the results in treated cells failed to follow this trend. The H_2O_2 levels in cells undergoing PEFE treatment was markedly lower than that in the control group at 1.5 hours post treatment and no significant difference was observed in the following hours, as shown in Figure 6.22, indicating that apoptosis was less likely to be induced by increasing ROS. Another factor which can impact redox homeostasis is RNS. The RNS level was quantified by NO levels in this research, as shown in Figure 6.10 and Figure 6.11. There was no significant difference between the treated samples and the control group, indicating that PEFE treatment did not affect RNS. As a result, it can be implied that apoptosis was not triggered by redox imbalance.

6.5 Summary

Collectively, based on the analyses of energy consumption and synthesis, this study has demonstrated that PEFE treatment resulted in an acute phase of changes in metabolism before 1 hour post treatment, which is in line with necrotic cell death and likely to be the outcome of non-specific cell death of a small portion of cancer cells immediately adjacent to the tip of the PEFE probe.

However, the most interesting observations are the sustained changes in metabolism following the acute phase of cell death, *i.e.* 1 hour post treatment. This is clearly linked to apoptosis induced by PEFE, as demonstrated in Chapters-4 and 5 and is a key discovery of the current study. The data presented here has clearly demonstrated that after PEFE treatment, glycolysis is reduced, as seen by a reduction of consumption of glucose and increase in lactose and ATP production. It is noteworthy however, that during this phase of apoptosis related metabolism, there appears to be no significant involvement of glutaminolysis, as both glutamine and glutamate showed little changes during this period compared with the non-treated control cells. Finally, this study provides clear evidence that ROS (reactive

oxygen species) plays little part in apoptotic cell death caused by PEFE treatment. This conclusion was drawn from the discovery that following PEFE treatment there is no change in the GSH/GSSG ratio nor in the levels of H_2O_2, both key indicators of Redox homeostasis.

These are interesting observations when considering the mode of action for PEFE, although the study remains at an early phase. It will be necessary, when time allows, to explore the expression of key enzymes in specific pathways following PEFE treatment.

Chapter 7

Conclusion and Future Work

7.1 Conclusion

In this research, a new technique named pulsed electromagnetic field exposure (PEFE) was developed based on dedicated microwave devices and advanced software. The entire PEFE system was calibrated at desired frequencies and power levels to ensure that PEFE was delivered correctly. *In vitro* and *in vivo* experiments were conducted to verify its efficacy in cancer cell-killing and tumour growth reduction and its potential significance as a clinical application.

The induced cell death in PEFE treatment varied according to different treatment conditions. In PEFE treatments with intensive electric fields, cell death included necrosis and apoptosis, which was confirmed by visual inspection using TEM. In the treatments using chronic PEFE, induced cell death was caspase-depended apoptosis, confirmed by overexpression of Caspase3 and Caspase9 compare with the untreated control group.

A well-studied protein Kidins220, which is a regulator in neuronal activities, was found to be involved in cell apoptosis in studies of other cell types. In human breast cancer cells, Kidins220 was confirmed to regulate cellular migration and then potentially impact cell motility or intercellular junctions using established cell models after Kidins220 knockdown. After PEFE treatment, the Kidins220 knockdown cells exhibited significantly higher death rates, and thus more receptive to PEFE. Potentially, proteins downstream of Kidins220 are also responsive to PEFE, namely ERK1/2 and MEK1/2 (Liao et al., 2007, Lopez-Menendez et al., 2009, Cai et al., 2017), supported by the finding the PEFE reduced both ERK1 and ERK2, and indeed MEK1 and MEK2 . It would indicate that in a cell with low Kidins220, PEFE would result in addition reduction of ERKs and MEKs, making the cells prone to apoptosis. Thus, Kidins220 could be a potential biomarker to ensure increased efficacy of PEFE treatment when used in clinical treatments.

The potential mechanism of how PEFE affects cellular signalling and potentially activated apoptosis related pathways was investigated. A protein microarray (Kinexus™ antibody microarray, Kinexus, British Columbia, Canada) revealed the potential links between cell to cell junctions and cell apoptosis after PEFE treatment, which could be regulated by HSP90 as this is reduced following

treatment, *i.e*. a significant reduction seen as early as 15 minutes post treatment. This reduction lasted for 1 hour before returning to control levels after 4 hours. Likewise, the current study has shown a striking disruption of cell-cell junctions by electron microscopy and immunofluorescence, a characteristic feature of damaged tight junctions. This was clearly indicated by first the disrupted distribution of ZO-1 in the tight junctions and then again early reduction of ZO-1 at protein level (within 15 minutes).

Thus, this study has shown a series of interesting molecular and cellular events in cancer cells after PEFE treatment. Immediately after PEFE treatment, cancer cells undergo disruption of tight junctions and reduction of tight junctional proteins. This is seen together with a reduction of HSP90 and Caspases, followed by a reduction of glycolysis of the cells and, over a longer time (after 6 hours), the manifestation of apoptosis.

As discussed in Chapter-5, it is established that HSP90 forms a protein complex with tight junctional proteins including ZO-1 and Src. On disruption of the tight junctions, the ZO-1/HSP90/Src protein complex is disrupted, resulting in the subsequent loss of HSP90 and an activation of caspases, which triggers apoptosis. It has also been reported recently that caspases are able to shut down metabolic pathways including that of glycolysis (Pradelli et al., 2014). Taken all the datasets and the literature reports together, we propose the following mode of action during PEFE induced cancer cell death and tumour suppression (Figure 7.1a and Figure 7.1b).

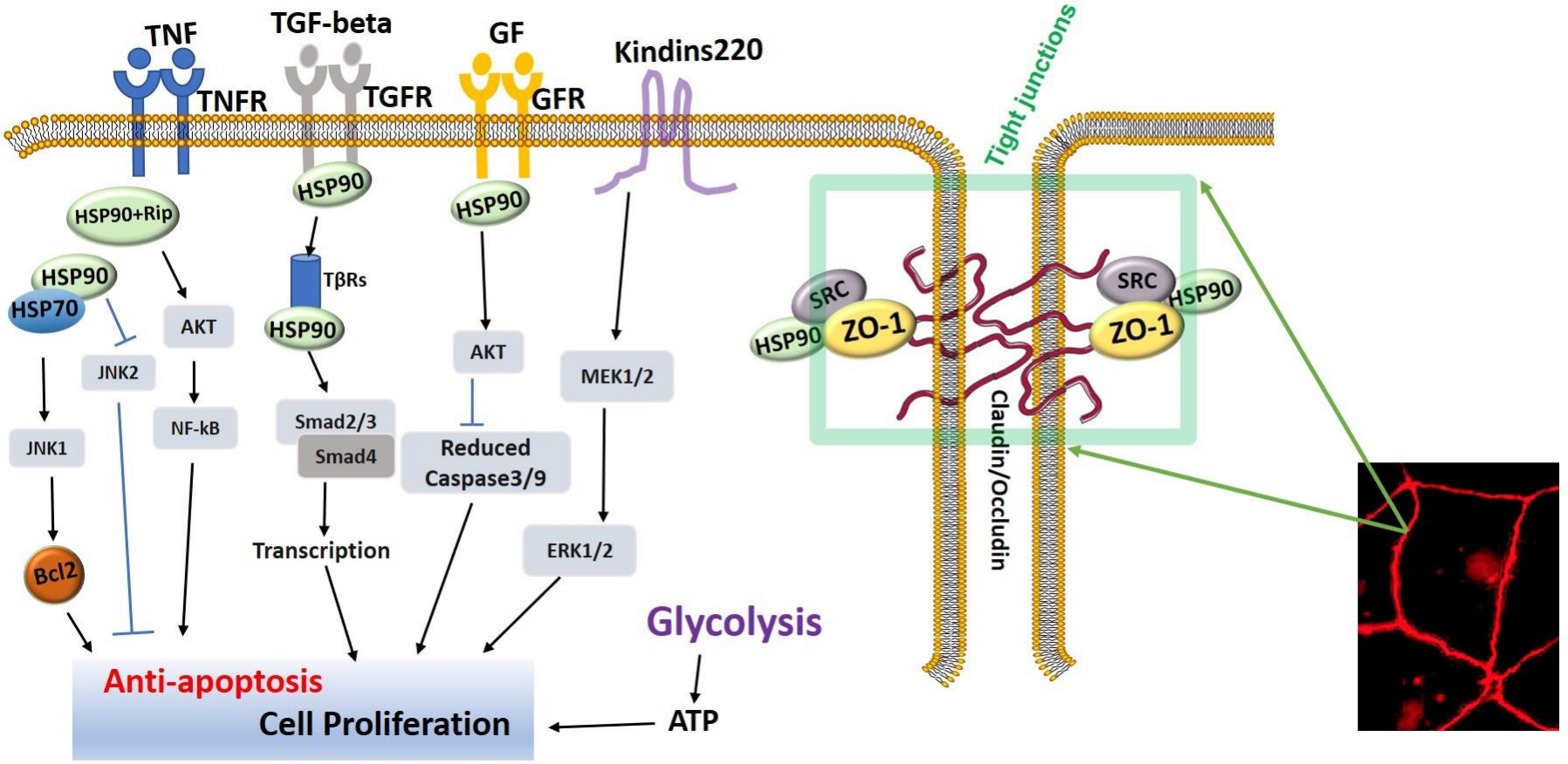
TNF
TNFR
TGF-beta
TGFR
GF
GFR
Kindins220
Tight junctions
HSP90+Rip
HSP90
HSP70
JNK2
AKT
JNK1
NF-kB
Bcl2
HSP90
TβRs
HSP90
Smad2/3
Smad4
Transcription
HSP90
AKT
Reduced
Caspase3/9
MEK1/2
ERK1/2
SRC
HSP90
ZO-1
SRC
HSP90
ZO-1
Claudin/Occludin
Glycolysis
ATP
Anti-apoptosis
Cell Proliferation

Figure 7.1 (A)

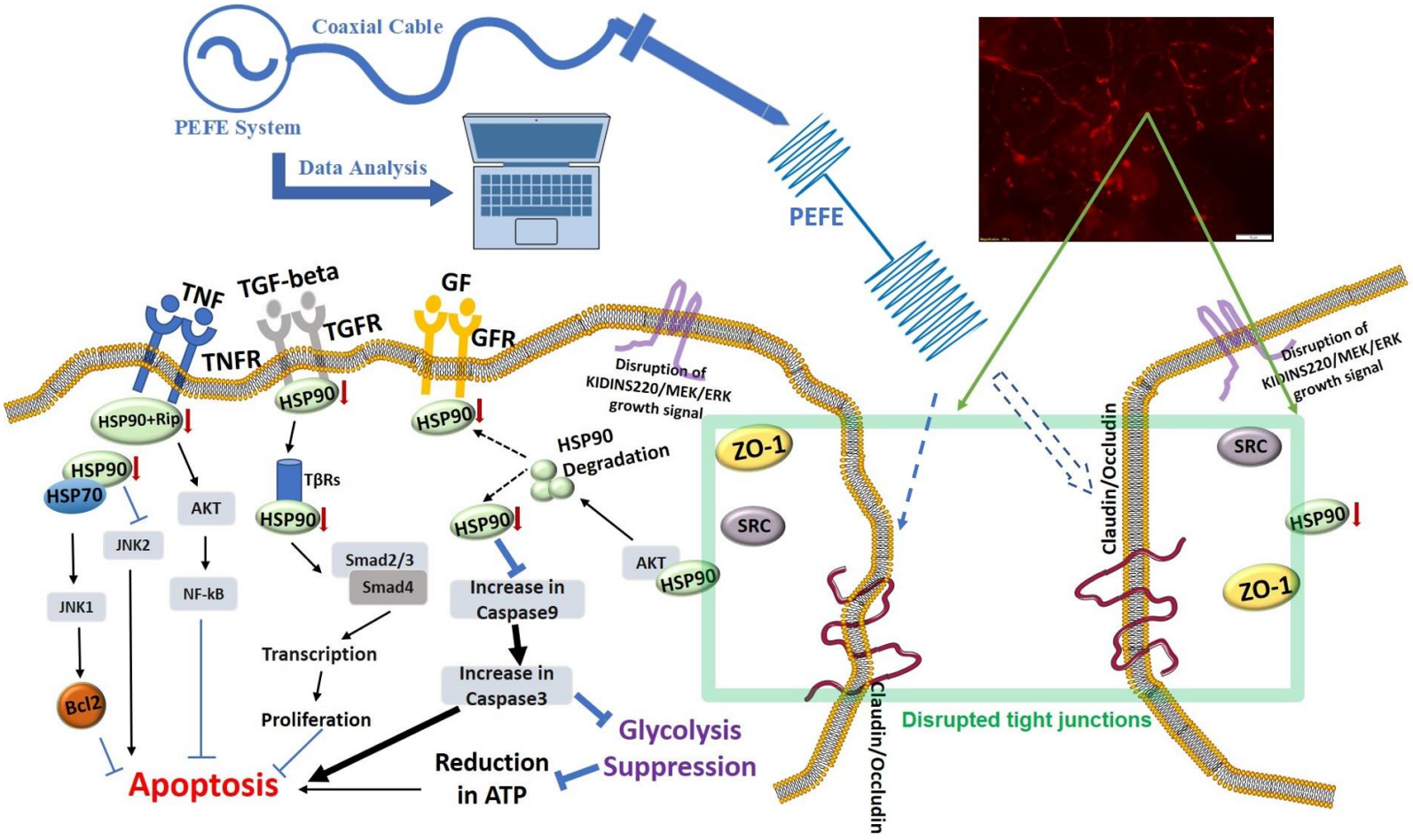
Coaxial Cable
PEFE System
Data Analysis
PEFE
TNF
TGF-beta
GF
TNFR
TGFR
GFR
HSP90+Rip
HSP90
HSP70
JNK2
AKT
JNK1
NF-kB
Bcl2
TβRs
Smad2/3
Smad4
Transcription
Proliferation
Apoptosis
HSP90 Degradation
Increase in Caspase9
Increase in Caspase3
Reduction in ATP
Glycolysis Suppression
Disruption of KIDINS220/MEK/ERK growth signal
ZO-1
SRC
Claudin/Occludin
Disrupted tight junctions

Figure 7.1 (B)

Figure 7.1 Proposed mode of action by which PEFE regulates the apoptosis of breast cancer cells. (A) Breast cancer cells with intact intercellular tight junctions before PEFE treatments. Multiple apoptotic and cell growth signalling pathways potentially involved HSP90 are: (1) HSP90/70 was found to activate JNK1, then Bcl2 was activated, leading to inhibition of apoptosis (Padmini et al., 2012). (2) HSP90/70 was studied to inhibits JNK2, thus block apoptosis(Padmini et al., 2012). (3) HSP90 and Rip complex can activate AKT, AKT then activates NFkappaB, thus inhibits apoptosis(Arya et al., 2007). (4) HSP90 combined with TβRs, activates SMAD2/3 involved with SMAD4. The activated SMAD2/3 can be co-activator in transcription and promote the proliferation, consequently inhibiting apoptosis(Zhang et al., 2012). (5) AKT, activated by HSP90, can lower the level of caspase9. As the downstream protein of caspase9, caspase3 is activated by caspase9 and is the effector of cell apoptosis(Cardone et al., 1998, Pandey et al., 2000, Li et al., 2013). Before PEFE treatments, the intact ZO-1/HSP90/SRC protein complex is exhibited. The cellular membrane sustains normal morphology. The biomarker, Kidins220, was studied to promote proliferation through MEK1/2 and ERK1/2 pathways (Liao et al., 2007, Lopez-Menendez et al., 2009, Cai et al., 2017). (B) Breast cancer cells with disrupted intercellular junctions after PEFE treatments. PEFE acts on intercellular tight junctions which subsequently triggers cell apoptosis, as indicated in blue hollow arrow in the upper figure. This apoptosis is associated with HSP90 through different signalling pathways. Once PEFE acts on intercellular junctions, it disrupts the ZO-1/HSP90/SRC protein complex. The breakdown of the tight junction complex contributes to disrupted intercellular junctions and altered morphology. A degradation of HSP90 was observed, leading to a much lower level of intracellular HSP90. HSP90 reduction would regulates cell apoptosis through caspase3 and caspase9 dependent pathways, which is not fully understood. The western blot results showed a downregulation of HSP90 and upregulation of caspase3 and caspase9. Furthermore, the upregulated caspase3 was studied to block glycolysis in metabolic signalling pathways(Pradelli et al., 2014), leading to a markedly reduction in cellular ATP level. The reduced production of ATP can promote cell apoptosis. Some other potential alterations in signalling pathways regulated by HSP90 are: (1) Downregulation of HSP90 weakens the inhibition of apoptosis through JNK1/Bcl2. (2) Downregulated HSP90 results in higher level of JNK2, thus promotes the cell apoptosis. (3) Decreased expression of HSP90 lower the level of HSP90/Rib protein complex, contributes to a downregulation of AKT and NFkappaB, which weakens the inhibition of cell apoptosis. (4) Downregulation of HSP90 blocks the formation of HSP90- TβRs protein complex, thus promote cell apoptosis through SMAD2/3. (5) Down-expression of HSP90 bonded with AKT, elevating the level of caspase9. Increased expression of caspase9 results in overexpression of caspase3, promoting cell apoptosis. The signalling pathway that Kidins220 regulated proliferation is also disrupted, resulting in promotion in cell apoptosis. Intensive PEFE may act on membrane structure, indicated in blue dotted arrow, and cause a breakdown of membrane structure and cellular organelles. This disruption results in rapid cell necrosis and potentially subsequent apoptosis. The activation and promotion in signalling pathways are indicated

using black arrows, while the inhibition is indicated using blue 'T'-shaped lines. The alterations in the expression of HSP90 after PEFE treatments are indicated by red arrows.

7.2 Future work

In addition to the current work completed in this thesis, this research also leads to future areas of research as follows:

7.2.1 PXI based PEFE system development

The current PEFE system was constructed with a series of microwave devices from varied manufacturers. Although the data acquisition and analysis can be done through software, the system has to be operated manually. Currently, a portable PXI based system consists of many compact PXIe modules from National Instruments (National Instruments, Ltd.) is under developing, as shown in Figure 7.2.

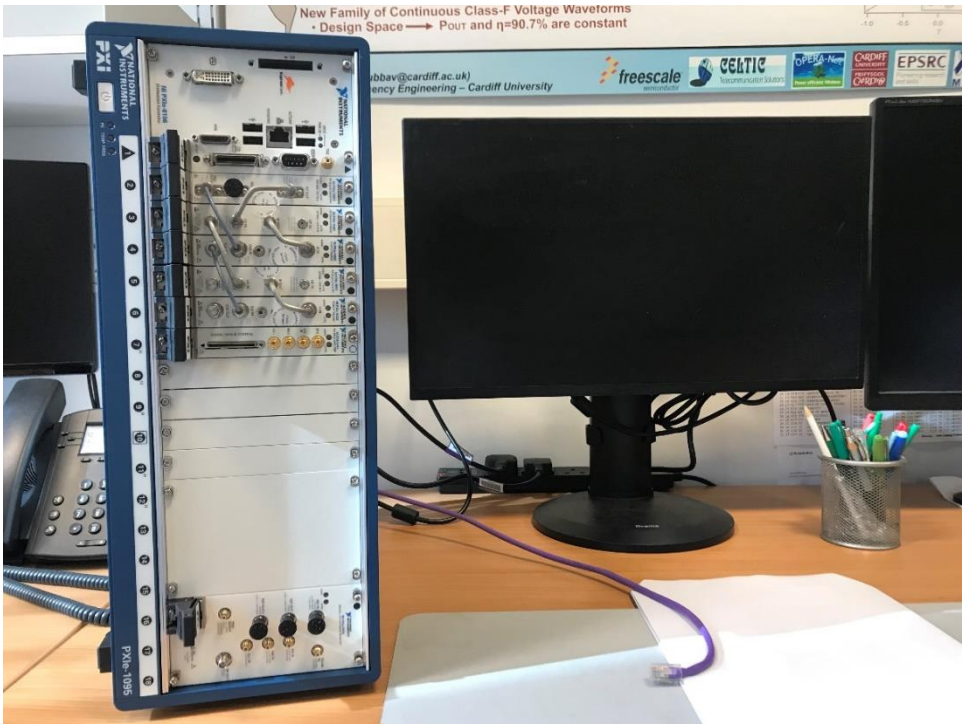

Figure 7.2 PXI based PEFE system which is current under development. The chassis on the left consists of signal generator and two vector signal analysers. The monitor on the right is used to visualise the user interface.

This new system now can generate PEFE and achieve data analysis more accurately. Temperature measurement will be integrated and the entire system will be controlled according to the measured temperature. Once the temperature exceeds 42℃, the PEFE will be stopped until the temperature falls back to 37℃.

7.2.2 Medical Needle design integrated with biopsy

Regarding the potential use in human trials, a new needle in PEFE treatments would be desired and will need to be manufactured. The current probe used *in vitro* and *in vivo* is standard coaxial cable with one pointed end. When inserting the probe into human tissues, the probe should be guided by ultrasound to precisely reach the tumour lesions. Thus, integration of the PEFE system with an ultrasound scanner will be required. Furthermore, a biopsy needle can be integrated into to the probe to minimize invasive incision and achieve histopathological analysis.

7.2.3 Cell apoptosis verification in intensive PEFE treatment

In chapter 4, a prolonged cell death was observed, which was posited to be cell apoptosis. This can be further confirmed by examining the expression of apoptosis-related proteins such as Caspase3 and Caspase9.

7.2.4 Investigation of PEFE treatment to achieve cell death selectively

The cells used in this research were cancer cells from human breast tissue. Many cell lines from other part of body could be investigated in the future by using PEFE treatment. These would include cancer cells from the liver, lung, and stomach. Since different cell lines have their own characteristics, this may lead to different responses to PEFE treatment. Moreover, an analysis of treatments using varied cell lines would contribute to a better understanding of how PEFE interacts with cancer cells.

Furthermore, since the dielectric properties of normal cells is significantly different from that of cancer cells, it will be worthwhile investigating whether PEFE can induce cancer cell death without damaging surrounding normal cells. The in vitro experiments can be conducted with primary cultured normal mammary epithelial cells under the same conditions. Should PEFE treatment effect cell death in cancer cells but not in surrounding, adjacent normal epithelial and stromal cells etc, then it

could be construed that this new device would be much safer than traditional treatments, as it would be better focussed and cause fewer side effects. In the continuing effort to find better, more targeted and more efficacious cancer therapies, potential PEFE therapy could be of great importance to patients with cancer in the future.

7.2.5 Confirmation of local high temperature produced within cancer cells

As discussed in Chapter 4, highly non-uniform the electric fields were generated during PEFE treatments. A local high temperature was likely to be produced inside cancer cells, which could be much higher than the global temperature. Some external thermometers can be applied in the different locations inside the well plate to measure the local temperature. Furthermore, some dedicated local temperature probes (for example: fluorophores) can also measure local temperature more precisely. Once the produced local higher temperature is confirmed, subsequent investigations will focus on how it can impact cancer cells.

7.2.6 Investigation on how heavy mental ions impact cancer cells

During the PEFE treatments, some mental ions can exist in the medium since the probed used in this research was made of copper. Although the concentration was low, these cupric ions were known to be biocides. As a result, further investigation should be done to explore whether the presence of cupric ions can be a factor to induce cancer cell death.

Bibliography

AARTS, B. M., PREVOO, W., MEIER, M. A. J., BEX, A., BEETS-TAN, R. G. H., KLOMPENHOUWER, E. G. & GOMEZ, F. M. 2020. Percutaneous Microwave Ablation of Histologically Proven T1 Renal Cell Carcinoma. *Cardiovasc Intervent Radiol*.

ABE, H., KURUMI, Y., NAKA, S., SHIOMI, H., UMEDA, T., NAITOH, H., ENDO, Y., HANASAWA, K., MORIKAWA, S. & TANI, T. 2005. Open-configuration MR-guided microwave thermocoagulation therapy for metastatic liver tumors from breast cancer. *Breast Cancer,* 12**,** 26-31.

ABOUL EZZ, H. S., KHADRAWY, Y. A., AHMED, N. A., RADWAN, N. M. & EL BAKRY, M. M. 2013. The effect of pulsed electromagnetic radiation from mobile phone on the levels of monoamine neurotransmitters in four different areas of rat brain. *Eur Rev Med Pharmacol Sci,* 17**,** 1782-8.

AGARWAL, A., DEEPINDER, F., SHARMA, R. K., RANGA, G. & LI, J. 2008. Effect of cell phone usage on semen analysis in men attending infertility clinic: an observational study. *Fertility and Sterility,* 89**,** 124-128.

AGARWAL, A., DESAI, N. R., MAKKER, K., VARGHESE, A., MOURADI, R., SABANEGH, E. & SHARMA, R. 2009. Effects of radiofrequency electromagnetic waves (RF-EMW) from cellular phones on human ejaculated semen: an in vitro pilot study. *Fertility and Sterility,* 92**,** 1318-1325.

AHDI REZAEIEH, S., ZAMANI, A., BIALKOWSKI, K. S. & ABBOSH, A. M. 2017. Novel Microwave Torso Scanner for Thoracic Fluid Accumulation Diagnosis and Monitoring. *Sci Rep,* 7**,** 304.

AHMED, M., BRACE, C. L., LEE, F. T., JR. & GOLDBERG, S. N. 2011. Principles of and advances in percutaneous ablation. *Radiology,* 258**,** 351-69.

AHMED, M., RUBIO, I. T., KLAASE, J. M. & DOUEK, M. 2015. Surgical treatment of nonpalpable primary invasive and in situ breast cancer. *Nat Rev Clin Oncol,* 12**,** 645-63.

AHMED, S., SNELLING, A., BAINS, M. & WHITWORTH, I. H. 2005. Breast reconstruction. *BMJ,* 330**,** 943.

AITKEN, R. J., BENNETTS, L. E., SAWYER, D., WIKLENDT, A. M. & KING, B. V. 2005. Impact of radio frequency electromagnetic radiation on DNA integrity in the male germline. *Int J Androl,* 28**,** 171-9.

AKRAM, M., IQBAL, M., DANIYAL, M. & KHAN, A. U. 2017. Awareness and current knowledge of breast cancer. *Biol Res,* 50**,** 33.

AMMARI, M., LECOMTE, A., SAKLY, M., ABDELMELEK, H. & DE-SEZE, R. 2008. Exposure to GSM 900 MHz electromagnetic fields affects cerebral cytochrome c oxidase activity. *Toxicology,* 250**,** 70-4.

AN, C., LI, X., ZHANG, M., YANG, J., CHENG, Z., YU, X., HAN, Z., LIU, F., DONG, L., YU, J. & LIANG, P. 2020. 3D visualization ablation planning system assisted microwave ablation for hepatocellular carcinoma (Diameter >3): a precise clinical application. *BMC Cancer,* 20**,** 44.

ANDOCS, G., SZASZ, O. & SZASZ, A. 2009. Oncothermia treatment of cancer: from the laboratory to clinic. *Electromagn Biol Med,* 28**,** 148-65.

ANDREANO, A. & BRACE, C. L. 2013. A comparison of direct heating during radiofrequency and microwave ablation in ex vivo liver. *Cardiovasc Intervent Radiol,* 36**,** 505-11.

ANTOCH, G., SAOUDI, N., KUEHL, H., DAHMEN, G., MUELLER, S. P., BEYER, T., BOCKISCH, A., DEBATIN, J. F. & FREUDENBERG, L. S. 2004. Accuracy of whole-body dual-modality fluorine-18-2-fluoro-2-deoxy-D-glucose positron

emission tomography and computed tomography (FDG-PET/CT) for tumor staging in solid tumors: comparison with CT and PET. *J Clin Oncol,* 22**,** 4357-68.

ARI ADI, W., YUNASFI, Y., MASHADI, M., SAHIDIN WINATAPURA, D., MULYAWAN, A., SARWANTO, Y., EDI GUNANTO, Y. & TARYANA, Y. 2019. Metamaterial: Smart Magnetic Material for Microwave Absorbing Material. *Metamaterial: Smart Magnetic Material for Microwave Absorbing Material*.

ARYA, R., MALLIK, M. & LAKHOTIA, S. C. 2007. Heat shock genes—integrating cell survival and death. *Journal of biosciences,* 32**,** 595-610.

ASANO, M., SAKAGUCHI, M., TANAKA, S., KASHIMURA, K., MITANI, T., KAWASE, M., MATSUMURA, H., YAMAGUCHI, T., FUJITA, Y. & TABUSE, K. 2017a. Effects of Normothermic Conditioned Microwave Irradiation on Cultured Cells Using an Irradiation System with Semiconductor Oscillator and Thermo-regulatory Applicator. *Sci Rep,* 7**,** 41244.

ASANO, M., TANAKA, S., SAKAGUCHI, M., MATSUMURA, H., YAMAGUCHI, T., FUJITA, Y. & TABUSE, K. 2017b. Normothermic Microwave Irradiation Induces Death of HL-60 Cells through Heat-Independent Apoptosis. *Sci Rep,* 7**,** 11406.

ATASOY, H. I., GUNAL, M. Y., ATASOY, P., ELGUN, S. & BUGDAYCI, G. 2013. Immunohistopathologic demonstration of deleterious effects on growing rat testes of radiofrequency waves emitted from conventional Wi-Fi devices. *Journal of Pediatric Urology,* 9**,** 223-229.

ATLI SEKEROGLU, Z., AKAR, A. & SEKEROGLU, V. 2013. Evaluation of the cytogenotoxic damage in immature and mature rats exposed to 900 MHz radiofrequency electromagnetic fields. *Int J Radiat Biol,* 89**,** 985-92.

AUFRANC, V., FAROUIL, G., ABDEL-REHIM, M., SMADJA, P., TARDIEU, M., APTEL, S. & GUIBAL, A. 2019. Percutaneous thermal ablation of primary and secondary lung tumors: Comparison between microwave and radiofrequency ablation. *Diagn Interv Imaging,* 100**,** 781-791.

AVENDANO, C., MATA, A., SANCHEZ SARMIENTO, C. A. & DONCEL, G. F. 2012. Use of laptop computers connected to internet through Wi-Fi decreases human sperm motility and increases sperm DNA fragmentation. *Fertil Steril,* 97**,** 39-45 e2.

BASILE, A., FAILLA, G., REFORGIATO, A., SCAVONE, G., MUNDO, E., MESSINA, M., CALTABIANO, G., ARENA, F., RICCERI, V., SCAVONE, A. & MASALA, S. 2014. The use of microwaves ablation in the treatment of epiphyseal osteoid osteomas. *Cardiovasc Intervent Radiol,* 37**,** 737-42.

BECKERS, A., ORGANE, S., TIMMERMANS, L., SCHEYS, K., PEETERS, A., BRUSSELMANS, K., VERHOEVEN, G. & SWINNEN, J. V. 2007. Chemical Inhibition of Acetyl-CoA Carboxylase Induces Growth Arrest and Cytotoxicity Selectively in Cancer Cells. *Cancer Research,* 67**,** 8180-8187.

BELFIORE, G., RONZA, F., BELFIORE, M. P., SERAO, N., DI RONZA, G., GRASSI, R. & ROTONDO, A. 2013. Patients' survival in lung malignancies treated by microwave ablation: our experience on 56 patients. *Eur J Radiol,* 82**,** 177-81.

BERTRAM, J. M., YANG, D., CONVERSE, M. C., WEBSTER, J. G. & MAHVI, D. M. 2006. A Review of Coaxial-Based Interstitial Antennas for Hepatic Microwave Ablation. 34**,** 187-213.

BHANGARI, M. D., BHAGALI, A. & KSHIRSAGAR, R. 2019. Analysis and Optimization of Microwave Wireless Transmission Hazards on Human tissues and its ramification.

BOLOMEY, J. & JOFRE, L. Three decades of active microwave imaging achievements, difficulties and future challenges. 2010 IEEE International Conference on Wireless Information Technology and Systems, 28 Aug.-3 Sept. 2010 2010. 1-4.

BOUJI, M., LECOMTE, A., HODE, Y., DE SEZE, R. & VILLEGIER, A. S. 2012. Effects of 900 MHz radiofrequency on corticosterone, emotional memory and neuroinflammation in middle-aged rats. *Exp Gerontol,* 47**,** 444-51.

BUCHNER, R., BARTHEL, J. & STAUBER, J. 1999. The dielectric relaxation of water between 0°C and 35°C. *Chemical Physics Letters,* 306**,** 57-63.

BUDIHARDJO, I., OLIVER, H., LUTTER, M., LUO, X. & WANG, X. 1999. Biochemical pathways of caspase activation during apoptosis. *Annu Rev Cell Dev Biol,* 15**,** 269-90.

BURCH, J. B., REIF, J. S., NOONAN, C. W., ICHINOSE, T., BACHAND, A. M., KOLEBER, T. L. & YOST, M. G. 2002. Melatonin metabolite excretion among cellular telephone users. *Int J Radiat Biol,* 78**,** 1029-36.

BURLAKA, A., TSYBULIN, O., SIDORIK, E., LUKIN, S., POLISHUK, V., TSEHMISTRENKO, S. & YAKYMENKO, I. 2013. Overproduction of free radical species in embryonal cells exposed to low intensity radiofrequency radiation. *Exp Oncol,* 35**,** 219-25.

BUTTIGLIONE, M., ROCA, L., MONTEMURNO, E., VITIELLO, F., CAPOZZI, V. & CIBELLI, G. 2007. Radiofrequency radiation (900 MHz) induces Egr-1 gene expression and affects cell-cycle control in human neuroblastoma cells. *J Cell Physiol,* 213**,** 759-67.

CAI, S., CAI, J., JIANG, W. G. & YE, L. 2017. Kidins220 and tumour development: Insights into a complexity of cross-talk among signalling pathways (Review). *Int J Mol Med,* 40**,** 965-971.

CAIRNS, R. A., HARRIS, I. S. & MAK, T. W. 2011. Regulation of cancer cell metabolism. *Nat Rev Cancer,* 11**,** 85-95.

CAM, S. T. & SEYHAN, N. 2012. Single-strand DNA breaks in human hair root cells exposed to mobile phone radiation. *Int J Radiat Biol,* 88**,** 420-4.

CAMPBELL, A. M. 1990. *Measurements and analysis of the microwave dielectric properties of tissues.* University of Glasgow.

CAMPISI, A., GULINO, M., ACQUAVIVA, R., BELLIA, P., RACITI, G., GRASSO, R., MUSUMECI, F., VANELLA, A. & TRIGLIA, A. 2010. Reactive oxygen species levels and DNA fragmentation on astrocytes in primary culture after acute exposure to low intensity microwave electromagnetic field. *Neuroscience Letters,* 473**,** 52-55.

CAPITANIO, U., BENSALAH, K., BEX, A., BOORJIAN, S. A., BRAY, F., COLEMAN, J., GORE, J. L., SUN, M., WOOD, C. & RUSSO, P. 2019. Epidemiology of Renal Cell Carcinoma. *European Urology,* 75**,** 74-84.

CARDONE, M. H., ROY, N., STENNICKE, H. R., SALVESEN, G. S., FRANKE, T. F., STANBRIDGE, E., FRISCH, S. & REED, J. C. 1998. Regulation of cell death protease caspase-9 by phosphorylation. *Science,* 282**,** 1318-21.

CARMELIET, P., DOR, Y., HERBERT, J.-M., FUKUMURA, D., BRUSSELMANS, K., DEWERCHIN, M., NEEMAN, M., BONO, F., ABRAMOVITCH, R. & MAXWELL, P. 1998. Role of HIF-1α in hypoxia-mediated apoptosis, cell proliferation and tumour angiogenesis. *Nature,* 394**,** 485.

CARRAFIELLO, G., IERARDI, A. M., FONTANA, F., PETRILLO, M., FLORIDI, C., LUCCHINA, N., CUFFARI, S., DIONIGI, G., ROTONDO, A. & FUGAZZOLA, C. 2013. Microwave Ablation of Pancreatic Head Cancer: Safety and Efficacy. *Journal of Vascular and Interventional Radiology,* 24**,** 1513-1520.

CATHERINO, W. H., MAYERS, C. M., MANTZOURIS, T., ARMSTRONG, A. Y., LINEHAN, W. M. & SEGARS, J. H. 2007. Compensatory alterations in energy homeostasis characterized in uterine tumors from hereditary leiomyomatosis and renal cell cancer. *Fertil Steril,* 88**,** 1039-48.

CAZZATO, R. L., DE MARINI, P., LECLERC, L., DALILI, D., KOCH, G., RAO, P., AULOGE, P., GARNON, J. & GANGI, A. 2020. Large nearly spherical ablation

zones are achieved with simultaneous multi-antenna microwave ablation applied to treat liver tumours. *Eur Radiol,* 30**,** 971-975.

CEJAS, P., CASADO, E., BELDA-INIESTA, C., DE CASTRO, J., ESPINOSA, E., REDONDO, A., SERENO, M., GARCIA-CABEZAS, M. A., VARA, J. A., DOMINGUEZ-CACERES, A., PERONA, R. & GONZALEZ-BARON, M. 2004. Implications of oxidative stress and cell membrane lipid peroxidation in human cancer (Spain). *Cancer Causes Control,* 15**,** 707-19.

CHANDRA, J., SAMALI, A. & ORRENIUS, S. 2000. Triggering and modulation of apoptosis by oxidative stress. *Free Radic Biol Med,* 29**,** 323-33.

CHANDRA, R., ZHOU, H., BALASINGHAM, I. & NARAYANAN, R. M. 2015. On the Opportunities and Challenges in Microwave Medical Sensing and Imaging. *IEEE Transactions on Biomedical Engineering,* 62**,** 1667-1682.

CHANG-QING, Y., JIE, L., SHI-QI, Z., KUN, Z., ZI-QIAN, G., RAN, X., HUI-MENG, L., REN-BIN, Z., GANG, Z., DA-CHUAN, Y. & CHEN-YAN, Z. 2020. Recent treatment progress of triple negative breast cancer. *Prog Biophys Mol Biol,* 151**,** 40-53.

CHEN, G., LU, D., CHIANG, H., LESZCZYNSKI, D. & XU, Z. 2012. Using model organism Saccharomyces cerevisiae to evaluate the effects of ELF-MF and RF-EMF exposure on global gene expression. *Bioelectromagnetics,* 33**,** 550-60.

CHEN, H., YUE, J.-X., YANG, S.-H., DING, H., ZHAO, R.-W. & ZHANG, S. 2009. Overexpression of transketolase-like gene 1 is associated with cell proliferation in uterine cervix cancer. *Journal of Experimental & Clinical Cancer Research,* 28**,** 43.

CHENG, Y. & FU, M. 2018. Dielectric properties for non-invasive detection of normal, benign, and malignant breast tissues using microwave theories. *Thorac Cancer,* 9**,** 459-465.

CHIANG, J., WANG, P. & BRACE, C. L. 2013. Computational modelling of microwave tumour ablations. *Int J Hyperthermia,* 29**,** 308-17.

CHU, K. F. & DUPUY, D. E. 2014. Thermal ablation of tumours: biological mechanisms and advances in therapy. *Nat Rev Cancer,* 14**,** 199-208.

CHUNG, S. H., CERUSSI, A. E., KLIFA, C., BAEK, H. M., BIRGUL, O., GULSEN, G., MERRITT, S. I., HSIANG, D. & TROMBERG, B. J. 2008. In vivo water state measurements in breast cancer using broadband diffuse optical spectroscopy. *Physics in Medicine and Biology,* 53**,** 6713-6727.

CLEATOR, S., TSIMELZON, A., ASHWORTH, A., DOWSETT, M., DEXTER, T., POWLES, T., HILSENBECK, S., WONG, H., OSBORNE, C. K., O'CONNELL, P. & CHANG, J. C. 2006. Gene expression patterns for doxorubicin (Adriamycin) and cyclophosphamide (cytoxan) (AC) response and resistance. *Breast Cancer Res Treat,* 95**,** 229-33.

CLEM, B., TELANG, S., CLEM, A., YALCIN, A., MEIER, J., SIMMONS, A., RASKU, M. A., ARUMUGAM, S., DEAN, W. L., EATON, J., LANE, A., TRENT, J. O. & CHESNEY, J. 2008. Small-molecule inhibition of 6-phosphofructo-2-kinase activity suppresses glycolytic flux and tumor growth. *Molecular Cancer Therapeutics,* 7**,** 110-120.

COLEMAN, M. P., QUARESMA, M., BERRINO, F., LUTZ, J.-M., DE ANGELIS, R., CAPOCACCIA, R., BAILI, P., RACHET, B., GATTA, G., HAKULINEN, T., MICHELI, A., SANT, M., WEIR, H. K., ELWOOD, J. M., TSUKUMA, H., KOIFMAN, S., E SILVA, G. A., FRANCISCI, S., SANTAQUILANI, M., VERDECCHIA, A., STORM, H. H. & YOUNG, J. L. 2008. Cancer survival in five continents: a worldwide population-based study (CONCORD). *The Lancet Oncology,* 9**,** 730-756.

CONKLIN, K. A. 2004. Chemotherapy-associated oxidative stress: impact on chemotherapeutic effectiveness. *Integr Cancer Ther,* 3**,** 294-300.

CZAJKA, M. L. & PFEIFER, C. 2020. *Breast Cancer Surgery*, StatPearls Publishing, Treasure Island (FL).

DARWEESH, S. K. & GAD, A. A. 2019. Percutaneous microwave ablation for HCV-related hepatocellular carcinoma: Efficacy, safety, and survival. *The Turkish Journal of Gastroenterology,* 30**,** 445-453.

DE COBELLI, F., PAPA, M., PANZERI, M., COLOMBO, M., STEIDLER, S., AMBROSI, A., CAO, R., GUSMINI, S., MARRA, P., CAPITANIO, U., BERTINI, R., VENTURINI, M., LOSA, A., GABOARDI, F., MONTORSI, F. & CARDONE, G. 2020. Percutaneous Microwave Ablation Versus Cryoablation in the Treatment of T1a Renal Tumors. *Cardiovasc Intervent Radiol,* 43**,** 76-83.

DE IULIIS, G. N., NEWEY, R. J., KING, B. V. & AITKEN, R. J. 2009. Mobile phone radiation induces reactive oxygen species production and DNA damage in human spermatozoa in vitro. *PLoS One,* 4**,** e6446.

DE TOMMASO, M., ROSSI, P., FALSAPERLA, R., FRANCESCO VDE, V., SANTORO, R. & FEDERICI, A. 2009. Mobile phones exposure induces changes of contingent negative variation in humans. *Neurosci Lett,* 464**,** 79-83.

DEL RE, B., BERSANI, F. & GIORGI, G. 2019. Effect of electromagnetic field exposure on the transcription of repetitive DNA elements in human cells. *Electromagn Biol Med,* 38**,** 262-270.

DESHAZER, G., MERCK, D., HAGMANN, M., DUPUY, D. E. & PRAKASH, P. 2016. Physical modeling of microwave ablation zone clinical margin variance. *Med Phys,* 43**,** 1764.

DESHMUKH, P. S., BANERJEE, B. D., ABEGAONKAR, M. P., MEGHA, K., AHMED, R. S., TRIPATHI, A. K. & MEDIRATTA, P. K. 2013a. Effect of low level microwave radiation exposure on cognitive function and oxidative stress in rats.

DESHMUKH, P. S., MEGHA, K., BANERJEE, B. D., AHMED, R. S., CHANDNA, S., ABEGAONKAR, M. P. & TRIPATHI, A. K. 2013b. Detection of Low Level Microwave Radiation Induced Deoxyribonucleic Acid Damage Vis-à-vis Genotoxicity in Brain of Fischer Rats. *Toxicology international,* 20**,** 19-24.

DIEGO, E. J., MCAULIFFE, P. F., SORAN, A., MCGUIRE, K. P., JOHNSON, R. R., BONAVENTURA, M. & AHRENDT, G. M. 2016. Axillary Staging After Neoadjuvant Chemotherapy for Breast Cancer: A Pilot Study Combining Sentinel Lymph Node Biopsy with Radioactive Seed Localization of Pre-treatment Positive Axillary Lymph Nodes. *Ann Surg Oncol,* 23**,** 1549-53.

DIEM, E., SCHWARZ, C., ADLKOFER, F., JAHN, O. & RUDIGER, H. 2005. Non-thermal DNA breakage by mobile-phone radiation (1800 MHz) in human fibroblasts and in transformed GFSH-R17 rat granulosa cells in vitro. *Mutat Res,* 583**,** 178-83.

DING, J., JING, X., LIU, J., WANG, Y., WANG, F., WANG, Y. & DU, Z. 2013a. Comparison of two different thermal techniques for the treatment of hepatocellular carcinoma. *Eur J Radiol,* 82**,** 1379-84.

DING, J., JING, X., LIU, J., WANG, Y., WANG, F., WANG, Y. & DU, Z. 2013b. Complications of thermal ablation of hepatic tumours: comparison of radiofrequency and microwave ablative techniques. *Clin Radiol,* 68**,** 608-15.

DONG, B., LIANG, P., YU, X., SU, L., YU, D., CHENG, Z. & ZHANG, J. 2003. Percutaneous sonographically guided microwave coagulation therapy for hepatocellular carcinoma: results in 234 patients. *AJR Am J Roentgenol,* 180**,** 1547-55.

DONG, B. W., LIANG, P., YU, X. L., ZENG, X. Q., WANG, P. J., SU, L., WANG, X. D., XIN, H. & LI, S. 1998. Sonographically guided microwave coagulation treatment of liver cancer: an experimental and clinical study. *AJR Am J Roentgenol,* 171**,** 449-54.

DONG, X., SUN, Z., WU, T., GUO, W., YAN, S. & ZHENG, S. 2019. 915-MHz microwave-assisted laparoscopic hepatectomy: a new technique for liver resection. *Surg Endosc,* 33**,** 395-400.

DOOLEY, W. C., VARGAS, H. I., FENN, A. J., TOMASELLI, M. B. & HARNESS, J. K. 2010. Focused microwave thermotherapy for preoperative treatment of invasive breast cancer: a review of clinical studies. *Ann Surg Oncol,* 17**,** 1076-93.

EBERHARDT, J. L., PERSSON, B. R., BRUN, A. E., SALFORD, L. G. & MALMGREN, L. O. 2008. Blood-brain barrier permeability and nerve cell damage in rat brain 14 and 28 days after exposure to microwaves from GSM mobile phones. *Electromagn Biol Med,* 27**,** 215-29.

EDRICH, J. Microwave Techniques in the Diagnosis and Treatment of Cancer. 1979 9th European Microwave Conference, 17-20 Sept. 1979 1979. 25-33.

EHTAIBA, M. H. 2017. *Use of microwave techniques in medical diagnostics and therapy.* Cardiff University.

ELMORE, J. G., ARMSTRONG, K., LEHMAN, C. D. & FLETCHER, S. W. 2005. Screening for Breast Cancer. *JAMA,* 293**,** 1245-1256.

EROGUL, O., OZTAS, E., YILDIRIM, I., KIR, T., AYDUR, E., KOMESLI, G., IRKILATA, H. C., IRMAK, M. K. & PEKER, A. F. 2006. Effects of Electromagnetic Radiation from a Cellular Phone on Human Sperm Motility: An In Vitro Study. *Archives of Medical Research,* 37**,** 840-843.

FAJARDO, L. F., EGBERT, B., MARMOR, J. & HAHN, G. M. 1980. Effects of hyperthermia in a malignant tumor. *Cancer,* 45**,** 613-623.

FEJES, I., ZAVACZKI, Z., SZOLLOSI, J., KOLOSZAR, S., DARU, J., KOVACS, L. & PAL, A. 2005. Is there a relationship between cell phone use and semen quality? *Arch Androl,* 51**,** 385-93.

FENG, W., LIU, W., LI, C., LI, Z., LI, R., LIU, F., ZHAI, B., SHI, J. & SHI, G. 2002. Percutaneous microwave coagulation therapy for lung cancer. *Zhonghua zhong liu za zhi [Chinese journal of oncology],* 24**,** 388-390.

FENN, A. J. 2007. *Breast cancer treatment by focused microwave thermotherapy*, Jones & Bartlett Learning.

FENTON, W. S., HIBBELN, J. & KNABLE, M. 2000. Essential fatty acids, lipid membrane abnormalities, and the diagnosis and treatment of schizophrenia. *Biological Psychiatry,* 47**,** 8-21.

FERLAY, J., SHIN, H.-R., BRAY, F., FORMAN, D., MATHERS, C. & PARKIN, D. M. 2010. Estimates of worldwide burden of cancer in 2008: GLOBOCAN 2008. *International Journal of Cancer,* 127**,** 2893-2917.

FERREIRA, A. R., KNAKIEVICZ, T., PASQUALI, M. A., GELAIN, D. P., DAL-PIZZOL, F., FERNANDEZ, C. E., DE SALLES, A. A., FERREIRA, H. B. & MOREIRA, J. C. 2006. Ultra high frequency-electromagnetic field irradiation during pregnancy leads to an increase in erythrocytes micronuclei incidence in rat offspring. *Life Sci,* 80**,** 43-50.

FIORENTINI, G. & SZASZ, A. 2006. Hyperthermia today: Electric energy, a new opportunity in cancer treatment. *Journal of Cancer Research and Therapeutics,* 2**,** 41-46.

FISHER, E. R., COSTANTINO, J., FISHER, B., PALEKAR, A. S. & REDMOND, C. 1995. Pathologic findings from the National Surgical Adjuvant Breast Project (NSABP) protocol B-17. Intraductal carcinoma (ductal carcinoma in situ). *Cancer,* 75**,** 1310-1319.

FöLDI, M., STICKELER, E., BAU, L., KRETZ, O., WATERMANN, D., GITSCH, G., KAYSER, G., ZUR HAUSEN, A. & COY, J. F. 2007. Transketolase protein TKTL1 overexpression: A potential biomarker and therapeutic target in breast cancer. *Oncology reports,* 17**,** 841-845.

FRAGOPOULOU, A. F., SAMARA, A., ANTONELOU, M. H., XANTHOPOULOU, A., PAPADOPOULOU, A., VOUGAS, K., KOUTSOGIANNOPOULOU, E., ANASTASIADOU, E., STRAVOPODIS, D. J., TSANGARIS, G. T. & MARGARITIS, L. H. 2012. Brain proteome response following whole body exposure of mice to mobile phone or wireless DECT base radiation. *Electromagn Biol Med,* 31**,** 250-74.

FURTADO-FILHO, O. V., BORBA, J. B., DALLEGRAVE, A., PIZZOLATO, T. M., HENRIQUES, J. A., MOREIRA, J. C. & SAFFI, J. 2014. Effect of 950 MHz UHF electromagnetic radiation on biomarkers of oxidative damage, metabolism of UFA and antioxidants in the livers of young rats of different ages. *Int J Radiat Biol,* 90**,** 159-68.

FURUSE, M., FUJITA, K., HIIRAGI, T., FUJIMOTO, K. & TSUKITA, S. 1998. Claudin-1 and -2: Novel Integral Membrane Proteins Localizing at Tight Junctions with No Sequence Similarity to Occludin. *Journal of Cell Biology,* 141**,** 1539-1550.

GABRIEL, C., GABRIEL, S. & CORTHOUT, E. 1996. The dielectric properties of biological tissues: I. Literature survey. *Physics in Medicine and Biology,* 41**,** 2231-2249.

GAJSKI, G. & GARAJ-VRHOVAC, V. 2009. Radioprotective Effects of Honeybee Venom (Apis mellifera) Against 915-MHz Microwave Radiation–Induced DNA Damage in Wistar Rat Lymphocytes: In Vitro Study. *International Journal of Toxicology,* 28**,** 88-98.

GARBER, K. 2010. Oncology's energetic pipeline. *Nature Biotechnology,* 28**,** 888-891.

GARDNER, R. A., VARGAS, H. I., BLOCK, J. B., VOGEL, C. L., FENN, A. J., KUEHL, G. V. & DOVAL, M. 2002. Focused microwave phased array thermotherapy for primary breast cancer. *Ann Surg Oncol,* 9**,** 326-32.

GIATROMANOLAKI, A., KOUKOURAKIS, M. I., PEZZELLA, F., SIVRIDIS, E., TURLEY, H., HARRIS, A. L. & GATTER, K. C. 2008. Lactate dehydrogenase 5 expression in non-Hodgkin B-cell lymphomas is associated with hypoxia regulated proteins. *Leukemia & Lymphoma,* 49**,** 2181-2186.

GLOBOCAN, W. 2012. Estimated cancer incidence, mortality and prevalence worldwide in 2012. *Int Agency Res Cancer*.

GOMPEL, A. & SANTEN, R. J. 2012. Hormone therapy and breast cancer risk 10 years after the WHI. *Climacteric,* 15**,** 241-9.

GRODZINSKY, E. & SUND LEVANDER, M. 2020. History of the Thermometer. *In:* GRODZINSKY, E. & SUND LEVANDER, M. (eds.) *Understanding Fever and Body Temperature: A Cross-disciplinary Approach to Clinical Practice.* Cham: Springer International Publishing.

GUL, A., CELEBI, H. & UGRAS, S. 2009. The effects of microwave emitted by cellular phones on ovarian follicles in rats. *Arch Gynecol Obstet,* 280**,** 729-33.

GULER, G., TOMRUK, A., OZGUR, E., SAHIN, D., SEPICI, A., ALTAN, N. & SEYHAN, N. 2012. The effect of radiofrequency radiation on DNA and lipid damage in female and male infant rabbits. *Int J Radiat Biol,* 88**,** 367-73.

GULER, G., TOMRUK, A., OZGUR, E. & SEYHAN, N. 2010. The effect of radiofrequency radiation on DNA and lipid damage in non-pregnant and pregnant rabbits and their newborns. *Gen Physiol Biophys,* 29**,** 59-66.

HACKER, G. 2000. The morphology of apoptosis. *Cell Tissue Res,* 301**,** 5-17.

HADDEN, J. 1999. Review Article The immunology and immunotherapy of breast cancer: an update. *International journal of immunopharmacology,* 21**,** 79-101.

HANAHAN, D. & WEINBERG, R. A. 2011. Hallmarks of cancer: the next generation. *Cell,* 144**,** 646-74.

HARBECK, N. & GNANT, M. 2017. Breast cancer. *The Lancet,* 389**,** 1134-1150.

HARBECK, N., PENAULT-LLORCA, F., CORTES, J., GNANT, M., HOUSSAMI, N., POORTMANS, P., RUDDY, K., TSANG, J. & CARDOSO, F. 2019. Breast cancer. *Nat Rev Dis Primers,* 5**,** 66.

HARVEY, C. & FRENCH, P. W. 1999. EFFECTS ON PROTEIN KINASE C AND GENE EXPRESSION IN A HUMAN MAST CELL LINE, HMC-1, FOLLOWING MICROWAVE EXPOSURE. *Cell Biology International,* 23**,** 739-748.

HASSAN, A. I. 2010. The role of hyperthermia in potentiation of chemotherapy and radiotherapy in mice bearing solid tumor. *Nat Sci,* 8**,** 100-8.

HASTED, J. B. 1972. Liquid Water: Dielectric Properties. *In:* FRANKS, F. (ed.) *The Physics and Physical Chemistry of Water*. Boston, MA: Springer New York.

HATHER, G., LIU, R., BANDI, S., METTETAL, J., MANFREDI, M., SHYU, W. C., DONELAN, J. & CHAKRAVARTY, A. 2014. Growth rate analysis and efficient experimental design for tumor xenograft studies. *Cancer Inform,* 13**,** 65-72.

HATZIVASSILIOU, G., ZHAO, F., BAUER, D. E., ANDREADIS, C., SHAW, A. N., DHANAK, D., HINGORANI, S. R., TUVESON, D. A. & THOMPSON, C. B. 2005. ATP citrate lyase inhibition can suppress tumor cell growth. *Cancer Cell,* 8**,** 311-21.

HEKMAT, A., SABOURY, A. A. & MOOSAVI-MOVAHEDI, A. A. 2013. The toxic effects of mobile phone radiofrequency (940 MHz) on the structure of calf thymus DNA. *Ecotoxicol Environ Saf,* 88**,** 35-41.

HENSLEY, C. T., WASTI, A. T. & DEBERARDINIS, R. J. 2013. Glutamine and cancer: cell biology, physiology, and clinical opportunities. *J Clin Invest,* 123**,** 3678-84.

HOUSSAMI, N., TURNER, R. M. & MORROW, M. 2017. Meta-analysis of pre-operative magnetic resonance imaging (MRI) and surgical treatment for breast cancer. *Breast Cancer Res Treat,* 165**,** 273-283.

HSU, P. P. & SABATINI, D. M. 2008. Cancer cell metabolism: Warburg and beyond. *Cell,* 134**,** 703-7.

HUNG, C. S., ANDERSON, C., HORNE, J. A. & MCEVOY, P. 2007. Mobile phone 'talk-mode' signal delays EEG-determined sleep onset. *Neurosci Lett,* 421**,** 82-6.

IANNITTI, D. A., MARTIN, R. C., SIMON, C. J., HOPE, W. W., NEWCOMB, W. L., MCMASTERS, K. M. & DUPUY, D. 2007. Hepatic tumor ablation with clustered microwave antennae: the US Phase II trial. *HPB (Oxford),* 9**,** 120-4.

ISSELS, R. D. 2008. Hyperthermia adds to chemotherapy. *Eur J Cancer,* 44**,** 2546-54.

IZUMI, N., ASAHINA, Y., NOGUCHI, O., UCHIHARA, M., KANAZAWA, N., ITAKURA, J., HIMENO, Y., MIYAKE, S., SAKAI, T. & ENOMOTO, N. 2001. Risk factors for distant recurrence of hepatocellular carcinoma in the liver after complete coagulation by microwave or radiofrequency ablation. *Cancer,* 91**,** 949-56.

JARUPAT, S., KAWABATA, A., TOKURA, H. & BORKIEWICZ, A. 2003. Effects of the 1900 MHz electromagnetic field emitted from cellular phone on nocturnal melatonin secretion. *J Physiol Anthropol Appl Human Sci,* 22**,** 61-3.

JEMAL, A., SIEGEL, R., WARD, E., HAO, Y., XU, J. & THUN, M. 2009. Cancer statistics. *Ca Cancer J Clin,* 59.

JONES, R. P., KITTERINGHAM, N. R., TERLIZZO, M., HANCOCK, C., DUNNE, D., FENWICK, S. W., POSTON, G. J., GHANEH, P. & MALIK, H. Z. 2012. Microwave ablation of ex vivo human liver and colorectal liver metastases with a novel 14.5 GHz generator. *Int J Hyperthermia,* 28**,** 43-54.

JUNIOR, L. C., GUIMARAES EDA, S., MUSSO, C. M., STABLER, C. T., GARCIA, R. M., MOURAO-JUNIOR, C. A. & ANDREAZZI, A. E. 2014. Behavior and memory evaluation of Wistar rats exposed to 1.8 GHz radiofrequency electromagnetic radiation. *Neurol Res,* 36**,** 800-3.

KAATZE, U. 1989. Complex Permittivity of Water as a Function of Frequency and Temperature. *Journal of Chemical and Engineering Data,* 34**,** 371-374.

KAATZE, U. & UHLENDORF, V. 1981. The dielectric properties of water at microwave frequencies. *Zeitschrift für Physikalische Chemie,* 126**,** 151-165.

KALAMIDA, D., KARAGOUNIS, I. V., MITRAKAS, A., KALAMIDA, S., GIATROMANOLAKI, A. & KOUKOURAKIS, M. I. 2015. Fever-range hyperthermia vs. hypothermia effect on cancer cell viability, proliferation and HSP90 expression. *PLoS One,* 10**,** e0116021.

KAMAL, A., ELMOETY, A. A. A., ROSTOM, Y. A. M., SHATER, M. S. & LASHEN, S. A. 2019. Percutaneous radiofrequency versus microwave ablation for management of hepatocellular carcinoma: a randomized controlled trial. *J Gastrointest Oncol,* 10**,** 562-571.

KARACA, E., DURMAZ, B., AKTUG, H., YILDIZ, T., GUDUCU, C., IRGI, M., KOKSAL, M. G., OZKINAY, F., GUNDUZ, C. & COGULU, O. 2012. The genotoxic effect of radiofrequency waves on mouse brain. *J Neurooncol,* 106**,** 53-8.

KESARI, K. K. & BEHARI, J. 2009. Fifty-gigahertz microwave exposure effect of radiations on rat brain. *Appl Biochem Biotechnol,* 158**,** 126-39.

KESARI, K. K. & BEHARI, J. 2010. Microwave exposure affecting reproductive system in male rats. *Appl Biochem Biotechnol,* 162**,** 416-28.

KIM, J. H., LEE, J.-K., KIM, H.-G., KIM, K.-B. & KIM, H. R. 2019. Possible Effects of Radiofrequency Electromagnetic Field Exposure on Central Nerve System. *Biomolecules & Therapeutics,* 27**,** 265-275.

KISHK, A. 2011. *Electromagnetic waves: propagation in complex matter*, BoD–Books on Demand.

KNAVEL, E. M. & BRACE, C. L. 2013. Tumor ablation: common modalities and general practices. *Tech Vasc Interv Radiol,* 16**,** 192-200.

KONG, D., PARK, E. J., STEPHEN, A. G., CALVANI, M., CARDELLINA, J. H., MONKS, A., FISHER, R. J., SHOEMAKER, R. H. & MELILLO, G. 2005. Echinomycin, a small-molecule inhibitor of hypoxia-inducible factor-1 DNA-binding activity. *Cancer research,* 65**,** 9047-9055.

KOSTRZEWA, M., DIEZLER, P., MICHAELY, H., RATHMANN, N., ATTENBERGER, U. I., SCHOENBERG, S. O. & DIEHL, S. J. 2014. Microwave Ablation of Osteoid Osteomas Using Dynamic MR Imaging for Early Treatment Assessment: Preliminary Experience. *Journal of Vascular and Interventional Radiology,* 25**,** 106-111.

KUANG, M., LU, M. D., XIE, X. Y., XU, H. X., MO, L. Q., LIU, G. J., XU, Z. F., ZHENG, Y. L. & LIANG, J. Y. 2007. Liver Cancer: Increased Microwave Delivery to Ablation Zone with Cooled-Shaft Antenna—Experimental and Clinical Studies. *Radiology,* 242**,** 914-924.

KUMAR, R. S., SAREESH, N., NAYAK, S. & MAILANKOT, M. 2009. Hypoactivity of Wistar rats exposed to mobile phone on elevated plus maze. *Indian journal of physiology and pharmacology,* 53**,** 283-286.

KUMAR, S., KESARI, K. K. & BEHARI, J. 2010. Evaluation of genotoxic effects in male Wistar rats following microwave exposure.

KUNG, A. L., ZABLUDOFF, S. D., FRANCE, D. S., FREEDMAN, S. J., TANNER, E. A., VIEIRA, A., CORNELL-KENNON, S., LEE, J., WANG, B., WANG, J., MEMMERT, K., NAEGELI, H.-U., PETERSEN, F., ECK, M. J., BAIR, K. W., WOOD, A. W. & LIVINGSTON, D. M. 2004. Small molecule blockade of transcriptional coactivation of the hypoxia-inducible factor pathway. *Cancer Cell,* 6**,** 33-43.

KWON, M. S., VOROBYEV, V., KANNALA, S., LAINE, M., RINNE, J. O., TOIVONEN, T., JOHANSSON, J., TERAS, M., LINDHOLM, H., ALANKO, T. & HAMALAINEN, H. 2011. GSM mobile phone radiation suppresses brain glucose metabolism. *J Cereb Blood Flow Metab,* 31**,** 2293-301.

LAHAT, E., ESHKENAZY, R., ZENDEL, A., ZAKAI, B. B., MAOR, M., DREZNIK, Y. & ARICHE, A. 2014. Complications after percutaneous ablation of liver tumors: a systematic review. *Hepatobiliary Surg Nutr,* 3**,** 317-23.

LAI, E. C. H. & LAU, W. Y. 2005. The continuing challenge of hepatic cancer in Asia. *Surgeon-Journal of the Royal Colleges of Surgeons of Edinburgh and Ireland,* 3**,** 210-215.

LAU, W.-Y. 2008. *Hepatocellular carcinoma*, World Scientific.

LAU, W. Y. & LAI, E. C. 2009. The current role of radiofrequency ablation in the management of hepatocellular carcinoma: a systematic review. *Ann Surg,* 249**,** 20-5.

LI, X., LUO, R., JIANG, R., MENG, X., WU, X., ZHANG, S. & HUA, W. 2013. The role of the Hsp90/Akt pathway in myocardial calpain-induced caspase-3 activation and apoptosis during sepsis. *BMC Cardiovasc Disord,* 13**,** 8.

LIANG, P., WANG, Y., YU, X. & DONG, B. 2009. Malignant liver tumors: treatment with percutaneous microwave ablation—complications among cohort of 1136 patients. *Radiology,* 251**,** 933-940.

LIAO, Y. H., HSU, S. M. & HUANG, P. H. 2007. ARMS depletion facilitates UV irradiation induced apoptotic cell death in melanoma. *Cancer Res,* 67**,** 11547-56.

LIEBE, H. J., HUFFORD, G. A. & MANABE, T. 1991. A model for the complex permittivity of water at frequencies below 1 THz. *International Journal of Infrared and Millimeter Waves,* 12**,** 659-675.

LIU, C., DUAN, W., XU, S., CHEN, C., HE, M., ZHANG, L., YU, Z. & ZHOU, Z. 2013a. Exposure to 1800MHz radiofrequency electromagnetic radiation induces oxidative DNA base damage in a mouse spermatocyte-derived cell line. *Toxicology Letters,* 218**,** 2-9.

LIU, C., GAO, P., XU, S. C., WANG, Y., CHEN, C. H., HE, M. D., YU, Z. P., ZHANG, L. & ZHOU, Z. 2013b. Mobile phone radiation induces mode-dependent DNA damage in a mouse spermatocyte-derived cell line: a protective role of melatonin. *Int J Radiat Biol,* 89**,** 993-1001.

LIVRAGHI, T., MELONI, F., SOLBIATI, L. & ZANUS, G. 2011. Complications of Microwave Ablation for Liver Tumors: Results of a Multicenter Study. *CardioVascular and Interventional Radiology,* 35**,** 868-874.

LIXIA, S., YAO, K., KAIJUN, W., DEQIANG, L., HUAJUN, H., XIANGWEI, G., BAOHONG, W., WEI, Z., JIANLING, L. & WEI, W. 2006. Effects of 1.8GHz radiofrequency field on DNA damage and expression of heat shock protein 70 in human lens epithelial cells. *Mutation Research/Fundamental and Molecular Mechanisms of Mutagenesis,* 602**,** 135-142.

LJUNGBERG, B., ALBIGES, L., ABU-GHANEM, Y., BENSALAH, K., DABESTANI, S., FERNANDEZ-PELLO, S., GILES, R. H., HOFMANN, F., HORA, M., KUCZYK, M. A., KUUSK, T., LAM, T. B., MARCONI, L., MERSEBURGER, A. S., POWLES, T., STAEHLER, M., TAHBAZ, R., VOLPE, A. & BEX, A. 2019. European Association of Urology Guidelines on Renal Cell Carcinoma: The 2019 Update. *Eur Urol,* 75**,** 799-810.

LOH, S. Y. & CHEW, S. 2011. Awareness and practice of breast self examination among Malaysian women with breast cancer. *Asian Pac J Cancer Prev,* 12**,** 199-202.

LOPEZ-MENENDEZ, C., GASCON, S., SOBRADO, M., VIDAURRE, O. G., HIGUERO, A. M., RODRIGUEZ-PENA, A., IGLESIAS, T. & DIAZ-GUERRA, M. 2009. Kidins220/ARMS downregulation by excitotoxic activation of NMDARs reveals its involvement in neuronal survival and death pathways. *J Cell Sci,* 122**,** 3554-65.

LORENTZEN, T., SKJOLDBYE, B. & NOLSOE, C. 2011. Microwave ablation of liver metastases guided by contrast-enhanced ultrasound: experience with 125

metastases in 39 patients. *Ultraschall in der Medizin-European Journal of Ultrasound,* 32**,** 492-496.

LOUGHRAN, S. P., MCKENZIE, R. J., JACKSON, M. L., HOWARD, M. E. & CROFT, R. J. 2012. Individual differences in the effects of mobile phone exposure on human sleep: rethinking the problem. *Bioelectromagnetics,* 33**,** 86-93.

LU, M.-D., CHEN, J.-W., XIE, X.-Y., LIU, L., HUANG, X.-Q., LIANG, L.-J. & HUANG, J.-F. 2001. Hepatocellular Carcinoma: US-guided Percutaneous Microwave Coagulation Therapy. *Radiology,* 221**,** 167-172.

LU, M. D., XU, H. X., XIE, X. Y., YIN, X. Y., CHEN, J. W., KUANG, M., XU, Z. F., LIU, G. J. & ZHENG, Y. L. 2005. Percutaneous microwave and radiofrequency ablation for hepatocellular carcinoma: a retrospective comparative study. *J Gastroenterol,* 40**,** 1054-60.

LUBNER, M. G., BRACE, C. L., HINSHAW, J. L. & LEE, F. T. 2010. Microwave Tumor Ablation: Mechanism of Action, Clinical Results, and Devices. *Journal of Vascular and Interventional Radiology,* 21**,** S192-S203.

LURIA, R., ELIYAHU, I., HAREUVENY, R., MARGALIOT, M. & MEIRAN, N. 2009. Cognitive effects of radiation emitted by cellular phones: the influence of exposure side and time. *Bioelectromagnetics,* 30**,** 198-204.

LUSTENBERGER, C., MURBACH, M., DURR, R., SCHMID, M. R., KUSTER, N., ACHERMANN, P. & HUBER, R. 2013. Stimulation of the brain with radiofrequency electromagnetic field pulses affects sleep-dependent performance improvement. *Brain Stimul,* 6**,** 805-11.

LUUKKONEN, J., HAKULINEN, P., MAKI-PAAKKANEN, J., JUUTILAINEN, J. & NAARALA, J. 2009. Enhancement of chemically induced reactive oxygen species production and DNA damage in human SH-SY5Y neuroblastoma cells by 872 MHz radiofrequency radiation. *Mutat Res,* 662**,** 54-8.

LYNGGAARD, P. & SKOUBY, K. E. 2015. Deploying 5G-Technologies in Smart City and Smart Home Wireless Sensor Networks with Interferences. *Wireless Personal Communications,* 81**,** 1399-1413.

MALVEZZI, M., CARIOLI, G., BERTUCCIO, P., ROSSO, T., BOFFETTA, P., LEVI, F., LA VECCHIA, C. & NEGRI, E. 2016. European cancer mortality predictions for the year 2016 with focus on leukaemias. *Annals of Oncology,* 27**,** 725-731.

MANSEL, R. E., FALLOWFIELD, L., KISSIN, M., GOYAL, A., NEWCOMBE, R. G., DIXON, J. M., YIANGOU, C., HORGAN, K., BUNDRED, N., MONYPENNY, I., ENGLAND, D., SIBBERING, M., ABDULLAH, T. I., BARR, L., CHETTY, U., SINNETT, D. H., FLEISSIG, A., CLARKE, D. & ELL, P. J. 2006. Randomized multicenter trial of sentinel node biopsy versus standard axillary treatment in operable breast cancer: the ALMANAC Trial. *J Natl Cancer Inst,* 98**,** 599-609.

MARTIN, R. C., SCOGGINS, C. R. & MCMASTERS, K. M. 2010. Safety and efficacy of microwave ablation of hepatic tumors: a prospective review of a 5-year experience. *Ann Surg Oncol,* 17**,** 171-8.

MARTIN, S. J. & HENRY, C. M. 2013. Distinguishing between apoptosis, necrosis, necroptosis and other cell death modalities. *Methods,* 61**,** 87-89.

MASOUD, V. & PAGES, G. 2017. Targeted therapies in breast cancer: New challenges to fight against resistance. *World J Clin Oncol,* 8**,** 120-134.

MATES, J. M. & SANCHEZ-JIMENEZ, F. M. 2000. Role of reactive oxygen species in apoptosis: implications for cancer therapy. *Int J Biochem Cell Biol,* 32**,** 157-70.

MATHUR, R. 2008. Effect of chronic intermittent exposure to AM radiofrequency field on responses to various types of noxious stimuli in growing rats. *Electromagn Biol Med,* 27**,** 266-76.

MCDONALD, E. S., CLARK, A. S., TCHOU, J., ZHANG, P. & FREEDMAN, G. M. 2016. Clinical Diagnosis and Management of Breast Cancer. *J Nucl Med,* 57 Suppl 1**,** 9S-16S.

MEISSNER, T. & WENTZ, F. J. 2004. The complex dielectric constant of pure and sea water from microwave satellite observations. *IEEE Transactions on Geoscience and Remote Sensing,* 42**,** 1836-1849.

METAXAS, A. C. & MEREDITH, R. J. 1988. Industrial Microwave Heating.

MIDORIKAWA, T., KUMADA, K., KIKUCHI, H., ISHIBASHI, K., YAGI, H., NAGASAKI, H., NEMOTO, H., SAITOH, M., NAKANO, H., YAMAGUCHI, M., KOH, Y., SAKAI, H., YOSHIZAWA, Y., SANADA, Y. & YOSHIBA, M. 2000. Microwave coagulation therapy for hepatocellular carcinoma. *Journal of Hepato-Biliary-Pancreatic Surgery,* 7**,** 252-259.

MOHANDAS, T. K., CHEN, X. N., ROWE, L. B., BIRKENMEIER, E. H., FANNING, A. S., ANDERSON, J. M. & KORENBERG, J. R. 1995. Localization of the Tight Junction Protein Gene TJP1 to Human Chromosome 15q13, Distal to the Prader-Willi/Angelman Region, and to Mouse Chromosome 7. *Genomics,* 30**,** 594-597.

MOTZER, R. J., JONASCH, E., AGARWAL, N., BHAYANI, S., BRO, W. P., CHANG, S. S., CHOUEIRI, T. K., COSTELLO, B. A., DERWEESH, I. H., FISHMAN, M., GALLAGHER, T. H., GORE, J. L., HANCOCK, S. L., HARRISON, M. R., KIM, W., KYRIAKOPOULOS, C., LAGRANGE, C., LAM, E. T., LAU, C., MICHAELSON, M. D., OLENCKI, T., PIERORAZIO, P. M., PLIMACK, E. R., REDMAN, B. G., SHUCH, B., SOMER, B., SONPAVDE, G., SOSMAN, J., DWYER, M. & KUMAR, R. 2017. Kidney Cancer, Version 2.2017, NCCN Clinical Practice Guidelines in Oncology. *J Natl Compr Canc Netw,* 15**,** 804-834.

MULLER, A., HOMEY, B., SOTO, H., GE, N., CATRON, D., BUCHANAN, M. E., MCCLANAHAN, T., MURPHY, E., YUAN, W., WAGNER, S. N., BARRERA, J. L., MOHAR, A., VERASTEGUI, E. & ZLOTNIK, A. 2001. Involvement of chemokine receptors in breast cancer metastasis. *Nature,* 410**,** 50-6.

NARAYANAN, S. N., KUMAR, R. S., POTU, B. K., NAYAK, S., BHAT, P. G. & MAILANKOT, M. 2010. Effect of radio-frequency electromagnetic radiations (RF-EMR) on passive avoidance behaviour and hippocampal morphology in Wistar rats. *Ups J Med Sci,* 115**,** 91-6.

NIKFARJAM, M., MURALIDHARAN, V. & CHRISTOPHI, C. 2005. Mechanisms of Focal Heat Destruction of Liver Tumors. *Journal of Surgical Research,* 127**,** 208-223.

NITTBY, H., BRUN, A., EBERHARDT, J., MALMGREN, L., PERSSON, B. R. & SALFORD, L. G. 2009. Increased blood-brain barrier permeability in mammalian brain 7 days after exposure to the radiation from a GSM-900 mobile phone. *Pathophysiology,* 16**,** 103-12.

NYLUND, R. & LESZCZYNSKI, D. 2004. Proteomics analysis of human endothelial cell line EA.hy926 after exposure to GSM 900 radiation. *Proteomics,* 4**,** 1359-65.

ODACI, E., BAS, O. & KAPLAN, S. 2008. Effects of prenatal exposure to a 900 MHz electromagnetic field on the dentate gyrus of rats: a stereological and histopathological study. *Brain Research,* 1238**,** 224-229.

ODAC‚, E., İKINCI, A., Y‚LD‚R‚M, M., KAYA, H., AKçA, M., HANC‚, H., SöNMEZ, O. F., ASLAN, A., OKUYAN, M. & BAŞ, O. 2013. The Effects of 900 Megahertz Electromagnetic Field Applied in the Prenatal Period on Spinal Cord Morphology and Motor Behavior in Female Rat Pups. *NeuroQuantology,* 11.

OLENYUK, B. Z., ZHANG, G.-J., KLCO, J. M., NICKOLS, N. G., KAELIN, W. G. & DERVAN, P. B. 2004. Inhibition of vascular endothelial growth factor with a sequence-specific hypoxia response element antagonist. *Proceedings of the National Academy of Sciences of the United States of America,* 101**,** 16768-16773.

OLIVEIRA, S. S. & MORGADO-DIAZ, J. A. 2007. Claudins: multifunctional players in epithelial tight junctions and their role in cancer. *Cell Mol Life Sci,* 64**,** 17-28.

OMATA, M., CHENG, A. L., KOKUDO, N., KUDO, M., LEE, J. M., JIA, J., TATEISHI, R., HAN, K. H., CHAWLA, Y. K., SHIINA, S., JAFRI, W., PAYAWAL, D. A., OHKI, T., OGASAWARA, S., CHEN, P. J., LESMANA, C. R. A., LESMANA, L. A., GANI, R. A., OBI, S., DOKMECI, A. K. & SARIN, S. K. 2017. Asia-Pacific clinical practice guidelines on the management of hepatocellular carcinoma: a 2017 update. *Hepatol Int,* 11**,** 317-370.

OTITOLOJU, A. A., OBE, I. A., ADEWALE, O. A., OTUBANJO, O. A. & OSUNKALU, V. O. 2010. Preliminary study on the induction of sperm head abnormalities in mice, Mus musculus, exposed to radiofrequency radiations from global system for mobile communication base stations. *Bull Environ Contam Toxicol,* 84**,** 51-4.

PACE, L. E. & KEATING, N. L. 2014. A systematic assessment of benefits and risks to guide breast cancer screening decisions. *JAMA,* 311**,** 1327-35.

PADMINI, E., VENKATRAMAN, U. & SRINIVASAN, L. 2012. Mechanism of JNK signal regulation by placental HSP70 and HSP90 in endothelial cell during preeclampsia. *Toxicol Mech Methods,* 22**,** 367-74.

PANDEY, P., SALEH, A., NAKAZAWA, A., KUMAR, S., SRINIVASULA, S. M., KUMAR, V., WEICHSELBAUM, R., NALIN, C., ALNEMRI, E. S. & KUFE, D. 2000. Negative regulation of cytochrome c-mediated oligomerization of Apaf-1 and activation of procaspase-9 by heat shock protein 90. *The EMBO journal,* 19**,** 4310-4322.

PANIERI, E. & SANTORO, M. M. 2016. ROS homeostasis and metabolism: a dangerous liason in cancer cells. *Cell Death Dis,* 7**,** e2253.

PARMAR, K., TANDON, R., KUMAR, N. & GARG, R. 2019a. Variations in electroencephalography with mobile phone usage in medical students. *Neurology India,* 67**,** 235-241.

PARMAR, K., TANDON, R., KUMAR, N. & GARG, R. K. 2019b. Variations in electroencephalography with mobile phone usage in medical students. *Neurology India,* 67**,** 235.

PEACOCK, J. R. 2009. Millimetre wave permittivity of water near 25 °C. *Journal of Physics D: Applied Physics,* 42**,** 205501.

PFANNENSTIEL, A., KEAST, T., KRAMER, S., WIBOWO, H. & PRAKASH, P. 2017. *Flexible microwave ablation applicator for the treatment of pulmonary malignancies,* SPIE.

PICARD, D. 2002. Heat-shock protein 90, a chaperone for folding and regulation. *Cell Mol Life Sci,* 59**,** 1640-8.

POGGI, G., MONTAGNA, B., DI CESARE, P., RIVA, G., BERNARDO, G., MAZZUCCO, M. & RICCARDI, A. 2013. Microwave Ablation of Hepatocellular Carcinoma Using a New Percutaneous Device: Preliminary Results. *Anticancer Research,* 33**,** 1221-1227.

POTRETZKE, T. A., ZIEMLEWICZ, T. J., HINSHAW, J. L., LUBNER, M. G., WELLS, S. A., BRACE, C. L., AGARWAL, P. & LEE, F. T. 2016. Microwave versus Radiofrequency Ablation Treatment for Hepatocellular Carcinoma: A Comparison of Efficacy at a Single Center. *Journal of Vascular and Interventional Radiology,* 27**,** 631-638.

PRADELLI, L. A., VILLA, E., ZUNINO, B., MARCHETTI, S. & RICCI, J. E. 2014. Glucose metabolism is inhibited by caspases upon the induction of apoptosis. *Cell Death Dis,* 5**,** e1406.

PRUD'HOMME, C., NUEFFER, J. P., RUNGE, M., DUBUT, J., KASTLER, B. & AUBRY, S. 2017. Prospective pilot study of CT-guided microwave ablation in the treatment of osteoid osteomas. *Skeletal Radiol,* 46**,** 315-323.

QIAN, G. J., WANG, N., SHEN, Q., SHENG, Y. H., ZHAO, J. Q., KUANG, M., LIU, G. J. & WU, M. C. 2012. Efficacy of microwave versus radiofrequency ablation for treatment of small hepatocellular carcinoma: experimental and clinical studies. *Eur Radiol,* 22**,** 1983-90.

QIN, F., YUAN, H., NIE, J., CAO, Y. & TONG, J. 2014. [Effects of nano-selenium on cognition performance of mice exposed in 1800 MHz radiofrequency fields]. *Wei sheng yan jiu = Journal of hygiene research,* 43**,** 16-21.

RAZAVINASAB, M., MOAZZAMI, K. & SHABANI, M. 2016. Maternal mobile phone exposure alters intrinsic electrophysiological properties of CA1 pyramidal neurons in rat offspring. *Toxicol Ind Health,* 32**,** 968-79.

REDMAYNE, M., SMITH, E. & ABRAMSON, M. J. 2013. The relationship between adolescents' well-being and their wireless phone use: a cross-sectional study. *Environmental Health,* 12**,** 90.

REIMANN, C., SCHüLSLER, M., SCHMIDT, S., HüBNER, F., BAZRAFSHAN, B., VOGL, T. & JAKOBY, R. Microwave Ablation Applicator with Sensing Capabilities for Thermal Treatment of Malignant Tissue. 2018 IEEE/MTT-S International Microwave Symposium - IMS, 10-15 June 2018 2018. 1278-1281.

REZK, A. Y., ABDULQAWI, K., MUSTAFA, R. M., ABO EL-AZM, T. M. & AL-INANY, H. 2008. Fetal and neonatal responses following maternal exposure to mobile phones. *Saudi Med J,* 29**,** 218-23.

RICHARDSON, H., JOHNSTON, D., PATER, J. & GOSS, P. 2007. The National Cancer Institute of Canada Clinical Trials Group MAP.3 trial: an international breast cancer prevention trial. *Curr Oncol,* 14**,** 89-96.

RIGGS, M. J., PANDALAI, P. K., KIM, J. & DIETRICH, C. S. 2020. Hyperthermic Intraperitoneal Chemotherapy in Ovarian Cancer. *Diagnostics (Basel),* 10.

RINZLER, E. S., SHIVARAM, G. M., SHAW, D. W., MONROE, E. J. & KOO, K. S. H. 2019. Microwave ablation of osteoid osteoma: initial experience and efficacy. *Pediatr Radiol,* 49**,** 566-570.

RISMAN, P. O. & WäPPLING-RAAHOLT, B. 2007. Retro-modelling of a dual resonant applicator and accurate dielectric properties of liquid water from −20 °C to +100 °C. *Measurement Science and Technology,* 18**,** 959-966.

RODRíGUEZ-ENRíQUEZ, S., MARíN-HERNáNDEZ, A., GALLARDO-PéREZ, J. C., CARREñO-FUENTES, L. & MORENO-SáNCHEZ, R. 2009. Targeting of cancer energy metabolism. *Molecular nutrition & food research,* 53**,** 29-48.

ROJAVIN, M. A. & ZISKIN, M. C. 1998. Medical application of millimetre waves. *QJM,* 91**,** 57-66.

ROSEN, A., STUCHLY, M. A. & VORST, A. V. 2002. Applications of RF/microwaves in medicine. *IEEE Transactions on Microwave Theory and Techniques,* 50**,** 963-974.

ROSS, K. F. A. & GORDON, R. E. 1982. Water in malignant tissue, measured by cell refractometry and nuclear magnetic resonance. *Journal of Microscopy,* 128**,** 7-21.

RYAN, D. G., MURPHY, M. P., FREZZA, C., PRAG, H. A., CHOUCHANI, E. T., O'NEILL, L. A. & MILLS, E. L. 2019. Coupling Krebs cycle metabolites to signalling in immunity and cancer. *Nat Metab,* 1**,** 16-33.

SABATH, E., NEGORO, H., BEAUDRY, S., PANIAGUA, M., ANGELOW, S., SHAH, J., GRAMMATIKAKIS, N., YU, A. S. & DENKER, B. M. 2008. Galpha12 regulates protein interactions within the MDCK cell tight junction and inhibits tight-junction assembly. *J Cell Sci,* 121**,** 814-24.

SADEGHI, M., ENFERADI, M. & SHIRAZI, A. 2010. External and internal radiation therapy: Past and future directions. *Journal of Cancer Research and Therapeutics,* 6**,** 239-248.

SALAMA, N., KISHIMOTO, T., KANAYAMA, H. O. & KAGAWA, S. 2009. The mobile phone decreases fructose but not citrate in rabbit semen: a longitudinal study. *Syst Biol Reprod Med,* 55**,** 181-7.

SCHENA, E., GIURAZZA, F., MASSARONI, C., FONG, Y., PARK, J. J. & SACCOMANDI, P. Thermometry based on computed tomography images during microwave ablation: Trials on ex vivo porcine liver. 2017 IEEE International Instrumentation and Measurement Technology Conference (I2MTC), 22-25 May 2017 2017. 1-6.

SCHMAUSS, D., MACHENS, H. G. & HARDER, Y. 2015. Breast Reconstruction after Mastectomy. *Front Surg,* 2**,** 71.

SCHULTZ, H., KäHLER, D., BRANSCHEID, D., VOLLMER, E., ZABEL, P. & GOLDMANN, T. 2008. TKTL1 is overexpressed in a large portion of non-small cell lung cancer specimens. *Diagnostic pathology,* 3**,** 35.

SCHWARZ, C., KRATOCHVIL, E., PILGER, A., KUSTER, N., ADLKOFER, F. & RUDIGER, H. W. 2008. Radiofrequency electromagnetic fields (UMTS, 1,950 MHz) induce genotoxic effects in vitro in human fibroblasts but not in lymphocytes. *Int Arch Occup Environ Health,* 81**,** 755-67.

SEMENZA, G. L., ROTH, P. H., FANG, H.-M. & WANG, G. L. 1994. Transcriptional regulation of genes encoding glycolytic enzymes by hypoxia-inducible factor 1. *Journal of biological chemistry,* 269**,** 23757-23763.

SHA, L. W., WARD, E. R. & STROY, B. 2002. A review of dielectric properties of normal and malignant breast tissue. *Ieee Southeastcon 2002: Proceedings***,** 457-462.

SHAPIRO, D. D., WELLS, S. A., BEST, S. L., HEDICAN, S. P., ZIEMLEWICZ, T. J., LUBNER, M. G., HINSHAW, J. L., LEE, F. T., JARRARD, D. F., RICHARDS, K. A., DOWNS, T. M., ALLEN, G. O., NAKADA, S. Y. & ABEL, E. J. 2020. Comparing Outcomes for Patients with Clinical T1b Renal Cell Carcinoma Treated With Either Percutaneous Microwave Ablation or Surgery. *Urology,* 135**,** 88-94.

SHIBATA, T., IIMURO, Y., YAMAMOTO, Y., MAETANI, Y., AMETANI, F., ITOH, K. & KONISHI, J. 2002. Small Hepatocellular Carcinoma: Comparison of Radio-frequency Ablation and Percutaneous Microwave Coagulation Therapy. *Radiology,* 223**,** 331-337.

SIDOFF, L. & DUPUY, D. E. 2017. Clinical experiences with microwave thermal ablation of lung malignancies. *Int J Hyperthermia,* 33**,** 25-33.

SIMON, C. J., DUPUY, D. E. & MAYO-SMITH, W. W. 2005. Microwave ablation: Principles and applications. *Radiographics,* 25**,** S69-S84.

SIRAV, B. & SEYHAN, N. 2011. Effects of radiofrequency radiation exposure on blood-brain barrier permeability in male and female rats. *Electromagn Biol Med,* 30**,** 253-60.

SOKOLOVIC, D., DJORDJEVIC, B., KOCIC, G., BABOVIC, P., RISTIC, G., STANOJKOVIC, Z., SOKOLOVIC, D. M., VELJKOVIC, A., JANKOVIC, A. & RADOVANOVIC, Z. 2012. The effect of melatonin on body mass and behaviour of rats during an exposure to microwave radiation from mobile phone. *Bratislavske lekarske listy,* 113**,** 265-269.

STANKIEWICZ, M. & MAYER MATTHIAS, P. 2012. The universe of Hsp90. *BioMolecular Concepts.*

STEIN, Y. 2019. Electromagnetic Radiation Including G5 Frequencies, Health Effects Summary and Policy Recommendations.

STEWART, B. & WILD, C. P. 2014. World cancer report 2014.

SURDUCAN, V., SURDUCAN, E. & CIUPA, R. 2010. Medical and scientific apparatus with microwave thermal and non-thermal effect. *Revista de Tehnologii Neconventionale,* 14**,** 42.

SUWA, K., SEKI, T., TSUDA, R., YAMASHINA, M., MURATA, M., YAMAGUCHI, T., NISHIO, A. & OKAZAKI, K. 2020. Short term treatment results of local

ablation with water-cooled microwave antenna for liver cancer: Comparison with radiofrequency ablation. *Molecular and Clinical Oncology*.

SYPNIEWSKA, R. K., MILLENBAUGH, N. J., KIEL, J. L., BLYSTONE, R. V., RINGHAM, H. N., MASON, P. A. & WITZMANN, F. A. 2010. Protein changes in macrophages induced by plasma from rats exposed to 35 GHz millimeter waves. *Bioelectromagnetics,* 31**,** 656-63.

SZASZ, O. 2013. Essentials of Oncothermia. *Conference Papers in Medicine,* 2013**,** 1-20.

TAL, N. & LEVIATAN, Y. A minimally invasive microwave ablation antenna. 2017 IEEE International Conference on Microwaves, Antennas, Communications and Electronic Systems (COMCAS), 13-15 Nov. 2017 2017. 1-3.

TENG, D.-K., LI, H.-Q., SUI, G.-Q., LIN, Y.-Q., LUO, Q., FU, P., DU, J.-R., JIN, C.-X. & WANG, H. 2019. Preliminary report of microwave ablation for the primary papillary thyroid microcarcinoma: a large-cohort of 185 patients feasibility study. *Endocrine,* 64**,** 109-117.

TEPPATI, V., FERRERO, A. & SAYED, M. 2013. *Modern RF and microwave measurement techniques*, Cambridge University Press.

THAMTORAWAT, S., HICKS, R. M., YU, J., SIRIPONGSAKUN, S., LIN, W.-C., RAMAN, S. S., MCWILLIAMS, J. P., DOUEK, M., BAHRAMI, S. & LU, D. S. K. 2016. Preliminary Outcome of Microwave Ablation of Hepatocellular Carcinoma: Breaking the 3-cm Barrier? *Journal of Vascular and Interventional Radiology,* 27**,** 623-630.

TINGUELY, P., DAL, G., BOTTAI, M., NILSSON, H., FREEDMAN, J. & ENGSTRAND, J. 2019. Microwave ablation versus resection for colorectal cancer liver metastases - A propensity score analysis from a population-based nationwide registry. *Eur J Surg Oncol*.

TKALEC, M., STAMBUK, A., SRUT, M., MALARIC, K. & KLOBUCAR, G. I. 2013. Oxidative and genotoxic effects of 900 MHz electromagnetic fields in the earthworm Eisenia fetida. *Ecotoxicol Environ Saf,* 90**,** 7-12.

TöPFER, F. & OBERHAMMER, J. 2017. Chapter 3 - Microwave cancer diagnosis. *In:* LI, C., TOFIGHI, M.-R., SCHREURS, D. & HORNG, T.-S. J. (eds.) *Principles and Applications of RF/Microwave in Healthcare and Biosensing.* Academic Press.

TRIVINO PARDO, J. C., GRIMALDI, S., TARANTA, M., NALDI, I. & CINTI, C. 2012. Microwave electromagnetic field regulates gene expression in T-lymphoblastoid leukemia CCRF-CEM cell line exposed to 900 MHz. *Electromagn Biol Med,* 31**,** 1-18.

TROSIC, I., PAVICIC, I., MILKOVIC-KRAUS, S., MLADINIC, M. & ZELJEZIC, D. 2011. Effect of electromagnetic radiofrequency radiation on the rats' brain, liver and kidney cells measured by comet assay. *Coll Antropol,* 35**,** 1259-64.

VANDER HEIDEN, M. G., CANTLEY, L. C. & THOMPSON, C. B. 2009. Understanding the Warburg effect: the metabolic requirements of cell proliferation. *Science,* 324**,** 1029-33.

VANHOVE, K., DERVEAUX, E., GRAULUS, G. J., MESOTTEN, L., THOMEER, M., NOBEN, J. P., GUEDENS, W. & ADRIAENSENS, P. 2019. Glutamine Addiction and Therapeutic Strategies in Lung Cancer. *Int J Mol Sci*, 20.

VARGAS, H. I., DOOLEY, W. C., GARDNER, R. A., GONZALEZ, K. D., VENEGAS, R., HEYWANG-KOBRUNNER, S. H. & FENN, A. J. 2004. Focused microwave phased array thermotherapy for ablation of early-stage breast cancer: results of thermal dose escalation. *Ann Surg Oncol,* 11**,** 139-46.

VECCHIO, F., BABILONI, C., FERRERI, F., BUFFO, P., CIBELLI, G., CURCIO, G., VAN DIJKMAN, S., MELGARI, J. M., GIAMBATTISTELLI, F. & ROSSINI, P. M. 2010. Mobile phone emission modulates inter-hemispheric functional coupling of EEG alpha rhythms in elderly compared to young subjects. *Clin Neurophysiol,* 121**,** 163-71.

VECCHIO, F., BABILONI, C., FERRERI, F., CURCIO, G., FINI, R., DEL PERCIO, C. & ROSSINI, P. M. 2007. Mobile phone emission modulates interhemispheric functional coupling of EEG alpha rhythms. *Eur J Neurosci,* 25**,** 1908-13.

VECCHIO, F., BUFFO, P., SERGIO, S., IACOVIELLO, D., ROSSINI, P. M. & BABILONI, C. 2012a. Mobile phone emission modulates event-related desynchronization of alpha rhythms and cognitive-motor performance in healthy humans. *Clin Neurophysiol,* 123**,** 121-8.

VECCHIO, F., TOMBINI, M., BUFFO, P., ASSENZA, G., PELLEGRINO, G., BENVENGA, A., BABILONI, C. & ROSSINI, P. M. 2012b. Mobile phone emission increases inter-hemispheric functional coupling of electroencephalographic alpha rhythms in epileptic patients. *Int J Psychophysiol,* 84**,** 164-71.

VECSEI, Z., CSATHO, A., THUROCZY, G. & HERNADI, I. 2013. Effect of a single 30 min UMTS mobile phone-like exposure on the thermal pain threshold of young healthy volunteers. *Bioelectromagnetics,* 34**,** 530-41.

VOGL, T. J., ECKERT, R., NAGUIB, N. N., BEERES, M., GRUBER-ROUH, T. & NOUR-ELDIN, N. A. 2016. Thermal Ablation of Colorectal Lung Metastases: Retrospective Comparison Among Laser-Induced Thermotherapy, Radiofrequency Ablation, and Microwave Ablation. *AJR Am J Roentgenol,* 207**,** 1340-1349.

VOGL, T. J., NAGUIB, N. N., GRUBER-ROUH, T., KOITKA, K., LEHNERT, T. & NOUR-ELDIN, N. E. 2011. Microwave ablation therapy: clinical utility in treatment of pulmonary metastases. *Radiology,* 261**,** 643-51.

WANG, H. Q., ALTOMARE, D. A., SKELE, K. L., POULIKAKOS, P. I., KUHAJDA, F. P., DI CRISTOFANO, A. & TESTA, J. R. 2005. Positive feedback regulation between AKT activation and fatty acid synthase expression in ovarian carcinoma cells. *Oncogene,* 24**,** 3574-82.

WARTERS, R. L. & JOSEPH, L. R. R. 1982. Hyperthermia and the Cell Nucleus. *Radiation Research,* 92**,** 458-462.

WDOWIAK, A., WDOWIAK, L. & WIKTOR, H. 2007. Evaluation of the effect of using mobile phones on male fertility. *Annals of Agricultural and Environmental Medicine,* 14.

WHEATLEY, D. N., KERR, C. & GREGORY, D. W. 1989. Heat-induced damage to HeLa-S3 cells: Correlation of viability, permeability, osmosensitivity, phase-contrast light-, scanning electron- and transmission electron-microscopical findings. *International Journal of Hyperthermia,* 5**,** 145-162.

WIGFIELD, S., WINTER, S., GIATROMANOLAKI, A., TAYLOR, J., KOUKOURAKIS, M. & HARRIS, A. 2008. PDK-1 regulates lactate production in hypoxia and is associated with poor prognosis in head and neck squamous cancer. *British journal of cancer,* 98**,** 1975.

WILKES, G. M. 2018. Targeted Therapy: Attacking Cancer with Molecular and Immunological Targeted Agents. *Asia Pac J Oncol Nurs,* 5**,** 137-155.

WILLIS, W. T., JACKMAN, M. R., BIZEAU, M. E., PAGLIASSOTTI, M. J. & HAZEL, J. R. 2000. Hyperthermia impairs liver mitochondrial function in vitro. *Am J Physiol Regul Integr Comp Physiol,* 278**,** R1240-6.

WOLF, F. J., GRAND, D. J., MACHAN, J. T., DIPETRILLO, T. A., MAYO-SMITH, W. W. & DUPUY, D. E. 2008. Microwave Ablation of Lung Malignancies: Effectiveness, CT Findings, and Safety in 50 Patients. *Radiology,* 247**,** 871-879.

WOOD, A. W., LOUGHRAN, S. P. & STOUGH, C. 2006. Does evening exposure to mobile phone radiation affect subsequent melatonin production? *Int J Radiat Biol,* 82**,** 69-76.

WUST, P., HILDEBRANDT, B., SREENIVASA, G., RAU, B., GELLERMANN, J., RIESS, H., FELIX, R. & SCHLAG, P. M. 2002. Hyperthermia in combined treatment of cancer. *The Lancet Oncology,* 3**,** 487-497.

XIE, H., VALERA, V. A., MERINO, M. J., AMATO, A. M., SIGNORETTI, S., LINEHAN, W. M., SUKHATME, V. P. & SETH, P. 2009. LDH-A inhibition, a therapeutic strategy for treatment of hereditary leiomyomatosis and renal cell cancer. *Molecular Cancer Therapeutics,* 8**,** 626.

XU, S., ZHOU, Z., ZHANG, L., YU, Z., ZHANG, W., WANG, Y., WANG, X., LI, M., CHEN, Y., CHEN, C., HE, M., ZHANG, G. & ZHONG, M. 2010. Exposure to 1800 MHz radiofrequency radiation induces oxidative damage to mitochondrial DNA in primary cultured neurons. *Brain Res,* 1311**,** 189-96.

YANG, X., YE, X., ZHENG, A., HUANG, G., NI, X., WANG, J., HAN, X., LI, W. & WEI, Z. 2014. Percutaneous microwave ablation of stage I medically inoperable non-small cell lung cancer: clinical evaluation of 47 cases. *J Surg Oncol,* 110**,** 758-63.

YAO, K., WU, W., WANG, K., NI, S., YE, P., YU, Y., YE, J. & SUN, L. 2008. Electromagnetic noise inhibits radiofrequency radiation-induced DNA damage and reactive oxygen species increase in human lens epithelial cells. *Mol Vis,* 14**,** 964-9.

YIN, X. Y., XIE, X. Y., LU, M. D., XU, H. X., XU, Z. F., KUANG, M., LIU, G. J., LIANG, J. Y. & LAU, W. Y. 2009. Percutaneous thermal ablation of medium and large hepatocellular carcinoma: long-term outcome and prognostic factors. *Cancer,* 115**,** 1914-23.

YOON, J., CHO, J., KIM, N., KIM, D. D., LEE, E., CHEON, C. & KWON, Y. 2011. High-frequency microwave ablation method for enhanced cancer treatment with minimized collateral damage. *Int J Cancer,* 129**,** 1970-8.

YU, J., YU, X.-L., HAN, Z.-Y., CHENG, Z.-G., LIU, F.-Y., ZHAI, H.-Y., MU, M.-J., LIU, Y.-M. & LIANG, P. 2017. Percutaneous cooled-probe microwave versus radiofrequency ablation in early-stage hepatocellular carcinoma: a phase III randomised controlled trial. *Gut,* 66**,** 1172-1173.

ZHANG, D.-Y., XU, Z.-P., CHIANG, H., LU, D.-Q. & ZENG, Q.-L. 2006. Effects of GSM 1800 MHz radiofrequency electromagnetic fields on DNA damage in Chinese hamster lung cells. *Zhonghua yu fang yi xue za zhi [Chinese journal of preventive medicine],* 40**,** 149-152.

ZHANG, K., LU, Y., YANG, P., LI, C., SUN, H., TAO, D., LIU, Y., ZHANG, S. & MA, Y. 2012. HILI inhibits TGF-beta signaling by interacting with Hsp90 and promoting TbetaR degradation. *PLoS One,* 7**,** e41973.

ZHANG, L., WANG, N., SHEN, Q., CHENG, W. & QIAN, G. J. 2013. Therapeutic efficacy of percutaneous radiofrequency ablation versus microwave ablation for hepatocellular carcinoma. *PLoS One,* 8**,** e76119.

ZHANG, M.-B., HE, J.-L., JIN, L.-F. & LU, D.-Q. 2002. Study of low-intensity 2450-MHz microwave exposure enhancing the genotoxic effects of mitomycin C using micronucleus test and comet assay in vitro. *Biomedical and environmental sciences : BES,* 15**,** 283-290.

ZHAO, R., ZHANG, S., XU, Z., JU, L., LU, D. & YAO, G. 2007a. Studying gene expression profile of rat neuron exposed to 1800MHz radiofrequency electromagnetic fields with cDNA microassay. *Toxicology,* 235**,** 167-75.

ZHAO, T.-Y., ZOU, S.-P. & KNAPP, P. E. 2007b. Exposure to cell phone radiation up-regulates apoptosis genes in primary cultures of neurons and astrocytes. *Neuroscience Letters,* 412**,** 34-38.

ZHIVOTOVSKY, B. 2004. Apoptosis, necrosis and between. *Cell Cycle,* 3**,** 63-65.

ZHOU, W. & ARELLANO, R. S. 2018. Thermal Ablation of T1c Renal Cell Carcinoma: A Comparative Assessment of Technical Performance, Procedural Outcome, and

Safety of Microwave Ablation, Radiofrequency Ablation, and Cryoablation. *Journal of Vascular and Interventional Radiology,* 29**,** 943-951.

ZHOU, W., ZHA, X., LIU, X., DING, Q., CHEN, L., NI, Y., ZHANG, Y., XU, Y., CHEN, L., ZHAO, Y. & WANG, S. 2012. US-guided percutaneous microwave coagulation of small breast cancers: a clinical study. *Radiology,* 263**,** 364-73.

ZIEMLEWICZ, T. J., HINSHAW, J. L., LUBNER, M. G., BRACE, C. L., ALEXANDER, M. L., AGARWAL, P. & LEE, F. T. 2015. Percutaneous Microwave Ablation of Hepatocellular Carcinoma with a Gas-Cooled System: Initial Clinical Results with 107 Tumors. *Journal of Vascular and Interventional Radiology,* 26**,** 62-68.